JOURNAL OF
GEOPHYSICAL RESEARCH

The continuation of

RRESTRIAL MAGNETISM AND ATMOSPHERIC ELECTRICITY
(1896-1948)

An International Quarterly

OLUME 59 March, 1954 NUMBER 1

CONTENTS

(Contents concluded on outside back cover)

Address all correspondence to

JOURNAL OF GEOPHYSICAL RESEARCH
5241 BROAD BRANCH ROAD, NORTHWEST
WASHINGTON 15, D.C., U.S.A.

THREE DOLLARS AND FIFTY CENTS A YEAR SINGLE NUMBERS, ONE DOLLAR

PRINTED BY
THE WILLIAM BYRD PRESS, INC.
P. O. Box 2-W—Sherwood Ave. and Durham St., Richmond 5, Virginia

JOURNAL OF GEOPHYSICAL RESEARCH

The continuation of

Terrestrial Magnetism and Atmospheric Electricity

(1896-1948)

An International Quarterly

Founded 1896 by L. A. BAUER *Continued 1928–1948 by* J. A. FLEMING

Fields of Interest

Terrestrial Magnetism
Atmospheric Electricity
The Ionosphere
Solar and Terrestrial Relationships
Aurora, Night Sky, and Zodiacal Light
The Ozone Layer
Meteorology of Highest Atmospheric Levels
The Constitution and Physical States of the Upper Atmosphere
Special Investigations of the Earth's Crust and Interior, including experimental seismic waves, physics of the deep ocean and ocean bottom, physics in geology
And similar topics

This Journal serves the interests of investigators concerned with terrestrial magnetism and electricity, the upper atmosphere, the earth's crust and interior by presenting papers of new analysis and interpretation or new experimental or observational approach, and contributions to international collaboration. It is not in a position to print, primarily for archive purposes, extensive tables of data from observatories or surveys, the significance of which has not been analyzed.

Forward *manuscripts* to one of the Associate Editors, or to the editorial office of the Journal at 5241 Broad Branch Road, Northwest, Washington 15, D. C., U. S. A. It is preferred that manuscripts be submitted in English, but communications in French, German, Italian, or Spanish are also acceptable. A brief abstract, preferably in English, must accompany each manuscript. A *publication charge* of $4 per page will be billed by the Editor to the institution which sponsors the work of any author; private individuals are not assessed page charges. Manuscripts from outside the United States are invited, and should not be withheld or delayed because of currency restrictions or other special difficulties relating to page charges. Costs of publication are roughly twice the total income from page charges and subscriptions, and are met by subsidies from the Carnegie Institution of Washington and international and private sources.

Back issues and *reprints* are handled by the Editorial Office, 5241 Broad Branch Road, N.W., Washington 15, D.C., U.S.A.

Subscriptions are handled by the Editorial Office, 5241 Broad Branch Road, N.W., Washington 15, D.C., U.S.A.

Entered as second-class matter at the Post Office at Richmond, Virginia, under the act of March 3, 1879.

Journal of

GEOPHYSICAL RESEARCH

The continuation of

Terrestrial Magnetism and Atmospheric Electricity

VOLUME 59 MARCH, 1954 No. 1

ON THE DYNAMO THEORY OF GEOMAGNETIC FIELD VARIATIONS

BY S. K. CHAKRABARTY AND R. PRATAP

Geophysical Laboratory, Bengal Engineering College, Howrah, India

(Received January 21, 1953)

ABSTRACT

The dynamo theory developed by Stewart, Schuster, and Chapman in order to explain the geomagnetic field variations no doubt give qualitative explanations for the observed variations but differ appreciably in details. In the present paper, the analysis of Chapman has been modified and the dynamo equations have been solved without introducing approximations which are difficult to justify. The solution of the dynamo equation has been given in the most general form, which can be used for any given "ionospheric conductivity" and "atmospheric oscillations." The results obtained have been compared with those of Chapman, which show the effect introduced in the final result by the approximations used by Chapman. The results have been utilized also to calculate the diurnal variations in horizontal and vertical intensities, and these have been compared with the observed data. The results show that with a reasonable assumption for the conductivity and the atmospheric oscillations, the dynamo theory can very well explain the observed facts.

The observational study of the various geomagnetic phenomena has been pursued for a long time and valuable records are available covering more than a century for a number of observatories distributed over the whole world. The physical theories to explain these observed results were brought forth from time to time, but they are not wholly satisfactory. The difficulties in the advancement

of the theoretical work are primarily due to the fact that the observations are mostly uncontrolled; the interesting phenomena that occur have a low periodicity and as such the observed results are also not very accurately known. The observed results on the nature of the solar diurnal variations, however, are known fairly accurately, and possibly for that reason various attempts were made to explain that from a theoretical standpoint. While the "diamagnetic theory" and the "drift-current theory" put forward to explain this phenomenon have their advantages, still at the present time the dynamo theory propounded by Schuster [see 1 of "References" at end of paper], and later modified and improved by Chapman [2], is possibly in best accord with observations. These analyses have also been summarized very lucidly by Chapman and Bartels [3], and also by Fleming [4]. There are, however, some physical assumptions as well as approximations in the underlying mathematical analysis, the validity of which is difficult to gauge. Since the publication of the analysis of Chapman, some important observational results have been obtained which make it necessary to revise or modify the analysis of Chapman. The anomalous behaviour of the *Sq* variation at Huancayo does not fit in with the analysis of Chapman. McNish [5], on the basis of his results obtained from a spherical harmonic analysis based on five American stations in the neighbourhood of 285° east longitude, tried to ascribe the anomaly to the large difference between the geographic latitude and the geomagnetic latitude, and concluded that the *Sq* variations should have a geomagnetic control rather than a geographic control. The possibility of a geomagnetic control is not only restricted to the equatorial regions, but its effect has also been noticed in higher latitudes. Chakrabarty [6] has also pointed out the existence of the difference in the *Sq* variations of Alibag and San Juan. Although these analyses of the observed data suggest the necessity of the modification of Chapman's analysis, no suggestion has so far been made as to how the analysis should be modified and through which factor the geomagnetic control can be incorporated into the analysis.

The uncertainties in the analysis of Chapman came through the neglect of the terms containing a_1^3 and a_2^2, and also higher powers of a_1 and a_2 in the expression deduced for the current function. In the later paper [7], however, the terms containing a_1^4 and a_2^2 were also retained. It will be shown in the subsequent sections that these approximations lead to a considerable difference in the final result. In a separate paper, Pratap has shown the order of error introduced by the approximations made in the analysis of Chapman. For comparison with the results of observations, Chapman has taken the average of the results of two or more observatories which are nearly in the same geographical latitude. This grouping tends to smooth out changes in variation with latitude and longitude, and, possibly as an effect of this, the discrepancy between the observed and the theoretical results based on Chapman's analysis [4, 8] were apparently reduced. The records of the Huancayo Observatory were not available at the time the analysis of Chapman was put forward, and it is now realized that the grouping of the stations in the same geographical latitude belt, particularly in low latitudes, will yield data of small statistical significance. A quantitative estimate of the magnetic variation cannot, therefore, be made from the results of Chapman. The special form of the integrated conductivity assumed by Chapman implies that the conductivity

distribution is symmetrical on the two sides of the noon meridian. Recent results obtained from ionospheric measurements, however, indicate that there is an asymmetry. It is, therefore, desirable to examine the effect of any change in the expression for the conductivity on the S variations. Chapman's expression for the conductivity, however, is superior to that used by Schuster, particularly because it introduces greater difference in the conductivity between day and night, and also makes the theoretical results agree in a much better way with the observed data. The conductivity of the upper atmosphere is primarily dependent on the ionizing power of the solar radiation, which possibly changes with sunspot activity. The variation of the Sq field with sunspot activity is now well established and any attempt to make a quantitative theoretical estimation of the field should provide for the possibility of incorporating the dependence of the conductivity on the sunspot cycle. The expression for the conductivity assumed by Chapman does not give proper weight to ion formation and recombination, and, as such, although broadly speaking the diurnal variation of the conductivity assumed by him agrees with that obtained from ionospheric measurements, it differs in details to some extent. Uncertainty also exists in the location of the layer that is the seat of the dynamo current. Recent ionospheric measurements, however, have shown that the height of the main ionized layer which is possibly the seat of the dynamo current associated with the Sq field should be in the neighbourhood of 100 km. The dynamo current depends critically on the nature of the atmospheric oscillation. The nature of the oscillation in the ionized layer where the dynamo current is produced is possibly different from the observed atmospheric oscillations on the surface of the earth. It may be noted that, whereas the main term in the daily barometric variations is semi-diurnal, in Sq the diurnal term, in general, is the predominating one. Schuster and Chapman deduced the air motion in the ionized shell by connecting it with the pressure variations observed on the earth's surface and neglecting all forces, including those due to the earth's rotation, except the pressure gradient. The work of Taylor [9] and Pekeris [10] suggests that the oscillation is reversed in phase at great heights and also its amplitude is magnified considerably, and as such, contrary to the assumptions of Schuster and Chapman, air motion in the ionosphere has no simple relation with the pressure variation at the ground-level. However, as pointed out by Chapman, it is possible to express the velocity potential in a series of surface harmonics, but the amplitude and the phase factor of each harmonic term need not be restricted by those obtained from the observed ground-level barometric variations, following the analysis of Chapman and Schuster. We propose to discuss the influence of the phase factor on the calculated geomagnetic field in a later paper. It will be clear from the following analysis that regular or irregular "wind" in the ionosphere has a considerable influence on the geomagnetic field. Observations on meteor trails occasionally reveal the existence of strong winds in the lower part of the ionosphere, and in some cases the trails are observed as twisted, suggesting local irregularities of wind direction and turbulence. The continuous geomagnetic records of horizontal intensity (H), vertical intensity (V), and declination (D) at different observatories show quite a large number of minor but irregular fluctuations, such as bays, micropulsations, and other similar disturbances, which are mostly local phenomena,

although a few of them are also of world-wide occurrence (Chakrabarty [11]). It is quite possible that at least considerable portions of these variations are due to the turbulence in the ionospheric level referred to above. A mathematical discussion on this point will be given in a subsequent paper.

In the present paper, we have obtained an expression for the current function without introducing any approximation which cannot be easily justified. Since fairly accurate observational data are now available from a world-wide net of observatories, it should be possible to make a quantitative comparison of the results of the analysis of this paper with the corresponding observed data and thus decide how far the dynamo theory can explain the observed variations. Such a quantitative analysis may possibly lead to the investigation of new phenomena for a proper understanding and explanation of the problems of geomagnetism. We have first carried out the analysis on the same physical assumptions as were made by Chapman and obtained the solution of the equation, and have shown the nature as well as the degree of difference that appear in the final result as a consequence of approximation introduced by Chapman. Later, we have also estimated the effect of the different physical assumptions on the final results.

Following Chapman, we assume that the dynamo current is produced in a spherical shell of mean radius r and thickness e, and that the conductivity ρ in this shell is supposed uniform throughout the thickness e, so that the integrated conductivity is given by

$$\rho e = a_0 + a_1 \cos\omega + a_2 \cos^2\omega \quad \ldots\ldots(1)$$

where

$$\cos\omega = \sin\delta \cos\theta + \cos\delta \sin\theta \cos t \quad \ldots\ldots(2)$$

δ is the declination of the sun, θ and λ are the colatitude and longitude of the point, and t is the local time. Terms containing higher powers of cos ω, however, can also be introduced in (1) without appreciably altering the following analysis.

Substituting (2) in (1) and making a Fourier resolution, we have

$$(\rho e) = K \sum_{s'=-\infty}^{\infty} f_{s'} \cos s't \qquad (\rho e)^2 = K^2 \sum_{s=-\infty}^{\infty} g_s \cos st \quad \ldots\ldots(3)$$

The general expressions are useful if we retain in (1) terms containing powers of cos ω higher than the second. In the particular case discussed in the present paper, where only the three terms as in (1) are retained, we have easily

$$\left.\begin{aligned} f_0 &= a_0 + a_1\beta\cos\theta + a_2\beta^2\cos^2\theta + \tfrac{1}{2}a_2\gamma^2\sin^2\theta \\ f_1 &= f_{-1} = \tfrac{1}{2}a_1\gamma\sin\theta + a_2\beta\gamma\sin\theta\cos\theta \\ f_2 &= f_{-2} = \tfrac{1}{4}a_2\gamma^2\sin^2\theta \\ f_s &= f_{-s} = 0 \qquad s > 2 \end{aligned}\right\} \quad \ldots\ldots(4)$$

and

$$
\left.\begin{aligned}
g_0 &= a_0^2 + 2a_0a_1\beta\cos\theta + (a_1^2 + 2a_0a_2)[\beta^2\cos^2\theta + \tfrac{1}{2}\gamma^2\sin^2\theta] \\
&\quad + 2a_1a_2[\beta^3\cos^3\theta + \tfrac{3}{2}\beta\gamma^2\cos\theta\sin^2\theta] \\
&\quad + a_2^2[\beta^4\cos^4\theta + \tfrac{3}{8}\gamma^4\sin^4\theta + 3\beta^2\gamma^2\cos^2\theta\sin^2\theta] \\
g_1 &= g_{-1} = a_0a_1\gamma\sin\theta + (a_1^2 + 2a_0a_2)\beta\gamma\sin\theta\cos\theta \\
&\quad + 3a_1a_2\beta^2\gamma\cos^2\theta\sin\theta + \tfrac{3}{4}a_1a_2\gamma^3\sin^3\theta \\
&\quad + 2a_2^2\beta^3\gamma\cos^3\theta\sin\theta + \tfrac{3}{2}a_2^2\beta\gamma^3\cos\theta\sin^3\theta \\
g_2 &= g_{-2} = \tfrac{1}{4}(a_1^2 + 2a_0a_2)\gamma^2\sin^2\theta + \tfrac{3}{2}a_1a_2\beta\gamma^2\cos\theta\sin^2\theta \\
&\quad + \tfrac{3}{2}a_2^2\beta^2\gamma^2\cos^2\theta\sin^2\theta + \tfrac{1}{4}a_2^2\gamma^4\sin^4\theta \\
g_3 &= g_{-3} = \tfrac{1}{4}a_1a_2\gamma^3\sin^3\theta + \tfrac{1}{2}a_2^2\beta\gamma^3\cos\theta\sin^3\theta \\
g_4 &= g_{-4} = \frac{1}{16}a_2^2\gamma^4\sin^4\theta \\
g_s &= g_{-s} = 0 \qquad s > 4
\end{aligned}\right\} \quad \ldots\ldots(5)
$$

where

$$\beta = \sin\delta; \qquad \gamma = \cos\delta$$

The dynamo field is produced by the motion of the medium in the presence of the earth's magnetic field. We assume that the oscillation of the ionospheric layer, where the dynamo current is produced, is of the harmonic type and has a velocity-potential Ψ given by

$$\Psi = \sum_{\sigma}\sum_{\tau} K_{\sigma}^{\tau}P_{\sigma}^{\tau}\sin[\tau t - \alpha] \quad \ldots\ldots(6)$$

The nature of the oscillation is not known accurately, nor has any relation between the atmospheric oscillations at the surface of the earth and that at the ionospheric layer been definitely established. But, whatever be the actual form, it is possible to express it by equation (6).

If, therefore, R be the current function, then following Chapman we have

$$
\left.\begin{aligned}
a(\rho e)^2\left[\frac{\partial(vH_z)}{\partial\phi} + \frac{\partial}{\partial\theta}(uH_z\sin\theta)\right] &= (\rho e)\left[\frac{1}{\sin\theta}\frac{\partial^2R}{\partial\phi^2} + \frac{\partial}{\partial\theta}\left(\sin\theta\frac{\partial R}{\partial\theta}\right)\right] \\
&\quad - \left[\frac{1}{\sin\theta}\frac{\partial R}{\partial\phi}\frac{\partial(\rho e)}{\partial\phi} + \sin\theta\frac{\partial R}{\partial\theta}\frac{\partial(\rho e)}{\partial\theta}\right]
\end{aligned}\right\} \quad \ldots\ldots(7)
$$

where H_z is the vertical component of the earth's magnetic field and u, v the southward and eastward components of the motion of the medium at the iono-

spheric layer where the dynamo current is produced. If the earth's field be regarded as that produced by a central magnetic dipole, then we have approximately

$$H_z = C \cos\theta + C \tan\theta_0 \sin\theta \cos(\phi - \phi_0) \quad \ldots\ldots\ldots\ldots (8)$$

where C is a constant and is approximately equal to $-2/3$ gauss, θ_0 and ϕ_0 being the coordinates of the geomagnetic north pole. The earth is assumed to be a uniformly magnetised sphere. Also

$$u = \frac{\partial \Psi}{a\,\partial\theta} \quad \text{and} \quad v = \frac{1}{a \sin\theta}\frac{\partial \Psi}{\partial \Phi} \quad \ldots\ldots\ldots\ldots\ldots (9)$$

where Ψ is given by (6).

Substituting (3) and (6) in (7) and simplifying, the left-hand side of (7) reduces to

$$\left.\begin{aligned} K^2 \sum_\sigma \sum_\tau \sum_{s=-\infty}^{\infty} g_s \sin\theta K_\sigma^\tau \Bigg[\left\{ \frac{\partial H_z}{\partial\theta}\frac{dP_\sigma^\tau}{d\theta} - \sigma(\sigma+1) H_z P_\sigma^\tau \right\} \sin[\tau t - \alpha] \cos st \\ + \frac{\tau}{\sin^2\theta}\frac{\partial H_z}{\partial\phi} P_\sigma^\tau \cos[\tau t - \alpha] \cos st \Bigg] \end{aligned}\right\}$$

or

$$\left.\begin{aligned} K^2 \sum_\sigma \sum_\tau K_\sigma^\tau \sum_{s=-\infty}^{\infty} g_s \sin\theta \Bigg[\left\{ \frac{\partial H_z}{\partial\theta}\frac{dP_\sigma^\tau}{d\theta} - \sigma(\sigma+1) H_z P_\sigma^\tau \right\} \sin[(\tau+s)t - \alpha] \\ + \frac{\tau}{\sin^2\theta}\frac{\partial H_z}{\partial\phi} P_\sigma^\tau \cos[(\tau+s)t - \alpha] \Bigg] \end{aligned}\right\} \quad \ldots\ldots (10)$$

It is, therefore, clear that R which must satisfy equation (7) should also be expressible as a series of surface harmonics, and without loss of generality we can, following Chapman, assume

$$R = \sum_\sigma \sum_\tau K_\sigma^\tau C K \sum_{n=0}^{\infty} \sum_{m=-\infty}^{\infty} p_n^m P_n^m \sin[mt - \alpha_m] \quad \ldots\ldots\ldots\ldots (11)$$

where p_n^m is a constant to be evaluated, and when m is a negative integer we assume that

$$P_n^m \equiv P_n^{-m}$$

Hence after simplifications, the right side of equation (7) reduces to

$$CK^2 \sum_\sigma \sum_\tau \sum_{s'=-\infty}^{\infty} \sin\theta K_\sigma^\tau \sum_n \sum_m p_n^m \Bigg[\left\{ \frac{ms'}{\sin^2\theta} - n(n+1) \right\} f_{s'} P_n^m - \frac{\partial f_{s'}}{d\theta}\frac{dP_n^m}{d\theta} \Bigg] \sin[\overline{m + s'}t - \alpha_m] \ldots (12)$$

by using the well-known relation

$$\frac{d}{d\theta}\sin\theta\frac{dP_n^m}{d\theta} + \sin\theta\left[n(n+1) - \frac{m^2}{\sin^2\theta} \right] P_n^m = 0 \quad \ldots\ldots\ldots\ldots (13)$$

Equation (7), therefore, reduces to

$$\left.\begin{aligned}\sum_{\sigma}\sum_{\tau}\sum_{s=-\infty}^{\infty} K_{\sigma}^{\tau} g_s \left[\frac{\partial H_z}{\partial\theta}\frac{dP_{\sigma}^{\tau}}{d\theta} - \sigma(\sigma+1)H_z P_{\sigma}^{\tau}\right]\sin[(\tau+s)t-\alpha] \\ + \frac{\tau}{\sin^2\theta}\frac{\partial H_z}{\partial\phi}P_{\sigma}^{\tau}\cos[(\tau+s)-\alpha] \\ = -C\sum_{\sigma}\sum_{\tau}K_{\sigma}^{\tau}\sum_{n}\sum_{m}\sum_{s'=-\infty}^{\infty} p_n^m\left[\left\{n(n+1)-\frac{ms'}{\sin^2\theta}\right\}f_{s'}P_n^m \right. \\ \left. + \frac{df_{s'}}{d\theta}\frac{dP_n^m}{d\theta}\right]\sin[(m+s')t-\alpha_m] \\ = -C\sum_{\sigma}\sum_{\tau}K_{\sigma}^{\tau}\sum_{n}\sum_{m}\sum_{s'=-\infty}^{\infty} p_n^m R_n^m(s')\sin[(m+s')t-\alpha_m]\end{aligned}\right\} \quad \ldots\ldots(14)$$

where

$$R_n^m(s') = \left[n(n+1) - \frac{ms'}{\sin^2\theta}\right]f_{s'}P_n^m + \frac{df_{s'}}{d\theta}\frac{dP_n^m}{d\theta} \quad \ldots\ldots\ldots\ldots(15)$$

Equation (14) is the "master equation" of our problem, which gives the values of p_n^m for all possible values of m and n for given values of atmospheric oscillations and the ionospheric conductivity, that is, for given values of σ, τ, and (ρe). We can solve (14) and get p_n^m as functions of δ. Without loss of generality, we can calculate p_n^m separately for different sets of values of σ and τ, and then sum it up to get the resulting expression for R. Chapman has also deduced the same equation, and up to this stage our analysis is similar to that of Chapman. In the next section, we shall solve equation (14) in the most general way, without the use of approximations as was done by Chapman.

For any preassigned value of σ and τ, we therefore have

$$\begin{aligned}-C\sum_{n}\sum_{m}\sum_{s=-\infty}^{\infty} p_n^m R_n^m(s')\sin[(m+s')t-\alpha_m] \\ = \sum_{s=-\infty}^{\infty} g_s\left[\left\{\frac{\partial H_z}{\partial\theta}\frac{dP_{\sigma}^{\tau}}{d\theta} - \sigma(\sigma+1)H_z P_{\sigma}^{\tau}\right\}\sin[(\tau+s)t-\alpha]\right. \\ \left. + \frac{\tau}{\sin^2\theta}\frac{\partial H_z}{\partial\phi}P_{\sigma}^{\tau}\cos[(\tau+s)t-\alpha]\right] \quad \ldots\ldots(16)\end{aligned}$$

We shall consider here the first term in the value of H_z given by (8). In another paper, Pratap [12] has shown that the contribution of the second term in (8) is very small as compared to that of the first. Hence, taking $H_z = C\cos\theta$, we get

$$\left.\begin{aligned}\sum_{n}\sum_{m}\sum_{s=-\infty}^{\infty} p_n^m R_n^m(s')\sin[(m+s')t-\alpha_m] \\ = \frac{1}{2\sigma+1}\{\sigma(\sigma+2)(\sigma-\tau+1)P_{\sigma+1}^{\tau} \\ + (\sigma^2-1)(\sigma+\tau)P_{\sigma-1}^{\tau}\}\sum_{s=-\infty}^{\infty} g_s\sin[(\tau+s)t-\alpha]\end{aligned}\right\} \quad \ldots\ldots(17)$$

Equating the coefficients of the corresponding harmonic terms, we get $\alpha_m = \alpha$ for all values of m and

$$\sum_n \sum_m p_n^m R_n^m(s') = \frac{1}{2\sigma+1}\{\sigma(\sigma+2)(\sigma-\tau+1)P_{\sigma+1}^{\tau} + (\sigma^2-1)(\sigma+\tau)P_{\sigma-1}^{\tau}\}g_s \quad \ldots\ldots(18)$$

where

$$s' = s + \tau - m \quad \ldots\ldots(18a)$$

Equation (18) in general gives an infinite number of equations, which when solved gives p_n^m and hence R.

If we take for the conductivity the expression given by (1), then by (5) we have

$$\left.\begin{aligned} g_s &= g_{-s} = 0 \quad \text{when} \quad s > 4; \quad \text{and} \\ R_n^m(s') &= 0 \quad \text{when} \quad s' > 2 \end{aligned}\right\} \quad \ldots\ldots(19)$$

It is possible that the main component in the atmospheric oscillation is a semi-diurnal one, and hence we also, like Chapman, calculate the coefficients p_n^m for the case $\sigma = 2, \tau = 2$. The method of calculation is perfectly general and can be carried out without much difficulty for other possible values of σ and τ. On the other hand, a different expression for the conductivity will give different values of g_s and f_s, and the above conditions (19) are to be modified.

With $\sigma = 2, \tau = 2$, equation (18) reduces to

$$\frac{8}{5} g_s P_3^2 = \sum_{n=0}^{\infty} \sum_{s'=-2}^{2} p_n^{s+2-s'} R_n^{s+2-s'}(s') \quad \ldots\ldots(20)$$

A typical form of the equation (20), for a particular value of s, say $s = 4$, when written in full stands as follows:

$$\frac{8}{5} g_4 P_3^2 = \sum p_n^4 R_n^4(2) + p_n^5 R_n^5(1) + p_n^6 R_n^6(0) + p_n^7 R_n^7(-1) + p_n^8 R_n^8(-2)$$

Using the expression for g_s given by (5) and the recurrence relations for the associated Legendre's functions, equation (20) can be reduced to the form in which both sides will be composed of terms containing associated Legendre's functions of different degrees and orders. Hence, equating the coefficients of the functions P_n^m of the same degree and order on the two sides, we get the values of coefficients p_n^m. The calculations are straightforward but tedious.

It is easily seen that solving equation (20) with $s = 4$, we get

$$p_5^4 = \frac{1}{3150} a_2 \gamma^2; \qquad p_n^4 = 0 \quad \text{for } n \neq 5 \quad \ldots\ldots(21)$$

Substituting these values in equation (20) with $s = 3$, we get p_n^m and so on. We have in this manner solved the equations exactly, without making any approximations. In his analysis, Chapman has assumed that $p_n^m s$ can be expressed in a series of power of a_2/a_0, a_1/a_0, and has neglected higher powers of these terms. With the values of a_0, a_1, a_2 used by him ($a_0 = 1$, $a_1 = 3$, $a_2 = 9/4$) for actual

calculations, it is difficult to justify these approximations. It appears that the terms neglected by him are of the same order and in some cases even larger than the terms retained. The effect of this approximation will be evident from Table 2, where the coefficients obtained by him are compared with those based on the analysis of the present paper.

In this way, we have been able to solve exactly and uniquely equations (20) for $s \geq 2$. The first difficulty arose when we took $s = 1$. Although the left side of (20) contained the five functions P_n^m ($m = 3, n = 3, 4, 5, 6, 7$) which would normally be sufficient to get all $p_n^1 s$, p_1^1 did not appear on the right side of the equation, since $R_1^1(2) = 0$. Consequently, p_1^1 could not be derived from these sets of equations. The coefficients of P_3^3 on the two sides of (20) can be equal and thus the equations with $s = 1$ satisfied exactly if we take

$$\tfrac{2}{3}a_0a_2 - \tfrac{1}{4}a_1^2 = 0 \qquad (22)$$

We can impose the condition that a_0 , a_1 , a_2 must be connected by the relation (22), or consider that the equations with $s = 1$ are satisfied approximately, since $2/3a_0a_2 - 1/4a_1^2$ forms a very small portion ($\backsim$ 5 per cent only) of the coefficients of P_3^3 on the left side of this equation. We are constrained, however, to believe that equation (22) may be a real one. If (22) is used, then equation (20) with $s = 0$ and $s = -1$ are also satisfied exactly. With our present-day knowledge about the ionospheric conductivity, we cannot say with certainty that the restrictions on the coefficients imposed by (22) are not real ones. For purpose of comparison, we have drawn in Figure 1 the curves showing (ρe) against ω, with $a_0 = 1$, $a_2 = 9/4$,

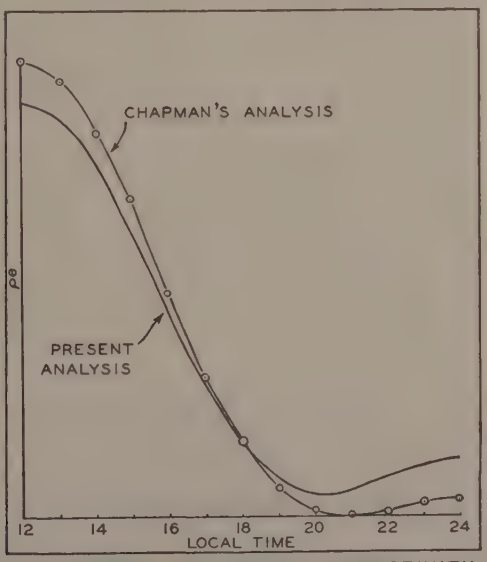

FIG. 1—DIURNAL VARIATION OF CONDUCTIVITY

and $a_1 = 2.45$, as obtained from (22), together with those obtained with Chapman's values, namely, $a_0 = 1$, $a_1 = 3$, $a_2 = 9/4$. Figure 1 suggests that the relation given by (22) is a possible one; still this question can be kept open till more accurate

observational data on the point are obtained, and as such no attempt has been made to give a physical interpretation to the condition (22).

Proceeding in the same way, we have solved equation (20) with $s = 0, -1, -2, -3, -4$, etc., and obtained all the coefficients p_n^m, which are given in Table 1. With the condition (22) and the coefficients p_n^m in Table 1, all equations of (20)

TABLE 1—*Coefficients of the current function* (11) *which satisfies equation* (20)

$$p_5^4 = \frac{1}{3150}\,a_2\gamma^2$$

$$p_5^3 = \frac{4}{1575}\,a_2\,\beta\gamma; \qquad p_4^3 = \frac{1}{140}\,a_1\gamma; \qquad p_3^3 = \frac{1}{45}\,a_2\,\beta\gamma$$

$$p_5^2 = \frac{4}{525}\,a_2(\beta^2 - \tfrac{1}{2}\gamma^2); \qquad p_4^2 = \frac{1}{35}\,a_1\beta; \qquad p_3^2 = \frac{2}{15}\,a_0 + \frac{2}{75}\,a_2; \qquad p_2^2 = \frac{1}{14}\,a_1\beta$$

$$p_5^1 = -\frac{16}{525}\,a_2\beta\gamma; \qquad p_4^1 = -\frac{3}{70}\,a_1\gamma; \qquad p_3^1 = \frac{2}{15}\,a_2\beta\gamma; \qquad p_2^1 = \frac{1}{7}\,a_1\gamma + \frac{1}{5}\,a_1\frac{1}{\gamma}$$

$$p_1^1 = \left(2a_0 - \frac{12}{5}\,a_2\right)\frac{\beta}{\gamma} + \frac{72}{35}\,a_2\beta\gamma$$

$$p_5^0 = \frac{4}{105}\,a_2\gamma^2; \qquad p_4^0 = 0; \qquad p_3^0 = -\frac{4}{15}\,a_2\gamma^2; \qquad p_2^0 = -\frac{4}{5}\,a_1\frac{\beta}{\gamma^2}$$

$$p_1^0 = 8a_0 - \frac{56}{5}\,a_0\frac{1}{\gamma^2} + \frac{48}{5}\,a_2\frac{\beta^2}{\gamma^2} + \frac{36}{35}\,a_2\gamma^2$$

$$p_5^{-1} = 0; \qquad p_4^{-1} = 0; \qquad p_3^{-1} = 0; \qquad p_2^{-1} = \frac{24}{5}\,a_1\frac{1}{\gamma^3} - \frac{18}{5}\,a_1\frac{1}{\gamma};$$

$$p_1^{-1} = 8\,\frac{a_0^2}{a_2}\frac{\beta}{\gamma^3} - \frac{112}{5}\,a_0\frac{\beta}{\gamma^3} + 20a_0\frac{\beta}{\gamma} + \frac{96}{5}\,a_2\frac{\beta^3}{\gamma^3} - \frac{24}{5}\,a_2\frac{\beta^3}{\gamma}$$

$$p_5^{-2} = p_4^{-2} = p_3^{-2} = 0; \qquad p_2^{-2} = -\frac{96}{5}\,a_1\frac{\beta}{\gamma^4}(1 + \beta^2)$$

$$p_5^{-3} = p_4^{-3} = p_3^{-3} = 0; \qquad p_5^{-4} = 0$$

with $s \geq -1$ and $s < -6$ are satisfied exactly. The equations corresponding to $-6 \leq s \leq -2$, however, are satisfied approximately. The residuals are only a small percentage of the complete expression that occurs on the right side of the corresponding equations. Most of the residuals again vanish when $\beta = 0$, that is, for the equinoxes.

It is thus clear that the values of p_n^m given in Table 1 are exact for all values of $m \geq -1$ and $m < -4$. The coefficients p_n^m for $-4 \leq m \leq -2$, however, are approximate, but their effect is not at all serious and the effect is very much less in the calculation of the coefficients when $\beta = 0$, that is, at the equinoxes, which

we have selected for purpose of comparison of the results of our calculations with the observed data. Until more accurate information is available about the nature of the atmosphere oscillations and the ionospheric conductivity, more accurate values of p_n^m for $-4 \leq m \leq -2$ may not be useful.

For purpose of comparison, we have given in Table 2 the values of some of the

TABLE 2—*Equinoctial values of* p_n^m *given in Table* 1 ($\beta = 0, \gamma = 1$), *together with Chapman's values*
[Present analysis ($a_1 = 2.45, a_2 = 2.25$); Chapman's analysis ($a_0 = 1, a_1 = 3, a_2 = 2.25$)]

p_5^4	0.000714	0.000721
p_4^3	0.0175	0.0212
p_5^2	−0.00857	0
p_3^2	0.193	0.203
p_4^1	−0.105	0
p_2^1	0.840	0.732
p_5^0	0.0857	0
p_3^0	−0.60	0
p_1^0	−0.8857	0
p_2^{-1}	2.94	0.0179
p_3^{-2}	0	0.032

coefficients p_n^m for the equinoxes, that is, $\beta = 0$ and $\gamma = 1$, together with the corresponding values obtained from Chapman's analysis. It will appear that some of the coefficients, namely, p_2^{-1}, p_4^1, p_3^0, p_1^0, differ appreciably from those of Chapman, and these possibly account for the large difference we obtain in the calculations of the ring currents and the *Sq* field.

In the next section, we have deduced the *Sq* variations of H and V, and have compared the results of our analysis with those deduced from observations and also those obtained from Chapman's analysis.

Substituting in (11) the values of p_n^m deduced above, we get the current function R. In another paper, we have drawn the ring currents and have shown their dependence on the phase α of the atmospheric oscillation. The magnetic potential W at the surface of the earth of radius a produced by the current functions deduced above is given by the relation

$$W = -\sum_{n=0}^{\infty}\sum_{m=-n}^{n} 4\pi \frac{n+1}{2n+1}\left(\frac{a}{r}\right)^n p_n^m P_n^m \sin\left[mt - \alpha_m\right] \quad \ldots\ldots\ldots (23)$$

where r is the mean radius of the ionospheric shell in which the dynamo current is produced. From the potential function W, one can easily calculate the geomagnetic force components and their variations. The position of the dynamo current is not known accurately, but from (23) it is evident that the values of W, and hence of H and V, do not depend very critically on r. For purpose of comparison, we have taken $r = a + 100$ km and $a = 6{,}368$ km. We have then calculated ΔH and ΔV for some different values of θ as a function of t. In Figure 2, we have plotted the

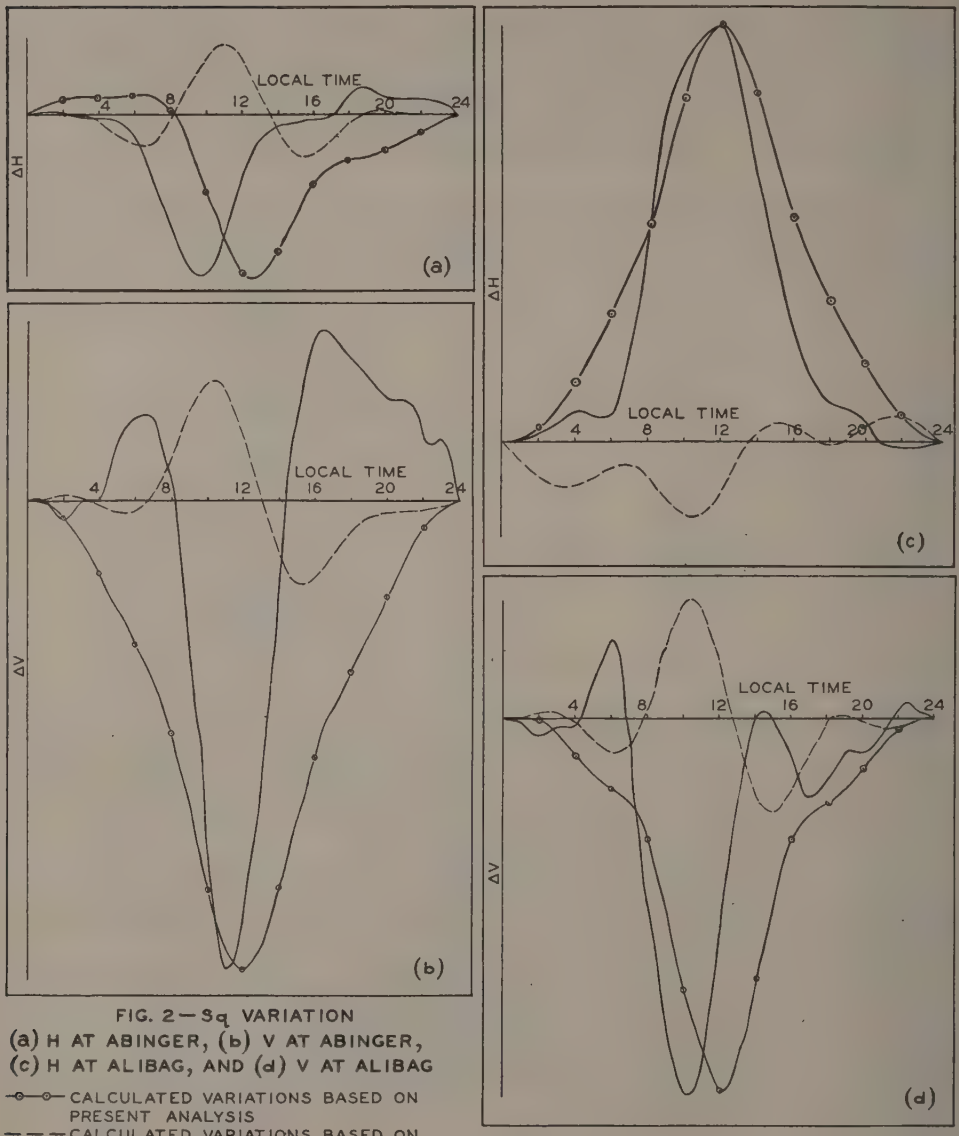

FIG. 2—Sq VARIATION
(a) H AT ABINGER, (b) V AT ABINGER,
(c) H AT ALIBAG, AND (d) V AT ALIBAG

—o—o— CALCULATED VARIATIONS BASED ON PRESENT ANALYSIS
— — — CALCULATED VARIATIONS BASED ON CHAPMAN'S ANALYSIS
——— OBSERVED VARIATIONS

values of ΔH and ΔV against local time for two different observatories, namely, Abinger ($\phi = 51°.2$, $\lambda = 359.6°$E, $\Phi = 54°.0$) and Alibag ($\phi = 18°.6$, $\lambda = 72.8$ E, $\Phi = 9°.5$). The observed data, which are extracted from the recent publications of the Department of Terrestrial Magnetism of the Carnegie Institution of Washington, have also been plotted in the Figures for purpose of comparison. We have also shown the corresponding curve based on Chapman's analysis, that is, using (23) with Chapman's values of p_n^m from Table 2. The phase of the atmospheric oscillations α has been taken as 275° throughout our calculations. For purpose of

comparison, we have also drawn (Fig. 3) the theoretical curve with $\alpha = 154°$ for the H variation at Alibag. This will show how critically our result depends on the

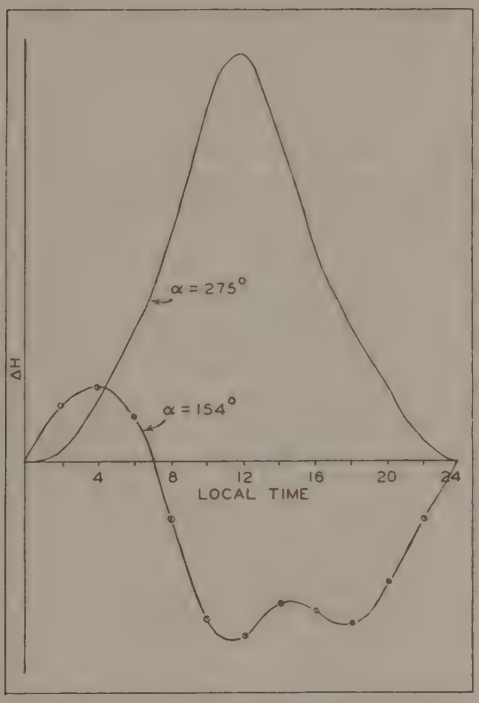

FIG. 3—CALCULATED S_q VARIATIONS IN H AT ALIBAG

magnitude of the phase α. This will be shown in details in another paper. It will be clear from the Figures that the calculations based on our analysis give a much better fit with the results of observation. It may be pointed out here that the expression for the conductivity assumed is only approximate and the approximation is worse at night time as well as in early morning. The differences between the theoretical curves and the observed curves, as shown in Figure 2, at these times are possibly due to those differences between the actual value of the conductivity and the theoretical value assumed. The theoretical curves of Figure 2 have been normalized to have the same maximum as those in the observed curves. This normalization should give the value of the product of a_0 and k_σ^τ, and should be the same for the ΔV and ΔH curves. Although both of them are of the order 10^3, they are not equal. It may be noted here that the observed curves are produced by the combined effects of dynamo currents in the ionosphere and that of the varying field produced by induction within the earth. The combined effects on ΔH and ΔV will possibly be different and, in order to get an estimate of the difference, accurate knowledge of the electrical conductivity and magnetic permeability throughout the earth is necessary. The curves are based on the assumption that the atmospheric oscillations in the ionospheric layer are semi-diurnal. If other components are present, as is quite likely, they will produce some contributions.

When more accurate knowledge about the atmospheric oscillations and the atmospheric conductivity becomes available, it will be possible from the analysis of the present paper to examine the extent to which the dynamo theory can explain the observed geomagnetic field variations.

References

[1] A. Schuster, Phil. Trans. R. Soc., A, **180**, 467 (1889) and A, **208**, 163 (1907).
[2] S. Chapman, Phil. Trans. R. Soc., A, **213**, 279 (1914).
[3] S. Chapman and J. Bartels, Geomagnetism, Oxford, Clarendon Press (1940).
[4] J. A. Fleming (Ed.), Terrestrial magnetism and electricity, New York, McGraw-Hill Book Co., Inc. (1939).
[5] A. G. McNish, Trans. Edinburgh Meeting, 1936; Internat. Union Geod. Geophys., Assoc. Terr. Mag. Electr., Bull. No. 10, 271-280 (1937).
[6] S. K. Chakrabarty, Curr. Sci., **15**, 246 (1946).
[7] S. Chapman, Phil. Trans. R. Soc., A, **218**, 1 (1919).
[8] J. Bartels, in Wien-Harms, Handbuch d. Experimentalphysik, Leipzig, Akad. Verlagsges., **25**, Teil I, 203–208 (1928).
[9] G. I. Taylor, Proc. R. Soc., A, **156**, 318 (1936).
[10] C. L. Pekeris, Proc. R. Soc., A, **158**, 650 (1937).
[11] S. K. Chakrabarty, Scientific notes, India Met. Dept., **10**, No. 126 (1947).
[12] R. Pratap, In press.

THE DISSOCIATION OF OXYGEN IN THE HIGH ATMOSPHERE*

BY M. NICOLET** AND P. MANGE

Ionosphere Research Laboratory, The Pennsylvania State University, State College, Pennsylvania

(Received June 23, 1953)

ABSTRACT

The question of the oxygen distribution in the high atmosphere is examined by studying the departure from photochemical equilibrium. An investigation of the transition region is made, utilizing recent rocket data on atmospheric transmission in the Schumann-Runge continuum of molecular oxygen. It is concluded that the molecular oxygen distribution above the dissociation region follows the distribution of the main atmosphere and depends on mixing effects. A limit for the time of mixing can be found when times of dissociation, recombination, and diffusion are considered.

It is shown that the level of the mesopause is related to the dissociation of the oxygen molecule. Some suggestions are made concerning dynamical effects affecting the airglow, formation of ionospheric regions, and dissociation of nitrogen.

I. Introduction

Since Chapman [see 1 of "References" at end of paper] found that oxygen is in a dissociated state above 120 km, and indicated that it is in a molecular state below 80 km, the problem of oxygen dissociation in the high atmosphere has been investigated by various authors.

Wulf and Deming [2] gave a complete distribution with height of atomic and molecular oxygen when the sun is assumed to radiate as a 6000°K black body and the recombination coefficient is determined by a three-body collision process. Using an atmospheric distribution subjected to diffusion, they found a complete dissociation of O_2 at 100 km.

In 1938 and 1947, Majumdar [3] and Rakshit [4] adopted Pannekoek's method which corresponds to a radiative equilibrium. Their results are not acceptable because the photochemistry of oxygen photodissociation and radiative recombination are not concerned with the same atomic states.

Recently, Penndorf [5] and Moses and Wu [6, 7] have again considered the problem of the oxygen photochemical equilibrium. Penndorf's method introduces the statistical equilibrium; that is to say, the number of O_2 photodissociation processes per cm^3 and sec equals the number of recombination processes per cm^3

*The research reported in this paper has been sponsored by the Geophysics Research Division of the Air Force Cambridge Research Center, Air Research and Development Command, under Contract AF 19(122)–44.

**Department of Radiation, Royal Meteorological Institute of Belgium, Uccle, Belgium.

and sec. The recombination process was computed according to the best known values from laboratory measurements involving three-body collisions. Some assumptions were made in order to simplify the computations, but his practical method must be accepted since further refinements are currently unrealistic due to the approximations involved in the numerical values of the coefficients.

Interesting considerations were given by Penndorf with regard to the emission of solar radiation. Instead of adopting the conventional 6000°K black body, he has also made computations with black bodies at 5000°K, 5300°K, and 5500°K, in order to follow the solar spectrum distribution in the spectral range in which molecular oxygen absorbs.

After a criticism of Penndorf's method, Moses and Wu [6] have attempted to establish a self-consistent method for calculating the oxygen equilibrium. In order to obtain the necessary number of equations, they have introduced a very restrictive condition; namely, a radiative equilibrium, where they assume that the rate of energy absorption by the photodissociation process equals the rate of energy emission in the recombination process. This hypothesis introduces the radiative recombinations of oxygen instead of a three-body recombination. Furthermore, in their mathematical theory, they have to make other assumptions regarding the solar emission and vertical distribution of the atmospheric constituents. We know that these assumptions are necessary in order to obtain a self-consistent result without any use of atmospheric data, but it is more desirable from a physical point of view to use observational data instead of making assumptions, when it is possible to do so.

In a more recent paper [7], Moses and Wu have dropped their radiative-energy balance hypothesis from the assumptions and have adopted a temperature distribution for their computation. However, the solar radiation is still represented by a black body of temperature 6000°K, which is very different from the published observational data. Furthermore, they assume diffusive equilibrium between oxygen and nitrogen. This assumption requires that the mixing effect due to advection or a dynamical disturbance is negligible compared with that of the diffusive equilibrium, and also that the time required to establish the oxygen photochemical equilibrium is less than the time necessary to establish the diffusion equilibrium between oxygen and nitrogen. Finally, it should also be noted that these assumptions are not independent of the assumed photodissociation process.

The purpose of the present work is to show that the treatment of oxygen dissociation is quite different from previous theories when the physical data obtained by rocket measurements are used. The results obtained from calculations in which a minimum of assumptions are made reveal that the theory differs materially from those of previous authors.

II. Absorption and dissociation of molecular oxygen

For the photodissociation of molecular oxygen, we know, from laboratory measurements,* of two absorption processes:

$$O_2 + h\nu(\lambda \leq 1759\ \text{A}) \rightarrow O(^3P) + O(^1D) \quad \ldots\ldots\ldots\ldots\ldots\ldots (1)$$

**Note added in proof:* New measurements by Herzberg lead to the exact values 1750 A and 2424 A; that is, 57,130 cm^{-1} or 7.08 eV and 41,260 cm^{-1} or 5.11 eV.

and

$$O_2 + h\nu(\lambda \leq 2420\ A) \rightarrow O(^3P) + O(^3P) \quad \ldots\ldots\ldots\ldots\ldots\ldots (2)$$

The intense Schumann-Runge continuum, starting at 56,850 cm^{-1} and corresponding to a dissociation potential of 7.047 eV, has been analyzed experimentally by Ladenburg and Van Voorhis [8] and discussed by Stueckelberg [9]. However, when the computation was ended using their data as indicated in the following pages, new experimental values of absorption coefficients were given by Watanabe [33]* and another computation was made using the more recent data.

The Herzberg continuum, commencing at 41,275 cm^{-1} and corresponding to the first dissociation potential of 5.116 eV, has been observed, thanks to measurements of the absorption of air [10, 11, 12, 13, 14, 15, 16].

The measurements of Ladenburg and Van Voorhis [8] cover, approximately, the spectral region from 60,000 cm^{-1} to 75,000 cm^{-1}. It is necessary to extrapolate their curve to the threshold at about 56,850 cm^{-1}. Graphical or theoretical extra-

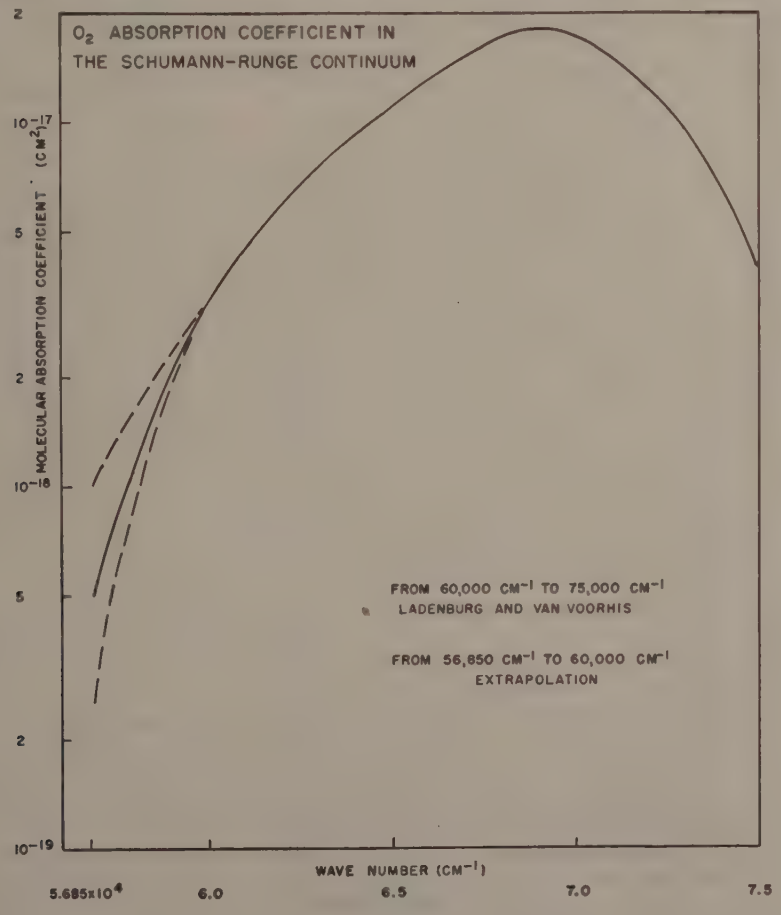

FIG. 1

*We keep both results in our discussion in order to compare data obtained by various workers.

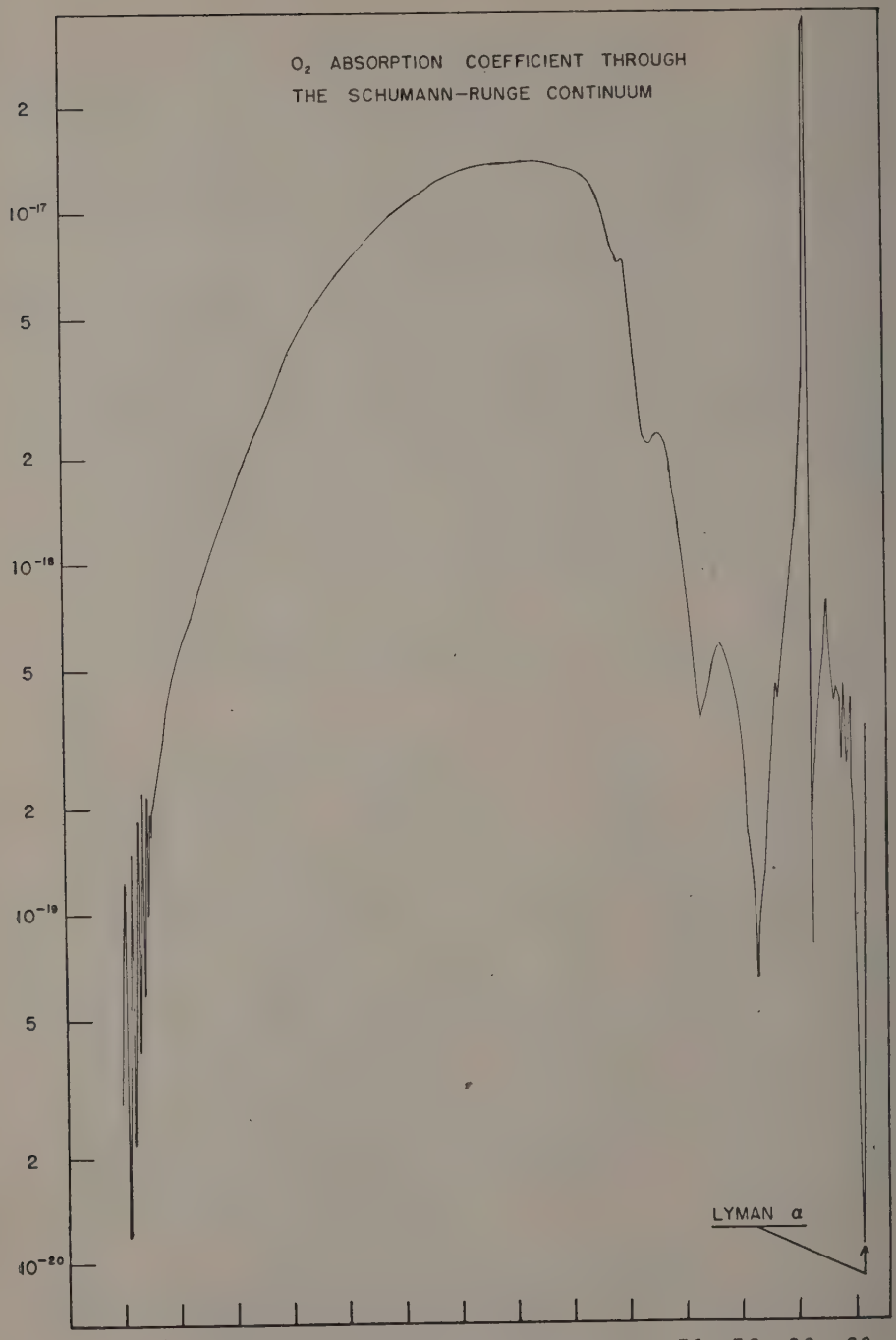
O_2 ABSORPTION COEFFICIENT THROUGH
THE SCHUMANN–RUNGE CONTINUUM
2
10^{-17}
5
2
10^{-18}
5
2
10^{-19}
5
2
10^{-20}
LYMAN α
5.6x10⁴ 5.8 6.0 6.2 6.4 6.6 6.8 7.0 7.2 7.4 7.6 7.8 8.0 8.2
WAVE NUMBER (CM⁻¹)

FIG. 2

polations lead to practically the same results. Penndorf [5], Bates and Nicolet [17], and Moses and Wu [6] have obtained different values, but, for a computation of the rate of O_2 dissociation, the most important effect is given by the black-body radiation temperature assumed. In considering here the general problem of the absorption of O_2 , we have represented in Figure 1 various extrapolations to the continuum head at 56,850 cm^{-1}; namely, 2.5×10^{-19}, 5×10^{-19}, and 10^{-18} cm^2. The value of 5×10^{-19} cm^2 was adopted considering the theoretical extrapolation [6] and as a mean between extreme possible values. An uncertainty at the continuum head is without great importance in the general computation, which takes into account the solar and absorption spectral distributions. In the shortest wavelength part of the Schumann-Runge continuum, we had based the spectral absorption on Weissler's [18] and Preston's [19] data. Values of the molecular absorption coefficient as deduced from Watanabe's data [33] are shown in Figure 2. In order to avoid approximations in the computations of integrals and to follow the absorption with the atmospheric optical depth, spectral ranges of 1000 cm^{-1} are used. Mean (con-

TABLE 1*a*—*Mean values of the O_2 absorption coefficient in the Schumann-Runge continuum, according to Ladenburg's and Van Voorhis's data* [8]

Spectral range	Absorption coefficient	Spectral range	Absorption coefficient	Spectral range	Absorption coefficient
(cm^{-1})	(cm^2)	(cm^{-1})	(cm^2)	(cm^{-1})	(cm^2)
56,847–58,000	7.60×10^{-19}	66,000–67,000	1.41×10^{-17}	75,000–76,000	1.87×10^{-18}
58,000–59,000	1.56×10^{-18}	67,000–68,000	1.62×10^{-17}	76,000–77,000	3.79×10^{-19}
59,000–60,000	2.59×10^{-18}	68,000–69,000	1.77×10^{-17}	77,000–78,000	1.00×10^{-19}
60,000–61,000	3.79×10^{-18}	69,000–70,000	1.73×10^{-17}	78,000–79,000	4.70×10^{-20}
61,000–62,000	5.19×10^{-18}	70,000–71,000	1.57×10^{-17}	79,000–80,000	2.77×10^{-20}
62,000–63,000	6.77×10^{-18}	71,000–72,000	1.35×10^{-17}	80,000–81,000	1.82×10^{-20}
63,000–64,000	8.45×10^{-18}	72,000–73,000	1.09×10^{-17}	81,000–82,000	1.28×10^{-20}
64,000–65,000	1.01×10^{-17}	73,000–74,000	7.95×10^{-18}	82,259	1.04×10^{-20}
65,000–66,000	1.20×10^{-17}	74,000–75,000	5.09×10^{-18}		

TABLE 1*b*—*Mean values of the O_2 absorption coefficient in the Schumann-Runge continuum as deduced from Watanabe's data* [33]

Spectral range	Absorption coefficient	Spectral range	Absorption coefficient	Spectral range	Absorption coefficient
(cm^{-1})	(cm^2)	(cm^{-1})	(cm^2)	(cm^{-1})	(cm^2)
56,847–58,000	3.43×10^{-19}	66,000–67,000	1.10×10^{-17}	74,000–75,000	3.22×10^{-18}
58,000–59,000	7.26×10^{-19}	67,000–68,000	1.24×10^{-17}	75,000–76,000	1.84×10^{-18}
59,000–60,000	1.24×10^{-18}	68,000–69,000	1.33×10^{-17}	76,000–77,000	5.59×10^{-19}
60,000–61,000	2.02×10^{-18}	69,000–70,000	1.38×10^{-17}	77,000–78,000	4.78×10^{-19}
61,000–62,000	3.22×10^{-18}	70,000–71,000	1.40×10^{-17}	78,000–79,000	1.57×10^{-19}
62,000–63,000	4.74×10^{-18}	71,000–72,000	1.36×10^{-17}	79,000–80,000	6.37×10^{-19}
63,000–64,000	6.33×10^{-18}	72,000–73,000	1.27×10^{-17}	80,000–81,000	7.93×10^{-18}
64,000–65,000	7.81×10^{-18}	73,000–74,000	8.44×10^{-18}	81,000–82,000	4.22×10^{-19}
65,000–66,000	9.44×10^{-18}				

stant) values of the absorption coefficient, which are adopted for these small spectral ranges in order to simplify the study of the absorption problem, are given in Tables 1*a* and 1*b*.

The absorption coefficient through the very feeble Herzberg continuum must be considered when the photodissociation due to the Schumann-Runge continuum cannot be effective after complete atmospheric absorption. In fact, this absorption by a forbidden transition is particularly effective in the ozonosphere. From comparisons between the experimental results [10 to 16], we adopt the value shown in Table 2, deduced from the curve of Figure 3.

It should be pointed out that the minimum values may be preferred because of the possibility of an absorbing process due to another molecule [13, 14].

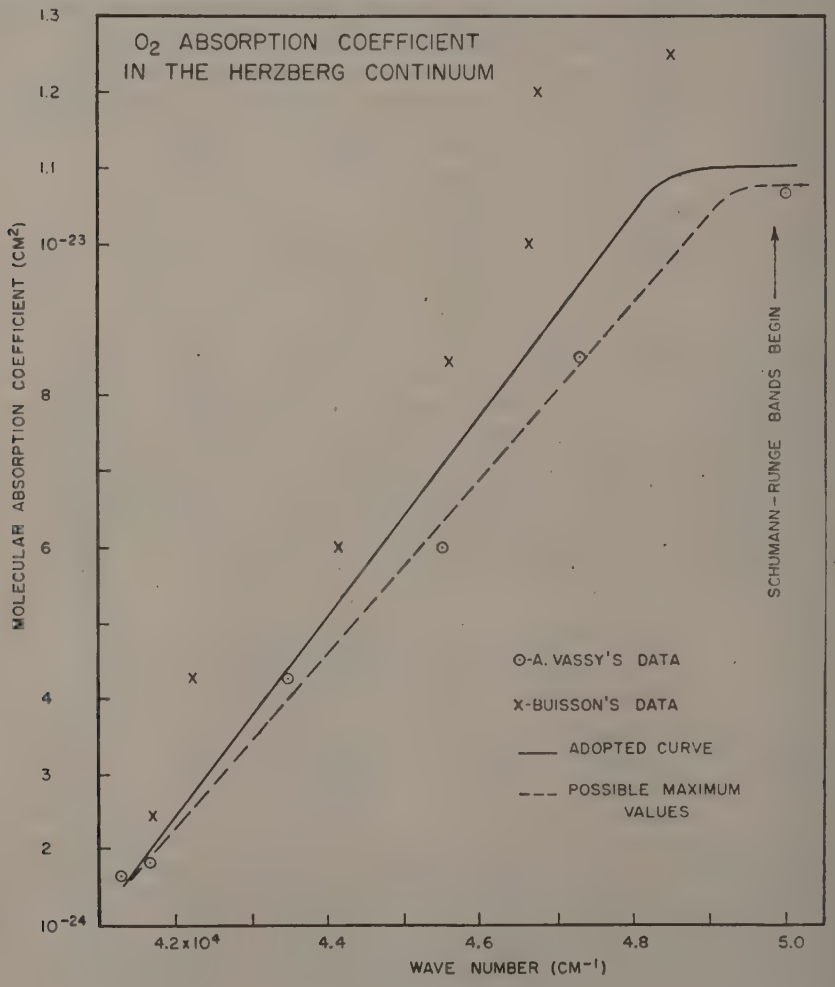

FIG. 3

(*Note:* The dashed line in Figure 3 represents possible *minimum* values rather than possible maximum values.)

TABLE 2—*Adopted values of O_2 absorption coefficient in the Herzberg continuum*

Wave number	Absorption coefficient	Wave number	Absorption coefficient
(cm^{-1})	(cm^2)	(cm^{-1})	(cm^2)
41,275	1.5×10^{-24}	46,000	7.7×10^{-24}
42,000	2.5×10^{-24}	47,000	9.0×10^{-24}
43,000	3.7×10^{-24}	48,000	10.5×10^{-24}
44,000	5.0×10^{-24}	49,000	1.1×10^{-23}
45,000	6.5×10^{-24}	50,000	1.1×10^{-23}

Comparing the values of the absorption coefficient given in Tables 1 and 2, it is easy to see that the optical depths involved in an atmospheric analysis for the two spectral ranges are different, and that the computation may be made separately for each continuum. Unit optical depth is reached with a total number of molecules between 10^{20} cm^{-2} and 1×10^{18} cm^{-2} for the Schumann-Runge continuum and between about 5×10^{23} and 10^{23} molecules per column of 1 cm^2 cross-section for the Herzberg continuum.

III. The solar radiation

If the solar radiation in the visible spectral range follows curves of black bodies for temperatures between 5800°K and 6000°K [cf. 20], a sharp decrease in flux density of the ultraviolet emission is indicated. According to classical astrophysical observations, the solar flux density becomes less than the 5800°K black-body flux density in the ultraviolet. The ratio of sun and 6000°K black-body flux densities decreases towards the shorter wavelengths, and rocket data [21] show that the radiation temperature is about 5000°K at $\lambda = 2500$ A and falls to 4500°K at about 2000 A.* This last temperature corresponds to a level in the solar photosphere where the weak (molecular, for example) lines occur. The temperature at the top of the photosphere [22] is still lower and is of the order of 3800°K. Such a temperature must be representative of the very low chromosphere. From these astrophysical results, we may say that the photospheric radiation cannot be below that of a 4000°K black-body emission. If a sufficient solar optical depth, where the weak absorption lines occur, must be considered, a 4500°K radiation temperature will generally be the lower limit.**

In order to compare the energies available in the spectral range in which molecular oxygen absorbs, we have considered black-body temperatures of 6000°K, 5000°K, 4500°K, and 4000°K. A very convenient form for comparison, which is useful for the determination of the rate of ionization or dissociation when a mean or constant value of the absorption coefficient can be used, is to give the emission by the number of photons per cm^2 and sec available at the top of the earth's

*According to recent rocket results [34], the radiation temperature at λ 2050 A would be 5000 $\pm$ 300°K.

**In the spectral region of the O_2 continuum, the solar spectrum should show an absorption leading to a low radiation temperature. Solar metallic atoms would have continuous absorption.

atmosphere. The calculation is made as follows. The radiation density, $\rho(\nu)$, of a black body may be represented by

$$\rho(\nu) = \frac{8\pi h\nu^3}{c^3}(e^{h\nu/kT} - 1)^{-1} \quad (3)$$

where $h = 6.623 \times 10^{-27}$ erg-sec is Planck's constant, $k = 1.38 \times 10^{-16}$ erg-degree^{-1}-mol^{-1} is Boltzmann's constant, $c = 2.99776 \times 10^{10}$ cm-sec^{-1} is the velocity of light in vacuum, and T is the absolute temperature.

At the top of the earth's atmosphere, the diluted solar radiation density, $\rho'(\nu)$, is

$$\rho'(\nu) = \beta_s\, \rho(\nu) \quad (4)$$

where $\beta_s = R^2/4\, r^2 = (\text{sun radius})^2/4 \times (\text{mean solar distance})^2 = 5.41 \times 10^{-6}$ is the dilution coefficient.

The number of photons at frequency ν, $q(\nu)$, available at the top of the atmosphere per cm^2 and sec is (3, 4)

$$q(\nu) = \frac{c\rho'(\nu)}{h\nu} = \frac{8\pi\beta_s}{c^2}\nu^2(e^{h\nu/kT} - 1)^{-1} \quad (5)$$

The total number, Q, of photons available at frequencies larger than ν is given by the integral

$$Q(\nu_1) = \int_{\nu_1}^{\infty} q(\nu)\, d\nu = \frac{8\pi\beta_s}{c^2}\left(\frac{kT}{h}\right)^3 \int_{x_1}^{\infty} \frac{x^2\, dx}{e^x - 1} \quad (6)$$

where $x_1 = h\nu_1/kT$.

Table 3 gives the values computed from (6) for various wave numbers and

TABLE 3—*Number of photons-cm^{-2}-sec^{-1} at the top of the earth's atmosphere*

Wave number	6000°K	5000°K	4500°K	4000°K
(cm^{-1})				
41,450	1.7×10^{15}	1.9×10^{14}	4.5×10^{13}	7.5×10^{12}
57,000	7.4×10^{13}	3.9×10^{12}	5.6×10^{11}	5.1×10^{10}
77,000	1.1×10^{12}	2.2×10^{10}	1.7×10^{9}	6.8×10^{7}
88,000	1.0×10^{11}	1.2×10^{9}	6.4×10^{7}	1.7×10^{6}
100,000	7.1×10^{9}	4.9×10^{7}	1.8×10^{6}	2.9×10^{4}

Figure 4 shows the variation of $Q(\nu_1)$ for $\nu_1 = 40{,}000$ cm^{-1} to $\nu_1 = 82{,}000$ cm^{-1}.

We may point out that the choice of the radiation temperature in the range of 6000°K—4000°K is of great consequence. For example, at about 57,000 cm^{-1}, where the Schumann-Runge continuum begins, a ratio of 20 is to be considered for 6000°K—5000°K black bodies and reaches more than 100 for 6000°K—4500°K. For this reason, a correct determination of the solar emission in this portion of the spectrum is more important than the exact extrapolation of the absorption coefficient, when the rate of photodissociation of O_2 in the Schumann-Runge continuum is to be computed.

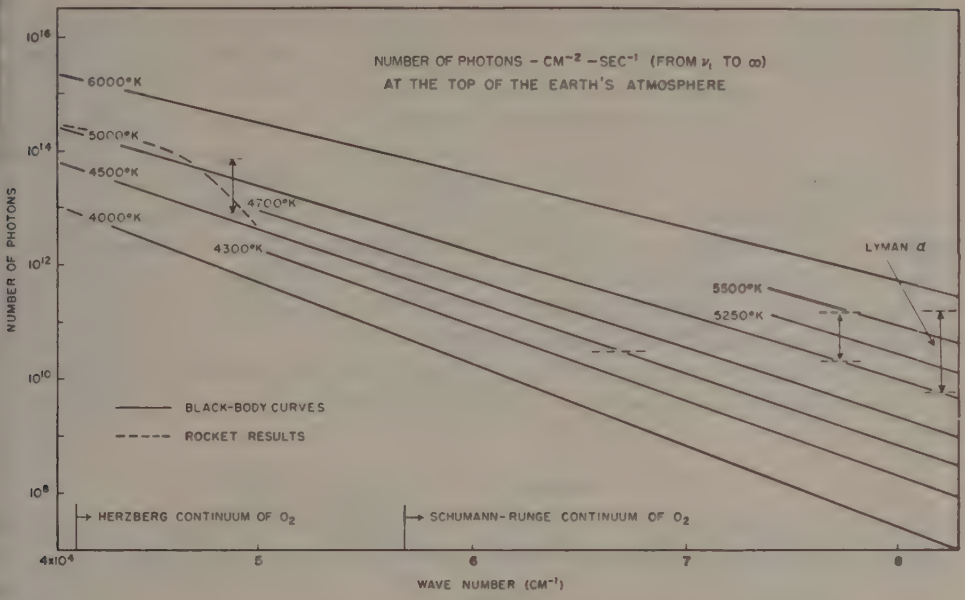

FIG. 4

We know that one may accept values little more than 5000°K in the 2500–2100 A range* and 5000 ± 300°K in the neighborhood of 2000 A. Between 2000–1500 A, no spectrum has as yet been obtained, but the rocket data published by Friedman, Lichtman, and Byram [23] provide, at about 1500 A, a flux density corresponding to a radiation temperature of 4500°K.** Consequently, we may adopt a 4500°K black-body curve between 1750–1500 A. At wavelengths shorter than 1300 A we have to deduce equivalent black-body curves from other rocket data [23, 24]. Unfortunately, the results can only be given in an approximate form.

According to the results of Tousey, Watanabe, and Purcell [24], the solar energy in the band 1230–1340 A is of the order of 0.2 erg-cm^{-2}-sec^{-1} and in the band of 1050–1230 A of the order of 0.4 erg-cm^{-2}-sec^{-1}. Considering the spectral distribution of the CaF_2 filter used by these workers, we may use a round figure of 1300 A as the effective wavelength, if we accept a black-body spectral distribution. In fact, in the effective spectral range 76,000 cm^{-1} to 80,000 cm^{-1}, there are 1.3×10^{10} photons-cm^{-2}-sec^{-1} at the top of the earth's atmosphere, a value which corresponds to a radiation temperature of 4900°K ± 100°K. In the range of 1230–1050 A, in which the first line, L_α, of the Lyman series of atomic hydrogen occurs, the solar flux density corresponds to a radiation temperature of about 5300°K. However, according to the results published by Friedman, *et al.* [23], the approximate value of 6,000°K is obtained at 1200 A; that is, 3.5×10^{11} photons-cm^{-2}-sec^{-1}, or about 6 ergs-sec^{-1}-cm^{-2}. As the value indicated for 1350–1150 A is .1 to 10 ergs-cm^{-2}-sec^{-1}, we have to choose between the two results. We adopt a

*Tousey [35] recently indicates a ratio of 1/15 at 2200 A for solar radiation and a 6000°K black body.

**Such a low value can be accepted, for solar absorption of Mg, Fe, and Si may be expected. Nevertheless, the temperature parameter is not known near the threshold.

radiation temperature of 5000°K at 1300 A and an equivalent black-body emission at 5500°K for the L_α radiation. With these values, we follow the data of Tousey, *et al.* [24] and the vertical distribution of the transmission factor given in Figure 4 of Friedman, *et al.* [23]. More recent data [34] show the importance of L_α radiation which is observed at 74 km for 18–20° solar elevation. The received energy* was 0.1 erg-cm^{-2}-sec^{-1} and is reliable within a factor of two. In short, in the spectral region where O_2 absorbs by its Herzberg continuum, a radiation temperature of 5000°K at 2400 A must be adopted. In the Schumann-Runge continuum, the radiation temperature is 4500°K in the main part of the spectrum. At 1300 A, the temperature is $\leq$ 5000°K; and at 1215 A (L_α), a radiation temperature $\geq$ 5000°K may be chosen.** We must also keep in mind that the chromospheric line, L_α, is very sensitive to the solar activity and increases in intensity during a solar flare. Its principal role is to ionize nitric oxide in region D, as shown in 1945 by Nicolet [25].

IV. The dissociation rate coefficient of O_2

Knowing now the number of photons-cm^{-2}-sec^{-1} available at the top of the earth's atmosphere and the absorption coefficients, we can compute D_∞, the number of photodissociations per molecule and second. Before using the values deduced for the solar emission, calculations were made for various black bodies from 6,000°K to 4,000°K, in order to follow the variation with temperature of the efficiency of the photodissociation (Table 4) and to compare the results obtained by various authors.

TABLE 4—*Number of O_2 photodissociation processes per mol-sec, D_∞*

Temp. (T)	4000°K	4500°K	5000°K	5500°K	6000°K
D_∞ (L)†	1.89×10^{-7}	2.34×10^{-6}	1.79×10^{-5}	9.50×10^{-5}	3.88×10^{-4}
D_∞ (W)†	1.23×10^{-7}	1.57×10^{-6}	1.26×10^{-5}	6.64×10^{-5}	2.76×10^{-4}

†$D_\infty(L)$ from Ladenburg's and Van Voorhis's data, and $D_\infty(W)$ from Watanabe's data.

At heights where the optical depth is negligible, Penndorf [5] has found $D_\infty = 1.83 \times 10^{-5}$, 1×10^{-4}, and 4×10^{-4} molecule^{-1}-sec^{-1}, respectively, for the temperatures 5,000°K, 5,500°K, 6,000°K. Nicolet [25], using a 5740°K black body with a mean value for the absorption coefficient, found $D_\infty = 3 \times 10^{-4}$ sec^{-1}, and Spitzer [26], with a 6000°K black body and an oscillator strength of 0.19, has obtained $D_\infty = 4 \times 10^{-4}$ sec^{-1}. More recently, Bates and Nicolet [17], adopting a small value of 10^{-19} cm^2 at the threshold for the absorption coefficient and a 5000°K black body have found $D_\infty = 1.84 \times 10^{-5}$ sec^{-1}. These results are remarkably consistent and indicate that the radiation temperature is the most

*Private communication of Naval Research Laboratory. A recent publication (Pietenpol, Rense, Walz, Stacey, and Jackson, in Phys. Rev., **90**, 156, 1953) indicates 0.3 erg-cm^{-2}-sec^{-1} with some solar activity.

**Photon values for various black bodies are as follows:

5000°K	5250°K	5500°K	6000°K	
5.9×10^9	1.9×10^{10}	5.6×10^{10}	3.7×10^{11}	at λ1220 A

important parameter which must be known. In order to follow the variation of D_∞ with the temperature, Figure 5 shows the complete results between $T = 6000°K$ and $T = 4000°K$.

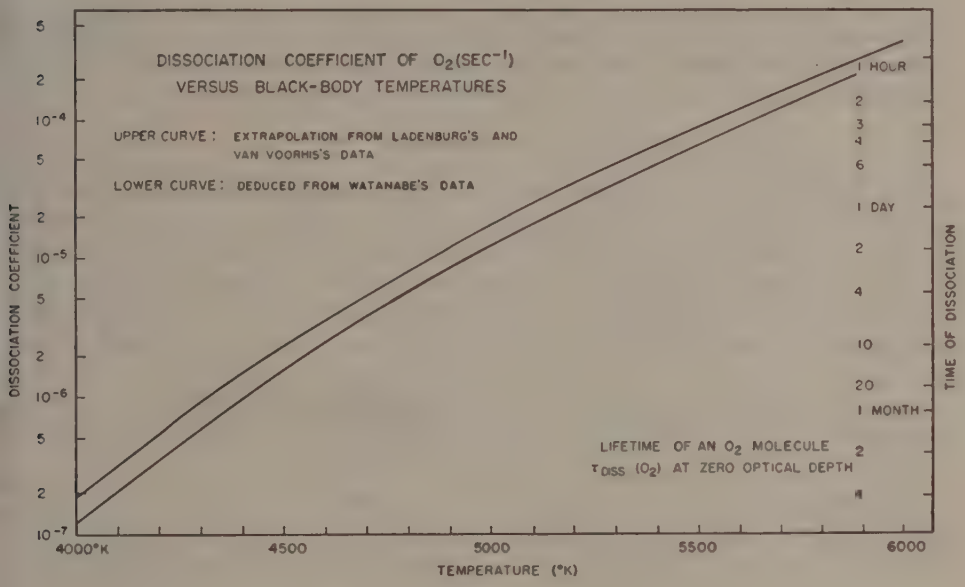

FIG. 5

A new step is now to consider the variation of D with the optical depth, $\tau(\nu)$, which is defined by

$$d\tau(\nu) = n(O_2)K(\nu)\,dz \quad \ldots\ldots(7)$$

Considering various spectral ranges of $\Delta\nu = 1000\ cm^{-1}$, we may obtain D by the following relations

$$D \equiv \Sigma D(\nu_i) = \Sigma D_\infty(\nu_i)e^{-\tau(\nu_i)} \quad \ldots\ldots(8)$$

where

$$\tau(\nu_i) = n(O_2)H(O_2)K(\nu_i) \quad \ldots\ldots(9)$$

for a vertical column.

The variation of D as a function of the total number of O_2 molecules absorbing the solar radiation is considered in three spectral ranges: (1) When the optical depth is negligible, the value of $D \equiv D_\infty$ is given by D_∞ (in Schumann-Runge continuum) $= 1.56 \times 10^{-6} sec^{-1}$. In fact,* 99 per cent of D_∞ is given by the spectral range 5.7×10^4 to $7.3 \times 10^4\ cm^{-1}$ and 90 per cent for $\nu_i < 7 \times 10^4\ cm^{-1}$. (2) With increasing total number of O_2 molecules giving a thick optical depth in the main part of the Schumann-Runge continuum, L_α radiation (λ 1216 A), which is in an atmospheric window, and the radiation of $\lambda < 2420$ A in the Herzberg con-

*The effect of bands superposed on the continuum towards the short wavelengths can be considered as negligible.

tinuum can play an important role. The minimum value is obtained by computing D_∞ when only the Herzberg continuum is effective. We find

$$D_\infty \text{ (Herzberg continuum)} = 5 \times 10^{-10} \text{ sec}^{-1} \quad (10)$$

corresponding to a radiation temperature of 5000°K at 2400 A and 4700°K at 2000 A.* (3) The Lyman-α effect is associated with an equivalent 5000°K radiation temperature

$$D_\infty \text{ (Lyman } \alpha) = 6 \times 10^{-11} \text{ sec}^{-1} \quad (11)$$

For such radiation, 10^{20} O_2 molecules cm^{-2} are required before obtaining the optical depth $\tau_{1216\,A} = 1$. However, as the intensity of L_α increases with solar activity, its photodissociation effect becomes more important under these conditions. With equivalent 5500° and 6000°K radiation temperature, $D_\infty(L_\alpha) = 6 \times 10^{-10}$ and 4×10^{-9} sec^{-1}. The final result, taking into account the various absorptions, is given in Table 5. When the total number of O_2 molecules reaches

TABLE 5—*Variation of D with the total number of O_2 molecules*

Number of molecules	D	Number of molecules	D
(cm^{-2})	*molecule-sec*$^{-1}$	(cm^{-2})	*molecule-sec*$^{-1}$
0	1.57×10^{-6}	10^{18}	1.31×10^{-7}
10^{15}	1.56×10^{-6}	2×10^{18}	5.81×10^{-8}
2×10^{15}	1.55×10^{-6}	5×10^{18}	1.37×10^{-8}
5×10^{15}	1.52×10^{-6}	10^{19}	2.98×10^{-9}
10^{16}	1.47×10^{-6}	2×10^{19}	1.06×10^{-9}
2×10^{16}	1.37×10^{-6}	5×10^{19}	8.60×10^{-10}
5×10^{16}	1.14×10^{-6}	10^{20}	7.04×10^{-10}
10^{17}	8.61×10^{-7}	2×10^{20}	5.70×10^{-10}
2×10^{17}	5.55×10^{-7}	5×10^{20}	5.02×10^{-10}
5×10^{17}	2.57×10^{-7}	10^{21}	5.00×10^{-10}

10^{19} cm^{-2}, L_α is strongly effective. Its effect rapidly becomes negligible with $n(O_2)$ $H(O_2) > 10^{20}$ cm^2. The radiation of $\lambda < 2400$ A plays the leading role until 5×10^{20} molecules-cm^{-2} are included in the vertical section involved.

In order to determine the penetration of the dissociative radiation into the atmosphere, conclusions must be reached regarding the vertical distribution of the pressure and molecular oxygen.

V. The vertical distribution of pressure and temperature

Various atmospheric models may be used to compute the temperature at each level for which we wish to discuss the dissociation of oxygen. It is not the intent to follow here the conclusions obtained from the combined rocket results as presented by the Rocket Panel [27] or other investigations. If the observational data are the

*Thus, a value of 1.5×10^{-9} sec^{-1} is not excluded, in accord with the most recent rocket results.

pressures or densities, the temperatures cannot be found without a hypothesis as to the mean molecular mass. Furthermore, above 80 km, the adopted temperatures depend only upon Naval Research Laboratory determinations of density from ram pressure, assuming a certain type of dissociation of O_2 and, perhaps, of N_2. Hence, instead of accepting any atmospheric model for which the temperature is given, it is considered preferable to accept the pressure data published by Havens, Koll, and LaGow [28], and determine two working models (Table 6) which will

TABLE 6—*Pressures, temperatures, and scale heights from* 60 *to* 120 *km*

Altitude, z	Small variation (Case A)				Pressure		Large variation (Case B)			
	Scale height, H	$T°K$		Pressure	Havens	Panel	Scale height, H	$T°K$		Pressure
		$N_2 + O_2$	$N_2 + O$					$N_2 + O_2$	$N_2 + O$	
km	*km*			*mm Hg*			*km*			*mm Hg*
50	7.80	260	...	6.76×10^{-1}	7.5×10^{-1}	6.76×10^{-1}	8.43	270	...	.....
60	7.40	245	...	1.82×10^{-1}	2.1×10^{-1}	1.87×10^{-1}	8.10	269	...	2.17×10^{-1}
70	6.60	218	...	4.34×10^{-2}	5.4×10^{-2}	4.56×10^{-2}	6.66	220	...	5.77×10^{-2}
80	5.80	190	158	8.63×10^{-3}	1.0×10^{-2}	9.31×10^{-3}	5.50	181	151	1.08×10^{-2}
90	6.25	205	171	1.63×10^{-3}	1.9×10^{-3}	1.90×10^{-3}	6.00	197	164	1.9×10^{-3}
100	7.25	237	198	3.69×10^{-4}	4.2×10^{-4}	4.45×10^{-4}	7.00	229	191	4.06×10^{-4}
110	8.50	277	231	1.04×10^{-4}	1.2×10^{-4}	1.24×10^{-4}	8.00	261	218	1.05×10^{-4}
120	10.00	325	271	3.5×10^{-5}	3.5×10^{-5}	4.0×10^{-4}	10.00	325	271	3.5×10^{-5}

permit the interpretation of the data obtained by various methods, such as grenade explosions or ram pressures.

Let us first consider the altitude of 120 km with a pressure of 3.5×10^{-5} mm of mercury and a scale height of 10 km. These figures are given by Havens, Koll, and LaGow [28] and must be accepted in view of the absence of other direct determinations near this level. We may determine the desired parameters at the level of 70 km by various methods, according to the hypotheses utilized regarding the distribution of the scale height. Two possibilities are discussed below, in which fixed scale-height variations result in low maxima of temperature and unpronounced minima. The pressure curves obtained are quite similar.

Computations are made based on the following: Let P, ρ, and T denote the pressure, density, and absolute temperature at height z, and let $P + dP$ equal the pressure at $z + dz$. Hence, if g denotes the acceleration due to gravity, the atmospheric statical equation is

$$dP = -g\rho\, dz \quad \ldots\ldots\ldots\ldots\ldots\ldots\ldots\ldots\ldots\ldots (12)$$

If the atmospheric constituents at height z have different molecular masses m_i and if the number density (concentration) of the j^{th} constituent is n_i, we may write

$$\rho = n_1 m_1 + n_2 m_2 + \cdots \quad = \sum_i n_i m_i = NM \quad \ldots\ldots\ldots\ldots (13)$$

so that

$$N = n_1 + n_2 + \cdots \quad \ldots\ldots\ldots\ldots\ldots\ldots\ldots\ldots\ldots\ldots (14)$$

Then (12) may be written in the equivalent form

$$dP = -gNM\,dz \quad \ldots\ldots(15)$$

Applying, to the atmospheric gas, the ideal gas law

$$P = NkT \quad \ldots\ldots(16)$$

where k is Boltzmann's constant, in (15) we may write the statical equation in the following form

$$\frac{dP}{P} = -\frac{gM}{kT}\,dz \quad \ldots\ldots(17)$$

and writing $H = kT/Mg$ = the scale height, we have the general form

$$\frac{dP}{P} = \frac{dN}{N} + \frac{dT}{T} = -\frac{dz}{H} \quad \ldots\ldots(18)$$

If complete mixing occurs in the atmosphere, the mean molecular mass, M, is a constant independent of the altitude. Assuming a mean value of g for a layer of definite thickness, we may write

$$\frac{dT}{T} = \frac{dH}{H} \quad \ldots\ldots(19)$$

and, from (18),

$$\frac{dN}{N} = -\frac{dH + dz}{H} \quad \ldots\ldots(20)$$

We feel confident that, at the present time, the available information concerning the behavior of the high atmosphere permits the use of a constant gradient of the scale height, so that we may write

$$dH = \beta\,dz \quad \ldots\ldots(21)$$

where β is a constant for various layers. Thus, from (21), we obtain by integration from (18) and (20), respectively,

$$\frac{P}{P_0} = \left(\frac{H}{H_0}\right)^{-1/\beta} \quad \ldots\ldots(22)$$

and

$$\frac{N}{N_0} = \left(\frac{H}{H_0}\right)^{-(1+\beta)/\beta} \quad \ldots\ldots(23)$$

and for the total number of particles in a vertical column above the level z,

$$\int_z^\infty N\,dz = NH \quad \ldots\ldots(24)$$

If the use of (19) is not valid, as in the case of a variable mean molecular mass, the exact distribution of temperature cannot be found from pressure or density measurements alone. In our case, the mean molecular mass, M, is altered because

of the dissociation of the O_2 molecule. For this reason, computations were made for an atmosphere with N_2 and O_2 molecules and with nitrogen molecules and atomic oxygen. At mesospheric* levels, we consider as an adequate approximation for this study

$$M_{N_2,O_2} = 0.8 \times 46.5 \times 10^{-24} + 0.2 \times 53.2 \times 10^{-24} = 47.8 \times 10^{-24} \text{ gm} \quad \ldots(25)$$

which gives a ratio

$$n(O_2)/n(N_2) = 1/4 \quad \ldots(26)$$

With complete dissociation of oxygen, the mean molecular mass is

$$M_{N_2,O} = 39.8 \times 10^{-24} \text{ gm} \quad \ldots(27)$$

which yields the ratio

$$n(O)/n(N_2) = 1/2 \quad \ldots(28)$$

These practical figures mean that there is uniform mixing following any small diffusive effect which may occur at heights considered here. The same hypothesis is adopted above 120 km and, with $dH/dz = 0.2$, we have computed the pressures and temperatures given in Table 7, assuming O_2 is completely dissociated.

TABLE 7—*Pressures, temperatures, and scale heights from* 120 *to* 220 *km*

Altitude, z	Scale height, H	Pressure	Temperature	Pressure, Havens [27]
km	*km*	*mm Hg*	°*K*	*mm Hg*
120	10	3.50×10^{-5}	271	3.5×10^{-5}
130	12	1.41×10^{-5}	324	1.5×10^{-5}
140	14	6.51×10^{-6}	377	7×10^{-6}
150	16	3.34×10^{-6}	430	3×10^{-6}
160	18	1.85×10^{-6}	482	2×10^{-6}
170	20	1.09×10^{-6}	534	.....
180	22	6.79×10^{-7}	586	.....
190	24	4.40×10^{-7}	637	.....
200	26	2.95×10^{-7}	688	.....
210	28	2.03×10^{-7}	738	.....
220	30	1.44×10^{-7}	789	2×10^{-7}

These data correspond to the rocket data and follow the results of Havens, Koll, and LaGow [28]. It should be noted that consideration of the diffusion and dissociation of molecular nitrogen can change the data of Table 7. However, it is known, by a research as yet unpublished, that diffusion is not strongly effective below 160 km and, also, that the ratio of atomic to molecular nitrogen is not larger than one hundredth in the height range of interest.

*Defined as proposed by S. Chapman, J. Geophys. Res., **55**, 395 (1950); indicated by M. Nicolet, Ann. Géophys., **6**, 318 (1950); and adopted by International Geodesy and Geophysics Union (1951).

Since we are interested in the determination of the absorption of the solar radiation by O_2 , we must determine the total number of molecules involved. For purposes of calculation, (17) was used in 2.5-km steps and, with β = constant, in 10-km steps, giving the results of Tables 6 and 7. From (23), we obtain the concentration, considering $O_2 + N_2$ and $O + N_2$. The results are given in Table 8 in 10-km steps and, in order to follow by 1-km steps, in Figure 6.

TABLE 8—*Values of the concentration N and the total number of molecules NH*

Altitude, z	Case *A*		Case *B*		Altitude, z	log $N^{(*)}$	log $NH^{(*)}$
	log $N^{(*)}$	log $NH^{(*)}$	log $N^{(*)}$	log $NH^{(*)}$			
km					*km*		
80	14.72	20.48	14.84	20.58	130	11.62	17.70
90	13.96	19.76	14.05	19.83	140	11.22	17.37
100	13.26	19.12	13.31	19.16	150	10.87	17.08
110	12.64	18.56	12.68	18.58	160	10.56	16.82
120	12.10	18.10	12.10	18.10	170	10.30	16.60

(*)These values are for an atmospheric composition of $N_2 + O$; for an atmosphere of $N_2 + O_2$, subtract 0.08 from the given figures.

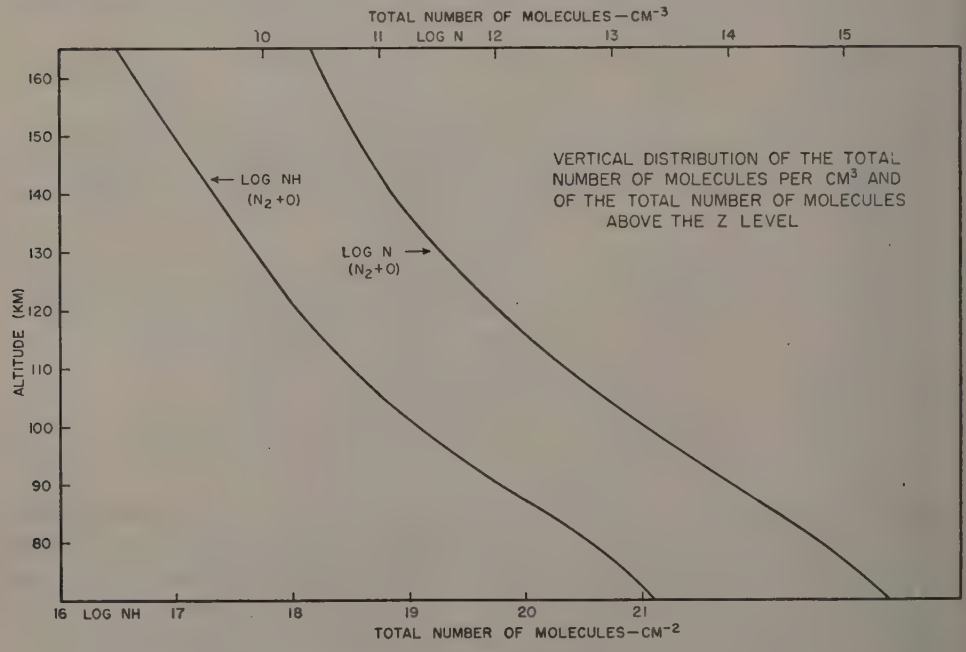

FIG. 6

VI. The vertical distribution of O_2

Friedman, Lichtman, and Byram [23], using a photon counter tube responding to a certain portion of the spectrum in one band covering λλ 1425 to 1650 A,

obtained in September 1949 a recording of the solar radiation intensity throughout a rocket flight.

In order to study the observational results, we reproduce, in Figure 7, the

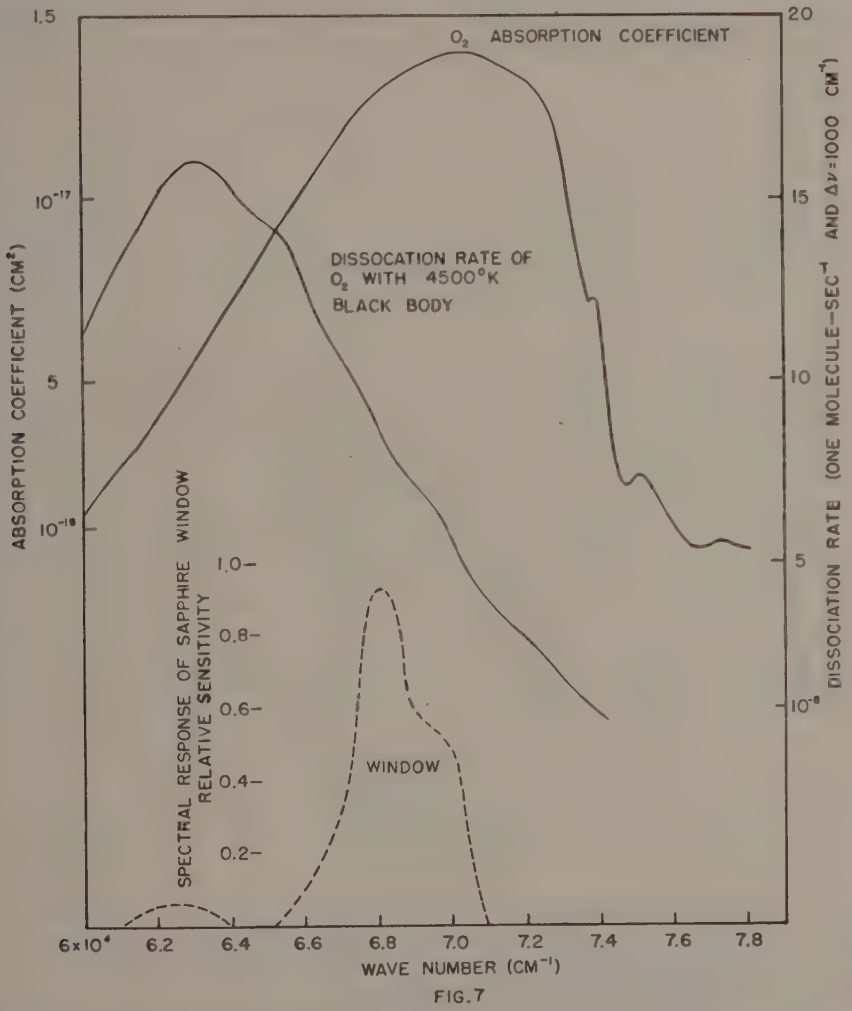

FIG.7

spectral variation of the absorption coefficient of the Schumann-Runge continuum (cf. Fig. 2) and the spectral response curve of the sapphire window used in the rocket flight [23]. The variation of the coefficient D_∞ for $\Delta\nu = 1000$ cm^{-1} at the top of the earth's atmosphere is plotted in the same Figure for a 4500°K black body. Comparison between these three curves indicates that the rocket measurements will yield results concerning the transmission of the solar radiation according to an oxygen absorption which may be represented by a round figure of 10^{-17} cm^2 as a mean value of the coefficient. The observed results are illustrated in Figure 8 according to the published data [23]. The maximum of absorption of solar photons (30 per cent of radiation not yet absorbed in an atmosphere with $dH/dz = 0.2$)

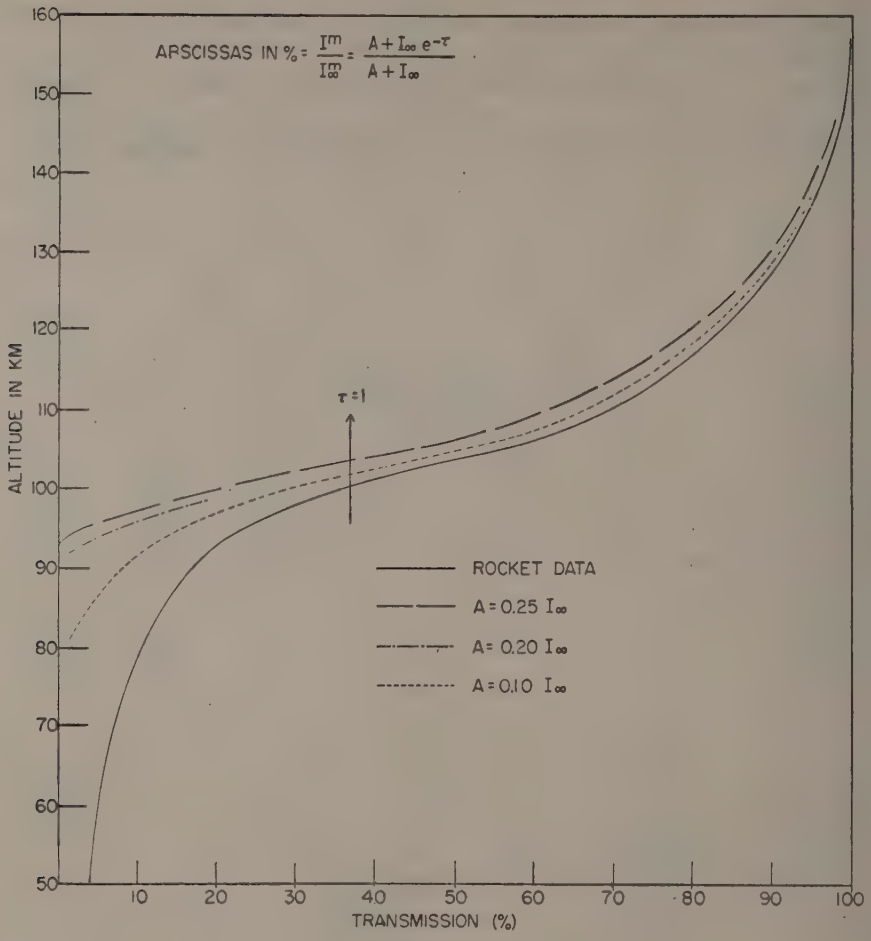

FIG 8

occurs just below 100 km and, for this reason, the response indicated on the observational curve at low heights (80 to 40 km) is an abnormal feature which cannot be explained by the observers.

Assuming that the source of the abnormal response in the measurements at 40 to 80 km was effective during the entire flight, its contribution may be represented by a constant A *above* a certain height. Thus, we may write

$$I^m_\infty = I_\infty + A \quad \ldots\ldots\ldots\ldots\ldots\ldots\ldots\ldots\ldots\ldots (29)$$

where I^m_∞, which denotes the measurement of the intensity at the top of the flight, is the sum of the actual intensity of the solar radiation without suffering absorption in the spectral range around $\lambda = 1500$ A and of the abnormal effect A yielding the supplementary response of the counter tube. In fact, this constant A may represent a solar radiation coming from outside the indicated spectral range of the sapphire window and reaching down to a height of 50 km. In this case, this radiation has

probably reached its maximum below 100 km, and in the range of height that we wish to study the effect of this radiation may be considered as a constant. Another interpretation could be given by an extra response of the system of measurement and here also, for a smooth curve, we may consider a constant effect.

Thus, in any case, it seems, according to the preceding equation, that we may write

$$\frac{I''}{I''_\infty} = \frac{A + I_\infty e^{-\tau(\nu)}}{A + I_\infty} \qquad (30)$$

where the ratio I''/I''_∞ denotes the atmospheric transmission found by rocket measurements; it is represented in Figure 8 by the solid line. $\tau(\nu)$ is the actual optical depth corresponding to the absorption by O_2 at about $\lambda = 1500$ A.

In order to discuss the possible values of $\tau(\nu)$, we assume three values for the constant A, as follows:

$$A = 0.25I_\infty ; \qquad A_2 = 0.20I_\infty ; \qquad \text{and} \qquad A_3 = 0.10I_\infty$$

A_1 , A_2 , and A_3 , respectively, correspond to an additional effect of 20 per cent at 83 km, of 16.5 per cent at 90 km, and of 9 per cent at 76 km to the assumed actual transmission in order to represent the observational results. The transmission curves for these three cases have been computed and are represented by broken-line curves in Figure 8. Such assumptions permit one to show the prominent effect of the abnormal feature at heights below 90 km and to follow the change of the curve shape above 100 km.

An investigation is still necessary in order to decide what is the best value to choose for the "extra-radiation effect." A computation has been made for each curve given in Figure 8 and gives the value of τ with height according to the relation

$$I/I_\infty = e^{-\tau(\nu)} \qquad (31)$$

Adopting the value $\tau = 1.2$ (maximum of absorption of λ 1500 A) for each case, we find that this optical depth is always at a level between 100 and 102.5 km. Thus, we have

$$n(O_2)H(O_2)K \sec \chi = 1.2 \qquad (32)$$

where K denotes a mean value of the absorption coefficient and $\chi = 45°$, the polar distance during the flight of September 1949. With values of $(1.2 \pm 0.1)10^{-17}$ m^2 for the absorption coefficient, we obtain for the number of O_2 molecules in a vertical column-cm^{-2}

$$16.83 \leq \log n(O_2)H(O_2) \leq 16.89$$

The log of the total number of molecules and atoms is, according to the results taken from Table 8 and Figure 6, 18.96 or 19.00 at 102.5 km. Taking the ratio, we see that the total number of O_2 molecules is not more than 1/100 and not less than 1/500 of the total number of particles above 100 km. A different value of A would change the ratio $n(O_2)/n(M)$.

In order to find the O_2 concentration, we must determine the scale height of

O_2 compared with the atmospheric scale height. The simplest way to do this is to attempt to follow the corrected transmission curve of Figure 8 above the maximum of absorption; that is to say, for a transmission of more than 30 per cent. Three hypotheses were made, as follows: (1) Photochemical equilibrium, (2) diffusive distribution of O_2, and (3) complete mixing of O_2.

The conditions for photochemical equilibrium, above the maximum of absorption where $D/D_\infty \simeq I/I_\infty$, may be put into the following form:

$$n(O_2)D_\infty e^{-\tau(\nu)} = Rn^2(O) \quad \ldots\ldots\ldots\ldots\ldots\ldots\ldots\ldots (33)$$

where R is a two- or three-body recombination coefficient.

It is not possible to follow the observational data with such a vertical distribution of O_2, because the O_2 concentration decreases too rapidly with the altitude.

A diffusive equilibrium for O_2, which is not very different from a photochemical equilibrium at heights where $\tau(\nu) < 1$ when the recombination process is a two-body collision, cannot be considered for the same reasons.

Finally, the observational data can be represented by a complete mixing of the atmosphere, which causes the vertical distribution of molecular oxygen to follow the atmospheric scale height. For example, choosing the *atmospheric scale height* for O_2 with $\tau = 1.25$ at 102.5 km, we obtain a vertical distribution of O_2 which is followed by the computed curve with $A = 0.25\, I_\infty$. These results are illustrated in Figure 9.

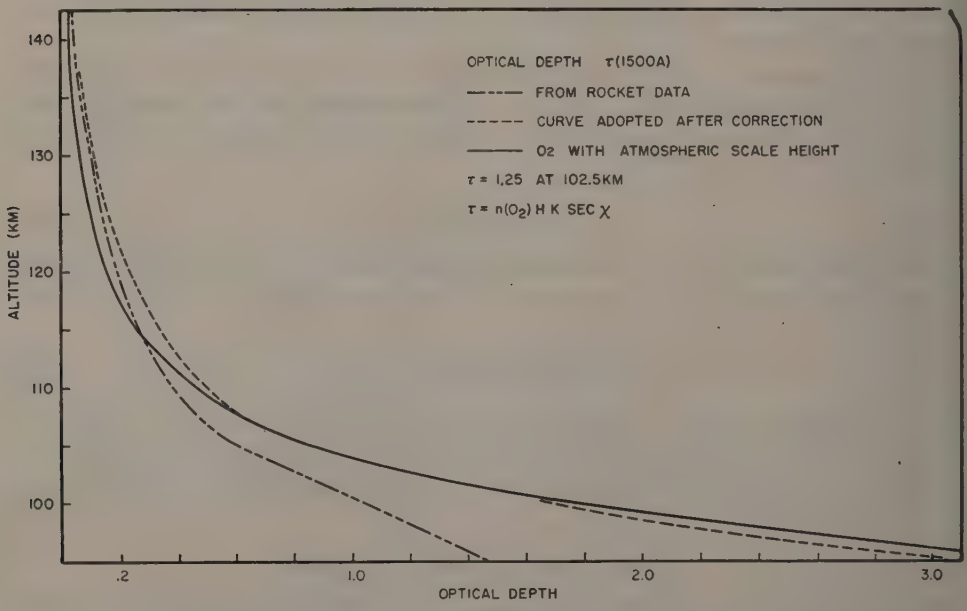

FIG. 9

At 102.5 km, a vertical column of 1 cm^2 cross-section has between 7 and 8 $\times$ 10^{16} O_2 molecules, and a total number of particles between 9×10^{18} and 10^{19}. Following the atmospheric distribution with one hundredth of the total number of particles, we obtain the solid-line curve which is remarkably consistent with the

lashed-line curve, representing the observational results modified by the constant 1 taking into account the abnormal feature occuring at low heights. For comparison, the uncorrected observational results are shown by a dot-dash curve in he Figure. This cannot be explained, below 100 km, by any atmospheric property vithout an extra effect not connected with the O_2 absorption in the spectral range of λ 1500 A.

In short, thanks to rocket measurements, it becomes possible to follow the vertical distribution of O_2 in the atmospheric region where this molecule is practically dissociated. This vertical distribution can be explained by a complete mixing of the atmosphere above 105 km. Other distributions give optical depths decreasing more rapidly with height than the observed optical depth.

If a mixing effect will account for the observational data, we must conclude that there is a complete departure from the oxygen photochemical equilibrium.

VII. The time of dissociation of an O_2 molecule

At levels where oxygen is in an atomic form, we may write the following equation:

$$\frac{dn(O_2)}{dt} = -n(O_2)D + R\,n^2(O) \quad \ldots\ldots\ldots\ldots\ldots\ldots (34)$$

where D still denotes the dissociation rate coefficient and R the recombination coefficient, independent of time but involving all the possibilities for the association of oxygen atoms. Because $n(O) \gg n(O_2)$, we may consider $n(O)$ as a constant when we study the variation of molecular oxygen. The solution of (34) is

$$n(O_2) = n_0(O_2)e^{-Dt} + \frac{R\,n^2(O)}{D}\,[1 - e^{-Dt}] \quad \ldots\ldots\ldots\ldots\ldots\ldots (35)$$

where $n_0(O_2) = n(O_2)$ when $t = 0$.

If we consider $Dt = 1$, that is to say, a value of t giving about two-thirds of the O_2 equilibrium value plus one-third of the initial value, we may define $\tau_{Diss} = \frac{1}{D}$ as a "time of dissociation."

From the D_∞ values given in Table 4, we find, at heights where the optical depth is negligible, a time of dissociation

$$\tau_{Diss}(O_2) = \frac{1}{1.57 \times 10^{-6}} = 6.4 \times 10^5 \text{ sec or 15 days of 12 hours duration} \ldots\ldots (36)$$

Thus, during a daylight interval of 12 hours, an O_2 molecule is not generally dissociated, since two weeks are required for dissociation to take place. In one day, more than 90 per cent of the number of O_2 molecules are not affected by photodissociation. Furthermore, where the optical depth increases, the time of dissociation also increases. The variation of τ_{Diss} with the total number of molecules is given in Figure 10. It can be seen that above 120 km, τ_{Diss} = 15 days, at 105.0 km about 20 days, and at 98 km about one month.

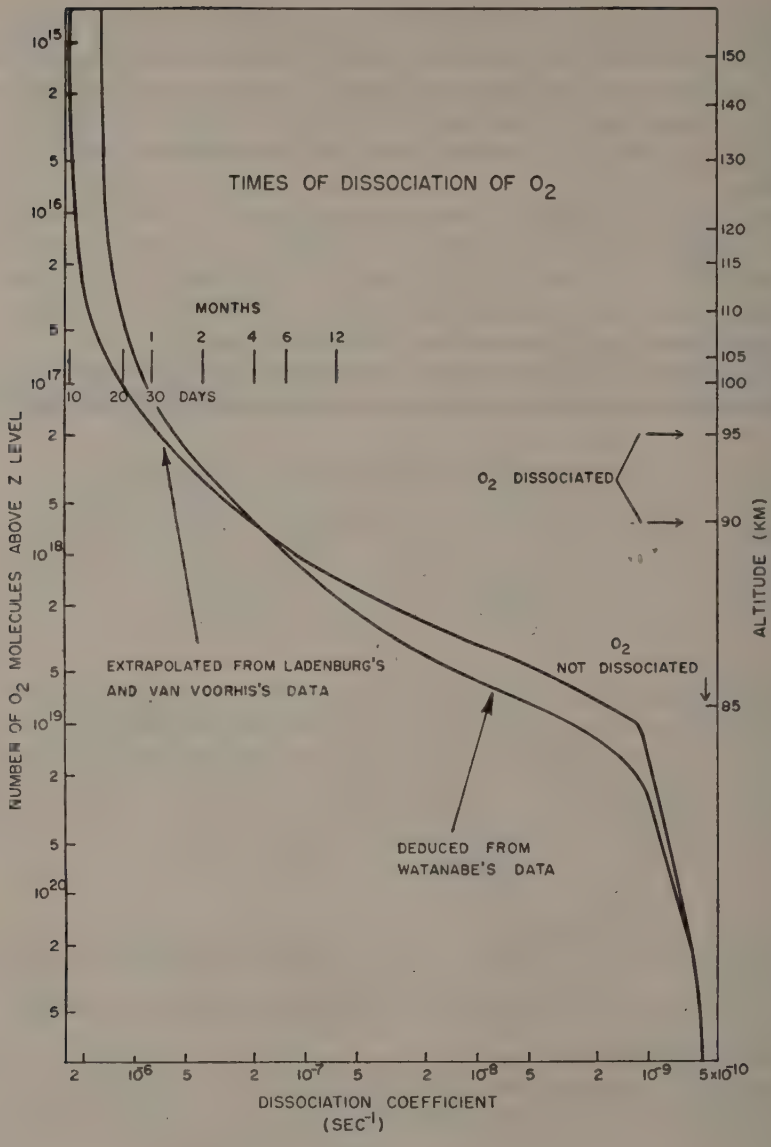

FIG. 10

N.B. The curves show the variation of times of dissociation as a function of the total number of O_2 molecules above a certain level. If $n(O_2) < n(O)$, that is, "O_2 dissociated," the associated altitudes between 90 km and 150 km are indicated in the vertical scale at right. The altitude 85 km labeled "O_2 not dissociated," which should read 95 km [*Note*: My error.—Ed.], shows that absorption of radiation in the Schumann-Runge region is already complete above this height if $n(O) < n(O_2)$.

In order to adopt a photochemical equilibrium, a time of mixing is required, τ_{mix}, which is less than 15 days above 120 km and less than one month at 100 km. Because deductions obtained from rocket results show a complete departure from the photochemical equilibrium, we are forced to conclude that dynamical effects

re operative, giving a τ_{mix} of less than 15 days. This conclusion is entirely different rom previous ideas concerning the O_2-O equilibrium. However, it is easy to under-tand that the dynamical effects leading to an atmospheric mixing at 100 km were neglected in the previous studies of the O_2-O equilibrium. For example, a 6000°K black body yields a time of O_2 dissociation of only one hour. Under these circum-tances, it is valid to consider a perfect photochemical equilibrium. τ_{Diss} is found o be less than one day, when a 5500°K black body is employed. In Figure 5, we an see $\tau_{Diss}(O_2)$ at zero optical depth plotted *versus* the black-body temperature used in the region of the Schumann-Runge continuum. The rapid variation of $\tau_{Diss}(O_2)$, depending on the assumed radiation temperature of the sun, is clearly seen.

Instead of the classical equation (34), the equation giving the local change of molecular oxygen concentration may be written, from the equation of continuity, as

$$\frac{\partial n(O_2)}{\partial t} = \frac{dn(O_2)}{dt} - \text{div}\,[n(O_2)\cdot \mathbf{V}] \quad \ldots\ldots\ldots\ldots\ldots\ldots (37)$$

in which $dn(O_2)/dt$ is given in (34), and $\mathbf{V}$ denotes the mixing velocity vector.

The net result is that the fundamental transport must be in the vertical direc-tion and shows an upward vertical drift of O_2. In other words, the O_2 molecules dissociated at each level are replaced by molecules coming from lower heights in order to maintain the observed vertical distribution.

In a vertical transport in which the dissociation effect is at least balanced by a vertical drift, we must have an upward velocity of O_2 molecules, $+w_{mix}(O_2)$ not less than

$$+w_{mix}(O_2) \simeq \frac{HD}{1+\beta} = \frac{10^6 \times 2.43 \times 10^{-6}}{1.2} = 2.0 \text{ cm sec}^{-1} \quad \ldots\ldots\ldots (38)$$

that is,

$$+w_{mix}(O_2) \simeq 1.7 \text{ km-day}^{-1}$$

VIII. The recombination process

The lifetime of an oxygen atom depends on the recombination process involved n the two-body or three-body collisions.

When a three-body collision is considered, one oxygen atom can recombine in a process for which the rate equation may be written

$$\frac{dn(O)}{dt} = -a_1\, n(M)\, n(X)\, n(O) \quad \ldots\ldots\ldots\ldots\ldots\ldots (39)$$

$n(M)$ being the number of particles and $n(X)$ the molecule or atom involved in the formation of a new molecule. For example, O_2 yields O_3 , which is destroyed by another rapid process not leading to an oxygen atom. Thus, the time of recombina-ion may be defined as (39)

$$\tau_{rec}(O) = \frac{1}{a_1\, n(M)\, n(X)} \quad \ldots\ldots\ldots\ldots\ldots\ldots\ldots\ldots (40)$$

If $n(X) \equiv n(O)$, the solution is

$$n(O) = \frac{n_0(O)}{1 + R\, n_0(O)\, t} \equiv \frac{n_0(O)}{1 + 2a_2\, n(M)\, n_0(O)\, t} \quad \ldots\ldots\ldots\ldots (41)$$

if $n_0(O)$ is the number of atoms at time $t = 0$, and $R \equiv a_2\, n(M)$ is the recombination coefficient with three-body collisions. Thus, if $n(O) = 1\ 3\ n_0(O)$, the time of recombination is found equal to

$$\tau_{rec}(O) \equiv \frac{1}{a_2\, n(M)\, n_0(O)} \qquad (42)$$

In the atmospheric region where $n(O_2) \gg n(O)$, $n(M) = n(O_2) + n(N_2)$, and $n(X) = n(O_2)$, or $n(X) = n(O)$ given by an equilibrium value or a certain fraction of $n(M)$.

Using data as shown in Figure 6 and coefficient values given by Bates and Nicolet [17], the numerical results obtained are presented in Table 9 and in the

TABLE 9—*Time of recombination of an oxygen atom*

Altitude	$n(O_2) = \frac{1}{5}\, n(M)$	$n(O)$ daytime equilibrium	$n(O) = \frac{1}{50}\, n(M)$	$n(O) = \frac{1}{5}\, n(M)$
km				
70	≥ 3 hours	≥ 5 days	≥ 1000 seconds	≥ 100 seconds
75	12 hours	20 days	1 hour	500 seconds
80	2 days	20 days	6 hours	2000 seconds
85	15 days	1 month	1 day	4 hours
90	3 months	2 months	10 days	1 day
95	1 year	4 months	1 month	5 days
100	7 years	4 months	9 months	27 days

form of curves in Figure 11. Using Bates' and Nicolet's values, $a_1 = 5 \times 10^{-36}\, T^{1/2}$ and $a_2 = 5 \times 10^{-34}\, T^{1/2}$ for $n(X) \equiv n(O)$. Since we cannot accept a photochemical equilibrium for which the time of recombination is not shorter than the time of mixing, we may say that, between 70 and 100 km, a departure from photochemical equilibrium does exist and leads to an increase of atomic oxygen toward the lowest altitudes. The magnitude of this departure depends on the altitudes considered. With an increase from an equilibrium value to $n(O) = 1\ 50\ n(M)$, it is necessary to select the 85-km level in order to obtain a time of recombination of the order of one day. If $n(O) \simeq n(O_2)$, 90 km is the appropriate level. In other words, if $n(O)$ attains the value $1\ 50\ n(M)$, the assumed disturbance has a lifetime of the order of one hour at 75 km and one day at 85 km. At higher altitudes, the departure becomes so important that it cannot be considered as a disturbance, but must be dealt with as a permanent state very different from the photochemical equilibrium.

In view of the above, an excess of atomic oxygen must exist below the maximum of O_2 dissociation, computed under the assumption of photochemical equilibrium. Further, large deviations can persist in the lower portion of the O_2-O region due to downward transport of atomic oxygen from the region of maximum equilibrium concentrations. This departure from the photochemical equilibrium is governed by the strength of the transport processes and by the rate of recombination. The

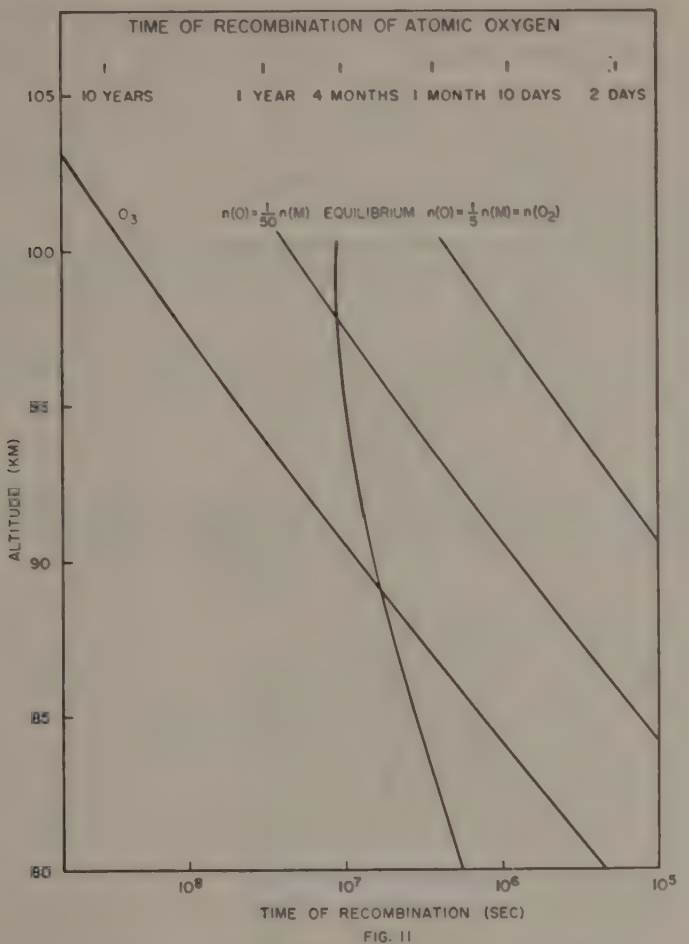

FIG. 11

vertical transport mechanisms which are operative are the mixing transport and the diffusive transport.

The basic equation governing these quantities is

$$\frac{\partial n(\mathrm{O})}{\partial t} = 2n(\mathrm{O}_2)D - 2R\,n^2(\mathrm{O}) - \mathrm{div}\,[n(\mathrm{O})\mathbf{V}_{\mathrm{mix}}] - \mathrm{div}\,[n(\mathrm{O})\mathbf{V}_{\mathrm{diff}}] \quad \ldots(43)$$

where $\mathbf{V}_{\mathrm{mix}}$ and $\mathbf{V}_{\mathrm{diff}}$ are the vector velocities of mixing and diffusion.

We may compare the time of mixing necessary for a departure from equilibrium with the time of recombination using the data of Table 9. At low heights, namely, 70 to 75 km, a disturbance due to advection dynamical effects is strongly effective, because the time of recombination is not less than one hour if $n(\mathrm{O}) \leq 1/50\ n(M)$. With such a ratio of atomic oxygen at 80 km, the disturbance may have a lifetime of the order of one day. At 85 km, a half dissociation of O_2 can be stable for more than four hours. Such a dissociation affects the mean molecular mass, and we may consider the mesopause to be related to the dissociation of oxygen. The qualitative

conclusion reached is that at such levels, there can permanently exist a number of oxygen atoms which is greater than the number resulting from a steady photochemical equilibrium.

At 100 km, the time of recombination is still further increased and the former deductions may be applied in the extreme. In fact, we reach a level where it is difficult to maintain a molecular oxygen concentration greater than an atomic oxygen concentration.*

Without a mixing effect producing a downward transport of atomic oxygen, it is still possible to show that the photochemical equilibrium is not stable in the transition region of molecular to atomic oxygen, the diffusion transport being effective.

In order to carry out computations of diffusive separation of atomic oxygen, let us consider a vertical distribution

$$n(\mathrm{O}) = n_M^*(\mathrm{O}) e^{(1+\beta)(1-\zeta-e^{-\zeta})} \quad \ldots\ldots\ldots\ldots\ldots\ldots\ldots\ldots\ldots\ldots (44)$$

in which $n_M^*(\mathrm{O})$ denotes the maximum concentration of atomic oxygen, ζ is a parameter related to the atmospheric scale height by

$$H/H_M^* = e^{\beta\zeta} \quad \ldots\ldots\ldots\ldots\ldots\ldots\ldots\ldots\ldots\ldots\ldots\ldots (45)$$

and β is the scale-height gradient given by (21).

The vertical velocity of an oxygen atom is given by the following equation:

$$w(\mathrm{O}) = -D\left[\frac{1}{n(\mathrm{O})}\frac{\partial n(\mathrm{O})}{\partial z} + \frac{1}{H}\frac{\partial H}{\partial z} + \frac{m(\mathrm{O})}{m(M)}\frac{1}{H}\right] \quad \ldots\ldots\ldots\ldots (46)$$

in which D denotes the diffusion coefficient [29].

Combining (44), (45), (46), and (20), we may write (46) as follows:

$$w(\mathrm{O}) = \frac{D_M^*}{H_M^*}\left[\left(1 - \frac{m(\mathrm{O})}{m(M)}\right)\exp\left\{\left(1 + \frac{\beta}{2}\right)\zeta - (1+\beta)\exp\left(\frac{\beta\zeta}{2}\right)\right\}\right] \quad \ldots\ldots (47)$$

and using atmospheric data as before, we obtain, for a maximum of $n(\mathrm{O})$ at 100 km, a downward velocity of atomic oxygen of not less than 0.14 km-day^{-1}. While this downward velocity of diffusion may seem very small, it affects considerably the photochemical equilibrium distribution. For example, the oxygen atoms produced at 100 km move down to a level one or two scale heights below in less than four months. In other words, the time of diffusion of atomic oxygen is less than the time of recombination at 95 km when a perfect photochemical equilibrium is considered. In any case, because the time of recombination $\geq 2 \times 10^6$ sec at 100 km, the oxygen atoms produced in the region of maximum concentration travel to lower heights and, as a consequence, destroy the vertical distribution arising from a photochemical equilibrium.

In short, mixing and diffusion processes are responsible for the shift in the transition region of O_2 and O to lower heights than given by the photochemical equilibrium. Furthermore, as diffusion increases with height, a mixing effect must

*An exact determination is not yet possible, because the coefficients of the chemical reactions are not well known. A change of the order of 5 km will be possible when accurate values are known.

be important above 120 km in order to maintain the distribution according to the atmospheric scale height.

IX. The theory and its significance

In studying the dissociation of oxygen molecules in the atmosphere, it is necessary to consider first as a primary factor the solar flux density which determines the dissociation rate. Assuming, in order to carry out computations, a radiation temperature of 6000°K, the dissociation rate coefficient leads to a lifetime for the O_2 molecule which is much less than one day, and, consequently, to a general photochemical equilibrium. However, since it is now known that the radiation temperature is less than 6000°K, namely, 4500°K, the time of dissociation at zero optical depth is actually about 15 days. As we know that, at mesospheric levels and above, winds of sufficient frequency and strength occur, we may assume that the possibility of vertical transport exists. From rocket data, we find that the time of mixing is shorter than the times of dissociation and diffusion. Furthermore, as has been established in earlier sections, below 100 km the relative time of recombination of an oxygen atom compared with the time of mixing is variable, depending on the heights and atomic oxygen concentrations considered The departure from photochemical equilibrium depends on the ratio τ_{rec}/τ_{mix} . If one supposes, for example, that τ_{rec} is of the order of one day, one finds that the altitudes at which this occurs are of the order of 80 km with a photoequilibrium, 85 km with a ratio $n(O)/n(M) = 1/50$ giving a disturbance, 90 km with a ratio $n(O)/n(M) = 1/5$ giving approximately a half dissociation of O_2 , and that above 95 km an approximate steady state occurs in which oxygen is dissociated. In this region, the ratio $n(O_2)/n(O)$ remains practically constant, thanks to the vertical drift of molecules while O and N_2 are mixed.

Since atomic oxygen moves downward in order to follow the vertical distribution of O_2 and N_2 below the transition region, its concentration increases compared with the photoequilibrium value. Hence, when the actual concentration is less than the possible concentration with complete mixing, a downward drift of atoms occurs until the recombination effect becomes important and destroys them. The rate at which oxygen molecules and atoms are, respectively, transported upwards and downwards cannot as yet be determined. Nevertheless, this rate is related to the rate at which the total number of molecules in a column of unit cross-section is dissociated above a certain level. Because the dissociation equilibrium can be reached in 15 days with an atomic oxygen atmosphere, one may consider that, from upper levels to 100-105 km, atomic oxygen predominates and that at 100 km it still constitutes an important fraction of the total population.

Thus, it is now clear that the transition region must be associated with the mesopause and that its altitude varies according to the transport processes affecting the vertical distribution of atomic oxygen. In the upper mesosphere, the atomic oxygen concentration is greater than the photoequilibrium concentration. In the thermosphere, the concentrations of all the constituents follow the values obtained from the ordinary barometric equation until the diffusive equilibrium is established at higher altitudes. In the future, it will be interesting to study the mixing in an atmospheric region in which tidal action must exist and turbulence is effective.

X. Conclusions

The physical arguments developed in the preceding sections show that the problem of the constitution of the high atmosphere may differ considerably from a problem based on equations made on self-consistent assumptions which do not represent physical parameters. It must, however, be emphasized that our quantitative deductions may be revised when relevant observational and experimental data become available. It is not possible to proceed further without knowing the exact scale height between 70 and 100 km. Nevertheless, it is now easily seen that in determining the vertical distribution of the oxygen dissociation in the mesosphere and thermosphere one cannot ignore the vertical transport. The views put forward here will lead, as consequences, to various other topics which require special discussion. Since a study of these topics is not the primary object of this paper, they will not be taken up here and will be published in the near future; but one may inquire whether or not some important problems should be reexamined.

An immediate result is that airglow data could be interpreted by considering the departure from a photochemical equilibrium in the chemosphere. Bates and Nicolet [17] have indicated that ozone increases to attain a value of (cf. eq. 33 of ref. 17) $n(O_3) \rightarrow k_2/k_3\ n(O_2)\ n(M)$, but never the combined initial concentrations of odd oxygen atoms. The ozone concentration is also predicted to be larger at night than during the day if no atomic hydrogen is involved. But hydrogen acts as a catalyst for the destruction of odd oxygen atoms and clearly causes $n(O)$ to diminish more pronouncedly. The net result is that OH and O_2 airglow emission, which depends on the O_3 and O concentrations, will be subject to their fluctuations. We know that OH and O_2 bands discovered by Meinel [30] at mesospheric levels exhibit variations and sometimes enhancement in the night-glow. Thus, we have here an indirect confirmation of the preceding deductions about the departure from the photoequilibrium.

In the E layer, we may assume now that the vertical distribution of O_2 follows the atmospheric distribution and the theory of a layer formation is much easier than before. A theory based on photoionization of oxygen molecules by ultraviolet radiation* as indicated by Nicolet [31], and a dissociative recombination as proposed by Bates and Massey [32], would describe the behavior of the normal E layer only if the number of photons at $\lambda 1025\ A$ is greater than the number of X-ray photons.

In region D where NO is present, the mixing effect must play an important part. As NO absorbs the Lyman-α radiation, Nicolet's theory [31] of the D region remains the most attractive explanation of the ionospheric region responding to solar-flare effects. Furthermore, the behavior of nitrogen oxides remains to be studied. This may play an important role in the airglow.

The problem of the dissociation of nitrogen molecules can be studied in the same way. Adopting the dissociative recombination according to Bates' process, $N_2^+ + e \rightarrow N + N$, we may see that at the level of maximum dissociation, namely, 160 km for an overhead sun, the lifetime of a nitrogen atom at the level of its

*The preionization is not necessary, since absorption coefficients for a direct photoionization are sufficient.

production is short, since the diffusion transport towards lower altitudes is very important. Its downward velocity is remarkable, and one may show that the formation of nitric oxide depends on it.

Because the recombination process cannot be effective above 100 km, the time duration of the cycle of atomic and molecular nitrogen will be of the order of several months. Finally, due to the small rate of dissociation, the ratio of atomic to molecular nitrogen concentrations will be of the order of one hundredth in the region where the mixing effect still exists. Because of the diffusive equilibrium above 160 km, this ratio must increase with height. However, it is not possible to consider a complete dissociation of molecular nitrogen.

We may also add that at the mesopause level, namely, the level of minimum temperature, values between 160°K and 170°K are possible (90-100 km) if O_2 is dissociated. Such temperatures are very near the temperature deduced by Meinel for the O_2 atmospheric bands. As the maximum of emission is associated with the region where O_2 is strongly absorbing near the maximum of atomic oxygen concentration, we again obtain a consistent physical picture.

Finally, it is interesting to determine the rate at which a loss of oxygen (or nitric oxide) molecules in the E layer or in region F is balanced by a diffusive transport, where the loss occurs by a dissociative recombination after an exothermic charge-exchange process converts the atomic into molecular ions. Using an equation such as (46), that is,

$$w(O_2) = -D\left[\frac{1}{n(O_2)}\frac{\partial n(O_2)}{\partial z} + \frac{1}{H}\frac{\partial H}{\partial z} + \frac{m(O_2)}{n(M)}\frac{1}{H}\right] \quad \ldots\ldots\ldots (48)$$

it is easy to find a vertical diffusion velocity.

The vertical distribution of the molecular oxygen concentration is given (23) by

$$n(O_2)/n_0(O_2) = (H/H_0)^{-x(1+\beta)/\beta} \quad \ldots\ldots\ldots\ldots\ldots\ldots (49)$$

where $x = 2$ if a photoequilibrium is assumed in an oxygen atmosphere with two-body recombination (Moses and Wu), $x = 3$ with three-body recombination (Penndorf), or $x > 3$ if a loss process is more effective than photodissociation.

Adopting numerical data which give minimum values for a diffusion effect, namely, $x = 2$, $\beta = \partial H/\partial z = 0.2$ and $m(O_2)/m(M) = 2$, we found the following values for upward velocities of oxygen molecules in order to attain the vertical diffusion distribution:

120 km	160	200	250
>0.16 cm-sec^{-1}	37	270	1600

That is to say, the velocity is more than 1 km/hour at 160 km, 10 km/hour at 200 km, and 60 km/hour at 250 km. Thus, it seems clear that molecules such as O_2 are present above the E layer and are distributed with height at least according to a diffusion equilibrium. One can say that the molecular oxygen concentration is of the order of 7×10^8 cm^{-3} at 160 km and 2×10^7 cm^{-3} at 200 km (minimum values, because mixing is an important process).

Such a result makes plausible the dissociative recombination theory for region F, as suggested by Bates and Massey, because the molecules involved in the charge transfer and destroyed by dissociative recombination are replenished rapidly by upward diffusion.

In short, physical arguments developed in the paper show that the point of view of departures from photoequilibriums by vertical transport is supported by observational data and suggest the study of the behavior of the high atmosphere by investigation of dynamical effects. Finally, the rocket measurements of *ultraviolet solar radiation absorption* as made by the Naval Research Laboratory are certainly the best means of determining the high atmosphere physical constitution and chemical composition.

The authors acknowledge with very great pleasure the benefit they have derived from visits to the Naval Research Laboratory, in Washington, D.C., and to the Evans Signal Laboratory, Belmar, N. J., and from discussing high atmosphere problems with Drs. E. O. Hulburt, H. E. Newell, R. Tousey, H. Friedman, T. R. Burnight, and their collaborators. Thanks to experimental data obtained from Watanabe before publication, it has been possible to include the more recent experimental results in this paper.

References

[1] S. Chapman, Phil. Mag., **10**, 369 (1930).
[2] O. R. Wulf and L. S. Deming, Terr. Mag., **43**, 283 (1938).
[3] R. C. Majumdar, Indian J. Phys., **12**, 75 (1938).
[4] H. Rakshit, Indian J. Phys., **21**, 57 (1947).
[5] R. Penndorf, J. Geophys. Res., **54**, 7 (1949).
[6] H. E. Moses and T. Y. Wu, Phys. Rev., **83**, 109 (1951).
[7] H. E. Moses and T. Y. Wu, Phys. Rev., **87**, 628 (1952).
[8] R. Ladenburg and C. C. Van Voorhis, Phys. Rev., **43**, 315 (1933).
[9] E. C. G. Stueckelberg, Phys. Rev., **42**, 518 (1932); **44**, 234 (1933).
[10] L. H. Dawson, L. P. Granath, and E. O. Hulburt, Phys. Rev., **34**, 136 (1929).
[11] L. P. Granath, Phys. Rev., **34**, 1045 (1929).
[12] H. Buisson, C. Jausseran, and P. Rouard, Revue Optique, **12**, 70 (1933).
[13] F. W. P. Götz and H. Maier-Leibnitz, Zs. Geophysik, **9**, 253 (1933).
[14] A. Vassy, Ann. Physik, **11**, Ser. 16, 145 (1941).
[15] W. Heilpern, Helv. Phys. Acta, **14**, 329 (1941).
[16] F. W. P. Götz, Ergebn. kosm. Physik, **3**, 261 (1938).
[17] D. R. Bates and M. Nicolet, J. Geophys. Res., **55**, 301 (1950).
[18] G. L. Weissler and Po Lee, J. Optical Soc. Amer., **42**, 200 (1952).
[19] W. M. Preston, Phys. Rev., **57**, 887 (1940).
[20] M. Nicolet, Ann. d'Astrophys., **14**, 249 (1951).
[21] T. R. Burnight, in Physics and medicine of the upper atmosphere, pp. 227-238, Albuquerque, University of New Mexico Press (1952).
[22] A. Unsöld, The constitution of the solar atmosphere, Roma, Accad. Naz. Lincei, 11 Convegno "Volta" (1952).
[23] H. Friedman, S. W. Lichtman, and E. T. Byram, Phys. Rev., **83**, 1025 (1951).
[24] R. Tousey, K. Watanabe, and J. D. Purcell, Phys. Rev., **83**, 792 (1951).
[25] M. Nicolet, Inst. R. Met. Belgique, Mém., **19**, 71 (1945).
[26] L. Spitzer, Jr., Chap. 7 in The atmospheres of the earth and planets, Chicago, University of Chicago Press (1949).
[27] Rocket Panel, Phys. Rev., **88**, 1027 (1952).
[28] R. J. Havens, R. T. Koll, and H. E. LaGow, J. Geophys. Res., **57**, 59 (1952).

[29] S. Chapman and T. G. Cowling, The mathematical theory of non-uniform gases, Cambridge, University Press (1939).
[30] A. B. Meinel, Astroph. J., **111**, 207, 433 (1950).
[31] M. Nicolet, J. Geophys. Res., **54**, 373 (1949).
[32] D. R. Bates and H. S. W. Massey, Proc. R. Soc., A, **192**, 1 (1947).
[33] K. Watanabe, E. C. Y. Inn, and M. Zelikoff, J. Chem. Phys., **20**, 1969 (1953); K. Watanabe, private communication.
[34] E. T. Byram, T. Chubb, H. Friedman, and S. W. Lichtman, J. Optical Soc. Amer., **42**, 876 (1952).
[35] R. Tousey, J. Optical Soc. Amer., **42**, 871 (1952).

IONOSPHERIC WIND ANALYSIS BY METEORIC ECHO TECHNIQUES

BY L. A. MANNING, A. M. PETERSON, AND O. G. VILLARD, JR.

Electronics Research Laboratory of the Department of Electrical Engineering, Stanford University, Stanford, California

(Received June 29, 1953)

ABSTRACT

The meteoric method for finding the velocities of winds in the lower *E*-region is extended. The previously given procedure for finding vector average wind is shown to be unaffected by the presence of turbulent wind components. A new procedure is worked out for finding root-mean-square values of the horizontal and vertical wind components. By looking at the statistics of the reduction procedures, estimates of the accuracies of the method are found; the sources of error are discussed. Relationships between sample size and accuracy are given. Typical results of the methods are presented.

INTRODUCTION

With the development of the meteoric reflection method for measuring upper atmosphere winds [see 1 of "References" at end of paper], a new insight into the structure of air motion and drift in the 80- to 120-km height range has become possible. Study of winds by noting the drift of meteoric ionization columns involves a simple physical picture, in which the danger of measuring apparent motions caused by wave-like disturbances, for example, appears to be small. The drift of distinct clouds of electrons and ionized particles, originating from a known mechanism, makes possible the interpretation of the results with confidence.

In a previous paper, the application of the meteoric method to the measurement of the average translational velocity of the air in the meteoric height region has been explained. It was pointed out at that time, however, that there were indications pointing to the existence of turbulent, stratified, and irregular air-motions in addition to the uniform drift components. In the present paper, the theory of wind reduction will be extended to include methods of measuring these non-uniform and turbulent velocities. The techniques will be illustrated with typical experimental results.

Since the methods for measuring upper atmosphere winds are basically statistical, it is important to be aware of the statistical limitations upon the accuracy of the results. A consideration of the means of estimating the accuracy of the procedures will be presented, both in relation to measurement of the uniform and of the turbulent components. In addition, detailed attention will be given to certain systematic errors and to their correction.

THE DETERMINATION OF AVERAGE WIND

In this section, the analysis of the previous paper will be extended to show that the uniform component of drift can be removed from the data without regard for the possible presence of a turbulent component.

Suppose that the velocity of the effective reflection point for a single reflection is given by the vector quantity $\mathbf{w}$. Then the radial velocity component v of the reflector is

$$v = \mathbf{n} \cdot \mathbf{w} \quad \ldots\ldots\ldots\ldots\ldots\ldots\ldots\ldots\ldots\ldots (1)$$

where the unit vector $\mathbf{n}$ is directed from the observer to the reflector. Consider now the group of all meteors detected towards a given azimuth. The vector drift velocity for each meteor will be given by an expression $\mathbf{w} = \bar{\mathbf{w}} + \hat{\mathbf{w}}$, if $\bar{\mathbf{w}}$ is defined as the average drift for the group, and $\hat{\mathbf{w}}$ is the deviation from the average drift which distinguishes each member of the group. Turbulent variations are thus described by the behavior of $\hat{\mathbf{w}}$, and the average wind is described by $\bar{\mathbf{w}}$. Similarly, the unit vector used to locate the position of each reflector may be written $\mathbf{n} = \bar{\mathbf{n}} + \hat{\mathbf{n}}$, and $\hat{\mathbf{n}}$ is the deviation of the meteor position from the mean $\bar{\mathbf{n}}$. With these definitions, (1) becomes

$$v = \bar{\mathbf{n}} \cdot \bar{\mathbf{w}} + \bar{\mathbf{n}} \cdot \hat{\mathbf{w}} + \bar{\mathbf{w}} \cdot \hat{\mathbf{n}} + \hat{\mathbf{n}} \cdot \hat{\mathbf{w}} \quad \ldots\ldots\ldots\ldots\ldots\ldots\ldots (2)$$

If we now compute the average radial velocity component v for all meteors in a given azimuthal direction, all terms but the first on the right of (2) drop out. The two central terms clearly are zero, since $\hat{\mathbf{n}}$ and $\hat{\mathbf{w}}$ have a zero average by definition. The average of the term $\hat{\mathbf{n}} \cdot \hat{\mathbf{w}}$ is zero, since the turbulent variations $\hat{\mathbf{w}}$ are independent of the position of the meteor as determined by $\hat{\mathbf{n}}$. For these reasons, (2) becomes

$$\bar{v} = \bar{\mathbf{n}} \cdot \bar{\mathbf{w}} \quad \ldots\ldots\ldots\ldots\ldots\ldots\ldots\ldots\ldots\ldots (3)$$

and the average radial velocity in a given sector is seen to depend upon the average drift velocity but not upon the turbulent velocity.

Returning to the formula (1) for the radial velocity component of the drift of a single trail, and introducing a system of coordinates, we can write

$$v = w \sin i \cos \alpha \cos (\theta_m - \theta_w) - w \cos i \sin \alpha \quad \ldots\ldots\ldots\ldots\ldots (4)$$

where w is the magnitude of the wind vector, i is the incidence angle of the received wave, α is the dip angle of the wind, θ_m is the azimuth to the meteor, and θ_w is the azimuth from which the wind comes. Flat earth is assumed, since the ranges are usually short enough. If we now consider the average radial velocity $\bar{v}$ for meteors of fixed azimuth, comparison of (1), (3), and (4) shows that

$$\bar{v} = \bar{w}\,\overline{\sin i}\,\cos \bar{\alpha} \cos (\theta_m - \overline{\theta_w}) - \bar{w}\,\overline{\cos i}\,\sin \bar{\alpha} \quad \ldots\ldots\ldots\ldots\ldots (5)$$

if it is realized that $\bar{\mathbf{n}}$ is not a unit vector as is $\mathbf{n}$, and that $|\,\bar{\mathbf{n}}\,| \sin \bar{i} = \overline{\sin i}$. Equation (5) demonstrates that when average radial wind velocity is plotted *versus* reflection azimuth, as in the reductions of the previous paper [1], the average wind velocity $\bar{w}$, the dip $\bar{\alpha}$ of the average wind, and $\overline{\theta_w}$ the azimuth of the average wind are the quantities determined. The existence of turbulent velocity components has been shown not to alter this conclusion.

THE TURBULENT VELOCITY COMPONENTS

The vector wind at a point has been described as $\mathbf{w} = \bar{\mathbf{w}} + \hat{\mathbf{w}}$. If $\bar{\mathbf{w}}$ is found by averaging $\mathbf{w}$ over all points in a plane of constant altitude, it represents the average

drift of the air in that height stratum. The quantity $\hat{\mathbf{w}}$ then represents the variation from the average wind in that stratum, caused by turbulent motion or similar irregularities. Description of the magnitude of $\hat{\mathbf{w}}$, which varies in a random manner from point to point, can best be achieved by giving the mean-square value.

When turbulence is present, equation (4) still gives the radial velocity component of the wind at a given reflection point, it being understood that w, α, and θ_w are functions of position. If we notice that $w \cos \alpha$ is the horizontal component of wind speed w_h, and that $w \sin \alpha$ is the vertical component w_v, we may write an expression for the squared velocity

$$v^2 = w_h^2 \sin^2 i \cos^2 (\theta_m - \theta_w) + w_v^2 \cos^2 i - w_h w_v \sin 2i \cos (\theta_m - \theta_w) \quad (6)$$

If we now restrict ourselves to meteors with the same elevation angle i, we may compute the average squared radial velocity, averaging over all angles θ_m from which meteors are received. When this mean is taken, using equal numbers of meteors from all azimuths, the final term of (6) becomes zero and we have

$$\overline{v^2} = \tfrac{1}{2} \overline{w_h^2} \sin^2 i + \overline{w_v^2} \cos^2 i \quad (7)$$

In this expression, $\overline{w_h^2}$ is the mean-square value of the horizontal wind, including any uniform drift velocity which may be present. The same is true of $\overline{w_v^2}$, the mean-square vertical wind velocity. Replacing w_h by $\overline{w_h} + \hat{w}_h$, and w_v by $\overline{w_v} + \hat{w}_v$ where the average is taken with respect to wind variation, and noticing that the average of $\hat{w}_h$ and $\hat{w}_v$, in the sense of (7), is zero, we obtain

$$\overline{v^2} = \tfrac{1}{2}(\overline{w_h}^2 + \overline{\hat{w}_h^2}) \sin^2 i + (\overline{w_v}^2 + \overline{\hat{w}_v^2}) \cos^2 i \quad (8)$$

Equation (8) suggests an experimental procedure for determining the mean-square turbulent wind. Notice, first, that $\overline{w_h}^2$ and $\overline{w_v}^2$ are found from the average drift analysis of the preceding section, performed as described in the earlier paper [1]. If $\overline{v^2}$ is plotted *versus* i, the elevation angle of the meteors, a curve of the form $a + b \cos 2i$ is obtained. By measuring the $i = 0$ and $i = 90°$ ordinates, (8) shows that the mean-square velocity coefficients can be found.

If instead of plotting $\overline{v^2}$ directly *versus* i, $\cos^2 i$ is used as abscissa, a linear plot results. Equation (8) then becomes

$$\overline{v^2} = \tfrac{1}{2}(\overline{w_h}^2 + \overline{\hat{w}_h^2}) - \left(\frac{\overline{w_h}^2 + \overline{\hat{w}_h^2}}{2} - \overline{w_v}^2 - \overline{\hat{w}_v^2} \right) \cos^2 i \quad (9)$$

The advantage which comes from such an anamorphosis is an increased ease in finding the parameters of the plot. A linear regression line can easily be fitted to the experimental data by least-squares analysis, and the $\cos^2 i = 0$ and 1 ordinates obtained by extrapolation. These ordinates are the respective coefficients on the right-hand side of equation (8).

THE TRUE AND APPARENT DISTRIBUTION OF BODY DOPPLER FREQUENCIES

When body Doppler frequencies F are measured experimentally, the radial velocity component v is determined by the relation $v = \lambda F/2$, where λ is the operating wavelength. If the observed Doppler frequencies are taken directly from the

experimental records, and their squares averaged in order to find the quantity $\overline{v^2}$ which is required in the analysis of the preceding section, a systematic error is introduced. This error results from the influence of the duration of meteoric echoes upon the minimum Doppler frequency which can be scaled from the records. Unless the echo duration is slightly greater than the reciprocal of the Doppler frequency, no more than a single cycle of the body Doppler waveform is traced out on the records, and frequency cannot be scaled by the usual methods. Figure 2 of the previous paper [1] will serve to illustrate the point.

The influence of echo duration is to cause the measured distribution of body Doppler frequencies to be deficient as F approaches zero. Figure 1 illustrates the

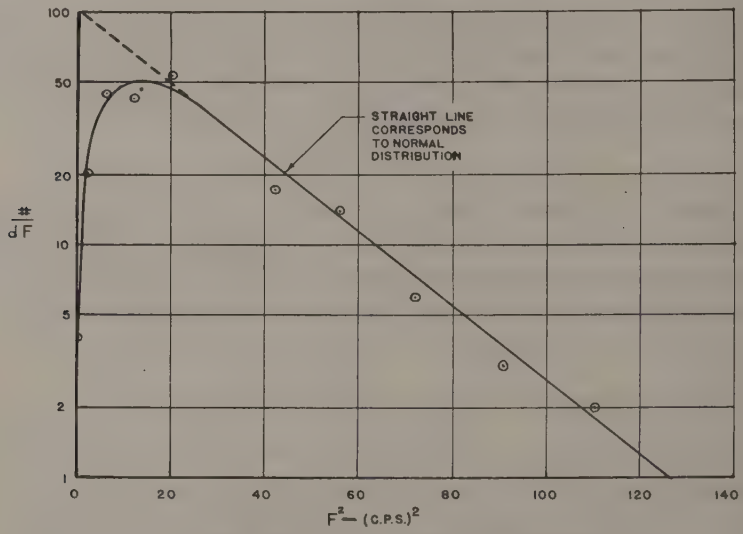

FIG. 1—DISTRIBUTION OF BODY DOPPLER FREQUENCIES IN TERMS OF THE SQUARE OF THE CENTER OF THE FREQUENCY INTERVAL

falling off as typically observed. In this Figure, the logarithmic ordinate scale represents $\#/\Delta F$, with $\#$ being the number of body Doppler frequencies scaled of value between F and $F + \Delta F$. The abscissa has a linear scale in F^2. Plotted in this way, a straight line corresponds to the normal distribution

$$\# = \#_0 \exp\left(-\frac{F^2}{2\overline{F^2}}\right) dF \qquad (10)$$

From Figure 1 it will be observed that measured body Doppler frequencies, averaged over all azimuths, are normally distributed except at the low body Doppler frequencies. The falling off is a result of the presence of only a fractional number of echo durations great enough for record scaling, among the potential low body Doppler meteors. If body Doppler data are to be used to determine mean-square wind velocities without error, the apparent mean-square Doppler frequency which is found directly from the records must be appropriately corrected to give the mean-square frequency $\overline{F^2}$ which corresponds to the extrapolated normal distribution. The true value $\overline{F^2}$ will always be less than the measured $\overline{F^2}_m$.

The curve of Figure 1 may be divided into the linear (normally distributed) part, and the low frequency (deficient) part. By plotting the ratio of the deficient to the extrapolated normal curves, Figure 2 is obtained. It is found, as shown in

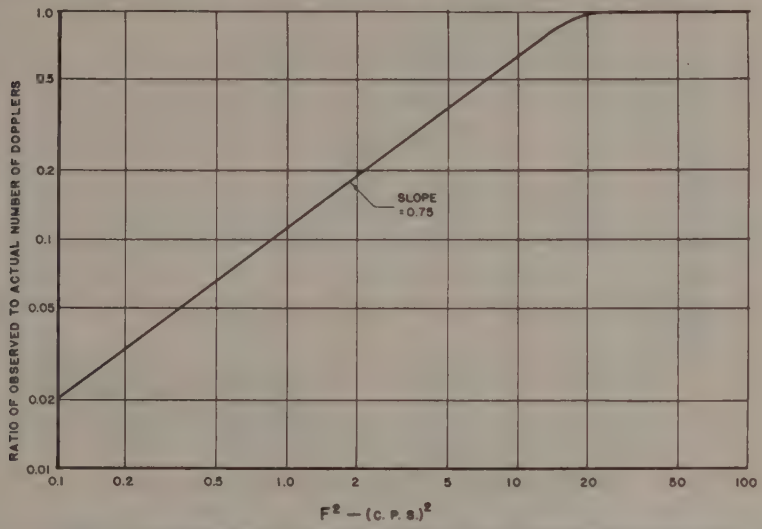

FIG. 2—THE OBSERVED DEFICIENCY IN THE NUMBER OF SCALED DOPPLER RECORDS, AS A FUNCTION OF SQUARED DOPPLER FREQUENCY, DERIVED FROM FIGURE 1

the Figure, that the deficiency can be closely expressed by a power law in the range of Doppler frequencies for which the deficiency exists. Mathematically expressed, then, the measured distribution of body Doppler frequencies is

$$\# = \#_0 \exp\left(-\frac{F^2}{2F^2}\right)\epsilon \, dF \qquad (11)$$

where

$$\epsilon = 1 \qquad F \geq F_0$$

$$\epsilon = \left(\frac{F}{F_0}\right)^{\alpha} \qquad F \leq F_0$$

and in the cases which have been examined, corresponding to summer mornings before dawn, the values $F_0 = 4.25$ and $\alpha = 1.5$, taken from Figure 2, are good approximations.

If the duration effect accounts for the deficiency factor ϵ, the implication is that the quantity $(F/F_0)^{\alpha}$ must be proportional to the number of meteors whose durations are greater than $(1/F)$. The plot in Figure 3 shows the latter function, for the test of Figure 2. Since it was based only upon the number of echoes whose body Doppler frequencies could be scaled, it is deficient itself at low durations, and so "saturates" less quickly than it otherwise would. However, the slope of 1.45 of the linear section of Figure 3 agrees very well with the doubled value from Figure 2 of 1.5 (note Fig. 2 abscissa is F^2, Fig. 3 just F). This agreement lends added weight to the supposition that the true radial component of velocity dis-

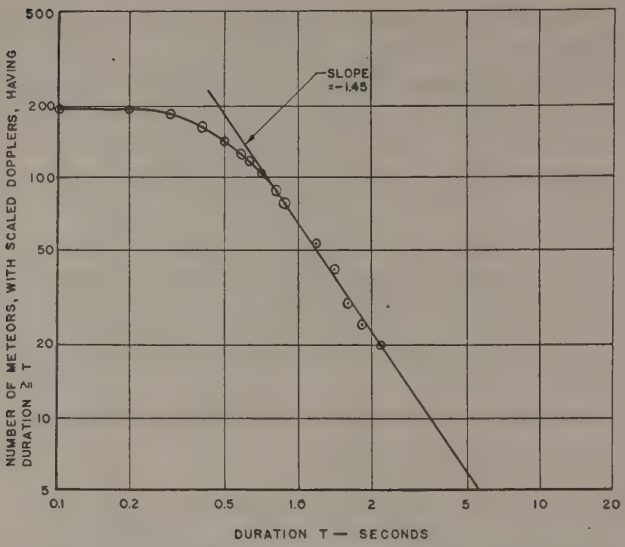

FIG. 3—THE NUMBER OF METEORS SCALED FOR DOPPLER FREQUENCY WITH DURATIONS GREATER THAN T VERSUS T (DATA OF JULY 16, 1949)

tribution of the observed meteor drifts is normal, since the theory fully accounts for the observed lack of low body Doppler frequencies. Additional evidence leading to this conclusion has been obtained from scatter plots of Doppler frequency *versus* duration. It is found that the area of such a plot above a curve $F = 1/(\text{duration})$ is solidly filled, and the area below vacant.

CORRECTION OF SYSTEMATIC ERROR IN MEAN-SQUARE BODY DOPPLER FREQUENCY

With the aid of the empirical equation (11) for the distribution of body Doppler frequencies, we can now calculate the relation between the mean-square Doppler frequency $\overline{F_m^2}$ scaled from the records and the value $\overline{F^2}$ without subscript which will represent the value characteristic of the actual wind velocities. We find, then that

$$\overline{F_m^2} = \frac{\int_0^{F_0} \exp\left(-\frac{F^2}{2\overline{F^2}}\right)\left(\frac{F}{F_0}\right)^\alpha F^2\,dF + \int_{F_0}^{\infty} \exp\left(-\frac{F^2}{2\overline{F^2}}\right)F^2\,dF}{\int_0^{F_0} \exp\left(-\frac{F^2}{2\overline{F^2}}\right)\left(\frac{F}{F_0}\right)^\alpha dF + \int_{F_0}^{\infty} \exp\left(-\frac{F^2}{2\overline{F^2}}\right)dF} \quad \ldots\ldots(12)$$

and if we call $a = F_0/\sqrt{\overline{F^2}}$, and $x = F/\sqrt{\overline{F^2}}$

$$\frac{\overline{F_m^2}}{\overline{F^2}} = \frac{\sqrt{\pi/2} + \int_0^a \exp\left(-\frac{x^2}{2}\right)\left[\left(\frac{x}{a}\right)^\alpha - 1\right]x^2\,dx}{\sqrt{\pi/2} + \int_0^a \exp\left(-\frac{x^2}{2}\right)\left[\left(\frac{x}{a}\right)^\alpha - 1\right]dx} \quad \ldots\ldots(13)$$

The simplest evaluation of the Doppler frequency corrections can be made by integrating (13) graphically with the aid of a planimeter. However, the integrals

in equation (12) can also be evaluated in terms of the incomplete gamma function. Using Pearson's [2] notation,

$$I(u, p) = \frac{1}{\Gamma(p+1)} \int_0^{u\sqrt{p+1}} v^p e^{-v}\, dv \quad \ldots\ldots\ldots\ldots\ldots\ldots (14)$$

where $\Gamma(p+1)$ is the complete gamma function. $I(u, p)$ is tabulated [2], and in terms of it (13) becomes

$$\frac{\overline{F_m^2}}{\overline{F^2}} = \frac{\sqrt{\frac{\pi}{2}} + \frac{2^{\frac{\alpha+1}{2}}}{a^\alpha} I\left(\frac{a^2}{\sqrt{2(\alpha+3)}}, \frac{\alpha+1}{2}\right) \times \Gamma\left(\frac{\alpha+3}{2}\right) - 2^{\frac{1}{2}} I\left(\frac{a^2}{\sqrt{6}}, \frac{1}{2}\right)\Gamma\left(\frac{3}{2}\right)}{\sqrt{\frac{\pi}{2}} + \frac{2^{\frac{\alpha-1}{2}}}{a^\alpha} I\left(\frac{a^2}{\sqrt{2(\alpha+1)}}, \frac{\alpha-1}{2}\right) \times \Gamma\left(\frac{\alpha+1}{2}\right) - 2^{-\frac{1}{2}} I\left(\frac{a^2}{\sqrt{2}}, -\frac{1}{2}\right)\Gamma\left(\frac{1}{2}\right)}$$

$\ldots\ldots\ldots (15)$

A useful approximate formula valid when $a < 0.5$ or so is

$$\frac{\overline{F_m^2}}{\overline{F^2}} = \frac{\sqrt{\pi/2}}{\sqrt{\pi/2} - \alpha a/(1+\alpha)} \quad \ldots\ldots\ldots\ldots\ldots\ldots (16)$$

while when $a = \infty$, $(\overline{F_m^2}/\overline{F^2}) = 1 + \alpha$. Figure 4 gives the relation between the

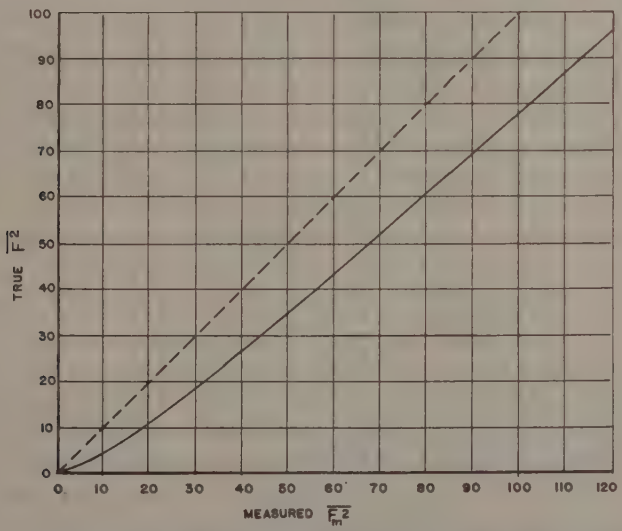

FIG. 4—THE RELATION BETWEEN THE TRUE AND MEASURED MEAN-SQUARE DOPPLER FREQUENCIES FOR PARAMETERS $F_0 = 4.25$, $\alpha = 1.5$, TYPICAL AT 23.1 MC/SEC

measured and true mean-square Doppler frequencies for $F_0 = 4.25$, and $\alpha = 1.5$, the constants being based upon representative conditions as observed at 23.1 Mc/sec. It should be noticed that at higher radio frequencies, the duration is decreased by the factor $1/f^2$, whereas the body Doppler frequency is increased by

the factor f. Consequently, the parameter a should vary directly with f. On the other hand, α should not vary markedly with frequency.

EXPERIMENTAL STUDIES OF TURBULENCE

To make actual use of the analysis so far developed, it is necessary to perform experiments in which the radially directed component of meteor drift velocity is measured as a function of elevation angle, for meteors distributed with respect to azimuth. Unfortunately, accurate measurement of meteoric elevation angles for arbitrary bearing angles is one of the hardest problems in the field of meteoric echo work. However, a remarkably good measure of turbulent velocity can be obtained by estimating elevation angle solely from measured slant range and assumed height. The pertinent relation is $\cos i = h/R$, where h is the height of the reflector, and R is the slant range. Using this method, equation (9) may be interpreted as a linear plot of $\overline{v^2}$ *versus* $(h/R)^2$.

The data obtained on the morning of July 27, 1949, have been analyzed and plotted in this way in Figure 5. A total of 330 meteors recorded between the hours of $02^h\ 30^m$ and $05^h\ 00^m$ PST were used; each plotted point represents the average squared Doppler frequency for meteors within a given range class, corrected with the use of Figure 4. A mean height h of 93 km was assumed for meteors whose range was 120 km or greater [3, 4, 5]. In the case of the shorter range meteors represented by the points to the right-hand side of the plot, lesser heights were assumed. For instance, the group of meteors with 90-km range could not be at a height greater than 90 km. Their mean height, therefore, was taken to be 85 km, the mean height for all meteors of height less than 90 km. Similarly, the 100-km range group was assumed to correspond to height 90 km, and $R = 110$ to $h = 92$, and $R = 120$ or above to $h = 93$ km. As a result of these necessary assumptions, the exact horizontal positions of the points in Figure 5 are somewhat ill-defined. Clearly, an uncertainty of 10 km in mean height would lead to an error in the abscissa which is equal to a corresponding 20 per cent of the abscissa.

The net effect of this uncertainty in mean height is not as great as might be anticipated, however. For small abscissas, the actual error in ordinate position, being reckoned on a percentage of abscissa basis, is insignificant. For large abscissas, the uncertainty in mean height can hardly be very large; the range for these latter points is less than the mean height for all meteors, so that the height distribution for short range meteors is reduced in extent and can be more accurately estimated.

Since the theory indicates a linear relationship exists between $\overline{F^2}$ and $(h/R)^2$, the method of least squares was used to determine a linear regression line.

In Figure 5 the heavy line indicates the result obtained from the July 27 data. The computed correlation coefficient of the means is 0.75, and implies that the sample size was adequate to importantly reduce the effect of variations caused by azimuth and the randomness in wind directions. Of greatest interest, however, is the probable accuracy of estimate of the $h/R = 0$ and 1 ordinates, since they are directly related to the constants descriptive of the wind. The values of these ordinates are affected first by the uncertainties in the mean of the distribution and in the regression coefficient which are associated with random sampling, and second with the uncertainty in the height distribution of the meteors. The possible

error associated with the sampling process can be estimated by statistical means, either by analysis of the statistical properties of each individual correlation, or by making use of the known statistical properties of the data in general. By either means, as considered in a later section, it can be shown that the error in the $h\ R = 1$ ordinate has a 50 per cent chance of being less than about $2.7\ \sqrt{N}$ of the mean ordinate of the distribution, where N is the number of meteors used in the correlation. As applied to the July 27 data, it is found that the overhead ordinate corresponds to 2.4 ± 4.7 c.p.s.^{2} with a certainty of 50 per cent. An estimate of the error resulting from the assumed height of 93 km (as reduced for short range) may be found by recomputing the regression line for a different set of assumed heights. The dashed line in Figure 5 shows the effect of assuming a height of 100 km. The variation in assumed height then leads to $h\ R = 1$ ordinates in this example of 8.8 as compared to 2.4 c.p.s.^{2}. However, the lower value is preferred, because 93 km appears to be a more representative mean height than does 100 km.

A second example is from the data of May 29, 1949, plotted in Figure 6. Again the heavy line corresponds to an assumed mean of the height distribution of 93 km, and the dotted line to a height of 100 km. As before, the heavy line is preferred. The ordinates of Figures 5 and 6 will be noticed to be identical to within the probable error of the sample.

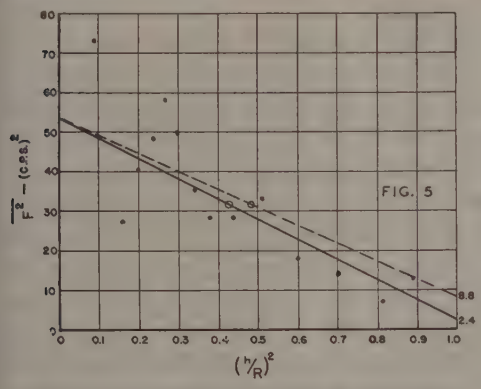

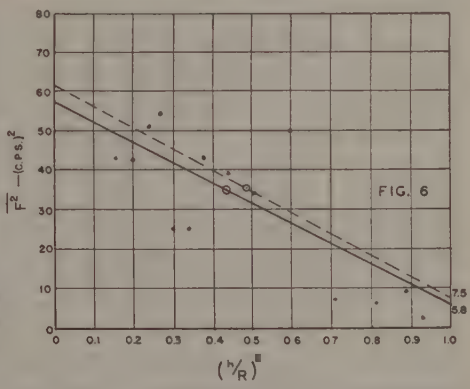

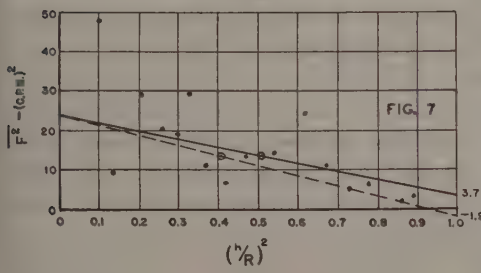

FIGS. 5-7—CORRECTED MEAN-SQUARE BODY DOPPLER FREQUENCY VERSUS $(h/R)^2$

FIG. 5—JULY 27, 1949, FROM 02^h30^m TO 05^h00^m LOCAL TIME; SAMPLE INCLUDES 330 METEORS; SOLID LINE BASED UPON $\bar{h}$=93 KM, DOTTED UPON $\bar{h}$=100; CARRIER FREQUENCY=23 MC

FIG. 6—MAY 29, 1949, FROM 02^h30^m TO 05^h00^m LOCAL TIME; SAMPLE INCLUDES 261 METEORS; SOLID LINE BASED UPON $\bar{h}$=93 KM, DOTTED UPON $\bar{h}$=100

FIG. 7—AUGUST. 2, 1949, FROM 03^h00^m TO 05^h50^m LOCAL TIME; SAMPLE INCLUDES 125 METEORS; SOLID LINE BASED UPON $\bar{h}$=110 KM, DOTTED UPON $\bar{h}$=93

A third example is shown in Figure 7, based on the data of August 2, 1949. On this occasion, heights were believed to be greater than usual, based upon actual angle of arrival data taken during the period. As a result, the heavy curve, corresponding to a 110-km height, was preferred to the light curve, corresponding to a height of 93 km.

INTERPRETATION

Considering the July 27, 1949, example further, we find that when

$$\left(\frac{h}{R}\right)^2 = 0, \qquad \overline{F^2} = 53.9 \text{ c.p.s.}^2 \qquad \text{and} \qquad \overline{v^2} = 15{,}700 \text{ (km/hr)}^2$$

and when

$$\left(\frac{h}{R}\right)^2 = 1, \qquad \overline{F^2} = 2.4 \text{ c.p.s.}^2 \qquad \text{and} \qquad \overline{v^2} = 1{,}310 \text{ (km/hr)}^2$$

Then

$$\tfrac{1}{2}(\overline{w_h}^2 + \overline{\hat{w}_h^2}) = 15{,}700$$

$$(\overline{w_v}^2 + \overline{\hat{w}_v^2}) = 1{,}310$$

As was found from the average wind analysis, on this date $\overline{w_h} = 98$ km/hr, and $\overline{w_v}$ for a single test is statistically indistinguishable from zero. Consequently, we find that $\sqrt{\overline{\hat{w}_h^2}} = 144$ km/hr (40 meters/sec), and $\sqrt{\overline{\hat{w}_v^2}} = 36$ km/hr (10 meters/sec). Root-mean-square vertical velocities of 15 and 12.5 meters/sec were obtained in the other examples. The differences are not significant.

In interpreting these results, we may first consider the root-mean-square-peak-horizontal wind velocity of 144 km/hr (40 meters/sec) found for July 27. This value may be attributed to variability of the horizontal drift velocity, either in time or in space. A time variation might be caused by a relatively steady air-motion, the direction of which changed during the period of the test. In this way, the average wind $\overline{w_h}$ would be assumed to be reduced because of vector additions of strong changeable winds. A test of this hypothesis might be to see if the ratio $\overline{w_h}/\sqrt{\overline{\hat{w}_h^2}}$ decreased as the period of averaging was increased. Spatial differences in wind velocity, on the other hand, might result from turbulence, stratification, or possibly from differences in wind properties within the region of meteoric observation. The last explanation is felt to be inadequate to explain the range and consistency of the observed effects. Stratification in height of the wind system would lead to peak horizontal variations such as are observed.

One important approximation was made in reducing the May 29 data, which has not been considered so far. It will be noticed, in the averaging process leading from equation (6) to (7), that it was assumed that equal numbers of echoes would be detected in each azimuthal direction. In practice, this is never true. However, examination of the distribution of rate of meteoric arrival *versus* azimuth shows that in the practical case the final term of (6) will be materially reduced. This is especially true, when it is realized that θ_w, as well as θ_m, tends to have a random, unpredictable variation. It is assumed that in averaging over all azimuthal directions $\cos(\theta_m - \theta_w)$ goes to zero. A rough test of the extent to which it does may be carried out by forming the ratio $\Sigma F/\Sigma \mid F \mid$ over all meteors. Experimentally, it is thus found that $\cos(\theta_m - \theta_w)$ is typically of the order of 1/5. Examination of equation (6) then shows that the cross-product term is reduced not only by the factor 1/5, but also by the small factor w_v/w_h, in comparison with the dominant

first term. In addition, the $\sin^2 i$ factor insures that the cross-product term vanishes completely at the $i = 0$ and 90° ordinates. For these reasons, little attention need be given to the distribution of meteors in azimuth.

STATISTICAL CONSIDERATIONS OF ACCURACY

The meteoric method of wind study is essentially statistical. A variable wind is sampled with the aid of a finite number of reflecting columns, and then averaging processes are utilized to determine the mean wind characteristics and to reduce to insignificance the variability of the results caused by uncontrolled factors. Because of the statistical nature of the sampling process, it is important to analyze the wind reduction procedures by statistical methods, in order to determine the sources of error and the accuracies that may be expected from a given sample size. The analysis may conveniently be divided into a study, first, of the vector average wind-reduction procedure, and second, of the r.m.s. wind-reduction procedure.

ACCURACY OF THE VECTOR AVERAGE WIND DETERMINATION

The procedure for determining the vector average wind was described in the previous paper [1]. If Doppler frequency is plotted *versus* the meteoric azimuth, as in Figure 8, a scatter plot is obtained, with widely different Doppler frequencies

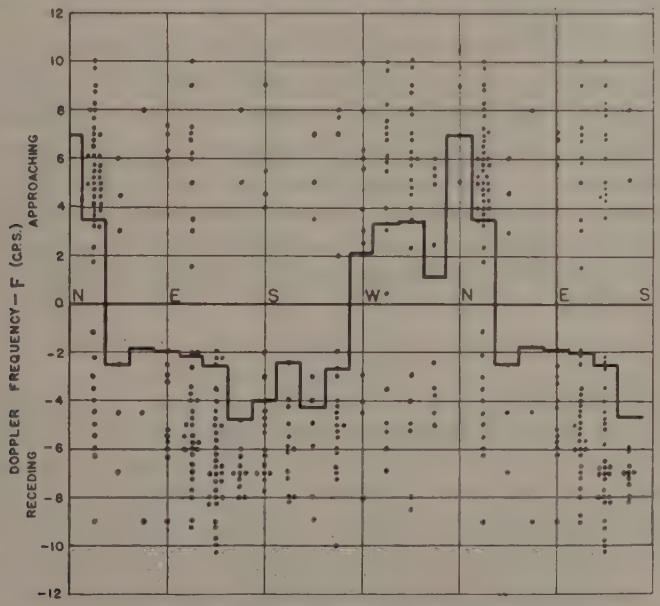

FIG. 8—MEASURED BODY DOPPLER FREQUENCIES VERSUS DIRECTION FOR DATA OF SEPTEMBER 11, 1949; THE RECTANGULAR CURVE IS THE MEAN

resulting for each given direction. Inspection of equation (4) reveals that the factors producing the scatter are (1) the variability in wind speed from observation to observation, caused by stratification, turbulence, and time variations; and (2) the influence of instantaneous wind direction with respect to the line from the observer to the meteor. As is shown by equation (5), if an average involving an infinite number of meteors is taken over the data in each azimuth class, the varia-

tions producing scatter will disappear, and to the extent that the average wind speed and direction are independent of the azimuth from which echoes are obtained, the average body Doppler *versus* azimuth curve will be a sine function. Before proceeding further, we may elaborate, by noting that even with an infinite sample size, a non-sinusoidal $\bar{v}(\theta_m)$ function could occur if, say, $\overline{\sin i}$ was a function of θ_m. Such a situation might result if meteors in one direction came from low radiants, and meteors in the opposite azimuths came from high radiants. The difference in zenith angle of the mean radiants would lead to a difference in $\overline{\sin i}$ *versus* detection azimuth. Similarly, large-scale horizontal variations in wind structure, of the order of a few hundred kilometers across, could lead to the same result.

In a practical wind plot, such as the one shown in Figure 8, a finite number of readings is obtained in each azimuth class. As a result, instead of a sinusoidal curve of regression (assuming such from an infinite sample), a broken curve is obtained which may be considered to be of the form of a sine variation plus a random sampling error S_m, varying randomly with azimuth. The sectional curve of Figure 8 receives its irregularity from S_m. Since the amplitude and direction of the vector average wind is determined from the amplitude A and phase ϕ of the sine curve best fitting the ordinates $\overline{F_m}$, the uncertainty in the wind velocity may be found by recognizing that

$$\overline{F_m} = a \cos (\theta_m - \overline{\theta_w}) + S_m + C \quad \ldots\ldots\ldots\ldots\ldots\ldots (17)$$

and Fourier analysis of $\overline{F_m}$ for A and ϕ will yield a and $\overline{\theta_w}$, with a probable error equal to the probable value of the Fourier coefficient of the m random ordinates, S_m. The constant C will be zero if the average vector wind is horizontal. It is related to the average $D = \overline{F_m}$ of the preceding paper by the relation $D = C + \overline{S_m}$, averaged over all m. The expectancy of error in the mean wind is the expected value of the Fourier coefficient of the M random ordinates S_m. If we denote by S the standard deviation of the sampling errors S_m, the expectancy of the root-mean-square error in A is [6]

$$E = \frac{2S}{\sqrt{M}} \quad \ldots\ldots\ldots\ldots\ldots\ldots\ldots\ldots\ldots\ldots (18)$$

Note that S is the standard deviation of the mean ordinates $\overline{F_m}$ from the true regression curve $a \cos (\theta_m - \theta_w)$, rather than from its estimate $A \cos (\theta_m - \phi)$. If, in computing the error, the standard deviation is measured from $A \cos (\theta_m - \phi)$, the difference is not important. In practice, more important errors in the estimate arise from the fact that there are not equal numbers of meteors in the averages used to obtain the ordinates $\overline{F_m}$, so that they become non-homoscedastic.

Although equation (17) can be applied as it stands to find the expectancy of error in a wind determination, it is laborious to compute S_m, requiring as it does the point for point calculation of the regression curve. An easier way to obtain the same answer can be found based upon use of the difference ordinates $\overline{F_{m+1}} - \overline{F_m}$, without computing the sine ordinates point by point. Only the amplitude A of the best-fitting sine curve need be known.

A quantity which can be conveniently scaled is

$$\Delta_m = \overline{F_{m+1}} - \overline{F_m} \quad \ldots\ldots\ldots\ldots\ldots\ldots\ldots\ldots\ldots\ldots (19)$$

which becomes, by virtue of (17), and the abbreviation $(\theta_m - \theta_w) = x_m$,

$$\Delta_m = A \sin\left(x_m + \frac{2\pi}{M}\right) - A \sin x_m + S_{m+1} - S_m$$

$$= AK \sin(x_m + \beta) + S_{m+1} - S_m$$

where $K = \sqrt{2(1 - \cos 2\pi/M)}$, and β is an irrelevant constant. Averaging Δ_m^2 over all M of the m's,

$$\overline{\Delta_m^2} = \frac{A^2K^2}{2} + \overline{S_{m+1}^2} + \overline{S_m^2}$$

$$= A^2\left(1 - \cos\frac{2\pi}{M}\right) + 2\,\overline{S_m^2}$$

since S_m is random with respect to m. Solving for the quantity $\overline{S_m^2}$, we have in our previous notation

$$S^2 = \frac{\overline{\Delta_m^2}}{2} - \frac{\left(1 - \cos\frac{2\pi}{M}\right)}{2} A^2 \quad \ldots\ldots\ldots\ldots\ldots\ldots (20)$$

Formula (20) is the most convenient way of obtaining S for use in (18). The final term of (20) vanishes for large numbers M of azimuth classes. It represents the variance of the M successive difference ordinates of the sinusoidal regression curve and so is subtracted from the observed variance to find the random component.

OBSERVED ERRORS IN VECTOR AVERAGE WIND VELOCITIES

The formulas (18) and (20) have been applied to the majority of the wind determinations presented in the earlier paper [1]. The actual expected error will in most cases be less than calculated, because the weighted Fourier analysis used in determining the vector average wind essentially rejects the information from the few poorly-determined ordinates, while the error analysis is not so weighted, and does not have this advantage. Table 1 summarizes the results of this study.

It will be seen that the values of error E are small compared with the typical root-mean-square horizontal winds of about 180 km hr. However, the expected errors are large compared with the vector average wind velocity, which appears to be physically a not too well determined average between opposing components of much higher speed.

In general, the determination of vector average wind velocity will have an error varying inversely as $\sqrt{P}$, with P being the total number of observations. Study of the results of Table 1 leads to a general semi-empirical formula for the expected error of velocity determination

$$E(\bar{w}) = \frac{400}{P^{1/2}} \quad \ldots\ldots\ldots\ldots\ldots\ldots\ldots\ldots (21)$$

where E is in km/hr. In the majority of cases in which unusual wind conditions do not exist, (21) probably will give a better estimate of accuracy than will (18).

The accuracy of the direction of the mean vector wind cannot so easily be specified in general, since in radians it is closely equal to the percentage error in average vector wind speed. The percentage error depends not only on the actual error as in (21), which is dependent principally on sample size, but also on the

TABLE 1—*Study of vector average wind errors*

Date	P	A	D	S	E
					km/hr
5-29-49	200	4.1	1.8	1.3	21
7-23-49	171	2.5	0.6	3.1	48
7-27-49	193	3.1	−0.1	1.9	30
7-30-49	254	1.5	0.4	1.9	30
8- 6-49	153	2.8	0.6	1.7	26
8-10-49	234	4.0	−1.7	1.4	22
8-13-49	215	2.2	1.2	1.4	22
8-17-49	143	4.0	0.5	2.2	34
8-20-49	181	1.6	−0.5	3.6	56
8-24-49	103	3.6	0.5	3.5	55
8-31-49	149	2.3	−1.5	2.3	36
9- 3-49	127	2.4	1.0	2.1	33
9-11-49	301	3.9	0.5	1.5	24

P = total number of meteors in test
A = amplitude of sine curve fitting $\overline{F_m}$ *versus* θ_m data (weighted)
D = average of $\overline{F_m}$ ordinates
S = Standard deviation caused by sampling error, neglecting weighting
E = expected error in vector average wind in km/hr, neglecting weighting

variable average vector wind magnitude, the difference between large opposing velocities. Probably the best estimate of the expected error in average vector wind direction then is

$$E[\angle \text{ of } (\overline{\mathbf{w}})] = \frac{400}{\overline{w}\, P^{1/2}} \qquad (22)$$

in radians. Typically $\overline{w}$ = 100 km/hr, P = 200, and the expected angular error becomes ± 16°.

THE VERTICAL AVERAGE WIND

From equation (5) it may be seen that the quantity $C = \overline{w}\ \overline{\cos i}\ \sin \bar{\alpha}$, based upon an infinite sample size, is a measure of the average vertical component of vector wind motion. If the wind is horizontal on the average, $\bar{\alpha} = 0$ and $C = 0$. The estimate of C, based upon the actual finite sample size, we shall call D. Experimentally, D is the average of the M ordinates $\overline{F_m}$. By virtue of (17), $D = C + \overline{S_m}$. The values of D for a number of tests are given in Table 1. The average D for the 13 tests is 0.25 c.p.s. The standard deviation of the D's is 0.41. With the aid of Student's distribution, it is found that the probability that $\overline{D}$ differ from 0.25 by more than 0.25 is 0.05. It is, therefore, slightly doubtful, on the basis of these data, that the true value of C is zero. On the other hand, much more data would be required to demonstrate the existence of a significant value of C different from zero. Certainly it is unlikely that C is greater than 0.50. A $\overline{D}$ of 0.25 would correspond to a downward average wind velocity of 1.5 meters per second.

ACCURACY OF THE R. M. S. WIND DETERMINATION

The factors affecting the accuracy of the r.m.s. vertical and horizontal velocity determinations of the type illustrated in Figures 1 to 3 are (1) uncertainty in

elevation angle, (2) random sampling errors, and (3) systematic errors in mean scaled Doppler frequency. The errors which result from estimating elevation angle from range and height have already been considered, as have the systematic scaling errors. The remaining error is a result of the fact that with a finite sample size the fluctuations in mean-square Doppler frequency caused by wind and detection-azimuth variations do not completely average out. If the sample size were infinite, an accurate measure of r.m.s. wind velocity would be obtained by recording the value of $\overline{F^2}$ when $(h/R)^2 = 0$ or 1. In the presence of scatter, these extreme values are in error, partly because of the uncertainty in the slope of the regression line and partly because of the uncertainty of the value of the mean ordinate. Since the mean abscissa is generally close to 0.50, the error in the $(h/R)^2 = 0$ or 1 ordinates caused by slope error is one-half the slope error. The total errors will have a variance which is the sum of the variance of the mean and the variance of half the slope.

With the use of Student's statistic, it is possible to obtain confidence limits on the values of the mean and of the slope. If we designate Student's statistic by t and the confidence limits of the mean by $\Delta\bar{y}$,

$$\Delta\bar{y} = \frac{\sigma_y t}{\sqrt{n}} \qquad (23)$$

where σ_y is the standard deviation of the ordinates F^2 measured from the mean, and n is the sample size. Fifty per cent confidence limits are obtained by using $t = 0.67$ for infinite sample size. In the example of Figure 5, $\sigma_y = 47$ c.p.s.^{2} and $n = 330$, giving $\Delta\bar{y} = 1.73$.

Confidence limits on the slope b of the regression line can be obtained from the formula

$$\Delta b = t\sqrt{\frac{\Sigma(y_i - Y_i)^2}{(n-2)\,\Sigma(x_i - \bar{X})^2}} \qquad (24)$$

where y_i are the individual values of F^2, x_i are the corresponding values of $(h/R)^2$, and Y_i represent the estimates of y_i from the regression line. In terms of the correlation coefficient r of the ordinates y_i and the standard deviations of the ordinates,

$$\Delta b = t\sqrt{\frac{(1 - r^2)\sigma_y^2}{(n-2)\sigma_x^2}} \qquad (25)$$

If there are equal numbers of meteors in each range class, (24) and (25) may be applied to the mean ordinates $\overline{y_i}$. Again, $t = 0.67$ for large sample size and in the example of Figure 5 $\Delta b = 8.7$ c.p.s.^{2}. The 50 per cent confidence limits on the $(h/R)^2 = 0$ and 1 ordinates will then be about 4.7 c.p.s.^{2}. This value suggests the formula $2.7\,\overline{F^2}/\sqrt{n}$, for the 50 per cent confidence limits, where $\overline{F^2}$ is the mean ordinate of the distribution and n is the sample size. The latter expression is a useful approximation for estimating the magnitude of statistical error in the velocity determination and may be used as a guide in planning more extensive experiments.

CONCLUSIONS

An appropriate extension of the methods for reducing meteoric body Doppler frequency data makes possible the determination not only of the vector average drift but also of the root-mean-square values of horizontal and vertical wind velocities. Whereas average vector horizontal wind components are typically of the order of 100 km per hour with considerable variability, the root-mean-square horizontal velocity is a more consistent 180 or so kilometers per hour. The average vector vertical wind is very nearly zero, but possibly as high as 3 meters per second. The root-mean-square vertical wind, on the other hand, is estimated to be somewhere between zero and 60 km per hour for the times that reduction has been attempted. This quantity can probably be taken to be descriptive of vertical components of irregular turbulent motion.

Comparison of wind measurements by the meteoric technique with those made by the layer reflection fading technique originated at Cambridge, lends further support to the supposition that the wind structure is quite stratified in the lower E-region. The Cambridge method yields mean velocities of the order of magnitude given by the meteoric r.m.s. technique, or even higher. It seems probable that layered winds exist which move with such speeds. The vector average winds, on the other hand, appear to have all the characteristics of a mean between opposing layered winds of greater velocity.

In order that reliance may be placed upon the meteoric velocity determinations to an appropriate extent, the statistics of the reduction procedures has been considered in detail. From the theory of the errors, several simple "rule of thumb" relations for the accuracy have been developed. It is found that, under typical conditions, the probable error in average wind velocity specification is of the order of $400/\sqrt{P}$ km per hour, where P is the number of meteors used in the reductions. The expected error of average vector wind direction is found to be $400/(\overline{w}\ P^{1/2})$ radians, where $\overline{w}$ is the magnitude of the average meteor wind velocity in kilometers per hour. The 50 per cent confidence limits for the value of the r.m.s. horizontal wind velocity are estimated to differ from the velocity by a fraction of the velocity of no more than $0.7/\sqrt{P}$, where P is the sample size. The error in vertical r.m.s. velocity is considered in detail, and is found to be limited by the accuracy of the means of estimating arrival angle, as well as by sample size.

References

[1] L. A. Manning, O. G. Villard, Jr., and A. M. Peterson, Meteoric echo study of upper atmosphere winds, Proc. Inst. Radio Eng., **38**, 877-883 (1950).

[2] K. Pearson, Tables of the incomplete Γ-function, published for the D. S. I. R. by His Majesty's Stationery Office, London, 164 pp. (1922).

[3] P. M. Millman and D. W. R. McKinley, Three-station radar and visual triangulation of meteors, Sky and Telescope, **8**, 114 (1949).

[4] J. A. Clegg and I. A. Davidson, Radio echo method for the measurement of the heights of the reflecting points of meteor trails, Phil. Mag., Ser. 7, **41**, 77-85 (1950).

[5] L. A. Manning, O. G. Villard, Jr., and A. M. Peterson, Radio Doppler investigation of meteoric heights and velocities, J. App. Physics, **20**, 475-479 (1949).

[6] S. Chapman and J. Bartels, Geomagnetism, **2**, Oxford, Clarendon Press, 1049 pp. (1940).

STUDY OF ATMOSPHERIC IONS IN A NON-EQUILIBRIUM SYSTEM

BY C. G. STERGIS

Geophysics Research Directorate, Air Force Cambridge Research Center, Cambridge, Massachusetts

(Received September 2, 1953)

ABSTRACT

The time variation of the concentration of atmospheric ions in a non-equilibrium system has been determined experimentally and theoretically. The results indicate that ionic equilibrium, once disturbed, may not again be attained until a time up to 15 minutes has elapsed.

INTRODUCTION

Ions of the atmosphere are continually being created and destroyed. Under conditions of ionic equilibrium, the rate of formation of ions is equal to the rate of destruction of ions. Once the equilibrium is destroyed, however, such as by the introduction or removal of an ionizing agent, the question arises as to how long a time will elapse before equilibrium will again be attained. This is more than an academic question, for it is a well-known fact that the strength of the ionizing agents in the atmosphere is far from constant with time. Thus, conclusions drawn from atmospheric ion measurements must take into account the existence or non-existence of ionic equilibrium.

THEORETICAL CONSIDERATIONS

The relation that is often assumed for the time rate of change of the small ion concentration is

$$\frac{dn}{dt} = q - \alpha n^2 - \beta n \qquad (1)$$

where n represents the concentration of small ions (ions per cc), q the rate of production of small ions (ion pairs per cc per sec), α the recombination coefficient for small ions, and β a factor which depends on the pollution present in the atmosphere in the form of large ions, nuclei, dust, smoke, soot particles, etc. The coefficient β, by virtue of its dependence on so many factors, is not easily determined directly. Hence, we eliminated β in equation (1) by making use of the equilibrium value of small ions, which we shall call n_∞. The value of n_∞ may be measured quite easily. Thus, from equation (1),

$$\beta = \frac{q - \alpha n_\infty^2}{n_\infty} \qquad (2)$$

Upon substituting this in equation (1) and integrating, we obtain

$$\left.\begin{aligned} ln\left(1 + \frac{A}{n - n_\infty}\right) &= A\alpha t + C \\ \text{where} \qquad A &= n_\infty + \frac{q}{\alpha n_\infty} \\ C &= ln\left(1 + \frac{A}{n_0 - n_\infty}\right) \end{aligned}\right\} \quad \ldots\ldots\ldots\ldots\ldots\ldots (3)$$

n_0 representing the concentration of small ions at time $t = 0$.

Equations (3) are plotted in Figure 1 for typical values of q, α, and n_∞ . In obtaining these curves, it has been assumed that the number of ions present initially is so great that the constant C in equation (3) is zero. When this is not the case, the same curves apply, except that the time axis is shifted by $(1/A\alpha)$ $ln\ [1 + A/(n_0 - n_\infty)]$, as is seen from equation (3).

An examination of Figure 1 shows that when the pollution is very great (n_∞ = 25), the concentration of small ions should reach its equilibrium value in about 30 seconds, whereas, when there is practically no pollution at all (n_∞ = 2500), equilibrium should not be reached until about 15 minutes after production of the ions. Theoretically, of course, equilibrium is never reached, but after a finite time the experimental values cannot be distinguished from the equilibrium value. The time at which this occurs depends on the sensitivity of the instrument used in making the measurements. In this discussion, we assume that the instrument is sensitive enough to distinguish a one per cent increase over the equilibrium value.

EXPERIMENTAL PROCEDURE

The principal instrument used in this investigation is the conductivity chamber, which was developed in this laboratory and is of the type first used by Gerdien. The instrument has been described previously [see 1 and 2 of "References" at end of paper].

The apparatus was arranged as follows: A pipe, 24 feet long and 4 inches in diameter, was placed in front of the conductivity chamber. By means of a fan attached to the other end of the chamber, air was caused to flow through the pipe and the chamber. A polonium alpha-ray source was placed at a given distance from the chamber and the conductivity of the air passing through it was measured. The source was then moved to another position inside the pipe and the conductivity again measured, etc. From the conductivity readings, the concentration of small ions in the air-stream was calculated. From the source-to-chamber distance and the air-speed, the time taken for the ions to travel from the source to the conductivity chamber was calculated. Thus, we were able to obtain a series of values of the concentration of small ions as a function of the time. The effect of the walls of the pipe on the ion decay measurements was considered and found to be negligible [2].

In the field, the experimental arrangement was as follows: A 5-curie cobalt-60 gamma-ray source was placed on a truck and the truck driven at constant speed

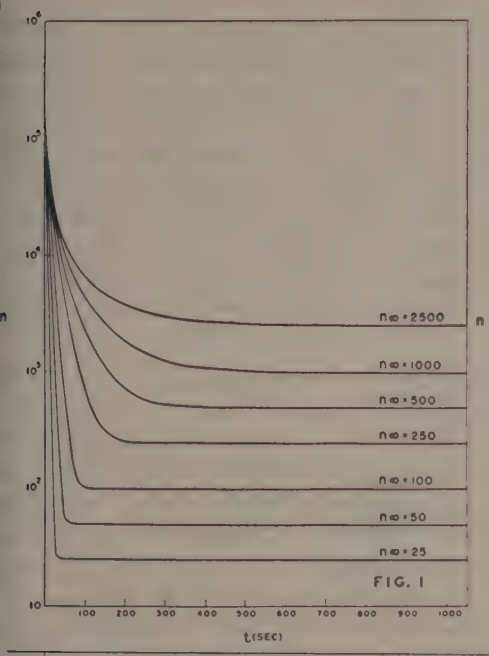

FIG. 1

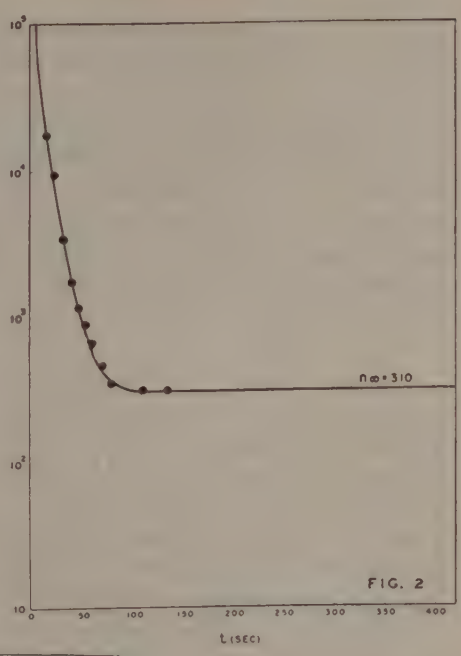

FIG. 2

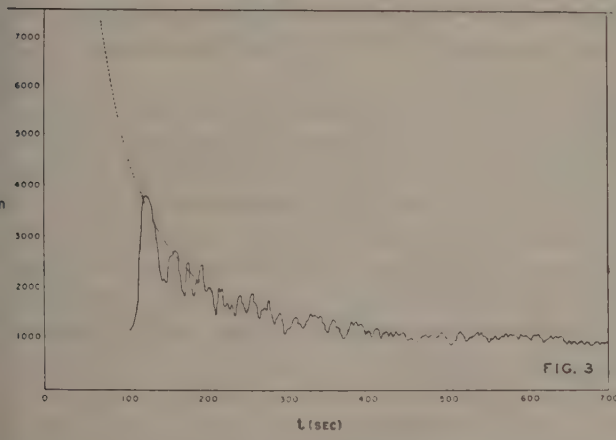

FIG. 3

FIG. 1—THEORETICAL ION DECAY CURVE (WITH $q=10$, $\alpha=1.6 \times 10^{-6}$, AND VALUES OF n_∞ FROM 25 TO 2500)

FIG. 2—ION DECAY RESULTS AT BEDFORD LABORATORY (CIRCLES INDICATE EXPERIMENTAL DATA, WHEREAS SOLID LINE IS THE THEORETICAL CURVE WITH $q=27$, $\alpha=1.6 \times 10^{-6}$, AND $n_\infty = 310$)

FIG. 3—ION DECAY RESULTS AT HOLLOMAN AIR FORCE BASE (SOLID LINE IS THE EXPERIMENTAL CURVE AND THE DASHED LINE THE THEORETICAL CURVE WITH $q=8$, $\alpha=1.55 \times 10^{-6}$, AND $n_\infty = 1000$)

along a straight road on days when the wind velocity was practically zero. An L-13 aircraft, equipped with conductivity instruments, made constant altitude passes over the road on which the truck was moving, thereby detecting the ion cloud generated by the gamma-ray beam. The time separation between passes was sufficient to prevent the aircraft from picking up the same cloud on two successive passes, as the passing of the aircraft through the ion cloud once is sufficient to disrupt the cloud considerably.

RESULTS

The results of ion decay measurements at the laboratory located at Bedford, Massachusetts, are shown in Figure 2. From this Figure, we see that the maximum

time that ions persist in this laboratory is about two minutes. This relativel short decay time is to be expected when we consider that the laboratory is locate near a region of considerable industrial activity, thereby causing the atmospher in that vicinity to be polluted to a large extent.

In order to compare the experimental results with the theoretical prediction we need to know the parameters q, α, and n_∞ . The value of n_∞ we obtained b direct measurement. The value of α we assumed to be 1.6×10^{-6} at room tempera ture and normal atmospheric pressure, as this value has been found by quite a fe investigators. The value of q was obtained in the following way: Equation (3 may be written as

$$ln(n - n_\infty) - ln\left(1 + \frac{n - n_\infty}{A}\right) = -A\alpha t + lnA - C \quad \ldots\ldots\ldots (4$$

The second term in the above expression may be shown to be small relative to th first term for the conditions of our experiment. Hence, by plotting $ln\ (n - n_\infty)$ a a function of t, we obtain a straight line, the slope of which gives $A\alpha$, from whic q may be obtained. Placing the values of q, α, and n_∞ in equation (3), we obtai the theoretical curve shown in Figure 2. It is observed that agreement betwee theory and experiment is very good.

Field tests were conducted at Holloman Air Force Base, New Mexico. Th reason for picking this location was the expectation of measuring a considerabl longer decay time than at Bedford because of the relatively purer air present i New Mexico. Such did, indeed, prove to be the case. Figure 3 shows typical result obtained there; namely, that ionic equilibrium, once disturbed, is not attaine again until a time of 10 minutes has elapsed. The theoretical ion decay curve is als shown in this Figure. The theoretical and experimental curves agree as well as ma be expected when measurements are made in the free atmosphere.

The author is pleased to acknowledge the assistance of the following: Mr. S. C Coroniti, of the Geophysics Research Directorate, who initiated this problem an gave many helpful suggestions; Mr. Roland Matson, who obtained the experimenta data with the aircraft; the personnel of Hanscom Air Force Base and Holloman Ai Force Base for making possible these experiments.

References

[1] R. C. Callahan, *et al.*, J. Geophys. Res., **56**, 545 (1951).
[2] C. G. Stergis, Air Force Cambridge Research Center, Geophys. Res. Paper (1953).

THE EFFECT OF ATMOSPHERIC SCATTERING AND GROUND REFLECTION UPON THE DETERMINATION OF THE HEIGHT OF THE NIGHT AIRGLOW

BY EDWARD V. ASHBURN

U. S. Naval Ordnance Test Station, Inyokern, China Lake, California; and Geophysical Institute, University of Alaska, College, Alaska

(Original manuscript received September 5, 1953, revised manuscript, September 21, 1953)

ABSTRACT

Chandrasekhar's theory of radiative transfer was used to calculate the effect of atmospheric scattering and ground reflection upon the determination of the height of the night airglow when the extinction coefficient is 0.15. It was found that the atmospheric scattering is a significant factor, but that the ground reflection is not important except for high albedo (snow cover).

The height of the night airglow emission layer is usually determined from the ratio of the intensity at the zenith to the intensity at some elevation near the horizon. The basic principle follows from simple geometry, since the apparent thickness of the emission layer near the horizon is a function of the height of the emission layer. The elementary theory, first proposed by Van Rhijn, has to be modified because of many complicating factors, such as background starlight, atmospheric scattering, non-uniformity of the emission layer, etc. Roach and Pettit [see 1 of "References" at end of paper] and Barbier [2] have given critical discussions of the various difficulties involved in the estimation of the heights from which the airglow arises. These discussions have not given a quantitative evaluation of the effect of the ground light due to the mathematical difficulties. Recently Sekera [3] has published tables of the numerical solutions of Chandrasekhar's [4] equations of radiative transfer for a Rayleigh atmosphere. The publication of these tables has made it possible to make a rigorous determination with a reasonable amount of computation of the effect of atmospheric scattering and ground light upon the calculation of the height of the airglow layer.

The problem that Chandrasekhar solved in a rigorous manner, for the first time, is as follows: A parallel beam of natural light of net flux πF per unit area normal to itself is incident in a specified direction on a plane-parallel atmosphere of optical thickness, τ. It is required to find the angular distribution of the light transmitted below the surface at τ.

The equations given by Chandrasekhar [4] express the light intensities (and the Stokes parameters giving the polarization of the light) as functions of τ; λ,

the albedo of the ground at the surface τ; μ_0, the cosine of the angle of incidence o the parallel light; μ, the cosine of the zenith angle of observation; and φ the azimuth angle. Sekera [3] published tables of the numerical values of the light intensities transmitted below the surface τ for the following values of the parameters:

$$\tau = 0.15,\ 0.25,\ \text{and}\ 1.00$$

$$\lambda = 0,\ 0.10,\ 0.25,\ 0.50,\ \text{and}\ 0.80$$

$$\mu_0 = 0.10,\ 0.20,\ 0.40,\ 0.60,\ 0.80,\ 0.90,\ 0.94,\ 0.98$$

$$\mu = 0.10, 0.20, 0.30, 0.34, 0.40, 0.436, 0.50, 0.60,$$
$$0.70, 0.90, 0.916, 0.98, 0.99, 1.00$$

$$\varphi = 0^\circ \text{ and } 180^\circ$$

The specific problem that is considered in this paper may be expressed as follows: A parallel beam of natural light of net flux πF per unit area normal to itself is incident from the zenith on a plane-parallel atmosphere of optical thickness $\tau = 0.15$. At all other zenith distances the incident parallel light has a net flux of

$$\left[1 - \left(\frac{R^2}{R+h}\right)^2 \sin^2\theta\right]^{-1/2} \pi F \qquad (1)$$

where R = radius of the earth, h = height of the airglow emission layer, and θ = zenith distance. The term in the brackets is the relative thickness of the airglow emission layer on a curved earth. What is the angular distribution of the intensity of the light transmitted below the surface at $\tau = 0.15$? Six cases are considered. The simplest case is that of the Van Rhijn formula, which takes account only of extinction of the airglow by the atmosphere below the airglow layer. The next cases are that of extinction of the airglow and the addition of the light due to the scattering of the incident light. The incident light is considered to be coming in from all directions of the hemisphere. The effect of albedos of 0, 0.10, 0.25, 0.50, and 0.80 at the surface $\tau = 0.15$ is computed. For purposes of comparison, the results given by Barbier's [2] formula for the case of albedo equal to zero are also given. The height of the night airglow is usually determined from the ratio of the light intensity at zenith distance θ to the intensity at zenith distance 0°. The height of the emission layer enters in the problem through equation (1).

To apply the results given in Sekera's [3] tables to the problem of the night airglow, it was necessary to determine the light intensities for all azimuths. The equations relating the intensities at an azimuth, φ, from the sun's azimuth, φ_0, are

$$I_l(\mu, \varphi) = I_l \cos^2 \tfrac{1}{2}(\varphi_0 - \varphi) + I_{la} \sin^2 \tfrac{1}{2}(\varphi_0 - \varphi) + \mu^2 Z \sin^2(\varphi_0 - \varphi)$$

$$I_r(\mu, \varphi) = I_r - Z \sin^2(\varphi_0 - \varphi)$$

where I_{la} and I_l are the intensity components parallel to the vertical plane containing the sun. I_l refers to the quadrant opposite the sun and I_{la} refers to the quadrant containing the sun. I_r is the intensity component normal to the vertical plane containing the sun, μ is the cosine of the zenith distance, φ is the azimuth angle, and

$$Z = \frac{3\mu_0(1-\mu_0^2)}{16(\mu - \mu_0)} [X^{(2)}_{(\mu_0)} Y^{(2)}_{(\mu)} - Y^{(2)}_{(\mu_0)} X^{(2)}_{(\mu)}]$$

where μ_0 is the cosine of the sun's zenith distance, and $X^{(2)}$ and $Y^{(2)}$ are as given in Table I of reference [3].

The light intensities were computed for eight azimuths for all the values of μ_0 and μ listed in Table VIII of reference [3]. These values were plotted and smooth curves were drawn giving the intensities for all μ_0's and φ's. From these curves, the integrated effects of the incident light having all directions throughout the hemisphere were determined for eight values of μ. The light due to atmospheric scattering and ground reflection was then added to the incident light reduced by the appropriate extinction. The results of these calculations are given in Table 1 following.

TABLE 1—*Ratio of light intensity at zenith distance, θ, to the intensity at zenith distance* 0° ($\tau = 0.15$)

Albedo of ground	Zenith distance							
	30°	40°	50°	60°	65°	70°	75°	78°
				Height of emission layer 100 km				
0	1.13	1.25	1.42	1.69	1.86	2.08	2.32	2.42
0.10	1.13	1.25	1.42	1.69	1.86	2.08	2.33	2.43
0.25	1.13	1.25	1.42	1.70	1.87	2.09	2.35	2.45
0.50	1.13	1.25	1.43	1.70	1.88	2.11	2.37	2.49
0.80	1.13	1.25	1.43	1.71	1.90	2.13	2.40	2.56
Van Rhijn	1.12	1.24	1.40	1.65	1.80	1.96	2.12	2.13
Barbier	1.13	1.25	1.44	1.71	1.90	2.11	2.33	2.42
				Height of emission layer 200 km				
0	1.13	1.24	1.41	1.63	1.77	1.92	2.09	2.11
0.10	1.13	1.24	1.41	1.63	1.77	1.93	2.10	2.12
0.25	1.13	1.24	1.41	1.64	1.78	1.94	2.12	2.15
0.50	1.13	1.24	1.41	1.64	1.79	1.96	2.15	2.19
0.80	1.13	1.24	1.41	1.65	1.80	1.99	2.19	2.28
Van Rhijn	1.12	1.22	1.38	1.58	1.71	1.83	1.87	1.81
Barbier	1.12	1.24	1.80	1.64	1.79	1.95	2.08	2.10
				Height of emission layer 300 km				
0	1.12	1.22	1.37	1.58	1.69	1.82	1.94	1.91
0.10	1.12	1.22	1.37	1.58	1.69	1.83	1.95	1.92
0.25	1.12	1.22	1.37	1.58	1.70	1.84	1.96	1.94
0.50	1.12	1.22	1.37	1.59	1.72	1.85	1.99	1.98
0.80	1.12	1.22	1.37	1.60	1.74	1.88	2.03	2.03
Van Rhijn	1.11	1.21	1.35	1.53	1.63	1.71	1.70	1.61
Barbier	1.12	1.23	1.38	1.59	1.72	1.84	1.91	1.90
				Uniform extraterrestrial light				
0	0.98	0.97	0.96	0.93	0.90	0.88	0.84	0.81
0.10	0.98	0.97	0.96	0.94	0.92	0.89	0.86	0.83
0.25	0.99	0.98	0.97	0.95	0.93	0.91	0.88	0.86
0.50	0.99	0.99	0.98	0.96	0.95	0.94	0.92	0.91
0.80	0.99	0.99	0.99	0.98	0.98	0.98	0.97	0.96
No atmos scattering	0.98	0.96	0.92	0.86	0.82	0.76	0.66	0.59

An inspection of Table 1 shows that the scattering in the atmosphere changes the I_θ/I_0 for angles $\geq 70°$ for the airglow by a significant amount and therefore would affect the deduced height of the airglow emission layer. The effect of the ground reflection is relatively small except when the albedo is high (a snow cover). For uniform extraterrestrial light, the reflected ground light produces a relatively larger effect than for the airglow, but the scattering by the atmosphere is still the predominate factor in changing the ratio of I_θ/I_0 . Table 1 also shows that for $\tau = 0.15$, Barbier's much simpler method of correcting for atmospheric scattering is adequate.

The value of $\tau = 0.15$ was chosen because it was the smallest τ given in Sekera's tables.* Unfortunately, this does not correspond to a Rayleigh extinction coefficient for a strong airglow line. The Rayleigh τ for the 5577 A line is 0.09 for a sea-level station. Due to scattering by haze and to absorption by ozone and water, the actual τ for relatively clear air is nearer 0.15 than to 0.09. However, most observatories are on mountain tops, which makes the extinction coefficient less than 0.15. The question then is: Are the figures in Table 1 useful in determining the effect of the atmospheric scattering and the ground reflection? Spot calculations from the Chandrasekhar theory have shown that the effect of the ground and of the atmospheric scattering decreases with decreasing τ. The values in Table 1 for the albedos less than 0.80 would then be higher than would be expected for a τ for the 5577 A, 5893 A, or red bands of the airglow. From this, it appears that the ground reflection may be neglected when the ratio I_θ/I_0 is to be used to estimate the height of the airglow lines when the corresponding $\tau \leq 0.15$. No definitive answer can be given, as yet, to the problem of the effect of large particle scattering or of a ground that does not reflect according to Lambert's law.

References

[1] F. E. Roach and H. B. Pettit, Mém. Soc. roy. sci. Liége, **12**, Fasc. 1-2, 13-42 (1952).
[2] D. Barbier, Mém. Soc. roy. sci. Liége, **12**, Fasc. 1-2 (1952).
[3] Z. Sekera, Tables relating to Rayleigh scattering of light in the atmosphere, University of California at Los Angeles, Department of Meteorology, Sci. Rep. No. 3.
[4] S. Chandrasekhar, Radiative transfer, Oxford, Clarendon Press (1950).

*Sekera and Ashburn will soon have in press an extension of Sekera's tables [3] for $\tau = 0.10$, 0.05, 0.02, and 0.01.

SOME RESULTS OF SWEEP-FREQUENCY INVESTIGATION IN THE LOW FREQUENCY BAND

BY J. M. WATTS AND J. N. BROWN*

Central Radio Propagation Laboratory, National Bureau of Standards, Washington 25, D. C.

(Received September 15, 1953)

ABSTRACT

Sweep-frequency techniques, long in use in high-frequency ionospheric research, have been used recently in low frequency research at the National Bureau of Standards. The discovery of a nighttime layer between the *E*- and *F*-layers, which is erratic in appearance, but which seems to have continuity with the daytime *E*-layer during sunset, is announced. Traces characteristic of magneto-ionic splitting are exhibited for the new layer and also for the low-level *E*-layer. Polarization and virtual height records of *F*-layer at night are shown and the effects of ionosphere storms on *E*- and *F*-regions are demonstrated.

Daytime reflections have been recorded from three distinct *E*-region boundaries, each of which appears to be quite sharp in ion gradient. These extend from about 70 km to over 100 km in virtual height. Several recordings of turbulent conditions in the lower levels of the daytime *E*-region are shown.

1. INTRODUCTION

When the Central Radio Propagation Laboratory first embarked on a low-requency propagation investigation program in 1948, two classical methods were vailable as tools. These were the phase-comparison method as used in England y Best, *et al.* [see 1 of "References" at end of paper], and the group-retardation nethod already being used in this country at low frequencies by Helliwell [2] and Benner, Grace, and Kelso [3]. Since the group-retardation or "pulse" technique ad resulted in much of our knowledge of ionospheric characteristics at high requencies, it was thought that it would also be effective in the low frequency and. As a result, in 1949 a fixed-frequency pulse transmitter was completed and ut into operation. This transmitter was used for the following two and one-half ears to make recordings of ionosphere height *versus* time. It was used successfully n frequencies of 37 kc, 50 kc, 100 kc, 160 kc, and 200 kc. The work on 50 kc was escribed briefly in an earlier paper [4]. During this same period, polarization

*Now at Barker and Williamson, Inc.

measuring equipment was developed that permitted examining the orientation and polarization sense of the downcoming echoes. Kilpatrick [5] and Watts [6] have described some of the fixed-frequency polarization findings.

While this work was going on, the effects of ionosphere disturbances were noted [7]. Since it was difficult to make frequency changes quickly in the transmitter, phenomena such as shown in Figure 1, recorded on 160 kc, never were explained satisfactorily.

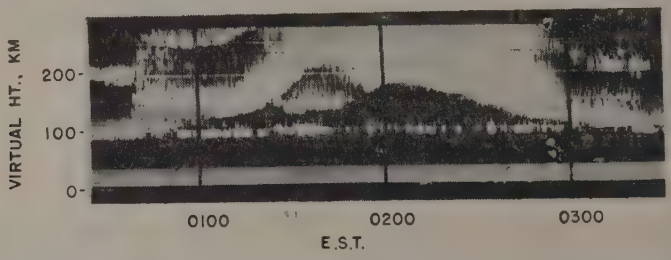

FIG. 1—VIRTUAL HEIGHT VS TIME AT CONSTANT FREQUENCY, 160 KC, OCT. 5, 1950

In January 1951, construction was started on a sweep-frequency exciter to cover the range from about 50 to 1100 kc. The transmitter [8] was completed and put into operation on a routine basis one year later. The first records were gratifying, even though they were not as good as the present records. Material improvement in the transmitter has recently been made by adding two more type 527 tubes to the push-pull parallel final amplifier, making a total of six tubes used in the output stage. The output broad-band transformer of the final amplifier has also been changed from one using steel cores to one using a ferrite core material. The result of these improvements has been to decrease the core losses and provide better coupling to the antenna circuit. The power remains practically constant over the entire frequency range when the output is fed into a dummy load, and is approximately one-half megawatt peak pulse power. The antenna characteristics, however, cause the loading to change with frequency, so that the power delivered to the antenna and the actual radiated power are extremely variable throughout the range covered.

While the transition from fixed-frequency operation to sweep-frequency operation was being made in the height measuring equipment, the polarization measuring equipment was also converted to operate on a sweep-frequency basis [10].

The following sections describe some of the results, and include groups of records reproduced to illustrate the different phenomena.

2. DAYTIME RECORDS

Figure 2 shows a typical early daytime virtual height *versus* frequency recording made on the sweep-frequency equipment. Broadcast-station interference, antenna radiation efficiency, and ionospheric absorption are the chief factors contributing to the appearance of the records. The "herring-bone" appearance at some frequencies is caused by interference from stations operating in the range covered by

the equipment. The receiver also suffers a reduction in sensitivity due to strong carrier interference. The interference on occasion has been severe enough to completely block the receiver and to obliterate even the transmitter pulse. Note the example of this in Figure 2 at 230 kc caused by a radio range station that is only

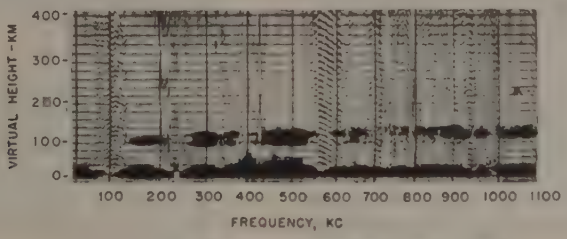

FIG. 2—VIRTUAL HEIGHT VS FREQUENCY, MAR. 7, 1953, 07:15 E.S.T., TYPICAL STRATIFICATION OBSERVED BEFORE ONSET OF DAYTIME ABSORPTION

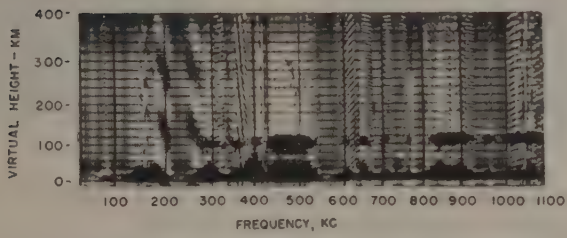

FIG. 3—VIRTUAL HEIGHT VS FREQUENCY, FEB. 11, 1953, 10:58 E.S.T., EXAMPLE OF LOW-LEVEL REFLECTION (BETWEEN 440KC AND 520KC)

three miles away from the receiving location. These adverse effects have been reduced to a great extent by installing an automatic bias control system that operates from the d-c level resulting from interfering carrier rectification.

The radiation efficiency of the transmitting loop antenna increases with frequency, approximately as the fourth power. However, the strongest daytime recorded echoes are in the range 400 to 500 kc. This is because there is normally little interference in this region, and there is also a natural antenna resonant condition in this range that further increases the radiated power. It is in this 400- to 500-kc region that the lowest *E*-region heights are usually recorded, in the height range of 68 to 80 km. Only occasionally are heights measured below this lower limit. This daytime layer, Figure 3, generally produces a weak echo and is recorded only part of the days. It was not recorded at all in midsummer, although the records showed reflections from other levels, which can also be seen in Figures 2, 3, and 4. On days when the low-level reflections are unusually persistent, they may show a scattered reflection as if from "blobs" randomly situated in the entire region from 70 to 100 km. The pattern of reflections then varies widely with frequency change and with time as shown in the six records of Figure 4. It is interesting, and perhaps significant, that scattering from this type of region (also the *E*-region) has been proposed as an explanation for a recently-discovered new type of VHF propagation [9].

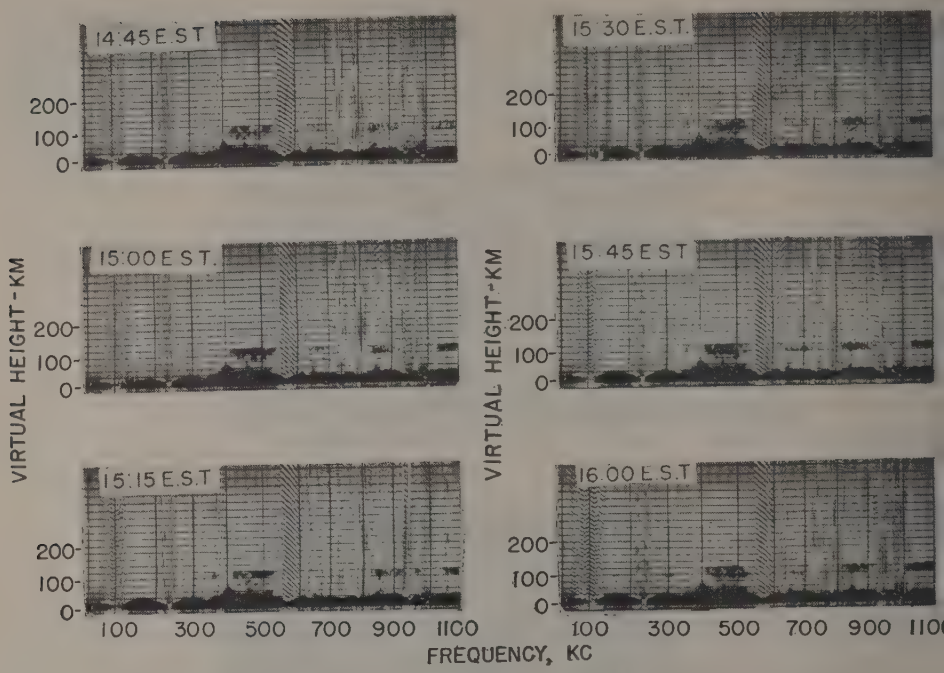

FIG. 4—DAYTIME RECORDS MARCH 11, 1953, SHOWING EVIDENCE OF TURBULENCE IN LOWER E-REGION

The next stratum which may be identified is the region that consistentl produces echoes in the height range of 85 to 95 km (Figs. 2 and 3). During th daylight hours, this region of reflection will produce echoes that are much stronge than the low-level returns. The upper frequency limit of the 90-km region echoe is usually within the 50- to 1100-kc range of the equipment and generally falls nea 800 or 900 kc. The phenomenon of this region's critical frequency is of interest, i that it shows no retardation characteristic in its own echoes or in the echoes fro the higher *E*-region stratum.

The third stratum in order of height seen during the daytime is the one tha varies from approximately 98 to 110 km in height. This is sometimes visible throug the lower strata between 400 and 500 kc, and the amplitude apparently depend on the amount of shielding that is provided by the 90-km region. The intensity o the echoes of this region is always greater toward the higher frequency end of th record, becoming quite high after the critical frequency of the 90-km region echo i passed. This third region seems to be at the level of the *E*-layer that is seen on th high-frequency ionosphere recording equipment with a critical frequency of fro 2 to 4 megacycles.

3. SUNSET AND SUNRISE TRANSITION PERIODS

The transition periods at sunset and sunrise are of special interest, as there i then an opportunity to see traces from layers that are either shielded by th lower *E*-region in the daytime or are non-existent when lower *E*-region ionizatio

is a minimum at night. During the latter part of the afternoon, the absorption decreases as sunset approaches. The next indication that sunset is taking place is the appearance of an *E*-region reflection above the normally visible lower layers. This is seen in Figure 5 on the record of 18:30, with a maximum frequency of

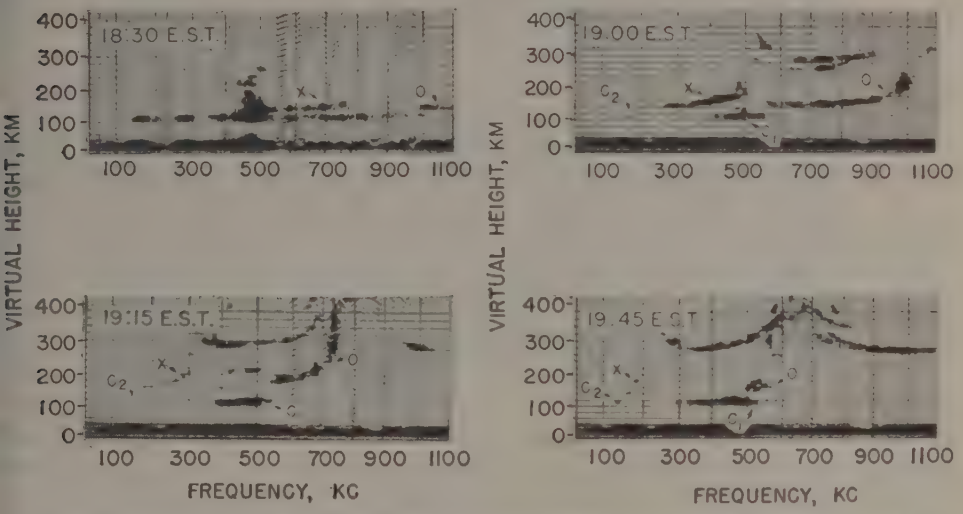

FIG. 5—VIRTUAL HEIGHT VS FREQUENCY DURING SUNSET, APRIL 3, 1953

760 kc (*X*). Simultaneously, we also see this same level at the high frequency end of the record (*O*) after the critical frequencies of the lower strata are exceeded.

As sunset progresses, two critical frequencies (of traces labeled "*O*" and "*X*") decrease and the layer heights begin to increase. The reflection from this region will be referred to below as "the intermediate-level reflection," although a more convenient name is desirable. When it has been possible to witness the complete sunset effect, the critical frequencies decrease and the slope of the $h' - f$ curve increases until the entire region is more or less obscured by reflections from the lower levels (95-120 km).

The correctness of the labels "*O*" and "*X*" may be deduced from the following: The ordinary and extraordinary critical frequencies of a slowly-varying electronic layer are related by

$$\frac{f_{(o)}^2 - f_{(x)}^2}{f_{(x)}} = \text{a constant, } f_{(H)} \text{ (the gyromagnetic frequency)}$$

when both criticals are below the gyromagnetic frequency. Table 1 shows the relationships as scaled from three of the Figure 5 records.

The accuracy resulting from the difference of two squares is poor, but the deduced gyromagnetic frequency values are not unreasonable. Note that below the gyromagnetic frequency the ordinary wave has a higher critical frequency than has the extraordinary.

Figure 5 also illustrates the first appearance of *F*-layer below 1100 kc after sunset. Its virtual height was about 280 km, and the two components were obscured

TABLE 1

Time	$f_{(o)}$	$f_{(x)}$	Deduced $f_{(H)}$
			kc
19:00	1000	500	1500
19:15	750	310	1510
19:45	580	200	1480

by the intermediate-layer components labeled "*O*" and "*X*" in a way familiar to workers at the higher frequencies when observing the *E*-, F_1-, and F_2-layer traces. In other words, the ordinary obscured ordinary *F*, and extraordinary obscured extraordinary *F*, and the familiar cusps due to retardation in the lower layer are in evidence. However, there is one unexpected feature. This is a cusp in the *extraordinary F*-layer trace which is associated with, but not necessarily at exactly the same frequency as, the *ordinary* intermediate-layer cusp. These may be seen in Figure 5 at 19:15 and 19:45 at 700 kc and 650 kc, respectively. One more feature of interest in Figure 5 is the residual 105-km reflection. It is quite evident in the 19:00 record and suggestive at 19:15 and 19:45 that this region was also producing two reflections having critical frequencies C_1 and C_2 , but there were no cusps at their critical frequencies and the transitions from the 105-km reflections to the higher level were quite abrupt. This is to be expected from the fact that the 105-km trace shows no change of virtual height with frequency and was, therefore, from a layer of near zero thickness or a sharp boundary. For wavelengths of the order of 1 km, then, the region may not be "slowly varying" and some departure from the classical behavior might be expected. However, the assumption that C_1 is the ordinary-wave critical frequency and C_2 is the extraordinary-wave critical frequency leads to the deduced values of $f_{(H)}$, which are as reasonable as those deduced from the intermediate level "*O*" and "*X*".

The normal night recordings usually do not have the elaborate display of traces shown in Figure 5. A typical one is Figure 6, which also contains a corresponding record of polarization. The method of polarization recording is presented in a paper by E. L. Kilpatrick [10], but the following brief explanation may be sufficient for understanding the ellipses: Sample polarization ellipses are recorded on moving film during the sweep just often enough to give visual continuity. At the same time, a time base perpendicular to the direction of film travel for delineating virtual height is applied and the rectified pulse output of one channel is connected so as to turn the oscilloscope beam on for each echo and also for the initial transmitted pulse. Two sets of ellipses are recorded on the same film. The top set of Figure 6 is the conventional polar presentation, and the electric vector orientations are shown to the right of the film. The bottom set with the caption "phase ellipse," is the result of a sum and difference arrangement devised primarily to show the direction of rotation of the polar ellipse; that is, the sense of the downcoming polarized echoes. As indicated at the right of the film, an ellipse or line in the second and fourth quadrants is produced by an echo of left-handed polarization and an ellipse or line in the first and third quadrants is produced by a right-handed

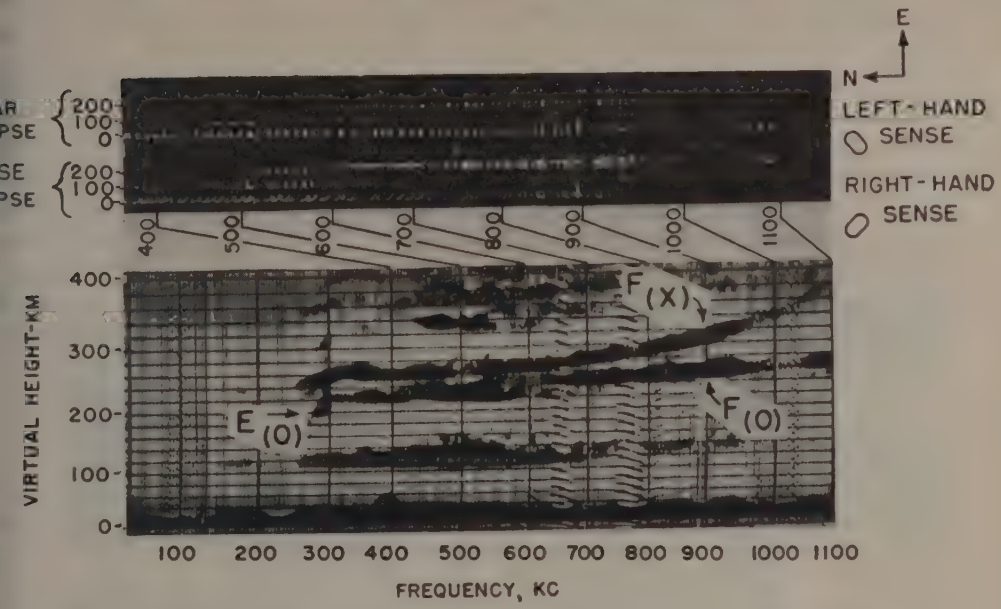

FIG. 6—VIRTUAL HEIGHT AND POLARIZATION VERSUS FREQUENCY, MARCH 12, 1953, 03:30 E.S.T.

echo. For a slowly varying layer in the northern geomagnetic hemisphere, these correspond, respectively, to ordinary and extraordinary echoes.

By careful matching of the traces of Figure 6, the following information can be deduced:

(1) The echo indicated by "$F_{(x)}$", extending from 260 to 1100 kc, was *F*-layer extraordinary echo
(2) The echo indicated by "$F_{(o)}$", extending from 530 to 1100 kc, was *F*-layer ordinary
(3) The echo at 105 km had left-hand sense

The "herring-bone" effect in the phase ellipses for the two *F*-layer traces is distinctive enough to readily suggest the conclusions (1) and (2).

Figure 6, in contrast with the sunset records of Figure 5, does not show much of the intermediate-level reflection for two reasons: (1) The critical frequency for that level was low; and (2) the 105-km reflection was stronger and less energy penetrated. However, the patch marked "$E_{(o)}$" is possibly the end of its ordinary-wave cusp, and there is a small amount of retardation evident in the extraordinary *F*-layer trace at about the same frequency, similar to the anomalous cusp in the extraordinary *F*-layer of Figure 5. It is unfortunate that lack of system sensitivity below 250 kc prevented a more complete record of that region.

The extraordinary *F*-layer trace of Figure 6 shows remarkable continuity down to a frequency of 260 kc, and other records have shown it to below 160 kc. This is due to the transparency of the lower regions to that component of the upgoing pulse energy producing a right-handed reflection. The ordinary *F*-layer trace, on

the other hand, is easily obscured by either a strong low-level reflection or a reflection of the ordinary wave from the intermediate level of reflection.

The transition at sunrise seems to be similar to that at sunset with one exception. The intermediate layer reforms as a separate and different entity from the residual of the old layer which was present during the night. On some series of records, the sunrise behavior indicates that a new group of ions grows quite clearly at the F-layer base level as soon as the exciting light from the sun touches the region. If there is a general absence of ionization below the F-layer, the new reflection shows a rapidly decreasing virtual height and increasing critical frequency as the whole region becomes ionized. One interval in the development is shown in Figure 7. Here, a reflection at a virtual height of 125 km appears from 700 kc, with

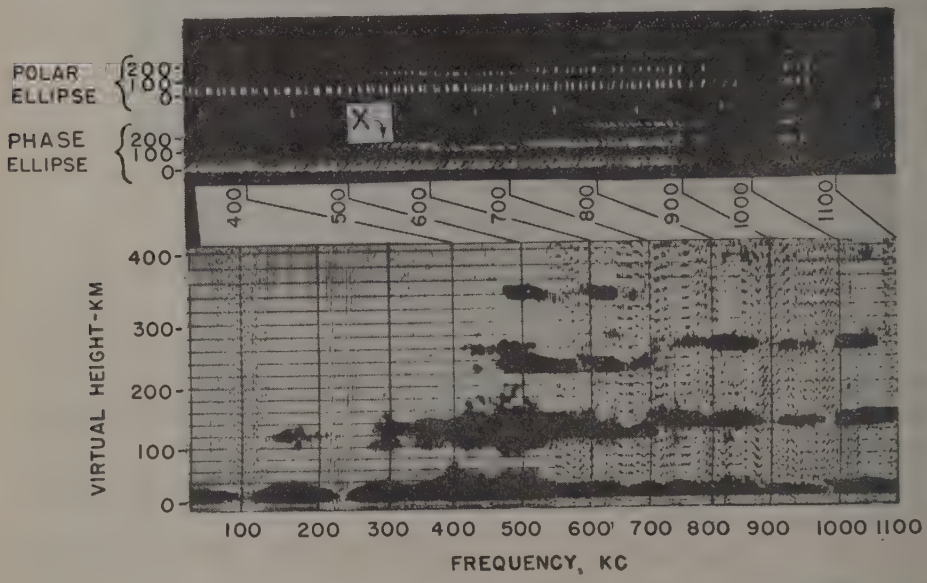

FIG. 7—VIRTUAL HEIGHT AND POLARIZATION VERSUS FREQUENCY, MARCH 12, 1953, 06:15 E.S.T., SHOWING SUNRISE TRANSITION

a critical frequency just above 1100 kc. Another reflection at 110 km has a critical frequency of 700 kc and appears to obscure the 125-km trace immediately below 700 kc. Some partial reflections appear between 300 and 530 kc at heights of 100 km and lower. However, between 500 and 600 kc, both 125- and 110-km reflections were recorded. A comparison with the polarization record shows definitely that the upper trace (indicated by "X" in Fig. 7) was extraordinary (right-handed) up to 600 kc, but all other traces were ordinary. Thus, again, at particular times, a phenomenon resembling classical magneto-ionic splitting may be observed at levels as low as 125 km. The fact that the two components are frequency selective in their amplitude characteristics suggests that their relative amplitudes may also vary with time when they are not resolved by the recorders, which would explain the changing of polarization patterns with time previously observed at 160 kc [5].

In general, the appearance of the night recording depends upon three factors, as follows:

(1) The amount of sporadic *E*
(2) The occurrence of intermediate-level reflections in the absence of strong low-level reflections
(3) The degree to which the *F*-layer ordinary and extraordinary reflections are recorded and their appearance

That these are not independent is illustrated in Figure 8. This rather unusual

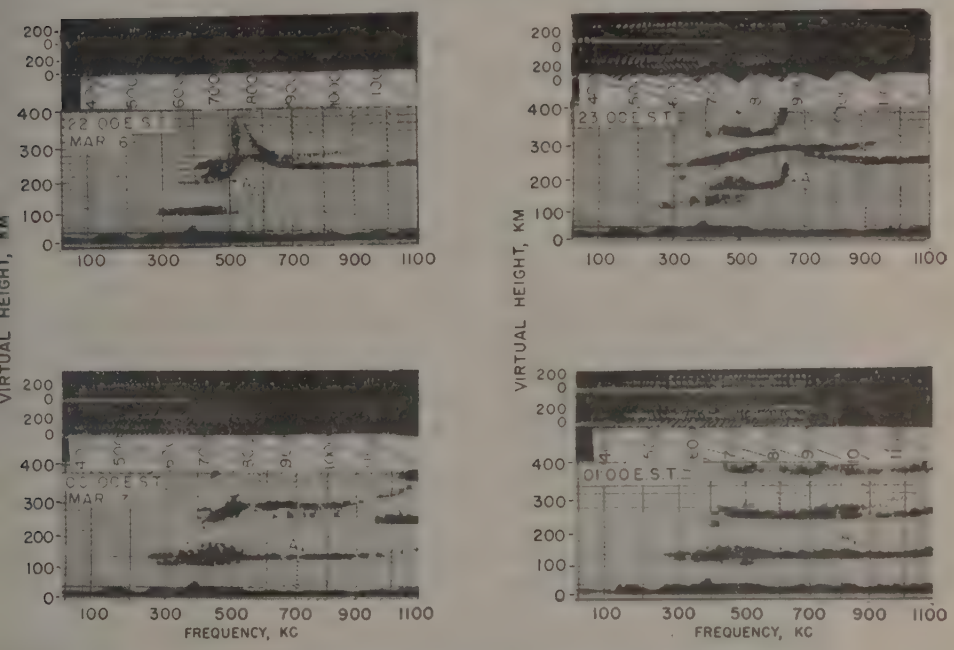

FIG. 8—VIRTUAL HEIGHT AND POLARIZATION VS FREQUENCY, MARCH 6-7, 1953, SHOWING TRANSITION OF INTERMEDIATE LAYER INTO SPORADIC E

series of records shows the appearance of an intermediate-layer trace, labeled "A", with a critical frequency of 520 kc and virtual height of 205 km at 22:00, and its subsequent change into sporadic *E* at a virtual height of 122 km and a maximum frequency above the range of the equipment. The entire process required about three hours and, while it is difficult to explain on a moving cloud basis, the concept of an ionizing agent coming from outer space is acceptable, since the sequence of gradual, but magneto-ionically selective, obscuring of the *F*-layer ordinary trace is almost ideal. Note that the trace "A" at 23:00 is from an excellent reflector for energy-producing ordinary-wave excitation, since a multiple is recorded, yet the medium is almost completely transparent to energy producing extraordinary-wave excitation of the *F*-layer. This is borne out by the polar ellipses, which are almost circular. The anomalous retardation in the extraordinary *F*-layer

trace near the ordinary cusp of trace "*A*" is nearly absent in this series of records. The "*A*" traces at 00:00 and 01:00 show little change of height with frequency, and at 01:00 the phase ellipse shows a cycle variation of orientation with frequency which has been noted to be characteristic of sporadic "*E*"-echoes. The explanation for this is not clear, but it could be caused by a combination of two echoes with non-identical frequency *versus* phase characteristics. Figure 8 is not intended to

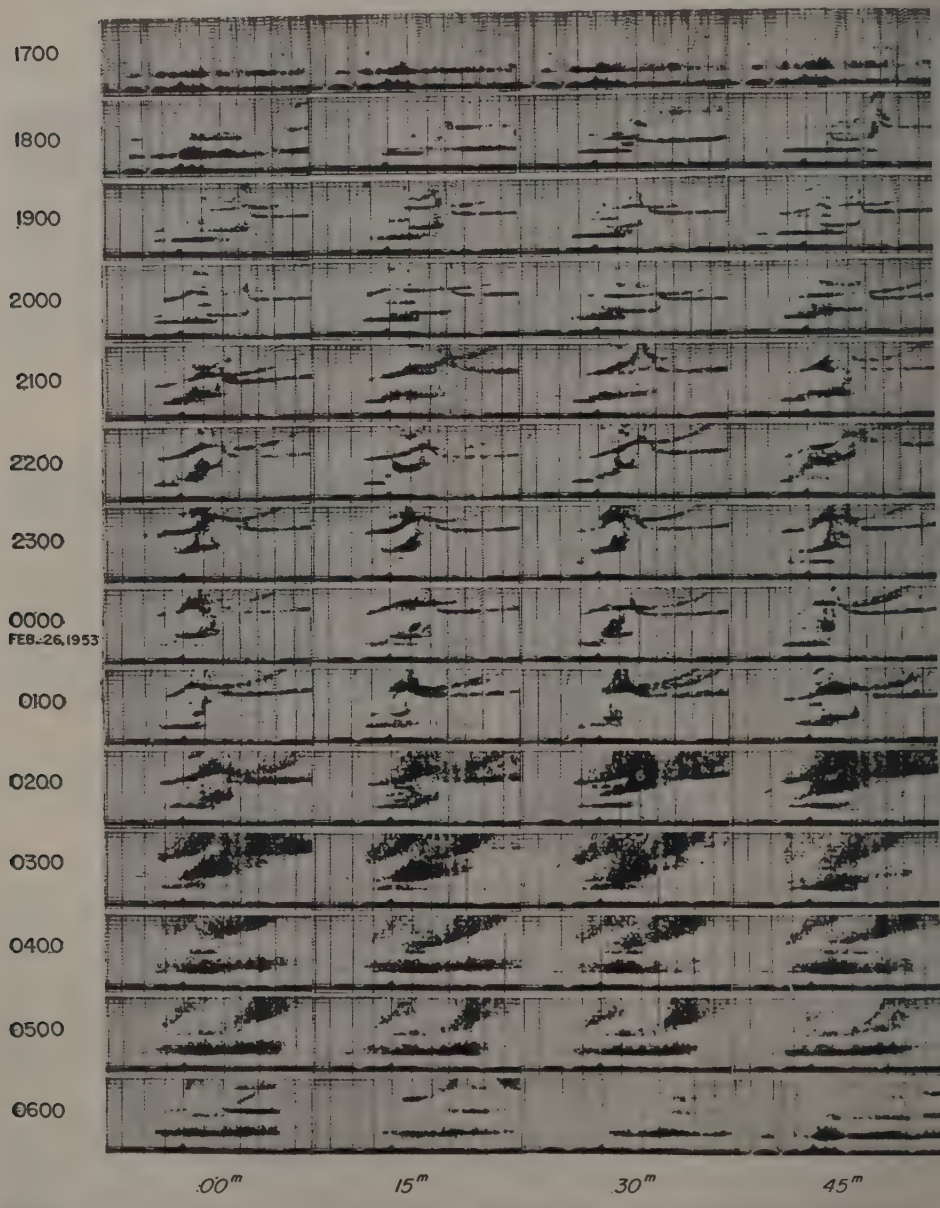

FIG. 9—ALL RECORDS, NIGHT OF FEB. 25-26, 1953, SHOWING INTERMEDIATE LAYER AND SPREAD ECHOES

illustrate the usual formation of a sporadic E-layer. The more common type produces records very similar to those at 00:00 and 01:00, but the sporadic E suddenly appears at the 100- to 130-km, level, as separate and distinct from the residual nighttime E which has a critical frequency of 400 to 600 kc.

4. EFFECTS OF IONOSPHERIC DISTURBANCES

The effects of ionospheric disturbances are quite apparent at night [7]. As an illustration, the records of Figure 9 were made during a moderately severe disturbance (I—Figs. 4 and 6 from CRPL F-Series publication). They show unusually complicated traces, especially those of the intermediate layer, and low critical frequencies and spread echo in the F-layer. From 03:00 to 06:00, practically no trace was recorded on the high-frequency ionosphere recorder used for regular measurements at the Fort Belvoir field station of the Central Radio Propagation Laboratory. The intensities and shapes of all traces were quite variable, and the anomalous retardation in the extraordinary F-layer trace by the intermediate layer was present to a varying degree on many of the records.

5. MEASURED CHARACTERISTICS

Figures 10, 11, 12, and 13 are the results of the first attempts to assign numerical values to characteristic features of the recordings. Lowest observable heights have

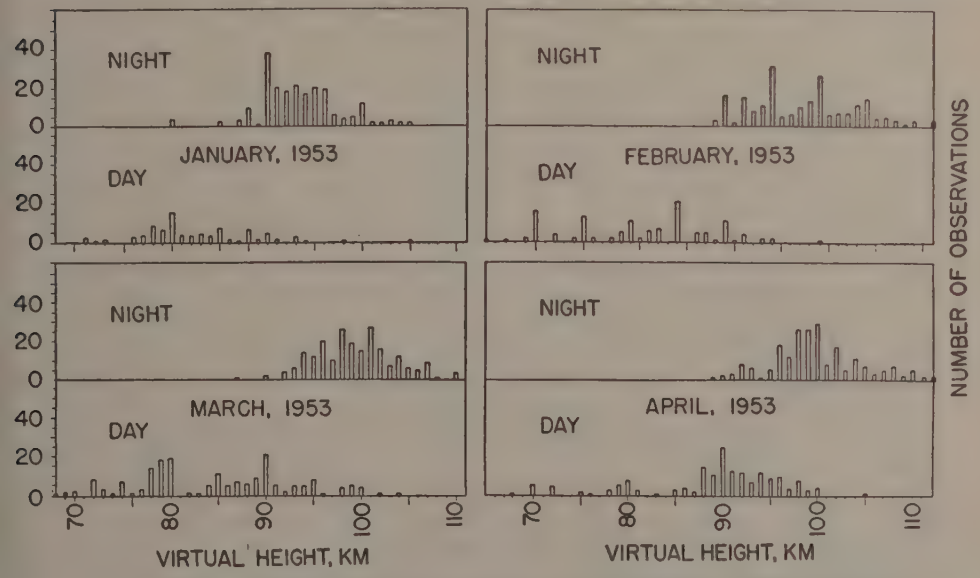

FIG. 10—LOWEST RECORDED HEIGHT HISTOGRAMS, DAY AND NIGHT

been recorded for four months in Figure 10. These usually are seen in the frequency range 400 to 500 kc, where the signal to noise ratio is best. The histograms contain all readings of lowest height, which were estimated at 1-km intervals. That this accuracy of ± 1 km was not achieved is evident, since the usual errors of personal judgment appear; that is, favoring even numbers, multiples of five, and avoiding

such numbers as 81. The plots were separated for night and day values to avoid too much mixing of different phenomena, and the sunrise and sunset transitions were eliminated for the same reason. At first view, the night values seem to have a progressive shift from 90-95 km in January to 98-100 km in April. A check of the operating log, however, indicates that a diurnally switched receiver-gain control was installed about January 23, 1953, and experimentation with different receiver sensitivities has shown that the 90-km boundary at night is recordable only with the highest sensitivity. The January plot, therefore, must be regarded in a different way from the other three. It is probably significant that the occurrence of values below 90 km is very rare during the night, as if the 90-km level were a very dependable night minimum height, but capable of giving only weak echoes at vertical incidence. The February night values are difficult to explain. The tendency to scale in multiples of five is quite evident, and the prominent maximum at 95 km does not appear in the other months. March and April data both show rather

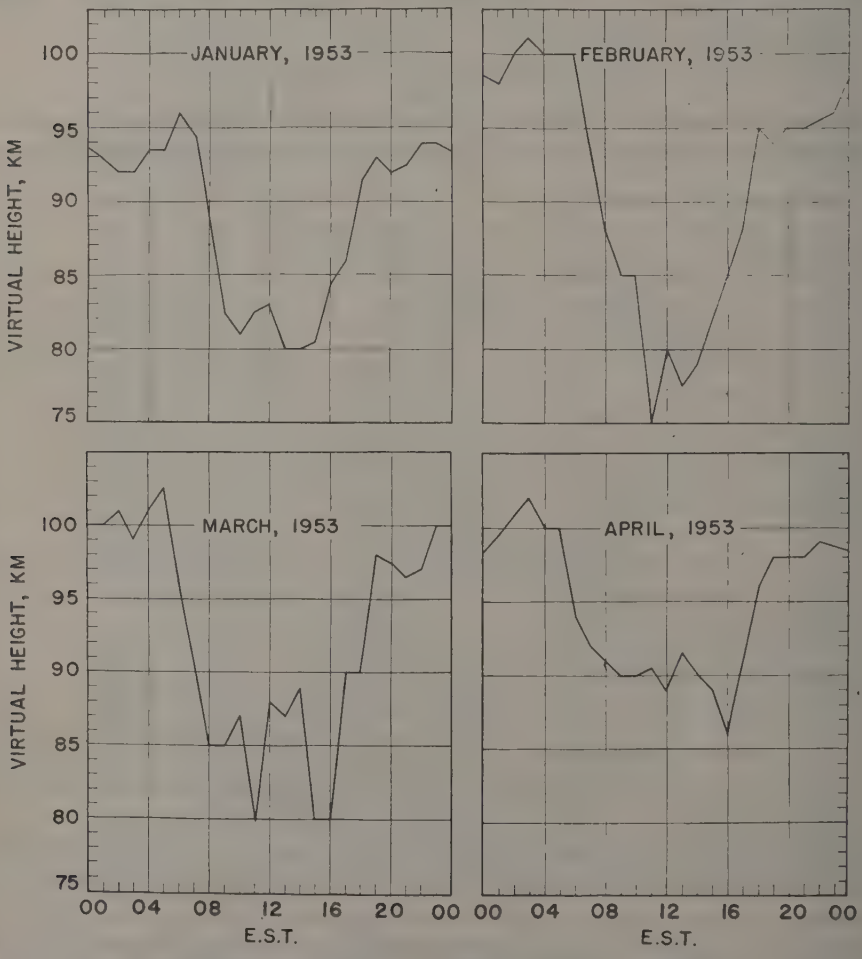

FIG. 11—HOURLY MEDIAN VALUES, LOWEST RECORDED HEIGHT

simple distributions with maxima at about 99 km and practically no values below 90 km.

Daytime values of observed minimum height may be expected to have considerable spread due to the great variability of echo intensity from the different levels with time (Figs. 2, 3, and 4), and Figure 10 verifies this. Here again, February data do not seem to fit in with the other months. Seventy-kilometer heights were recorded 16 times during that month, and four entries were below 70 km. The other months have clusters at 70, 80, and 90 km, and it appears that most readings will be near 90 km as summer advances because the lower level reflections will be too weak to record.

Figure 11 contains hourly median values of the data from Figure 10 with the addition of the sunrise and sunset periods. It is subject to the same limitations in interpretation.

Figure 12 contains hourly median values of all strata associated with the

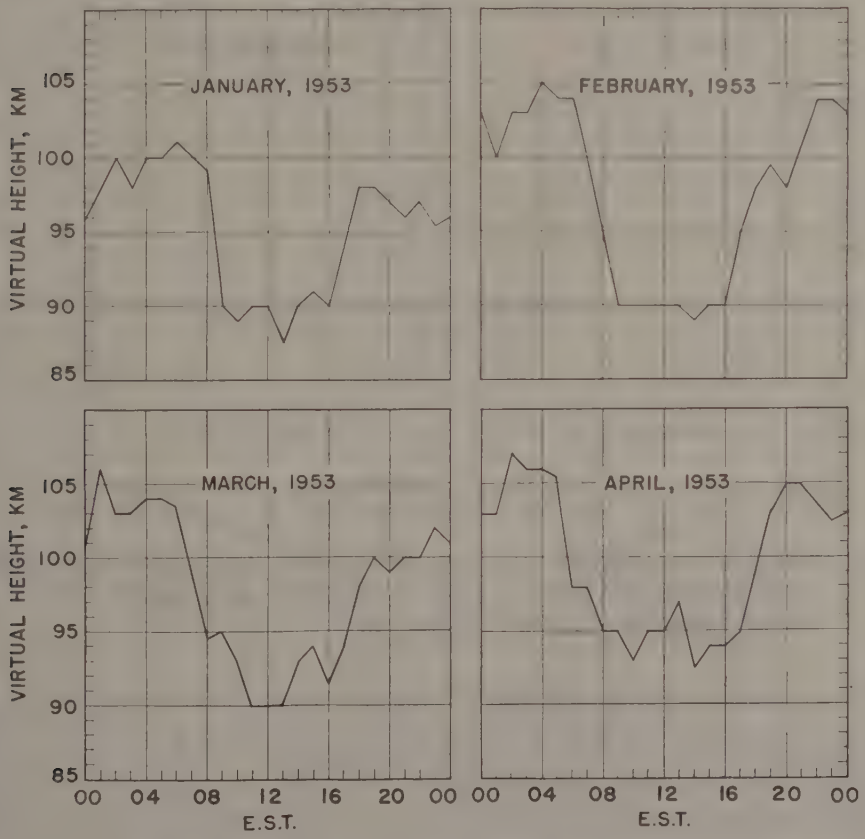

FIG. 12–HOURLY MEDIAN VALUES, E-REGION HEIGHTS

E-layer, excluding data for the intermediate level, which was arbitrarily assumed to be above 140 km. As an example, for the record of Figure 2, values of 90, 108, and 120 km would be recorded. The month's median for that hour would then in-

clude the effects of all strata in determining which level was recorded most often.

Figure 13 contains hourly median values of two more characteristics, the minimum frequency at which the F-layer ordinary ray was recorded and the maximum frequency at which any reflection occurred in the region below 140 km. The two characteristics might be expected to be identical, since the low-level

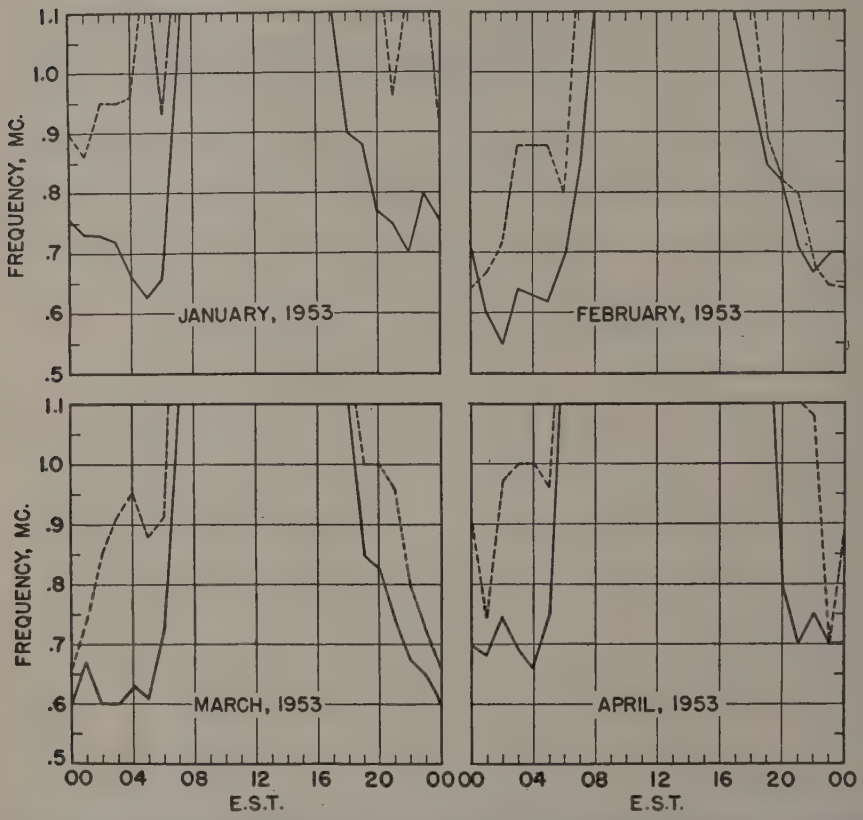

FIG. 13-HOURLY MEDIAN VALUES, F-LAYER MINIMUM FREQUENCY OF ORDINARY RAY; ALSO E-REGION MAXIMUM FREQUENCY (DASHED LINES)

reflection usually obscures the F-layer ordinary trace, but it often was of a sporadic E-type which was not wholly opaque, similar to the "fringe" type of sporadic E seen at high frequencies. For this reason, the E-region medians are consistently higher than the F-layer minimum frequency medians and the difference is a measure of this fringing effect. It should be pointed out that these are the only data available on nighttime E-region critical frequencies in the United States, except those from the pioneer sweep-frequency ionosphere recorders of the Carnegie Institution of Washington, Department of Terrestrial Magnetism, and the Model-B equipment of the National Bureau of Standards. The lower limit of some of these machines was 500 kc, but the power output was low, their definition was limited by the

galvanometers used to record the reflected pulses, and the time of sweep was as long as 15 minutes, which tended to distort patterns which changed much in that length of time.

6. CONCLUSION

The presence of the intermediate-level reflection has been noted at fixed frequency. Workers at The Pennsylvania State College have called it "the 150-km, or sporadic, echo." It has, no doubt, been the cause of unexplained echoes, such as part of the changing pattern of Figure 1. The conclusion from sweep-frequency observations must be that this echo at 160 kc is probably either the extraordinary or the ordinary ray from the intermediate level. The degree of transparency that the lower regions have for its energy determines whether or not it may be recorded. In addition, its critical frequency varies in a manner which is at present unknown, and in at least one instance (Fig. 8), the whole layer seemed to form at a high height and gradually descend to form a sporadic *E*-layer. These conditions tend to make its appearance unpredictable, although, of course, it can appear only at night. The continuity of the intermediate-level reflections with the daytime *E*-layer during the sunrise and sunset transitions infers that it is, in fact, the nighttime *E*-layer and that the two reflections occasionally received from it, such as "*O*" and "*X*" in Figure 5, correspond to the familiar conditions for magneto-ionic reflection. The occasional retardation in the extraordinary *F*-layer trace, which appears to be associated with the ordinary critical frequency of the intermediate-level reflection, is at present anomalous.

Assuming that the foregoing assumptions are correct, the low-level (70-140 km) reflections must be considered in a different way. There are two distinct possibilities. The first possibility is that they result from heretofore obscure conditions for reflection in the lower part of the *E*-layer where collision rates are high and gradients are steep. These conditions, if they exist, might not necessarily require a separate "layer" to explain the low-level reflections, at least at night. The second possibility is that the low-level reflections result from at least one separate layer or boundary which at night is quite thin—perhaps even approaching a wavelength at some frequency within the sweep range. It is apparent from the sweep-frequency records that its change of virtual height with frequency is almost zero until a discrete increase to the next level occurs. This is true in the day as well as at night. The last discrete increase in the daytime, however, is to the region which, on further increase in frequency, shows a retardation cusp and then the regular *E*-layer critical penetration frequency. If the intermediate-level reflection is included in the sequence, this same order prevails at night, but only on special occasions when the low-level reflections do not obscure the intermediate level. The nighttime low level appears to be similar to sporadic *E* in its characteristics, except that a genuine instance of high frequency sporadic *E* at night is often seen as a separate trace on the low frequency record with a separate, distinct, virtual height.

The authors do not intend to advocate the use of sweep-frequency techniques for all phases of low frequency experimentation. They are obviously of no use at very low frequencies where it is virtually impossible to design wide band antennas of practical size. They also are not suited for measuring quantities such as absorp-

tion and polarization with a high degree of accuracy when these quantities vary with time, since the frequency change superimposed upon the other variations would cause useless complication. However, it is believed that the technique is as valuable to low frequency research as it has been in helping to understand complex regions at high frequencies. The following phenomena appear to be subject to analysis using the low frequency data now on hand and will be treated in subsequent papers:

(1) Relationships between the nighttime intermediate-level ionization and magnetic storms
(2) Further study of the intermediate level and its relation to the other regions
(3) Relationship between ionization in the 70- to 140-km region and meteors during the night hours
(4) *F*-layer critical frequencies when they are below 1100 kc.

References

[1] J. E. Best, J. A. Ratcliffe, and M. V. Wilkes, Experimental investigations of very long waves reflected from the ionosphere, Proc. R. Soc., **156**, 614-633 (1936).
[2] R. A. Helliwell, Ionospheric virtual height measurements at 100 kilocycles, Proc. Inst. Radio Eng., **37**, 887-889 (1949).
[3] A. H. Benner, C. H. Grace, and J. M. Kelso, Polarization of low frequency radio waves reflected from the ionosphere, Proc. Inst. Radio Eng., **38**, Correspondence, 951-952 (1950).
[4] J. N. Brown and J. M. Watts, Ionosphere observations at 50 kc, J. Geophys. Res., **55**, 179-181 (1950).
[5] E. L. Kilpatrick, Polarization measurements of low frequency echoes, J. Geophys. Res., **57**, 221-226 (1952).
[6] J. M. Watts, A note on the polarization of low frequency ionosphere echoes, J. Geophys. Res., **57**, 287-289 (1952).
[7] J. M. Watts and J. N. Brown, Effects of ionosphere disturbances on low frequency propagation, J. Geophys. Res., **56**, 403-408 (1951).
[8] J. C. Blair, J. N. Brown, and J. M. Watts, An ionosphere recorder for low frequencies, J. Geophys. Res., **58**, 99-107 (1953).
[9] D. K. Bailey, *et al.*, A new kind of radio propagation at very high frequencies observable over long distances, Phys. Rev., **86**, 141-145 (1952).
[10] E. L. Kilpatrick, A technique for making sweep frequency measurements of polarization in the range from 50 kc ot 1100 kc, to be published.

CORRELATION OF MAGNETIC, AURORAL, AND IONOSPHERIC VARIATIONS AT SASKATOON—PART 2

BY J. H. MEEK*

Physics Department, University of Saskatchewan, Saskatoon, Saskatchewan, Canada

(Received November 2, 1953)

ABSTRACT

The relations between magnetic, auroral, and ionospheric observations are summarized with reference to the occurrence of positive and negative magnetic bays. Auroral light associated with positive bays occurs at a higher geomagnetic latitude than that associated with negative bays. The magnetic and auroral light variations are compared to Martyn's theory of the aurora. If the latter is accepted, the conclusion is reached (1) that most aurora is caused by positively charged particles, and (2) that the conditions described for the early phase actually exist throughout most of a disturbance.

INTRODUCTION

Since submission of the first paper under the above title [see 1 of "References" at end of paper], a considerable amount of additional information has been acquired. The present paper summarizes the previous observations and expands the material on early evening variations, especially those connected with positive magnetic bays.

Data accumulated during the last two years include (1) continuous records of three components of the earth's magnetic field (H, D, and Z); (2) vertical incidence and northerly directed ionosonde records, made at 20-second intervals throughout the night, and covering ranges up to 800 km and frequencies between 1 and 18 Mc/sec; and (3) records of amplitude of auroral light intensity, made by a photoelectric device, scanning from the northern to southern horizon along a magnetic meridian at 10-minute intervals.

COMPARISON OF OBSERVATIONS

Statistical treatments, of the type carried out in the past, mask many of the significant related effects. On examining in detail the recorded variations throughout individual nights, definite relationships between the different types of observations are quite evident. Due to the overlapping of the disturbance effects, no one night will show all the main features.

In order to simplify the presentation and to show the more typical patterns

*The author is on the staff of the Defence Research Board, Radio Physics Laboratory, and is seconded to the University of Saskatchewan for this work.

clearly, an idealized set of observations is depicted in Figure 1. A detailed explanation of this type of diagram was given in Part 1 of this paper [1].

It is clear from the Figure that the ionospheric and auroral light observations may be related directly to the observed changes in the H component of the earth's magnetic field, and in particular to the occurrence of positive and negative magnetic

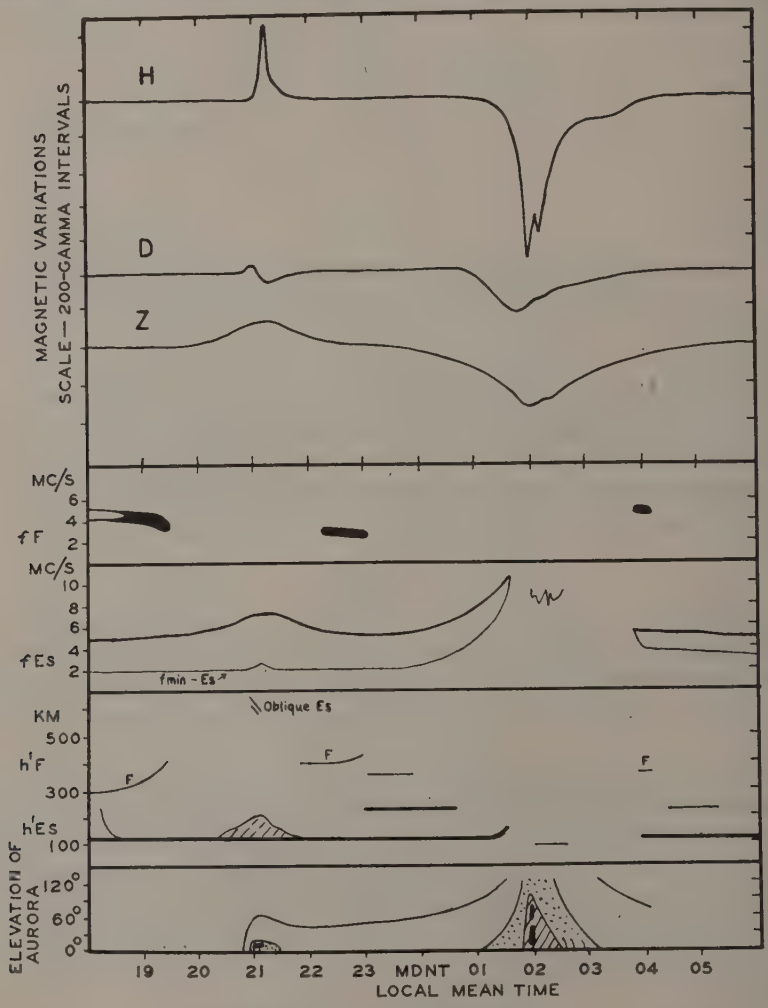

FIG. 1—AN IDEALISTIC GEOPHYSICAL DISTURBANCE AT SASKATOON

bays (increases and decreases, respectively, in H). The following points are worth noting.

(*a*) The occurrence of a negative bay on a particular night is not necessarily preceded by a positive bay, although a negative bay almost always follows a positive bay.

(*b*) The duration of a positive bay is less than one hour; that of a negative bay is usually less than two hours.

(*c*) The local times of most frequent occurrence of positive bays are centered around 8 p. m.; those of negative bays around 2 a. m. This differs considerably from the 6 p. m. and 6 a. m. times of the Chapman-Martyn model [2] for geophysical disturbances.

(*d*) The time of change-over from positive to negative bays is nearer to 10 p. m. than to midnight.

(*e*) On very disturbed nights, a number of bays may occur, often overlapping. These bays appear to exist independently of each other. There is no clear evidence that the same bay repeats at 24-hour intervals, as has been suggested in the past [3, 4]. The inference is that each bay, positive or negative, is due to a separate group of particles entering the ionosphere in the auroral zone. The general geomagnetic disturbance is made up of a great many bay-type disturbances, which collectively may be world-wide, but individually are localized, the individual effects being confined to a band that is probably less than 1,000 km in length along the auroral zone.

(*f*) There have been few very severe geomagnetic disturbances during the past two years; consequently the conclusions in this paper are based on slight and moderate disturbances.

MAIN FEATURES CONNECTED WITH A POSITIVE BAY

Ionosonde measurements show spreadiness of the *F*-region echoes in the afternoon or early evening of a disturbed night (some hours before the occurrence of the first positive bay). Then the sporadic *E*-region echoes become more prominent and soon obscure the *F*-region. They increase in intensity up to the time of the bay.

At the start of the bay, as the value of *H* begins to increase sharply, a bright auroral arc appears at an elevation usually not more than about 10° above the northern horizon and often west of the magnetic meridian. Coincident with this aurora, long-range echoes (400 to 800 km) are observed sporadically on frequencies between 10 Mc/sec and 18 Mc/sec. Observations with a north-pointing rhombic antenna indicate that these echoes are from the same part of the sky as the auroral light [5]. As the magnetic field returns towards normal, the intensity of the aurora decreases and its structure is more diffuse.

Throughout the course of the bay, the maximum reflection frequency of the sporadic *E*-region shows some increase; a slight temporary increase of *D*-region absorption is evident; the position of the auroral display is relatively constant during a positive bay. On a few occasions, it has appeared at a certain elevation in the sky and subsequently moved northward.

Again, during the course of the bay, a few records examined in detail show that the magnetic disturbance vector rotates once in an anticlockwise direction, agreeing with McNish [6]. This would be equivalent to a concentrated group of negative charge moving eastward along the auroral zone. The direction of the vector usually is in a nearly horizontal plane, corresponding to an ionospheric current much closer to the zenith than the auroral light visible during the bay. This is true even after making the usual adjustments for the effect of induced currents in the earth [6].

MAIN FEATURES CONNECTED WITH A NEGATIVE BAY

Several hours before the commencement of a large negative bay, the sporadic E-region echoes become more solid, the top reflection frequencies show retardation and "z", "o", and "x" ray separation to their respective critical frequencies. The region becomes more uniform and of appreciable vertical thickness. Multiple reflections between the layer and ground are usually observed. There is not much abnormal absorption of high frequency radio waves until the H component of the magnetic field starts dropping at the beginning of a large negative bay. Faint aurora is usually seen in the north during this period and, as H drops, auroral curtains and bands are seen to higher elevations. In contrast to the case of a positive bay, the maximum elevation of aurora above the northern horizon may be roughly related to the amount of change of H. A drop in H of 100 gammas corresponds to a maximum elevation of about 60°, while a drop of 200 gammas indicates aurora overhead.

The intensity of the auroral light is related to the rate of change of H, as in the case of the positive bays. For small negative bays, the equivalent current system indicates a negative charge moving westward (clockwise rotation of the disturbance vector). For the larger bays—more than about 300 gammas drop in H— the same rotation predominates but is less sharply defined. This is probably due to the presence of currents on both sides of the zenith.

During that part of a large negative bay when H is several hundred gammas below normal, no high frequency radio echoes from above 100 km are observed. Since this is the period when auroral light is overhead, it appears logical to associate the D-region radio-wave absorption with the base of the auroral light, which is also just below the 100-km level.

Both the auroral light and the radio-wave absorption region persist after the peak of the magnetic bay is long past. The former becomes diffuse and patchy, while the latter breaks up, allowing occasional reception of high frequency echoes from the E- or F-regions.

COMPARISON WITH MARTYN'S THEORY

Martyn's theory of the aurora [7] assumes that the auroral zone is a band some 5° latitude in width. Auroral effects are due to precipitation along the magnetic lines of force of positively and negatively charged particles from an equatorial ring-current, approximately five earth radii out. During the early stages of a disturbance and in the afternoon and early evening, the positively charged particles tend to come down at the northern edge of the auroral zone, while the negative particles come down at the southern edge of the auroral zone. After midnight, the situation is reversed, with the positive particles at the southern edge and the negative particles at the northern edge. In the final stage of the disturbance, the latter is thought to prevail both evening and morning.

If this theory is accepted, realizing, of course, that it is actually based on statistical information and not upon individual disturbances, we can apply it to our present observations with the following results.

Auroral light is produced along the outer (northern) precipitation surface in the early evening, but not usually along the inner surface. In the morning, the

conditions are reversed and the auroral light is produced along the more southerly surface. The observed variations in magnetic field can be accounted for if it is assumed that drift currents are set up along both surfaces, although light may be observed along only one.

Some observations made over a period of a year in 1948-49, at Portage la Prairie (59° north geomagnetic latitude) and at Baker Lake (75° north geomagnetic latitude) [8], showed that statistically the auroral light was observed more frequently north of Baker Lake in the evening than in the morning, while at Portage la Prairie the reverse was true. It may also be noted that during this same period there was definite evidence of a double peak of occurrence of auroral light (at approximately 65° north and 68° north geomagnetic latitudes), throughout the night.

It would appear then that the auroral light in the evening connected with positive bays is on the northern side of a Martyn-type auroral zone, while in the morning the auroral light connected with negative bays is on the southern side. Following Martyn, both of these would be the result of positively charged precipitation.

During moderate disturbances, it has been shown clearly that the auroral light expands or at least extends southward during the growth of a negative magnetic bay. It now appears likely that in the evening the aurora connected with a positive bay expands or extends northward from a higher geomagnetic latitude. Calculations show that the electric currents producing the magnetic field variations exist at both sides of the auroral belt, although light is produced mainly at one or the other edge. It is concluded that higher energy than exists in slight or moderate disturbances is required for the appearance of auroral light due to precipitation of negatively charged particles. Consequently, auroral light due to the latter may be expected only during severe disturbances.

Positive bays may be observed on any day during a long period disturbance. This indicates that the model proposed for the early phase actually carried on through most of the disturbance, while the final phase or decay, if present, is of fairly short duration. This can be reconciled if it is assumed that the disturbances being observed are actually due to separated packets of incoming particles. Martyn's model was designed to describe the course of a very severe geophysical disturbance, in which the incoming particles are in a lasting, more or less continuous stream.

ACKNOWLEDGMENTS

This work has been carried out as a project of the Radio Physics Laboratory, Defense Research Board of Canada. The author wishes to express his appreciation of the assistance and encouragement given by Dr. B. W. Currie and other members of the Department of Physics, University of Saskatchewan.

References

[1] J. H. Meek, J. Geophys. Res., 58, 445-458 (1953).
[2] S. Chapman and J. Bartels, Geomagnetism, Oxford, Clarendon Press, 1, 310 (1940).
[3] S. Chapman and J. Bartels, Geomagnetism, Oxford, Clarendon Press, 1, 340 (1940).

[4] H. W. Wells, Terr. Mag., **52**, 315 (1947).
[5] J. H. Meek and A. G. McNamara, to be published in Can. J. Phys., June 1954.
[6] A. G. McNish, Trans. Amer. Geophys. Union, 17th Ann. Meet., Pt. I, 166 (1936); Terr. Mag., **43**, 67 (1938).
[7] D. F. Martyn, Mixed Commission on Ionosphere, International Council of Scientific Unions, Proc. of Second Meeting, Brussels, Sept. 4-6, 1950, pp. 49-56 (1951).
[8] J. H. Meek, Defence Research Board, Radio Physics Laboratory, Rep. No. 6 (Aug. 1950).

WINDS IN THE UPPER ATMOSPHERE DEDUCED FROM THE DYNAMO THEORY OF GEOMAGNETIC DISTURBANCE*

BY E. H. VESTINE

Department of Terrestrial Magnetism, Carnegie Institution of Washington, Washington 15, D. C.

(Received August 7, 1953)

ABSTRACT

Average features of geomagnetic disturbance are represented by atmospheric-electric current-systems. These cannot be uniquely inferred from the magnetic observations at ground level. Using the Balfour Stewart dynamo theory, these electric current-systems are then tentatively replaced by equivalent atmospheric wind-systems, using order of magnitude calculations. It is found that these supposed wind-systems will differ in accordance with the degree of electric polarization of the atmosphere, and with the intensity of toroidal or solenoidal electric currents likely to be present, as a consequence of zonal winds.

A simple monthly mean wind-system of geomagnetic disturbance shows good general agreement with a wind-system derived by Kellogg and Schilling from meteorology. A qualitative version of a possible wind-system for the main phase of a magnetic storm is derived and found to show some measure of agreement with diurnal features of atmospheric motions deduced from radio-star scintillations and auroral motions.

The causes of such wind-systems, and the effective transverse conductivity of the atmosphere, are briefly but inconclusively discussed. It is shown that the flux of X-rays producing ionization of the *E*-region is apparently the same on days of magnetic storm as on days prior to the storm, and that the dynamo air-flow at the *E*-region yielding the quiet-day diurnal variation also appears inappreciably affected by the presence of a magnetic storm.

I. INTRODUCTION

In 1882, Balfour Stewart proposed that the geomagnetic variations might be due to electric currents in the atmosphere, produced by motion of electrically conducting air across the lines of force of the geomagnetic field [see 1 of "References" at end of paper]. The theory for the quiet-day diurnal variation was developed

*In part an invited discussion prepared for the Conference on Atmospheric Motions, September 7-9, 1953, at Albuquerque, New Mexico.

by Schuster [2], and extended by Chapman [3] in an extensive memoir in 1919. Meanwhile, Kennelly [4] and Heaviside [5] had postulated a conducting layer as early as 1902. Chapman suggested in his 1919 paper that there was probably more than one ionized layer in the atmosphere. The height of the first of these layers was then found in the Appleton and Barnett [6] and the Breit-Tuve experiments in 1925 and 1926 [7], and later experiments by many workers soon greatly clarified, or at any rate exposed, the complicated electrical state of the upper atmosphere. These activities were markedly accelerated after about 1940, because of the importance to radio-wave propagation.

The vast volume of new observational material has provided estimates of the electrical conductivity of the atmosphere contributed by electrons and positive ions. However, little information has yet been forthcoming about the contribution of negative ions, though the present view suggests that they are unimportant [8]. Consequently, radio techniques have been indicative of the lower limit of integrated conductivity (with a good chance of a fair approximation to the actual value) for the various ionized regions. On the other hand, radio methods have shown also that the apparent oscillations in the upper atmosphere were much larger than had been originally supposed. Although the augmentation above that for the oscillation at ground level was considerable, the lower limit of conductivity from radio methods was at first computed to be too small to confirm the dynamo theory experimentally, though it now seems possible that suitable electric polarization suffices [9, 10]. Moreover, the height of one region of interest has been found by a direct rocket experiment [11].

In recent years, there has been much renewed interest in dynamo theories of the upper atmosphere. One such study by Wulf [12] has provoked some discussion of the possibility that practically all except secular geomagnetic variations are due to winds in the upper atmosphere, including magnetic storms, magnetic bays, and aurora. Wulf also brought into the foreground the possibility that the experimentally determined winds in the stratosphere were correlated with the motions of electrically conducting air in the upper atmosphere. His actual studies of data were limited mainly to North America, so that, although he showed that many of his ideas were plausible enough, he did not succeed in clarifying them fully in terms of the detailed observations. However, his work has been timely in emphasizing three things; namely, the importance of solar radiation in feeding heat engines of the atmosphere, the fact that turbulence and Reynold's numbers would have to be considered in the upper atmosphere, and finally the expectation of zonal wind-belts at different levels. He also revived interest in some quarters in the old ultraviolet theory of magnetic storms and aurora proposed by Hulburt and Maris [13] (and its modern variations), which had been attacked rather vigorously by McNish [14], and by Chapman and Bartels [15]. However, even today it must be admitted that a great deal of the spirited discussion of such matters is carried out on the basis of a rather obscure experimental background and relates to ideas which at present are immature.

Accordingly, at the present time, there are a few students who are hopeful that magnetic storms can be explained by winds in the upper atmosphere. Harang [16] has discussed geostrophic winds in this connection, and Bartels [17] has called

further attention to the matter. Chapman and Ferraro [18], and Martyn [19], are hopeful that their incomplete corpuscular theory will eventually suffice, for both magnetic storms and auroras. However, it is not unlikely that they will be willing to include also a dynamo theory based on atmospheric winds to explain those effects which their corpuscular theory may fail to demonstrate. There have, in fact, already been signs of this. Chapman in 1919 [20] considered compressions and expansions of the atmosphere as the cause of magnetic storms, and in 1927 and again together with the writer in 1938 [21] noted that an atmospheric circulation of the harmonic type P_2^1 could have a rôle in the production of the "diurnally varying" part D_S of storms, and this possibility has recently been considered in some detail by Fukushima [52]. Corpuscular theories possess also other evidence of flexibility, as exemplified by Alfvén's outline of such a theory, including an electric-discharge theory of aurora [22] and a recent plasma theory of aurora due to Lebedinski [23].

The advocates of corpuscular theories were considerably cheered recently when Gartlein [24] and Meinel [25] detected effects of protons in auroral spectra, and Meinel measured components of their incoming velocities by Doppler effects. To date, those who believe the ultraviolet theory has been unduly maligned have not come forward with the statement that these incoming protons are evidence of the runaway atoms of Hulburt and Maris moving along the geomagnetic field, perhaps because their terminal velocity would be too low to penetrate to the E-region and below. They may also have a possibility of linking this effect to the recent theory and observations ascribing the zodiacal light to the very high concentration of about 600 electrons (and positively charged particles) per cm^3 outside the earth. Siedentopf's suggestion is that the supply is from the extension of the solar corona to the earth [26]. A check seems afforded by radio whistlers (verbal comment by J. A. Ratcliffe).

It is accordingly desirable to consider briefly the rôle of winds in the atmosphere in relation to ionospheric, magnetic, and auroral phenomena. In recent years, radio techniques have afforded estimates of the motion of electric charges at various levels or heights in the ionosphere, principally in Europe, North America, and Australia [27, 28, 29, 30, 31, 32, 33], though it is not yet quite clear that the motions of electric-charge concentrations describe the winds that carry the greatly preponderant neutral atoms and molecules there.* So far, there is considerable evidence of highly systematic motion. There is also evidence at times suggestive of turbulence. Finally, a rather dominant effect is in evidence, that of zonal motion, reminiscent of the suggestions of Wulf [12] and of Kellogg and Schilling [34], as well as of the early formal studies of winds in general by Jeffreys [35]. But it has not yet been possible to interpret the now numerous observations (at only a few points) in terms of the wind-system required for the dynamo theory of the magnetic diurnal variation, perhaps because of vertical gradients in the zonal winds estimated by fixed radio-frequency measurements. This, of course, raises the question as to what part of the supposed winds may contribute nothing to an actual electric

*Recent brilliant experiments reported by Whipple and Millman, on the motions of trains of meteors at the "Conference on Atmospheric Motions," l.c., confirm many of the indications of the radio data.

current-system, or to current-systems other than that of the diurnal variation. For instance, current-systems associated with magnetic disturbance may be present.

As a first approach, it may be desirable to consider only those current-systems which may be specially simple. Accordingly, in the present paper, there will be considered at first only those cases in which the lines of current-flow are perpendicular or along the geomagnetic field. In this case, only the conductivity perpendicular to the magnetic field may need consideration. Accordingly, the dynamo theory for an isotropic medium may be successful, and the wind-systems may also have a desirable simplicity. If under these conditions there be considered only the daily mean winds, the longitudinal variation in transverse conductivity can, at least initially, be replaced by the conductivity averaged along parallels of magnetic latitude. Of course, this procedure restricts comparisons with observed winds to daily mean, monthly mean, and seasonal wind-changes and current-systems.

The present paper aims only to discuss the possible rôle of winds in relation to geomagnetic disturbance, on a rather broad basis, using order of magnitude calculations. The immediate purpose is to roughly deduce the wind-systems required to produce magnetic storms, so that experimental measures of ionospheric winds can then be used to confirm or disprove the dynamo theory of disturbance.

A dynamo theory of meridional winds is first considered. The theory for magnetic north-south wind-components is derived for the case in which the transverse conductivity varies only with geomagnetic latitude. The contribution of zonal winds is then discussed. Current-systems are next derived for geomagnetic data in terms of daily, monthly, or seasonal means, regardless of whether they are to be attributed to averages of magnetic storms or otherwise; if the electric current-systems yielding daily or monthly means flow outside the atmosphere, there should, of course, be found no evidence of the causative wind-pattern in the radio or other observations of winds.

Finally, it is observed that since the zonal winds of the troposphere are shown to account for seasonal fluctuation in the earth's rate of rotation, the latter may be correlated with seasonal changes in north-south winds in the lower ionosphere. If so, aspects of the geomagnetic annual variation may be correlated with the rate of the earth's rotation [36], although, of course, the zonal winds of the upper atmosphere contribute insignificantly to changes in angular momentum of the atmosphere. However, Dr. Clemence, of the United States Naval Observatory, suggests that present values of the seasonal changes in rate of the earth's rotation are not accurate enough for this purpose.

II. THE AVERAGE GEOMAGNETIC ANNUAL VARIATION ON DISTURBED MINUS QUIET DAYS

If geomagnetic disturbance is to be ascribed to departures from normal in the wind-velocity in the upper atmosphere, corresponding departures are expected in the mean monthly global circulation of air. Although this view may be incorrect, it is not at all unreasonable in view of abundant evidence of commotion in the ionosphere during magnetic disturbance, as well as evidence of concentrated electric currents and aurora at the auroral zone at such times near the height 100 or 150 km.

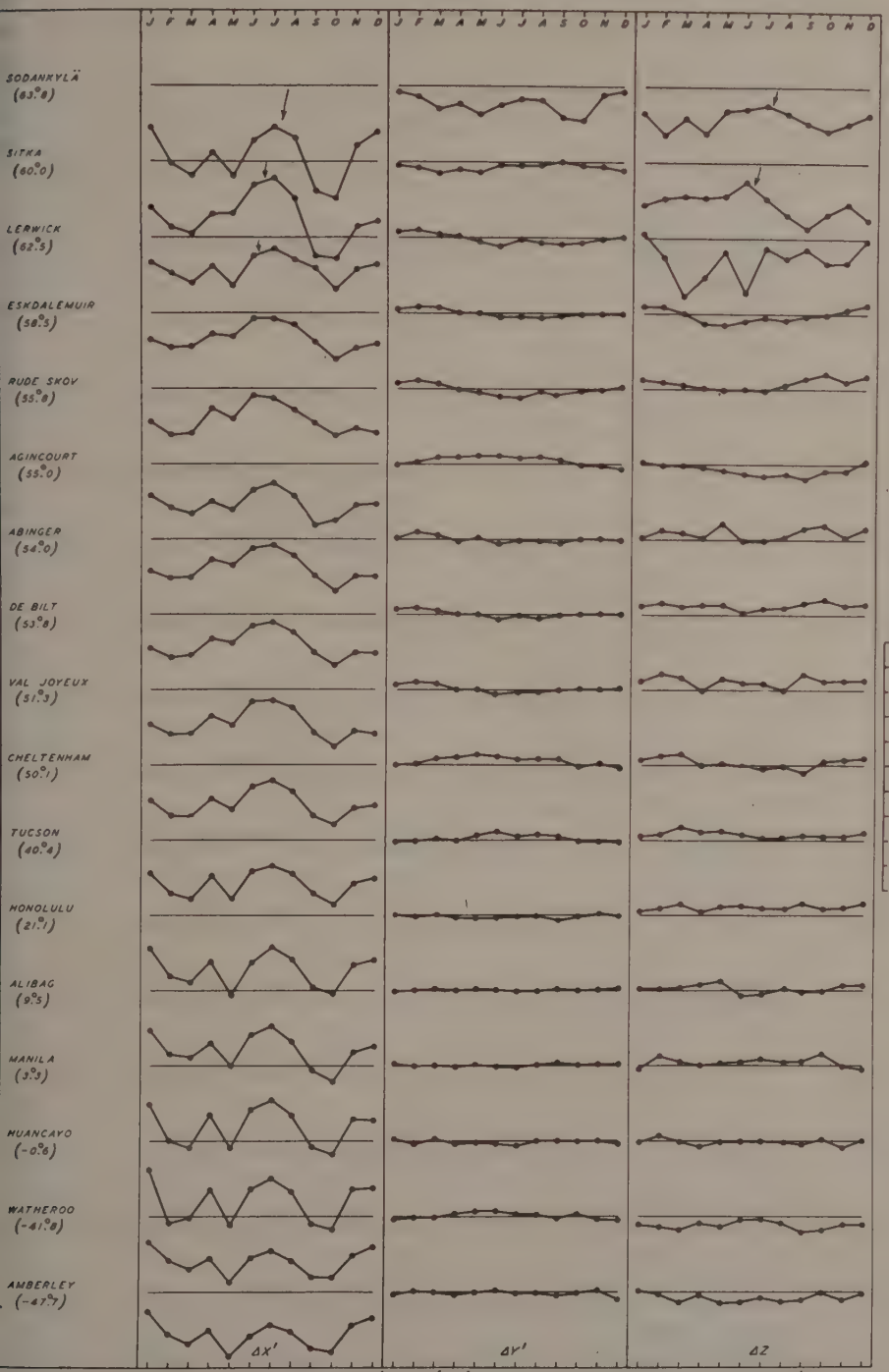

FIG. 1 — DISTURBED MINUS QUIET-DAY MEANS (D_{mi}), X', Y', AND Z-COMPONENTS, MEAN OF 1922-33 (GEOMAGNETIC LATITUDES INDICATED IN PARENTHESES)

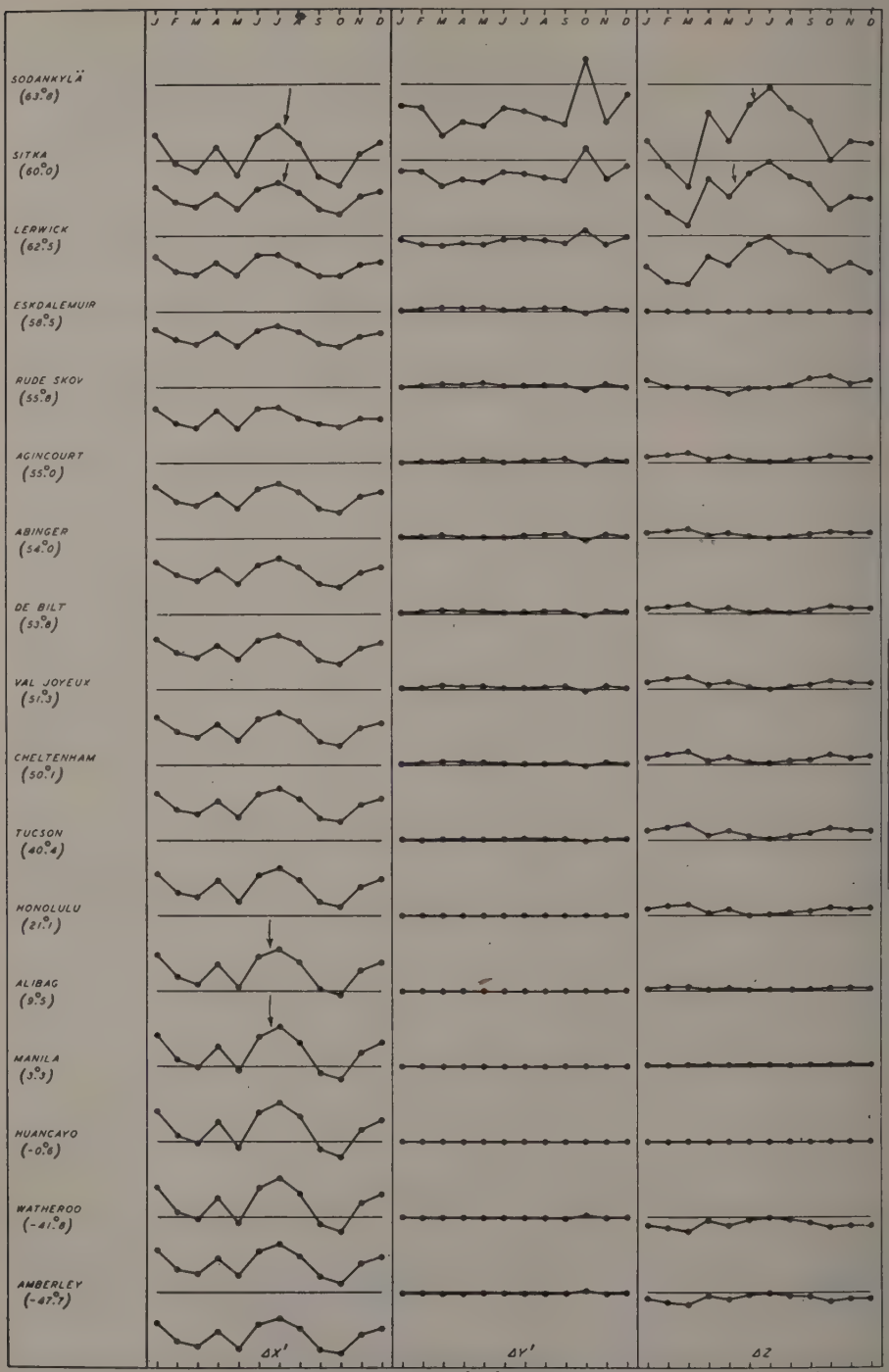

FIG. 2 — PART OF D_{mi} SYMMETRICAL ABOUT EQUATOR, X'-, Y'-, AND Z-COMPONENTS, MEAN OF 1922-33 (GEOMAGNETIC LATITUDES INDICATED IN PARENTHESES)

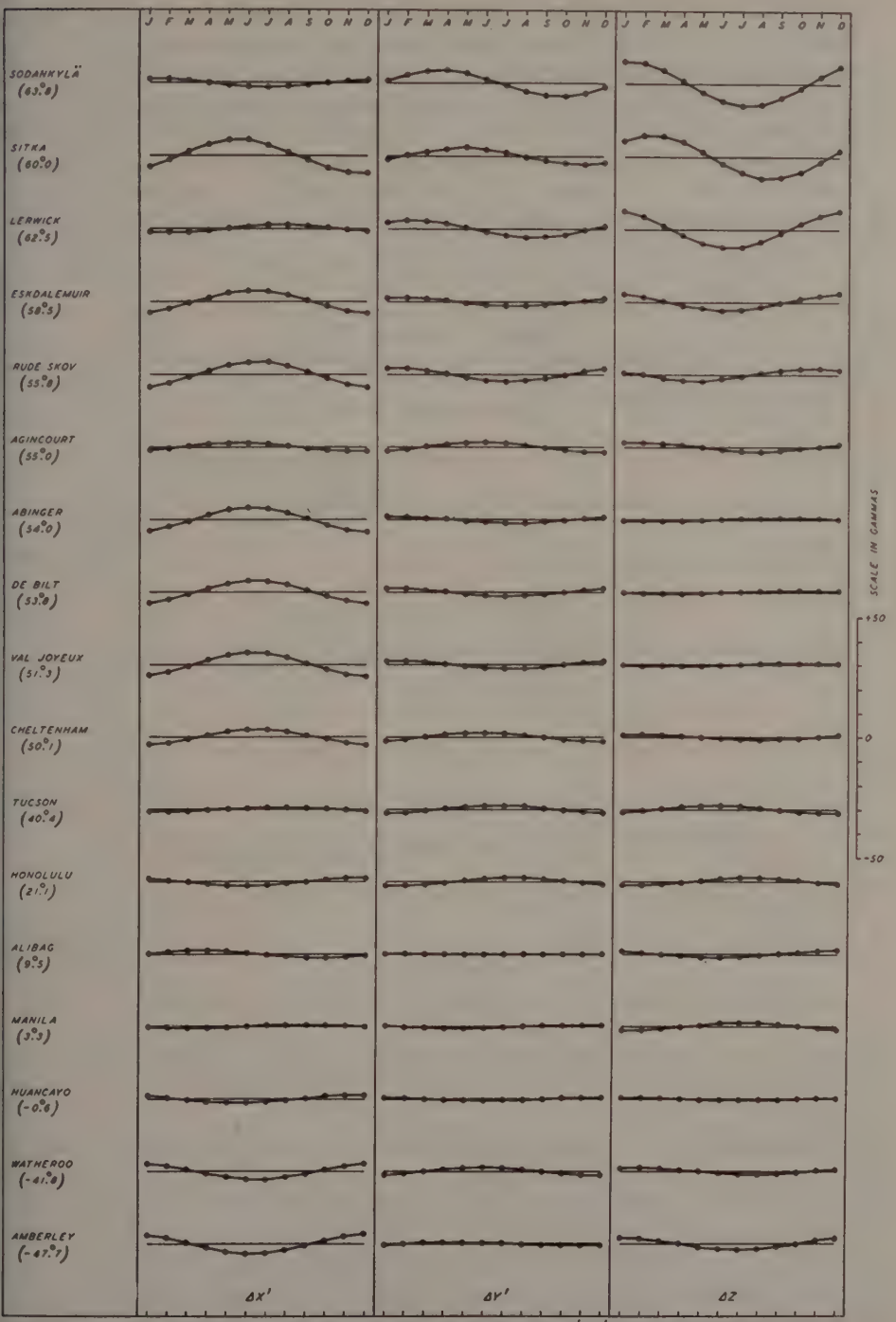

FIG. 3 — SINUSOIDAL PART OF D_{mi} ANTI-SYMMETRICAL ABOUT EQUATOR, X'_-, Y'_-, AND Z-COMPONENTS, MEAN OF 1922-33 (GEOMAGNETIC LATITUDES INDICATED IN PARENTHESES)

Figure 1 shows the disturbed minus quiet-day monthly means at various stations [37] in terms of geomagnetic coordinates and components; the distinction between geomagnetic and geographic coordinates will be dropped in this study, by assuming the geomagnetic and geographic axes (displaced through 11°.5 of latitude) are coincident. The components tangential to the earth's surface are the geomagnetic north component ($\Delta X'$), east component ($\Delta Y'$), and vertical component, positive downwards (ΔZ). Attention will be restricted mainly to $\Delta X'$, as $\Delta Y'$ is small, and ΔZ difficult to measure as accurately as $\Delta X'$ and $\Delta Y'$.

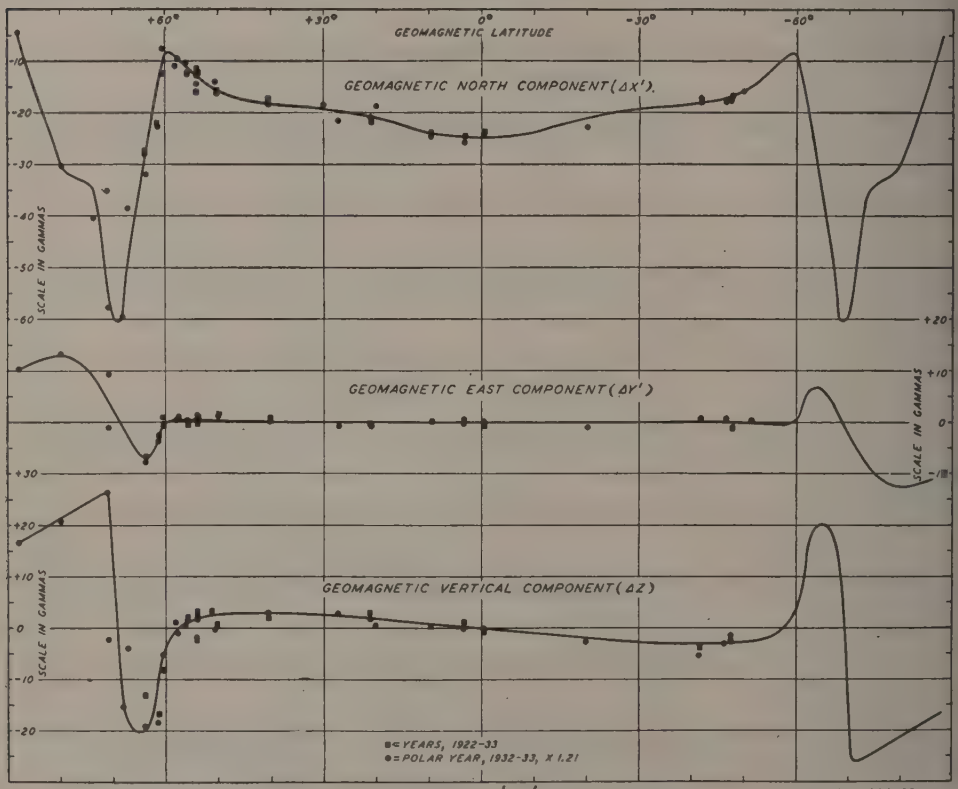

FIG. 4—VARIATION WITH GEOMAGNETIC LATITUDE OF X^L, Y^L, AND Z-COMPONENTS OF D_{mi}, MEAN OF 1922-33

The units are in terms of gammas, where one gamma = 10^{-5} cgs unit. From Figure 1 it will be noted that $\Delta X'$ is always directed southwards and varies with time of year.

The data of Figure 1 analyze nicely into two parts: (1) a part symmetrical about the geomagnetic equator (Fig. 2), and (2) a part of sinusoidal character with a period of one year (Fig. 3). The remarkable regularity of (2) is not due to the mode of analysis, as an equally regular sinusoidal variation can be derived by subtracting, for instance, results in $\Delta X'$ for Amberley, New Zealand, from Cheltenham, Maryland, as was first shown by Cynk [38]. It may be remarked that equally interesting and similar sinusoidal variations are found in $F2$-region critical fre-

quency [39], and cosmic-ray ionization associated with the meson layer at 16 km [40], and possibly in north-south wind-velocities at modest atmospheric levels.

Figures 4 and 5 show the latitude distribution of the symmetrical and sinusoidal parts, based on 12-year averages; Figure 6 gives the observed tentative latitude distribution for both parts combined, based in polar regions upon monthly means for the International Polar Year, 1932-33.

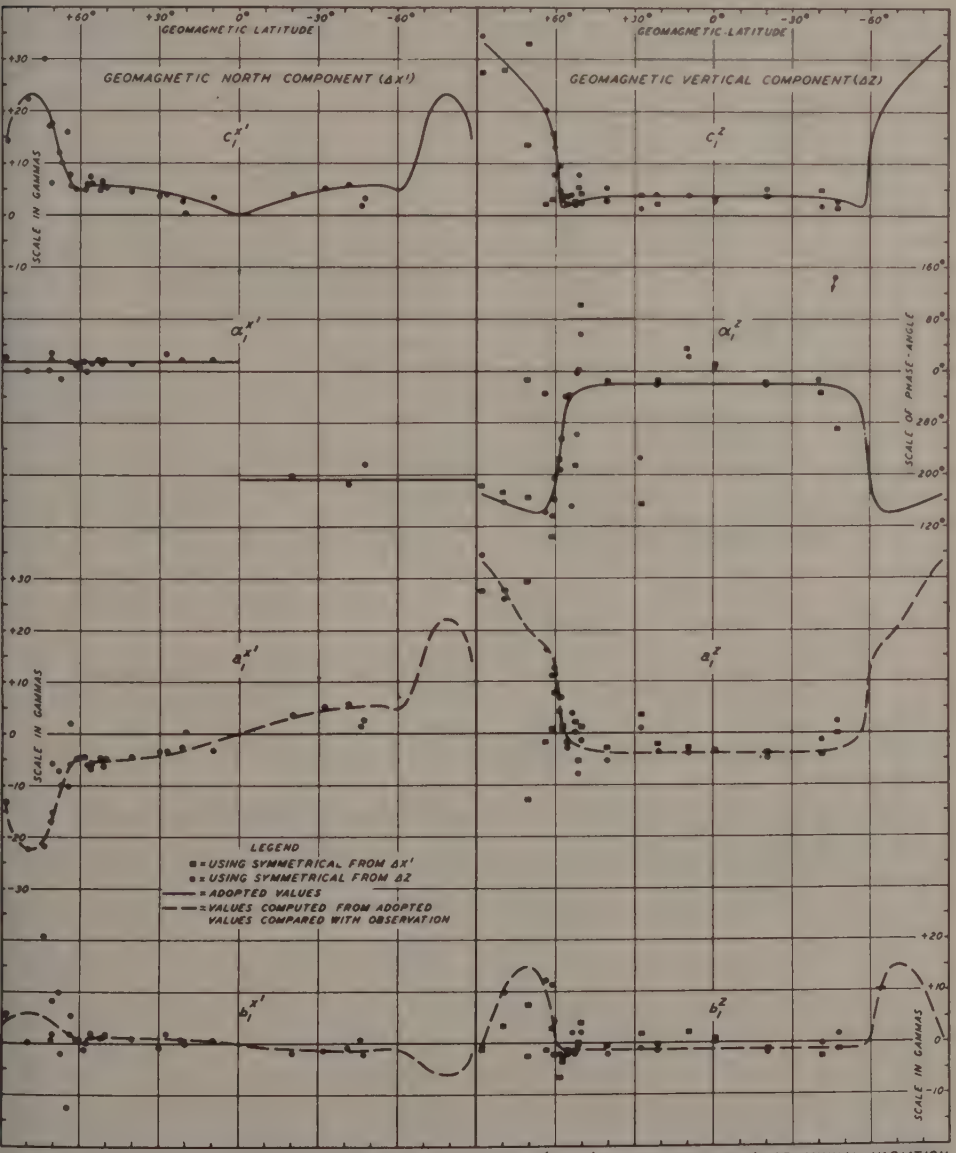

FIG. 5 — VARIATION WITH LATITUDE OF SINUSOIDAL PART $-c_1 \cos(t+\alpha_1) = a_1 \cos t + b_1 \sin t$ OF ANNUAL VARIATION, ALL DAYS, IN GEOMAGNETIC NORTH (x') AND VERTICAL (z) COMPONENTS, VARIOUS GROUPS OF YEARS 1905-41, REDUCED TO MEAN OF 1922-33

III. SIMPLE DYNAMO THEORY OF WINDS MOVING ALONG AND PERPENDICULAR TO THE GEOMAGNETIC FIELD

(*a*) *Meridional and zonal horizontal winds confined to a thin shell*—The motion of a medium with velocity **v**, in the presence of a magnetic field **H**, induces a "dynamo" electric field **E**, equal to $\mathbf{v} \times \mathbf{H}$. If the southward, eastward, and upward vertical components of **v** are u, v, w, and those of **H** are H_x, H_y, H_z,

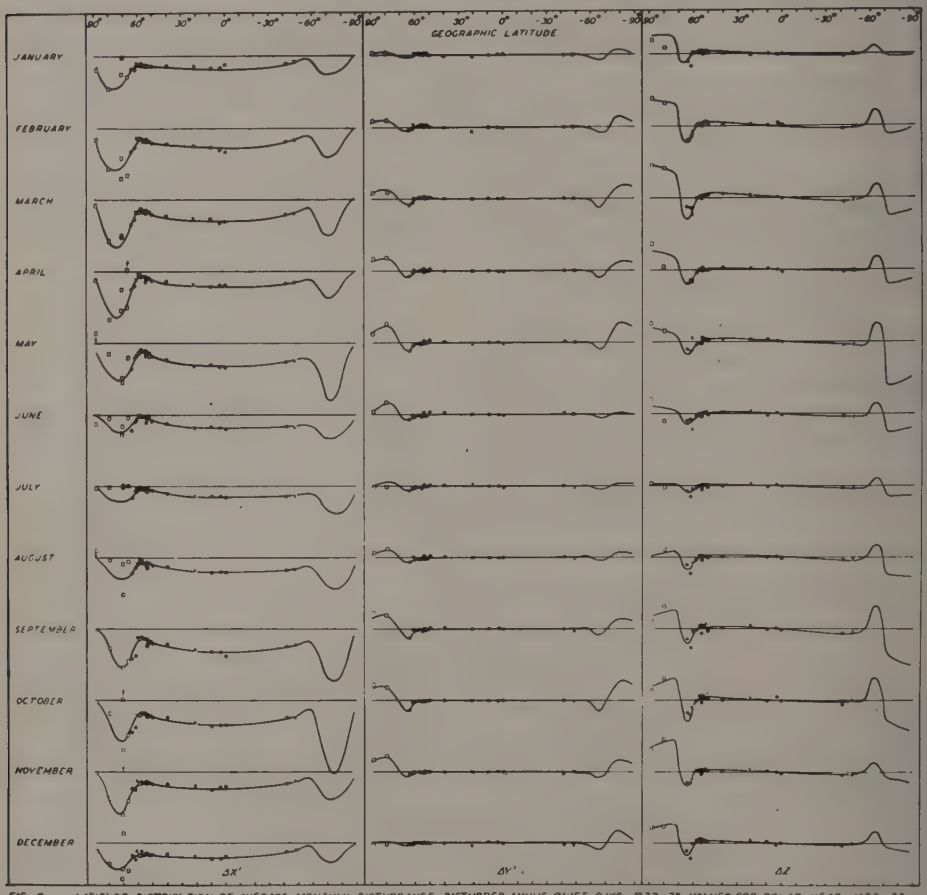

FIG. 6 — LATITUDE-DISTRIBUTION OF AVERAGE MONTHLY DISTURBANCE, DISTURBED MINUS QUIET DAYS, 1922-23, VALUES FOR POLAR YEAR, 1932-33, REDUCED TO 1922-33

LEGEND: ○=STATIONS, 1922-33; □=STATIONS, 1932-33; ×=LERWICK, 1926-30, RUDE SKOV, 1927 33, VAL JOYEUX, HONOLULU, AND AMBERLEY, 1922-33

$$\left.\begin{aligned} E_x &= vH_z - wH_y \\ E_y &= wH_x - uH_z \\ E_z &= uH_y - vH_x \end{aligned}\right\} \qquad (1)$$

When the shell is thin, the vertical component E_z is productive of polarization and is hence neglected [15].

If we ignore self or mutual induction and suppose the air-flow irrotational, from Ohm's law

$$\left.\begin{aligned} vH_z &= \partial S/a\,\partial\theta = (1/K)\,\partial R/a\sin\theta\,\partial\varphi \\ -uH_z &= \partial S/a\sin\theta\,\partial\varphi = -(1/K)\,\partial R/a\,\partial\theta \end{aligned}\right\} \quad \ldots\ldots\ldots\ldots (2)$$

where S is the electrostatic potential of any charge distribution set up in the shell of radius a, K the electric conductivity, and R the current-function. Here θ is the colatitude and φ the east longitude.

On eliminating S, Chapman found [15]

$$K\left\{\frac{\partial^2 R}{\sin\theta\,\partial\varphi^2} + \frac{\partial}{\partial\theta}\left(\sin\theta\,\frac{\partial R}{\partial\theta}\right)\right\} - \left\{\frac{\partial K}{\partial\varphi}\frac{\partial R}{\sin\theta\,\partial\varphi} + \sin\theta\,\frac{\partial K}{\partial\theta}\frac{\partial R}{\partial\theta}\right\}$$
$$= aK^2\left\{\frac{\partial v\,H_z}{\partial\varphi} + \frac{\partial(uH_z\sin\theta)}{\partial\theta}\right\} \quad \ldots\ldots (3)$$

Martyn [41] has shown that an important modification is necessary in the case of an ionized gas, since the ions tend to move also along the magnetic field, but this will be ignored in the present paper.

It may be helpful initially to consider the consequences of (3) in a particularly simple case. Suppose the geographic and geomagnetic axes are coincident, so that $H_z = -C\cos\theta$, say, and that K is independent of φ, as will be the case where only the daily mean conductivity is considered. Also imagine a spherical current-sheet flowing from east to west along all parallels of geomagnetic latitude, with a current per unit width given by $i = i_0\sin\theta$. Then R referred to the north pole will be $ai_0(1-\cos\theta)$, and the magnetic field inside the sheet will be uniform, parallel to the geomagnetic axis, and directed from north to south, and equal to $8\pi i_0/3$. It will also be noted that only the transverse conductivity is involved.

Using (3), there results

$$u = -\frac{i_0}{CK}\tan\theta \quad \ldots\ldots\ldots\ldots\ldots\ldots\ldots\ldots (4)$$

where K can be arbitrary, but independent of longitude.

Obviously, the equatorial singularity arises because $H_z = 0$ there, since $K(\theta) = \infty$ is physically inadmissible. This difficulty is not due to the choice of R; the day-to-day changes in the geomagnetic field throughout low and middle latitudes are physically compatible to good approximation with such a supposed current-system. Of course, a ring-current in the equatorial plane at a distance of a few earth-radii in which the daily mean current varied would remove the immediate difficulty. However this may be, the present aim will be directed towards the view that the currents are located in the atmosphere, in which case a physically admissible wind-system is required for its generation and maintenance.

The wind u confined to the shell lacks continuity. It is also clear that poleward flow of air within a rotating shell on a rotating earth should be accompanied by some form of an eastward air-flow to conserve angular momentum. Accordingly, the existence of poleward winds requires the coexistence of some form of zonal wind-system.

(*b*) *Zonal winds in a thin uniformly conducting shell*—The consequences of (3) in the case of a zonal wind-system will next be considered.

Taking, for example, $v = v_0 \sin^2 2\theta$, from (2),

$$-v_0 C \sin^2 2\theta \cos\theta = \frac{\partial S}{a\,\partial\theta}$$

$$S = \frac{-4av_0C}{15}\sin^3\theta(2 + 3\cos^2\theta) + C_1 \quad \ldots\ldots(5)$$

which gives $S = 0$ at $\theta = 0, \pi$; $S = -8/15\ (av_0C)$ at $\theta = \pi/2$, when $C_1 = 0$. If $v_0 = 10^3$, $S \sim 2{,}000$ volts. It is evident that all that results is a polarization of the conducting sheet which stops all north-south flow of current [Fig. 7(*C*)]. This is true also when $v = v(\theta)$.

The foregoing two rough calculations for a thin shell refer tentatively to the symmetrical part of the geomagnetic annual variation. For the sinusoidal part in January, say, a westward current $i = i_0' \sin 2\theta$ flowing in a thin spherical shell would reproduce most of the observed effect between the auroral zones. This yields $R = ai_0' \sin^2\theta$. Using (3), it is then easily shown that

$$u = -[2i_0'/CK(\theta)]\sin\theta \quad \ldots\ldots(6)$$

which is a wind blowing from south to north, and strongest at the equator. In June, this wind is reversed, so that

$$u = [2i_0'/CK(\theta)]\sin\theta \quad \ldots\ldots(7)$$

These results are shown schematically in Figure 7(*A*) and (*B*).

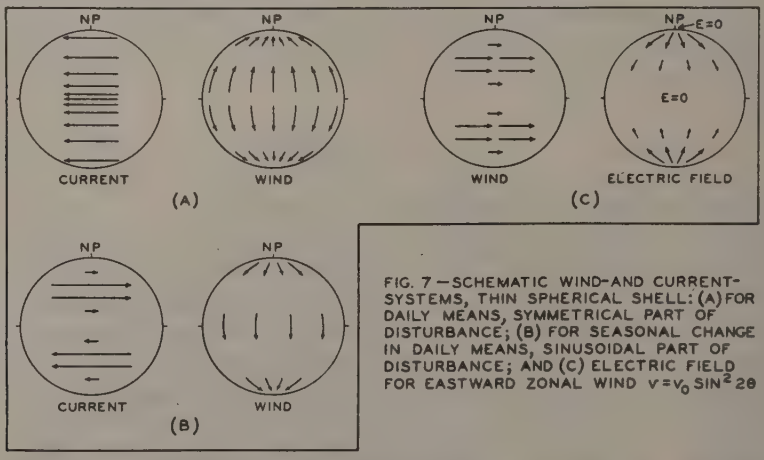

FIG. 7—SCHEMATIC WIND-AND CURRENT-SYSTEMS, THIN SPHERICAL SHELL: (A) FOR DAILY MEANS, SYMMETRICAL PART OF DISTURBANCE; (B) FOR SEASONAL CHANGE IN DAILY MEANS, SINUSOIDAL PART OF DISTURBANCE; AND (C) ELECTRIC FIELD FOR EASTWARD ZONAL WIND $v = v_0 \sin^2 2\theta$

The rough indications of wind-systems found thus far for the geomagnetic annual variation by themselves mean little, unless some kind of independent check can be found, and the equation of continuity has not been satisfied. Figure 8 shows a pioneering attempt from meteorology to deduce a general circulation of the upper atmosphere, for northern winter and summer [34]. Now the height of the hypothetical electric current-system assumed responsible for the geomagnetic annual variation is unknown, except near the auroral zone where the height may be estimated as of the order of 100 to 140 km. From Figure 8, the winds for 100-

to 120-km height flow polewards, and are qualitatively in accord with the result found for the symmetrical part of the annual variation, but in the equatorial regions the air-flow is upwards. This upward air-flow across the horizontal component of field would also generate westward electric currents in this region, thus removing the singularity in u at the equator.

As in the case of the seasonal part of the geomagnetic annual variation, there may also be present a north to south wind; in middle latitudes, Kellogg and Schilling give 75 m/sec to the east in the northern hemisphere, and 105 m/sec to the east in the southern hemisphere, so that a north to south wind in middle latitudes is suggested, although the phase discrepancy appears to be 180°, or six months.

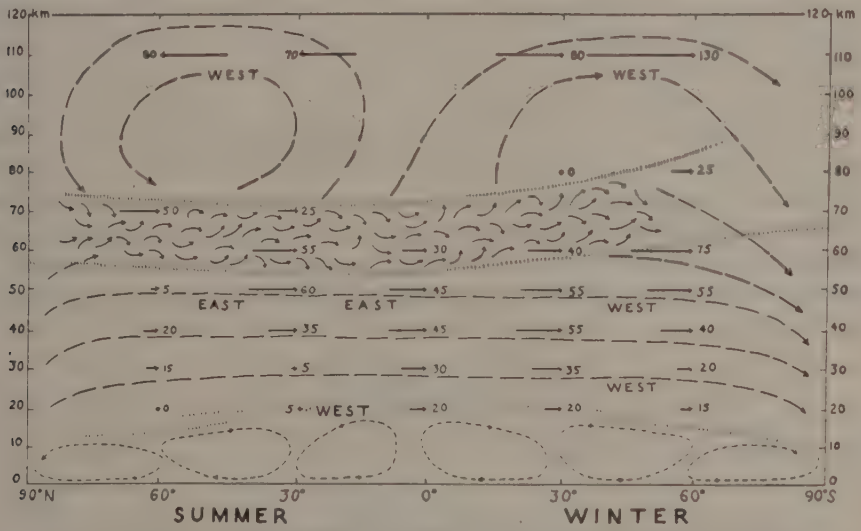

FIG. 8—SCHEMATIC REPRESENTATION OF GENERAL CIRCULATION IN MERIDIONAL CROSS-SECTION FOR NORTHERN SUMMER

The tentative results of the radio data on conductivity [10], geomagnetism, and meteorology probably agree about as well as might be hoped. At the auroral zone, if the conductivity is enhanced due to incoming charged particles, possibly by a factor of say 50 at times over that in middle latitudes, the same tentative wind-systems might suffice to give the observed enhancement in the geomagnetic annual variation noted in auroral regions.

(*c*) *Meridional and zonal horizontal and vertical winds confined to thick shell; the lower half of thickness a poor electrical conductor*: 1. *Meridional winds for mean annual disturbances*—It has just been noted that the agreement found between the results of the previous crude dynamo theory of the geomagnetic annual variation and the tentative results from meteorology may not necessarily be accidental. Accordingly, it may be instructive to proceed as before, on a very simple basis, remarking that the singularity in u at the equator is physically inacceptable, in the case of the symmetrical part. It was noted that this singularity arose because H_z was zero at the equator, and that the necessary westward-flowing currents there may be generated by an upward circulation in conducting air in the equatorial belt,

poleward motion in middle latitudes, and downward air-flow in polar regions, the circuit being completed at levels of low electric conductivity. At lower levels, the conducting quality of the air introduced could, for instance, be rapidly reduced by recombination. In the equatorial belt, the slow vertical rise of air may be unable to affect the height of the E-region and lower F-region much, even when this rising air fluctuates in speed.

Assume then that the meridional wind-vector is constant and equal to $\mathbf{v}_0$. From (1), the westward-directed electric field is given by $\mathbf{v}_0 \sim \mathbf{H}$, or $E_y = wH_x - uH_z$, all other terms, including the contribution of S to E_y, being zero. Actually, zonal winds abstracting from the vector velocity $\mathbf{v}_0$ should coexist, but would generate polarization, or toroidal fields parallel to E_y, and hence exert no mechanical force on currents generated due to E_y. Also suppose K_0 is the conductivity averaged around the equator, decreasing polewards as $[1 + (3/2) \sin \theta]^2$. Then $i = KE = K_0 [1 + (3/2) \sin \theta]^2 v_0 F \sin \psi$, where ψ is the angle between v_0 and F, and F is the total magnetic intensity.

Since F is known, knowing i from the data, the angle ψ can then be found, and hence the products of both u and w with K_0, since the dip I is also known.

If $0.6\ \Delta X'$ is taken to give the value of $\Delta X'$ corrected for induced earth-currents [15] for the observed values $\Delta X'$ of the symmetrical part of the annual geomagnetic variation, the approximate value of i will then be $i = (3 \times 0.6/8\pi)\ \Delta X' = 0.07 \Delta X'$, using a spherical current-sheet approximation locally [15], except near the auroral zone. Hence,

$$\sin \psi = \frac{0.07\ \Delta X'}{K_0 v_0 (1 + \frac{3}{2} \sin \theta)^2 F}$$

at the time of equinox, whereas in other months

$$\sin \psi = \frac{0.07\ \Delta X'}{K_0 v_0 (1 + \frac{3}{2} \cos \chi)^2 F} \qquad (8)$$

where χ is the mean monthly zenith angle of the sun at the parallel of colatitude θ. Accordingly, (8) will fail if $K_0 v_0$ is not such that $0 < \sin \psi < 1$. When $\theta = 50°$, according to hypothesis, v_0 is to be horizontal, and since $\tan I = 2 \cot \theta = 2 \cos 50° = 1.6782$, $I = 59°.2$, or $\psi = 59°.2$, then $\sin \psi = 0.859$, whence $Kv_0 = 0.18\ \Delta X'$, for $F = 0.449$. From Figure 4, the annual average of $\Delta X'$ at $\theta = 50°$ is about -18.3γ, so that $Kv_0 = 3.3 \times 10^{-5}$. If then $v_0 \sim 100$ m/sec, K will be $3.3 \times 10^{-5}/10^4 = 3.3 \times 10^{-9}$, or 4.4×10^{-9} cgs at $\chi = 0$. This value of the integrated conductivity at the equator will be tentatively adopted here for purposes of calculation, as well as the corresponding tentative value $v_0 = 100$ m/sec; it is, of course, assumed that K_0 is appropriate to the value averaged around the equator.

Accordingly, (8) becomes

$$\sin \psi = \frac{0.324\ \Delta X'}{(1 + \frac{3}{2} \sin \theta)^2 (1 + 3 \cos^2 \theta)^{1/2}} \qquad (9)$$

where $\Delta X'$ is in gammas, for the annual average.

The results of applying (9) to the daily means of disturbances (Fig. 4) are given in Table 1. It will be noted that if we added a suitable conductivity at the

TABLE 1—*Calculated meridional wind-directions* α *measured as upward departures from northward horizontal direction; also values total intensity* (F), *inclination* (I), *and angular departures* ψ *of wind-vector* v_0 *from* F, *at various colatitudes* θ, *using* (9)

$\Delta X'$	θ	F	I	sin ψ	ψ	α
γ		cgs			°	°
....	0	0.600	90°	.....	..	....
5	2	0.600	89	0.732	47	−42
30.5	10	0.593	85	3.14	..	....
59.5	20	0.573	80	4.42	..	....
8.2	30	0.541	74	0.482	29	−45
15.8	40	0.498	67	0.800	53	−14
18.3	50	0.449	59	0.859	59	0
20.4	60	0.397	49	0.946	71	22
22.0	70	0.349	36	(1.06)	(90)	(54)
24.0	80	0.313	19	(1.21)	(90)	(71)
24.5	90	0.300	0	(1.27)	(90)	(90)

uroral zone, the strong electric currents there might also be reproduced. It will e seen also that the equation of continuity is violated, since v_0 is constant.

2. *Meridional winds for mean monthly disturbance*—Figure 6 gives the average ombined symmetrical and sinusoidal parts of monthly mean disturbance in the eomagnetic north component $\Delta X'$, for disturbed minus quiet days, 1922-33.

Proceeding as in the case of the annual means of disturbance, using (8), the orresponding relative wind-velocities and directions may be estimated. This was one by adopting a value of $K_0 v_0$ for each month such that sin ψ would equal unity t a point in middle latitudes, taking v_0 to increase polewards as sec φ, due to change n orifice area. The results are shown in Figure 9 (full lines). The wind-vectors are rawn proportional to $K_0 v_0$, where K_0 is the average conductivity in each month long the subsolar parallel. If K_0 is due to a constant flux of wave radiation from he sun, its monthly mean value would change by only a few per cent during the ear, since it would depend on the distance to the sun. The wind-vectors of Figure would then be proportional to the velocity, if the latitude distribution assumed or the conductivity were correct. The actual wind-velocity change in the 12-year verages from May to July would then be by about a factor of two (Fig. 6), provided hat when the average wind-velocity of the ionospheric region doubled the regi n nvolved did not become extended so that motion took place also in levels having igher or lower electric conductivity. Inspection of Mitra's results in Table 3 although for K_0) shows that the region involved in the circulation need change n height by only about a few kilometers to change the conductivity by a factor f two, and completely absorb the factor two in wind-velocity. In the same way, the upper limit in $\Delta X'$ for a very great magnetic storm be taken as 2,000γ at he equator, the factor 100 required for the increase in v_0 could be completely bsorbed by a not too considerable change in the height of conductivity in relation o circulation, for example, for a region of height between 100 and 150 km, on the oubtful basis of adequate integrated conductivity. Actually the vertical gradients n conductivity are quite considerable until the height of maximum in $F2$-ioniza-

tion is reached. In fact, during the maximum of the main phase of magnetic storm of which we are here considering the monthly mean, marked motions of th $F2$-region relative to ground level usually appear. Martyn [43] has shown that th vertical motions of the $F2$-region seem satisfactorily explained by the electrostat fields of the auroral-zone electrojets, for which a dynamo theory is sketched late in this paper.

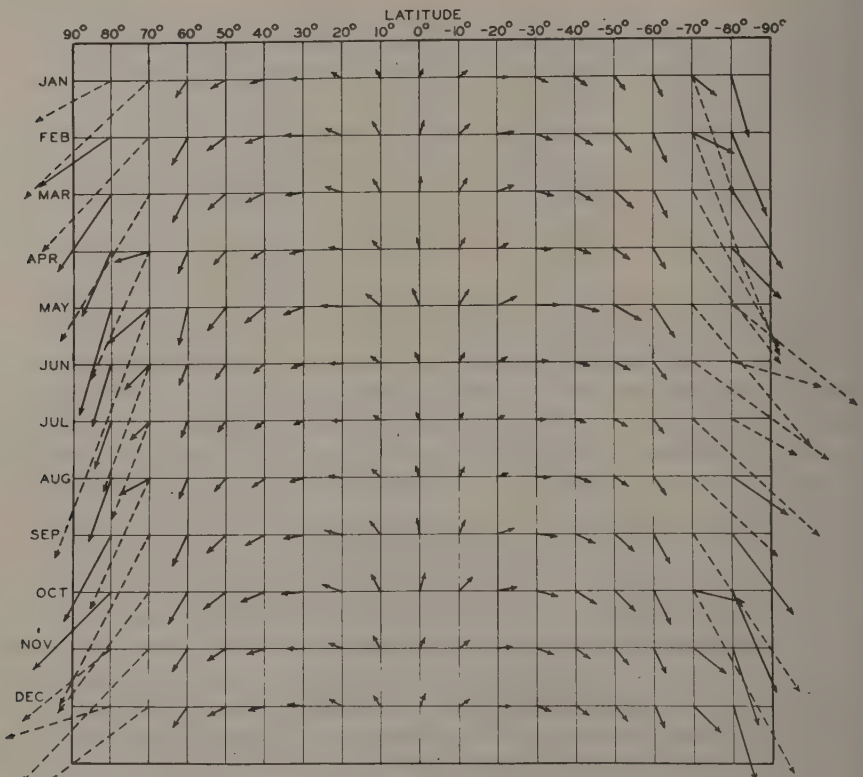

FIG. 9 —MERIDIONAL WIND-COMPONENTS, MONTHLY MEANS OF DISTURBED MINUS QUIET DAYS, VELOCITY $V = V_0 \sec \varphi$, ADDED CONDUCTIVITY AT AURORAL ZONE

Figure 8 shows that the simple law of conductivity, $K = K_0 [1 + (3/2) \cos \chi$ does not appear to give enough conductivity in auroral regions in the northe winter. Of course, this is not surprising, if it be supposed that incoming proto noted by Meinel [25], neglected here, contribute sensibly to augment the ioniz tion. What probably really is surprising is that a simple wind-pattern suffic so well for the simple law of conductivity assumed.

The added conductivity K_A in polar regions required to give the dotted win vectors at $\varphi = 70°$ and $80°$ (direction of vector only), also shown in Figure 9, listed in Table 2 as a multiple of $K_0 [1 + (3/2) \cos \chi]^2$. Actually the vector directi for $\varphi = 80°$ derived in this crude way has little meaning, because the factor sec will not insure approximate conformity to the question of continuity.

3. *Zonal winds and toroidal fields*—If the wind-system of Figure 9 is qualitatively rrect, it would be accompanied by zonal winds to the east at the higher level. owever, quite high in the *F*-region, the kinematic viscosity may be so high at this eastward drift of air is reduced to zero. For small-scale motion this is doubt true, but for large-scale motion the effect should be very greatly reduced. auroral regions, the electric conductivity may be considerably higher near the -region, and near and above the *D*-region there may be a westward tendency in

ABLE 2—*Added polar transverse conductivity* K_A *in terms of* $K_0[1 + (3/2)\cos\chi]^2$ *to give assumed continuity in wind-system*

Month	φ =		φ =	
	80° N	70° N	70° S	80° S
nuary	0.43	3.14	2.92	....
bruary	....	2.34	2.96	....
arch	....	2.76	2.85	....
ril	....	2.94	2.96	....
ay	....	3.73	3.33	0.43
ne	....	3.09	2.90	0.43
ly	....	2.94	3.05	0.43
ugust	....	3.03	2.42	....
ptember	....	2.83	2.71	....
tober	....	2.60	2.95	....
ovember	0.43	3.39	3.82	....
ecember	0.43	3.01	3.06	....

nal winds extending down to lower levels, a part of the return circuit for the eridional component of the wind-system previously considered. Under these nditions, when a part of the conductor remains stationary with respect to the agnetic field while another part of the thick conducting shell experiences zonal otion relative to the field, a toroidal field generator probably results. Obviously e same is true whenever the daily mean zonal winds vary in velocity with height. t present, the observational data are very sparse, but it seems desirable never-eless to attempt at least a rough estimate of the strengths of the toroidal fields d currents expected under assumed conditions.

Suppose a uniformly conducting thick region is made up of two thick adjacent herical shells, the outer shell moving with the earth and its dipole field, while e inner shell has a zonal motion to the east, moving as a whole with a relative gular velocity ω. Bullard [42] has written down the solutions for this type of oblem, but in order to avoid the difficulties naturally inherent, it is convenient attempt here the solution for a cruder idealization of the problem: This is forded by regarding the inner thick shell to extend throughout the earth. The oblem then becomes identical with a toroidal field problem solved by Bullard his theory of the earth's main field.

If the conductivity is uniform and equal to K, a the radius of the outer shell and b the radius of the concentric sphere, Bullard found that within a uniform field F, parallel to the axis of rotation of the sphere, that in the outer shell the currents are

$$I_r = \tfrac{1}{5}K\omega F b^5(1/r^5 - 1/a^5)(1 - 3\cos^2\theta)$$

$$I_\theta = -\tfrac{1}{5}K\omega F b^5(1/r^5 + 3/2a^5)\sin 2\theta$$

The magnetic field in this shell consists of the initial field F and the field produced by the induced currents. The latter field H_φ has lines of force which are circles of latitude and are of maximum intensity at $r = b$, $\theta = \pi/4$, where

$$H_\varphi(\max) = -\tfrac{2}{5}K\omega F b^2(1 - b^5/a^5) \quad \ldots\ldots\ldots\ldots\ldots\ldots (10$$

There is an external electric field outside the whole system (and within the outer shell) given by

$$\left.\begin{aligned} E_r &= -\tfrac{1}{2}\omega F(3\cos^2\theta - 1)\, b^5/r^4 \\ E_\theta &= -\tfrac{1}{2}\omega F \sin 2\theta\, b^5/r^4 \end{aligned}\right\} \quad \ldots\ldots\ldots\ldots\ldots\ldots (11$$

The present interest centers largely around computations for (10) and (11).

Taking $K = 10^{-12}$, a surface rotation of the sphere at the equator of 200 m/sec $a = 6{,}550$ km, $b = 6{,}450$ km, $F = 1/2$, and using (10) there results $H_\varphi = 0.6$ gauss. If the outer shell is only 10 km in thickness, all results are reduced by a factor of about 10.

If at the auroral zone the conductivity were 10 times as great, and the relative wind-velocity 300 m/sec, there would be hence good prospects for quite strong toroidal fields. The estimates are clearly uncertain, and one might perhaps equally well affirm that H_φ is between zero and 30 gauss. But since zonal winds of the type imagined actually should occur, unstable toroidal fields of 3,000γ to one gauss or so would not be unexpected. This may affect the separation of the ordinary and extraordinary wave components of radio waves, and their plane of polarization at higher levels, as well as experimental radio determinations of the gyrofrequency of electrons.

The electric field external to the atmosphere is of the order $E = \omega F b^5/2a^5 \sim 0.5 \times 10^{-5}$, or about 10^{-13} volt/cm, and hence negligible, when the toroidal currents are flowing.

Actually the earth's poloidal (main) field is different from the axial approximation to this field just considered, but Bullard has shown that the important quantity is the strength of field at the boundary of the shell and sphere, at $r = b$. Hence the foregoing rough calculation of the toroidal field should be little affected by this approximation.

According to Mitra (The upper atmosphere, p. 380, 2nd ed., 1952) the noon values of conductivity along the field at the equator are as follows:

TABLE 3—*Value of conductivity K_0 at various heights h in cgs*

h	$K_0 = n_e K_e + n_i K_i$
km	
60	8×10^{-18}
100	1.4×10^{-17}
150	8.4×10^{-13}
200	1.3×10^{-11}
250	1.1×10^{-10}
300	1.8×10^{-10}

But this assumes no negative ions present. Hence the estimates of specific conductivity along the field are minimum values in this sense. Unfortunately, the height of zonal winds which might enter into the production of toroidal fields is not known, so the tentative value $K = K_0 = 10^{-12}$ may be too high. Also, the model used may not be too well suited, though a simple check can be made.

Imagine a layer 100 km thick, in which the top 50 km experience a constant zonal wind v perpendicular to a field H. Suppose also that the lower 50-km thickness is fixed relative to the earth's surface. Then if $H = 0.4$, $v = 100$ m/sec, $E = 4.10^3$. The current density will be $KE = 4.10^3 \cdot 10^{-12} = 4 \times 10^{-9}$ and the circuit is completed in the lower half of the layer. The total current in the top layer may be of the order 50 km $\times 10^5 \times 4 \times 10^{-9} = 200 \times 10^{-4} = 0.02$ emu, and the field $\delta H = 2\pi i = 0.12\Gamma$. At the auroral zone, magnetic disturbance is about 20 times as great on an average as in middle latitudes, and if this means the conductivity is 20 times as great, a toroidal field of the order of 2.4 gauss, perpendicular to the magnetic field and parallel to the earth, might arise, for example, adjacent to homogeneous auroral arcs, where incoming charged particles might be found spiraling down this toroidal field, emerging in the poloidal field below.

4. *Conductivity of the atmosphere and the dynamo theory of disturbance*—Up to the present, the poloidal and toroidal magnetic fields generated by winds in the upper atmosphere have been discussed without much regard to available estimates of electric conductivity. The present discussion follows Bates and Massey [8] in neglecting negative ions as unimportant.

The conductivity of an ionized gas in a magnetic field has been discussed by Cowling [44], Hirono [9], Maeda [45], Martyn [10], Westfold [46], and some experimental rocket results by Singer, Maple, and Bowen [11]. In Martyn's notation, if e is the electronic charge (taken positive always), ν the collision frequency with neutral and other atoms and molecules, ω the gyrofrequency, and H the magnetic field, writing

$$\omega_{e,i} = He/m_{e,i} \qquad (12)$$

where H is the intensity of the geomagnetic field, $m_{e,i}$ the mass. Writing tan $(\alpha, \beta) = \omega_{e,i}/\nu_{e,i}$ and denoting the number density by N,

$$\left.\begin{aligned} K_0 &= \frac{Ne}{H}(\tan\alpha + \tan\beta) = A(\tan\alpha + \tan\beta) \\ K_1 &= A\sin(\alpha+\beta)\cos(\alpha-\beta) \\ K_2 &= A\sin(\alpha+\beta)\sin(\alpha-\beta) \end{aligned}\right\} \quad \ldots\ldots\ldots\ldots (13)$$

where K_2 is the Hall conductivity which is appropriate when the electric and magnetic fields and current are mutually perpendicular, without hindrance to the flow of current due to polarization. But, when the Hall current cannot flow due to polarization,

$$\left.\begin{aligned} K_3 &= A\sin(\alpha+\beta)\sec(\alpha-\beta) \\ &= K_1 + K_2^2/K_1 \\ &= A(\tan\alpha+\tan\beta)/(1+\tan\alpha\tan\beta) \\ &= K_0/(1+\tan\alpha\tan\beta) \end{aligned}\right\} \quad \ldots\ldots\ldots\ldots (14)$$

The interrelationships can be seen more readily by considering the contribution of a single electron, namely, $K_0 = e^2/m\nu$, $K_1 = K_0\nu^2/(\nu^2+\omega^2)$, $K_2 = K_0\nu\omega/(\nu^2+\omega^2)$. Also $K_3 = K_0$, the same as (14) when $\tan\beta = 0$.

As Cowling noted in 1932, polarization effects may be important. If the electric force $\mathbf{E}$ is due to the velocity $\mathbf{u}$ of the gas perpendicular to the magnetic field, $\mathbf{E} = \mathbf{u}\wedge\mathbf{H}$ and the current $\mathbf{i}$ is given by

$$\begin{aligned} \mathbf{i} &= K_1\mathbf{u}\wedge\mathbf{H} - K_2(\mathbf{u}\wedge\mathbf{H})\wedge\mathbf{H}/H \\ &= K_1\mathbf{u}\wedge\mathbf{H} + K_2H\mathbf{u} \end{aligned}$$

and a Hall current flows in the direction of $\mathbf{u}$. The intensity E of a field stopping the Hall current is given by $K_1E = -K_2Hu$, or the new current density is

$$\left.\begin{aligned} \mathbf{i} &= K_1(\mathbf{E}+\mathbf{u}\wedge\mathbf{H}) - K_2(\mathbf{E}+\mathbf{u}\wedge\mathbf{H})\wedge\mathbf{H}/H \\ &= K_1\mathbf{u}\wedge\mathbf{H} - K_2(\mathbf{E}\wedge\mathbf{H})/H \\ &= K_1(1+K_2^2/K_1^2)\mathbf{u}\wedge\mathbf{H} = K_3\mathbf{u}\wedge\mathbf{H} \end{aligned}\right\} \quad \ldots\ldots\ldots\ldots (15)$$

and the apparent conductivity has now increased to K_3. If an additional electric field $\mathbf{E}' = \mathbf{v}\wedge\mathbf{H}$, where $\mathbf{v}$ is the zonal wind-velocity, and is such that $\mathbf{E}'$ is applied in the direction $\mathbf{u}$, then

$$\begin{aligned} \mathbf{i} &= K_1(1+K_2^2/K_1^2)\mathbf{u}\wedge\mathbf{H} + K_2\mathbf{E}'\wedge\mathbf{H}/H \\ &= K_1(1+K^2/K_1^2)\mathbf{u}\wedge\mathbf{H} + K_2(\mathbf{v}\wedge\mathbf{H})\wedge\mathbf{H}/H \end{aligned}$$

or

$$i = [(K_1(1+K_2^2/K_1^2)u + K_2v]H$$

In the absence of polarization

$$i = (K_1u + K_2v)H \quad \ldots\ldots\ldots\ldots (16)$$

and, since $K_2 = (\omega/\nu)K_1$, a material increase in i may result due to the zonal wind. If i flows along parallels of latitude, this effect is not readily reduced by

olarization. The field $\mathbf{E}'$, when adjacent stationary or more slowly moving con-ucting regions are present, may produce toroidal magnetic fields, directed either estward or eastward, depending on the velocity and conductivity distributions ith height. Clearly the direction and magnitude of $\mathbf{i}$ depends on the signs of $\mathbf{u}$ nd $\mathbf{v}$, and their magnitudes.

It may clarify matters to consider these possibilities of an effective increase n transverse conductivity in physical terms for moderately low to high latitudes. n the northern hemisphere, northward-flowing conducting air of velocity $-u$ roduces the electric field $\mathbf{E} = -\mathbf{u} \times \mathbf{H}$, so that $\mathbf{E}$ is directed westward. As a onsequence, positive ions move westward and the electrons eastward, the latter aving greater mobility in the E- and lower F-regions. The electric field $\mathbf{E}$ thereby reated will in turn provide a force $\mathbf{E} \times \mathbf{H}$, causing both positive ions and electrons o drift downwards and southwards, the electrons at a greater rate, at least in the -region. This lowers the effectiveness with which the field $\mathbf{E}$ produces the west-ard-flowing current, because the time spent between collisions has been used n executing motions other than that to the west or east. If then the force $\mathbf{E} \times \mathbf{H}$ is alanced out by eventual self-polarization, the rate of flow of positive ions west-ard and electrons eastward will greatly increase, as Cowling has shown. The onditions under which this can happen in an ionized region are worthy of fuller nvestigation, but the modern view based on analogous laboratory experiments uggests that the effective reduction in transverse conductivity by a magnetic eld in fact may be slight [47].

In the case of the associated zonal winds of velocity $\mathbf{v}$ to the east, the actual ffect is likewise obscure in a thick layer. The electromotive force is $\mathbf{E}' = \mathbf{v} \times \mathbf{H}$ o the north and across the layer, depending in the case of the latter also on latitude, nd insofar as circuits are available may produce toroidal magnetic fields not bservable at ground level. In the latter event, the Hall effect $\mathbf{E}' \times \mathbf{H}$ will drive ns and electrons westward (except in return circuits), the electrons more rapidly, o that the Hall current flows eastward, reducing the westward current due to $\mathbf{E}$. n fact, a reversal in current might sometimes be expected, though balanced by estward Hall currents in the returning toroidal circuits, if the Hall mobilities re there the same. Accordingly, the rôle of zonal winds, insofar as effective pro-uction of the required westward-flowing current is concerned, relates to the extent o which return circuits of toroidal currents are available. If only partially available or the use of $\mathbf{E}'$, a polarization enhancing westward current-flow may result. The all currents associated with toroidal currents would have fields, observable at round level. Hence a dynamo theory for the real atmosphere may be quite complex.

Finally, a dynamo theory of disturbance would seem to require satisfactory onductivity at night as well as by day. Hence the currents might flow mainly the F-region, throughout low and middle latitudes, at least at night. In auroral gions, the electric currents generated should extend downwards to below the -region as well. However, it is difficult to understand how there can be any gnificant Hall effects in the F-region, on the classical theory. Although $K_2 = \omega/\nu)K_1$, and the ratio ω/ν rapidly increases with height above the E-region for ns and electrons alike, for singly charged ions of any mass, the computed mobilities re the same for ions and electrons, in the F-region. An electrically neutral F-region ould have only weak Hall currents.

Actually the currents may be generated in both the lower ionosphere and the F-region. The number of negative ions in the E- and D-regions at night are unknown, and if present in sufficient numbers would permit adequate conductivity at night. However, it would probably then be necessary to explain why the ordinary quiet-day diurnal variation is smaller in amplitude at night than by day.

The foregoing discussion, on the whole, suggests that it may not be inappropriate to speculate on the possible nature of a wind-system of magnetic storms.

5. *The wind-systems of magnetic storms*—It is probable that every student of the subject of magnetic storms has at one time or another considered some form of the dynamo theory of disturbance, since Balfour Stewart first suggested this possibility in 1882. The name storm itself indicates an early felt analogy with tropospheric storms. Following the work of Jesse in the late nineteenth century, on the wind-speeds of noctilucent clouds near the height of 80 km, some interest was shown then in connecting these with aurora. Jesse concluded prior to 1894 that the winds near this height in general tended to move the clouds with a component away from the sun [48]. The interest in dynamo effects also increased greatly after ionospheric measurements appeared. But the grave difficulties found in explaining the conductivity required for the much smaller quiet-day magnetic daily variation has probably been the most serious deterrent to intensive study.

In the present paper, a tentative wind-system for an individual hour of a magnetic storm is schematically described, in the hope that it may prove of assistance to the experimentalist interested in upper-air winds. It is hoped later to compare it in quantitative terms with observation. It can lay little claim to originality, as one pattern of meridional circulation and zonal winds has been previously discussed by Harang [16], and by Wulf [12]. It is considered here in relation to the field of storms averaged around parallels of latitude, and denoted D_{st} . The remaining and more prominent part of the storm field, especially in polar regions, is denoted D_S . It varies markedly with longitude, and therefore with local time, as well as with time measured from the onset of storm. For this part, all that has been done is to extend the P_2^1 type of atmospheric circulation proposed by Vestine and Chapman [21] so that it includes vertical motion and zonal winds. The suggestion that a vertical motion might be involved in a dynamo theory of disturbance has been made also by McNish [49] and others [52]. The consideration of two superposed atmospheric circulations is mainly a matter of convenience, as the first may be the most prominent in low and middle latitudes, whereas the second circulation for D_S is supposed to apply to those disturbance features which appear almost daily, as well as to the dominant part in the polar regions during storms.

Figure 10 shows the partial current-systems derived for the maximum of the main phase of the magnetic storm, for 16^h GMT, May 1, 1933 [37]. The current-systems are shown as viewed from above the geomagnetic north pole. A total of 100,000 amperes flows between successive current-lines. Figure 11(A) shows a qualitative meridional and zonal wind-pattern as seen from above the geomagnetic north pole, a sectional view being shown in Figure 11(B), which provides a current-system such as that of Figure 10(A) [averaged round parallels of latitude]. It is intended to resemble that for the geomagnetic annual variation already discussed, and includes rising air near the equator which flows poleward and then flows downward, returning in a region of poor electric conductivity at lower levels of

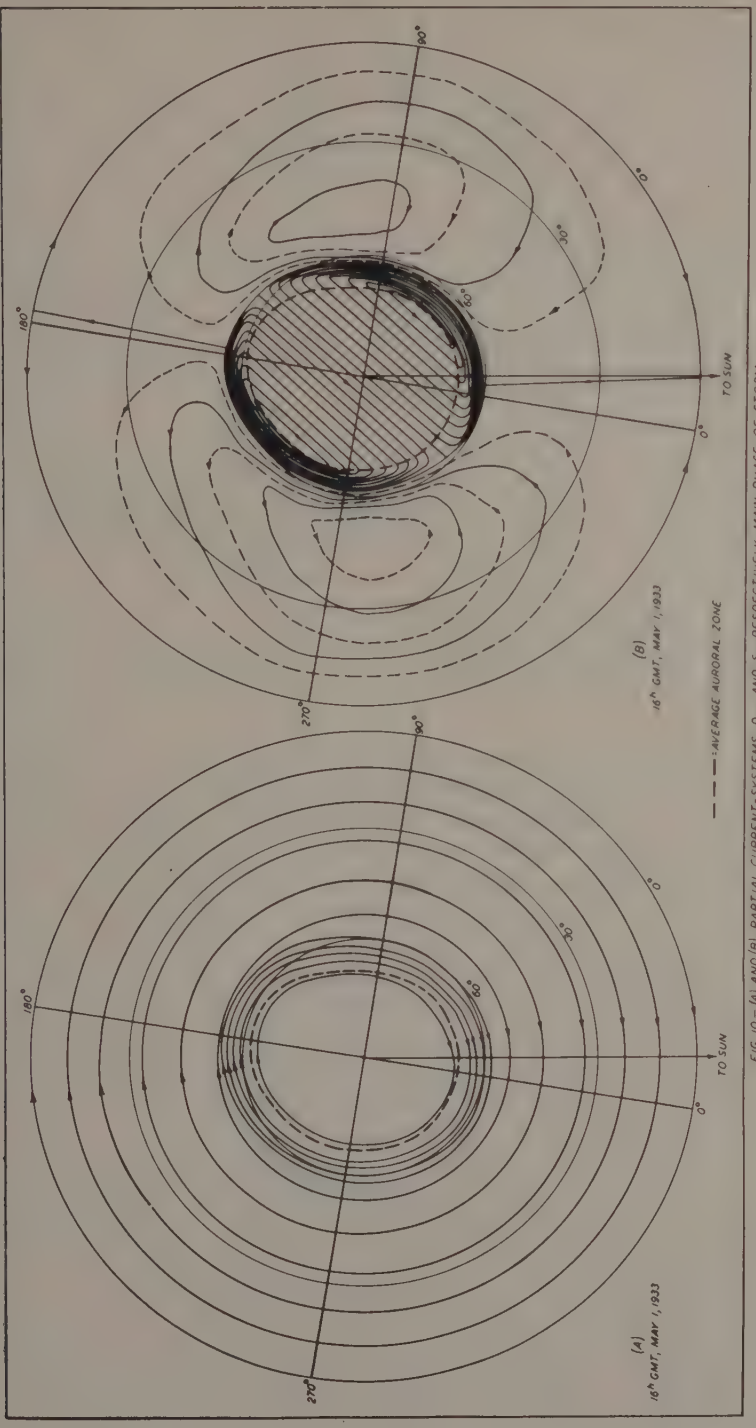

FIG 10 – (A) AND (B), PARTIAL CURRENT-SYSTEMS, D_{st} AND S_D, RESPECTIVELY, MAIN PHASE OF STORM
(100,000 AMPERES FLOW BETWEEN SUCCESSIVE FULL-DRAWN CURRENT-LINES)

the atmosphere. It probably cannot exist by itself alone and without time changes in intensity [35].

Figure 12(*A*) shows a corresponding meridional and zonal pattern for the

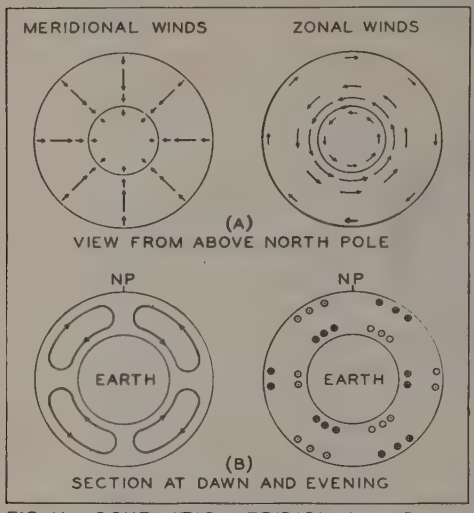

FIG. 11—SCHEMATIC MERIDIONAL AND ZONAL WINDS, MAIN PHASE, MAGNETIC STORMS FOR D_{st}

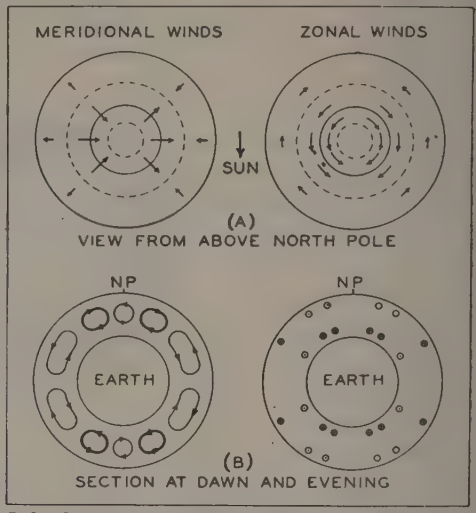

FIG. 12—SCHEMATIC MERIDIONAL AND ZONAL WINDS, MAIN PHASE, MAGNETIC STORMS FOR D_S

more or less diurnally varying part of the storm D_S [Fig. 10(*B*)]. This includes the largest field-producing part of the storm, and unlike the system of Figure 11(*A*), found strongly only during magnetic storms, is likely to represent nearly all of regular magnetic disturbance on most days of the year. The circulation near the auroral zone is supposed to provide electrojets. In order to reproduce the geomagnetic data, these two wind-systems should change very considerably in intensity, relative to one another, and in their orientation relative to the sun during the course of a storm. At main phase, they should combine to yield weak or zero eastward-flowing electric currents at the equator on the 6 a.m. meridian, and strong westward-flowing electric currents at the auroral zone. At 18^h, weak eastward-flowing currents at the auroral zone, and strong westward-flowing currents at the equator, are indicated. These results accord with those of Figure 13, the complete current-system for 16^h GMT, May 1, 1933.

It would be most interesting to attempt an extension of the foregoing comparisons in quantitative rather than qualitative terms, but this will not be attempted here. The most obvious need is for consideration of available conductivity in likely regions of interest. For instance, the wind-system for D_S , in a very great magnetic storm must provide a field of about 5,000 gammas at the (expanded) auroral zone, and 2,000 gammas at the equator. For the latter, at such times the current i per unit width of the current-system for D_S must provide a field $2\pi i = 0.02$ gauss, and since $i = KE = KuH$, for $H = 0.5$, $u = 1{,}000$ m/sec, there results $K = 10^{-7}$ for the effective integrated conductivity of the ionized region experiencing the motion. This conductivity is so high and the assumed velocity u so great that it appears likely that it is incompatible with present concepts of the transverse

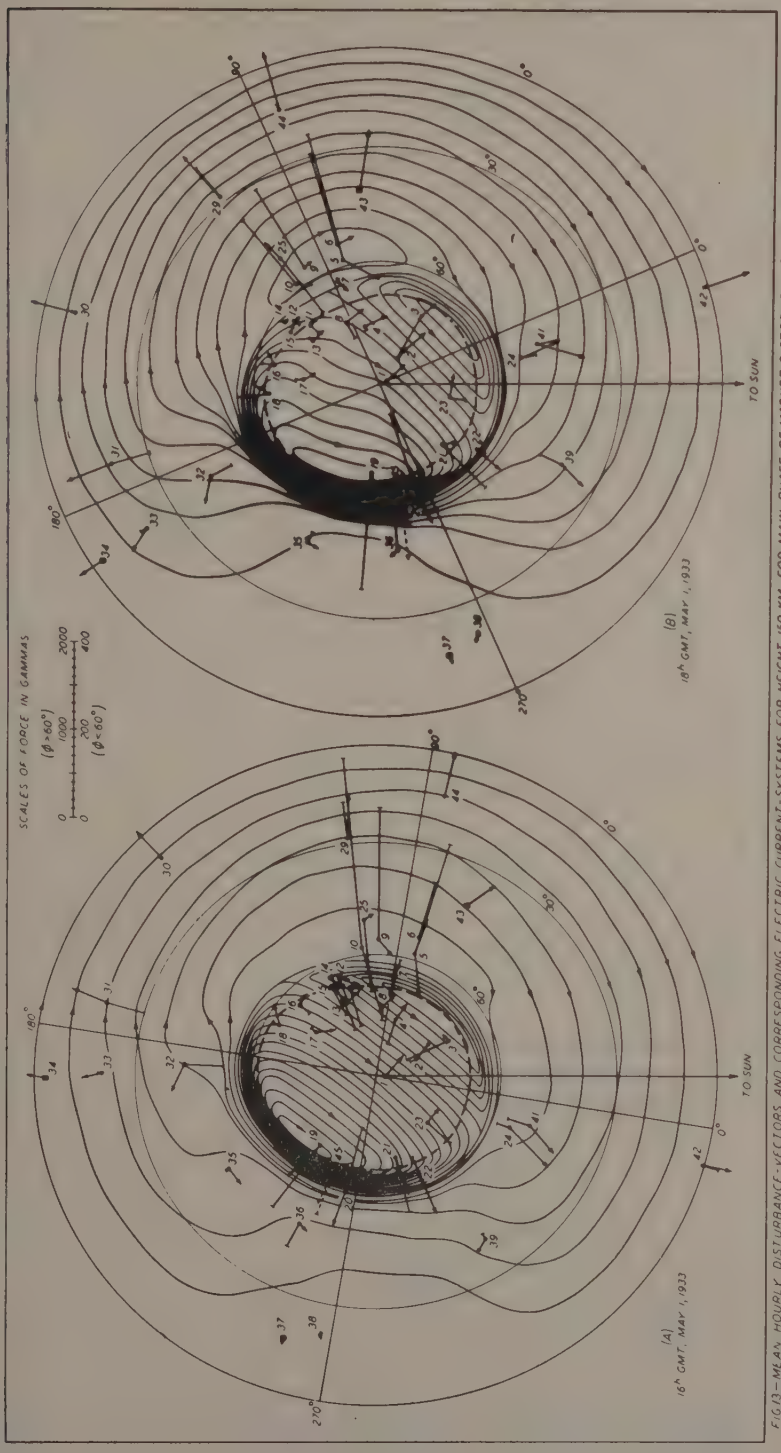

FIG 13—MEAN HOURLY DISTURBANCE-VECTORS AND CORRESPONDING ELECTRIC CURRENT-SYSTEMS FOR HEIGHT 150 KM FOR MAIN PHASE OF MAGNETIC STORMS; VIEW FROM ABOVE GEOMAGNETIC NORTH POLE

conductivity. If as suggested by Alfvén [22], the effective conductivity is likely to be about equal to that along the magnetic field in any case, or if enough polarization is present, the conductivity may of course be adequate, provided the generating winds flow throughout much of the ionosphere, as can be seen on inspection of Table 3.

It is also evident, however, that the very concentrated currents flowing along the auroral zone require a very considerable concentration of conductivity there, in order that the equation of continuity be satisfied. This question of conductivity will be referred to later in this paper. Since both wind-systems vary in intensity with time, in combined form they may satisfy the requirements for possible wind-systems [35].

Finally, from Figure 12, it can be seen that at the lower level of the circulation between north latitudes 45 to 60 degrees, there is agreement with the results for noctilucent clouds, if taken for the 80-km level. Before midnight, Jesse found several cases of winds blowing from the southwest; after midnight, the winds blew mainly from the east northeast. The smaller southward component also checks satisfactorily.

At the upper level, the wind-directions agree fairly well with those of Little and Maxwell [28] and Ryle and Hewish [29], and others, for the top of the *F*-region. The results also agree with Meinel's determination of auroral motions [50]. This remarkable agreement, showing a reversal in zonal winds at midnight and noon, is not necessarily an indication of the height of the supposed air-flow, since the same result would probably be found for several geared circulations; toroidal $\mathbf{E} \wedge \mathbf{H}$ forces may also be driving the electrons. Of course, similar comparisons should be made for other latitudes, but there seems at least a measure of agreement thus far.

6. *The initial phase of magnetic storms*—Figure 14 shows an atmospheric current-system which could reproduce the maximum of the initial phase of the storm of October 14, 1932. A wind-system which would give this result is likely to closely resemble that for Figure 11, with its circulation temporarily diminished during the initial phase, plus a system resembling that of the solar daily variation, in this particular case.

Figure 15 shows the record in horizontal intensity for the great magnetic storm of May 13, 1921, and though the data are scanty, the indications of reversals in the initial phase, at stations only some thousands of kilometers apart, probably mean that a dominant atmospheric component was present. It is clear that the differences shown between Agincourt and Cheltenham, less than a thousand kilometers apart, cannot be simply explained on potential theory in terms of sources at this or a greater distance. Thus an important part, but not necessarily all of the field change, can with reasonable certainty be ascribed to atmospheric sources, though the ultimate cause is solar.

7. *The auroral-zone currents, aurora, and toroidal fields*—It was noted that the meridional winds, for reasons of continuity, could probably not produce the exceedingly concentrated electric currents flowing along the auroral zone during magnetic disturbances without a marked local concentration in the conductivity there. It has been suggested that this added conductivity is due to protons of solar origin. No doubt the protons entering from outside will provide a major

FIG. 14— (A) AND (B), PARTIAL CURRENT-SYSTEMS, D_{ST} AND S_D, RESPECTIVELY, INITIAL PHASE OF STORM
(10,000 AMPERES FLOW BETWEEN SUCCESSIVE FULL-DRAWN CURRENT-LINES)

source of ionization, but the sequence of events in auroral displays and importan features of aurora such as the transition of homogeneous auroral arcs to ray arc have never been convincingly explained. It is hence of interest to inquire whethe toroidal magnetic fields in this region of possible high and variable zonal wind may assist in explaining some of the observed effects which have evaded effort at an explanation for so long a time.

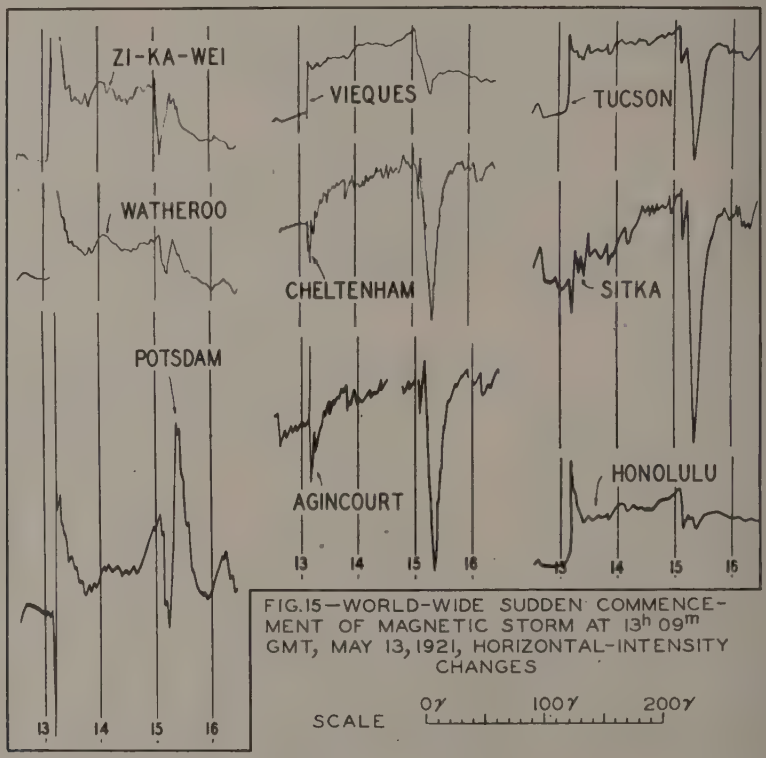

FIG. 15—WORLD-WIDE SUDDEN COMMENCEMENT OF MAGNETIC STORM AT $13^h\ 09^m$ GMT, MAY 13, 1921, HORIZONTAL-INTENSITY CHANGES

It was noted that a toroidal field of as much as a gauss would not be unexpecte along the auroral zone. If the zonal winds roughly resemble those of Figure 11 for the storm-time part D_{st} , a westward-directed toroidal field should exten around the auroral zone, between the upper and lower levels of zonal air-flow if otherwise, the toroidal field would be reversed.

The polar zonal winds in Figure 12 would predict incomplete or defectiv toroidal fields (in which the flux returns outside the region near the axis), stron at 6 a.m., and directed westward at its axis, and at 18^h directed eastwards. I large enough, these toroidal fields may exert a powerful local guiding influenc on the incoming auroral particles. Consequently, homogeneous and persisten auroral arcs would be explained as due to particles moving mainly along th poloidal and toroidal fields, ionizing the atoms along the path, with productio of auroral spectra. This would also explain the average perpendicularity of dis turbance-field changes to auroral arcs, the conductivity being that for current flow along the toroidal field, along a path already possessing excess ionization

t would be interesting to check this by methods similar to those of Gartlein [24] nd Meinel [25].

8. *The auroral electrojet*—A more daring possibility seems worth considering. f the foregoing explanation for the concentration of auroral-zone currents is orrect, as seems at least possible in view of the coexistence of possible changes in he toroidal field with time due to changes in the speed of zonal winds with time, n atmospheric "betatron" might result. This possibility will next be examined.

If $\dot{\mathbf{T}}$ is the time rate of change of the toroidal induction, from Maxwell

$$-\dot{\mathbf{T}}/c = \text{curl } \mathbf{E} \quad \ldots\ldots(17)$$

Taking cylindrical coordinates z, r, θ, with Oz along the toroidal field as axis f symmetry, and neglecting field curvature, the problem becomes similar to that onsidered by Swann [51], for generating cosmic rays in the field of sunspots, hough it is not necessary here to use his relativistic mechanics.

It is first supposed that at a distance $r = R$ from the axis the field T reaches ome value T_0 after a time τ. Suppose further that T varies as $1/r$, so that at a ime t the field T_s at $r < R$ is given by

$$T_s = RT_0 t/\tau r \quad \ldots\ldots(18)$$

From (17)

$$-RT_0/r\tau c = \text{curl}_z \mathbf{E}$$

$$= (1/r)[\partial/\partial r(rE_\theta) - \partial E_r/\partial\theta]$$

nd since by symmetry $\partial E_r/\partial\theta = 0$,

$$(\partial/\partial r)(rE_\theta) = -RT_0/\tau c$$

$$E_\theta = -RT_0/\tau c$$

The energy W of the electron after the time t is thus $W = (eT_0Rt)^2/2m\tau^2$ ergs, f all quantities are in emu, or $W = 8.7 \times 10^{-2}\ (\dot{T}_0Rt)^2$ electron volts. Swann oints out that the infinite value assumed for the field at the origin is irrelevant, ince the variation of the field as $1/r$ need persist only within a very thin range of r.

The mean free path of an electron at a height of about 200 km in the atmosphere s of the order of 100 cm, and the collision frequency at this level or somewhat igher is about 10^3. Thus, if $\dot{T}_0$ is taken as 100 gammas per second (which may be ppropriate, because changes at ground level of 5 gammas per second are common n auroral regions for the poloidal field), $R = 100$ km, $t = 10^{-3}$, there results $V = 8.7$ ev before a collision takes place, usually with a positive ion. The electric ield would have to be applied nearly parallel to the earth's main field. These equirements are hence rather extreme. Although a value of W as great as 8.7 v need not be acquired per single collision, a value of about 0.1 ev would be ecessary in order to exceed the energy kT of the gas, where T is the temperature, n order that W be permitted to increase to values of interest. After suitable data n ionic cross-sections become available, for collisions with low energy electrons, t will be possible to examine the latter point more closely. It may also be noted hat, since $\dot{T}_0$ will depend on the transverse conductivity and hence on ν^2, the roduct $\dot{T}_0 t$, other things being equal, is in this sense proportional to $1/t$. The echanism seems unlikely to be capable of yielding much acceleration of electrons

by weak electric fields in long free-path regions of the upper atmosphere. Hence if any interest in the mechanism appears warranted at all, this interest concern itself with the possibility that electrons can be driven upward from near the 150-km level, with protons being driven downward from about this level, with energies o the order of 5,000 ev, as estimated by Meinel [25]. It is then embarrassing to fin that hydrogen is almost certainly in short supply in this region, so that it has t arrive from outside the atmosphere, or be driven down slowly by the electri field of the accelerator from the upper atmosphere, in the form of protons. Th major constituent of the downgoing beam would then be positive ions, movin more slowly than the protons, and for which observational evidence is at presen wanting. An obvious requirement is that the accelerator should yield about 5,00 volts, nearly parallel to the main magnetic field along the path in which accelera tion occurs. If this path length is 50 km, say, which might be reasonable, the mini mum electric field required is then $5 \times 10^{11}/5 \times 10^{6}$ or 10^{5} emu/cm in the absenc of losses due to collision. This is 10 times as great as that assumed for the acceler ator considered above, so that an accelerator of larger linear dimensions would b required; in the absence of collisions, if $E = 10^{4}$ along this path of 50 km, th velocity will be 10^{8} cm/sec, from simple dynamics. But, if the mechanism wer altered to provide values of E slightly in excess of 10^{5} emu, the suggestion ma merit serious consideration.

The motions of the energized particles will be determined by the combine field of the earth and the toroidal field. Regarding these as represented by vector at any point, it will be clear that for any finite toroidal field all that happens i that the lines of force of the main field are bent within the toroidal volume o field, the lateral displacement of the line of force being greatest near the axis o the toroidal field. Hence the horizontal changes in toroidal field will not be paralle to the combined field. It may prove more realistic also to regard the toroidal fiel as defective, so that it resembles that of a long solenoid, with its axis along th auroral zone. The trajectories of the accelerated particles will then be determine by the net magnetic field, the velocity of the particles, the electric field (includin that of the auroral electrojets directed along the auroral zone toward the region o local midnight). It should also be noted that only when E_θ is directed nearl parallel to the poloidal field, with T small, so that $E_\theta > T$, would there seen much chance of effective acceleration of particles.

Under the conditions stated, it is clear that the particles, if accelerated in th fluctuating solenoidal field, should escape to move mainly along the lines of forc of the earth's main field, producing aurora in their passage. The initial effect ma be a homogeneous auroral arc due to protons, perhaps mainly urged downward because of initial causes. The efficiency of electron capture should increase to maximum and then decline with increasing speed of the proton, with correspondin fluctuation in the arc intensity. Meanwhile, the electric conductivity havin increased, due to production of ion pairs by the protons, it may be possible t accelerate electrons adequately by the mechanism. These may emerge first nea the ends of the solenoidal field and move upward to form rays, developing into ray arc, draperies, curtains, and corona. The elements for generation of magneto hydrodynamic waves being evidently at hand, namely, changing zonal air-flo

and changing toroidal field, it is not unlikely that the very regular progressive trains of luminosity proceeding upwards along the magnetic field are visible evidence of the propagation of such waves, in flaming aurora. The display then soon ends, and a homogeneous auroral arc later appears when conditions more favorable to the creation of a stable accelerating mechanism again arise and the sequence may be continued. Before the generation of magnetohydrodynamic waves takes place, the mechanism may possess a capacity for reversibility, such as would probably be expected for differential motions of zonal winds. This flexibility again accords well with observation, as according to Stagg [53]: "In a transition from homogeneous arc to ray arc, rayed structure developed first at the extremities of the arc; conversely, when ray arc reverted to homogeneous arc, the constituent rays persisted longer at the extremities."

It would hence be interesting to make some detailed calculations based on the foregoing or some similar model,* supposing the height to be somewhat greater, so that there would be better chances of an adequate supply of hydrogen for the creation of protons, as well as a longer time interval between collision of protons and electrons. The prelude to the formation of a homogeneous auroral arc in the early evening is usually an auroral glow, and this would seem barely explicable by the type of mechanism just considered. If the glow is also associated with an increase in ionization, due to incoming protons, this may permit adequate electric conductivity to allow a build up of the accelerating mechanism. Ionization from a jet stream of air along the auroral zone might also be a possibility. The need for a considerable electric conductivity may be illustrated by noting that, if $\dot{T} = 2\pi KHd\dot{v} = 30\gamma/\text{sec}$, for $H = 0.5$, $d = 10$ km, $\dot{v} = 1$ m/sec/sec, $v = 100$ m/sec as relative zonal wind-velocity, then $K = 10^{-12}$, which is too high an initial value.

One objection to this type of mechanism would seem to be the absence of much curvature in auroral rays. While it is a matter of abundant record that homogeneous auroral arcs in changing to ray arcs do so chiefly at the extremities of the homogeneous arc at first [53], where they may appear to show sharp curvature at the base of the rays, it is necessary to suppose that toroidal fields are very concentrated, and always very small within ray arcs themselves. Since very straight ray structure has been noted at all levels from 60 to 1,000 km by Störmer and others, it is clear that only transitory toroidal fields of appreciable magnitude can be contemplated in auroral regions, and not within any observed ray structure. However, this objection may not be valid, since if T is large no acceleration may take place. Also, as has been noted, the mechanism may appear to have some promise in explaining the usual sequential transitional changes noted at the auroral zone: homogeneous arcs to ray arcs to curtains to rays and to coronas, and their variations. The magnetic bay associated with the electrojet often shows marked oscillations near its beginning. Micropulsations of the geomagnetic field have also been noted to occur simultaneously with longitudinal oscillations in the luminosity of weak, thin, homogeneous auroral arcs [55]. Formally, changing toroidal and poloidal fields should be linked. Hence the suggestion may merit some serious consideration.

*O. R. Wulf has discussed another effect of zonal winds in this connection at "Conference on Atmospheric Motions," l.c. See J. Geophys. Res., 58, 531-538 (1953).

According to these views, the qualitative wind-system of Figure 11 is supposed to give rise to two electrojets at the auroral zone, and it is not unlikely that the electric currents generated in these electrojets close their circuits across the polar cap and in low latitudes.

9. *Toroidal fields in the F-region*—When more detailed measurements of zonal winds in the *F*-region become available, it should be possible to estimate the strengths of the toroidal fields in low and middle latitudes as well. For this purpose, it is necessary to know the vertical gradient in the zonal winds, as well as the effective transverse conductivity. For instance, if the kinematic viscosity were greatest near the height of 200 km, say, so that it is less above and below, conditions favoring the production of a vertical gradient in zonal wind-velocity might result. At a very high level, actual slippage of the atmosphere as a whole may occur. Under these conditions, toroidal fields extending from near the equator to the poles might result, with their fields directed nearly along parallels of latitude. Our present classical theory of the transverse conductivity of the atmosphere suggests that these fields are likely to be quite small and uninteresting. However, it has been suggested that the transverse conductivity in practice is likely to approach that along the geomagnetic field. From Table 3 this reaches 10^{-10} at height 300 km, and then might yield toroidal fields during magnetic storms which are strong and extensive enough to explain the observed decreases in cosmic-ray intensity at such times; of course, an alternative explanation may be afforded by meridional electric fields caused by zonal motion within solar streams and the ring-current of Chapman and Ferraro. It is likely that eastward-flowing zonal winds generate meridional currents which flow equatorwards near the *E*-region; the magnetic field at ground level would then be mainly due to the westward-flowing Hall currents, yielding the storm-time variation. In return circuits at higher levels, the Hall currents would be zero. If homogeneous auroral arcs tend to appear near the axes of localized toroidal fields, the long, thin, homogeneous auroral arcs noted by Störmer [54] and the writer [55] may be evidence of additional toroidal fields just south of the average position of the auroral zone, and near the 200-km level, as well as of a substantial vertical gradient in zonal wind-velocity.

10. *Remarks on the flux of X-ray radiation on days preceding and during magnetic storms*—The possibility of increased solar radiation during magnetic storms will next be considered. The solar daily variation on magnetically quiet days (S_q) is augmented during solar flares of ultraviolet light [56]. The amplitude of S_q on individual days may then roughly indicate the X-ray flux absorbed near and within the *E*-region, in which the current-system responsible for S_q appears to flow.

Figure 16 illustrates the average amplitude of S_q as given by its noon maximum minus the average of the preceding and following midnight value near the equator, for five days preceding and during those major magnetic storms of the period 1905 to 1942. The amplitudes were those used in another study [37]. They are given in terms of the 12-year average for 1922-33 taken as unity. The amplitudes are averaged for four groups of about 30 storms each (or less), during four periods of the Greenwich day.

Since the four samples of data give essentially the same amplitudes, it is concluded that the flux of radiation absorbed in the *E*-region is substantially the same on days preceding and during magnetic storms. The average amplitude is

about 1.2, which is expected since the magnitude of S_q is greater near sunspot maximum, when magnetic storms are more frequent. A small increase in amplitude is shown for the day of sudden commencement, in the case of storms beginning at 13^h to 18^h GMT. This probably reflects mainly the apparent additive effect on the noon values of field due to the initial phase of storms at Huancayo, about five hours west of the Greenwich meridian; for years prior to 1922, the amplitude of S_q was based on Apia, Samoa, and Manila, P.I. It may also be remarked that the determination of the average amplitude of S_q on storm days was possible because D_S is on the average about zero near noon and midnight. Although it should be possible to correct roughly for any spurious effects of the initial phase on the apparent amplitude of S_q , the initial phase is ordinarily so short in duration that this has not been attempted here.

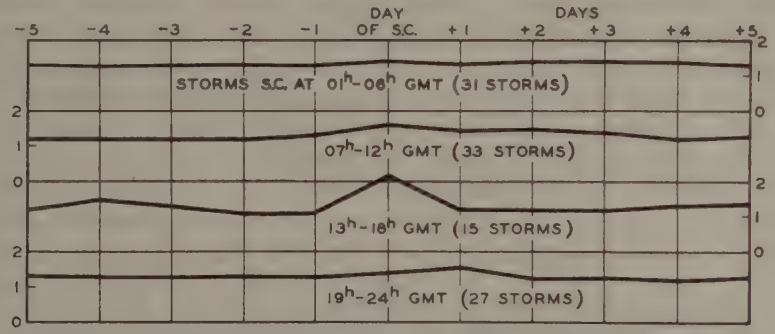

FIG. 16—AVERAGE AMPLITUDE OF SOLAR DAILY MAGNETIC VARIATION ON DAYS PRECEDING AND DURING MAGNETIC STORMS IN TERMS OF 12-YEAR AVERAGE, 1922-33, TAKEN AS 1.0

From Figure 16, it is concluded that the average integrated conductivity of the E-region is the same on days preceding and during magnetic storms. If S_q is due to a wind-system giving rise to dynamo action, this wind-system is about the same in intensity on days preceding and during magnetic storms. If magnetic storms are due to enhanced wind-systems and dynamo action, these wind-systems do not seem in the least degree to have affected a possible wind-system for S_q . The latter conclusion may appear strange and unnatural. Of course, if magnetic storms are not due to the dynamo action of winds in the ionosphere, the lack of a correlation would be simply explained. It may then be necessary to explain why the observed motions of conducting air in the ionosphere correlated with magnetic activity [28] fail to give rise to observable magnetic effects. Accordingly, it appears likely the explanation is that S_q is generated by the tidal air-motions due to gravitational causes [15], with transitory changes in conductivity during solar flares as suggested by McNish [56].

Having arrived at the conclusion that the solar flux of X-rays ionizing the E-region is sensibly unchanged during magnetic storms, and adopting the prevalent view that S_q is of tidal origin, it is next necessary to consider how a wind-system responsible for magnetic disturbance might arise. It is rather clear that transient solar heating due to the part of the spectrum ionizing the E-region can scarcely be of interest, because it appears to be about the same both before and during a storm, according to the results of Figure 16. This may suggest that the accumula-

tion of the solar energy takes place over a period of many days, until as Wulf [12] proposes, a condition of instability arises, precipitating marked changes in the circulation, which, if the dynamo theory is correct, would then give rise to a magnetic storm.

Another possible source which may merit careful consideration is that the solar and terrestrial atmospheres may be dynamically linked *via* magnetohydrodynamic waves. If these can be generated by zonal flow, in the solar streams considered in the Chapman-Ferraro theory of storms, a wave of period a few hours to a day or more should be able to penetrate, perhaps to the *E*-region, along the lines of force of the earth's atmosphere. On this view, some transient zonal winds would be merely a manifestation of long-period magnetohydrodynamic waves entering and being absorbed, accompanied by toroidal fields, currents, and evidence of rapid downward motion in the *F*-region. At the ground, polarized disturbance as in bays would be noted. In regions of non-uniform conductivity and magnetic field, the transmission of such waves would be inefficient and complex. However, the mechanism may be sufficiently interesting to warrant more complete examination of this special form of electromagnetic wave accompanied by mass motions.

It is probably simpler to suppose that the energy driving the wind-system of Figure 11 is given up by the general circulation of the atmosphere at lower levels. On this view, the wind-system of Figure 11, decaying steadily since the last magnetic storm, will reach the stage when it is relatively weak, due to the counter-accelerating action of zonal winds. A small sudden increase in conductivity in the low ionosphere, due to solar radiation, would then be required to produce the sudden commencement. Unhappily, there is no present observational evidence of this increase in conductivity, though electrical effects occur [57].

IV. SUMMARY AND CONCLUSIONS

Order of magnitude calculations and qualitative considerations show that the greater part of the field of magnetic storms may possibly arise from atmospheric-electric current-systems produced by the dynamo action of winds. Tentative wind-systems are deduced from the geomagnetic data and, though these cannot be inferred uniquely, they may conform to some indications of the motions of noctilucent clouds, tentative radio-measurements, and radio-star scintillation results, as well as with several features of a circulation proposed by Kellogg and Schilling from meteorology. It is by no means clear that such wind-systems play a part in the production of magnetic storms.

The wind-systems described are subject to grave uncertainties respecting the rôle of winds in modifying the effective transverse conductivity of the ionosphere.

A beginning is made in the treatment of the dynamo theory of a thick layer of conducting atmosphere. Estimates of toroidal fields accompanying zonal winds in the ionosphere indicate that these are likely to be significant, and under certain conditions may attain values comparable with or larger than the observed poloidal field.

It is shown that in equatorial regions the average amplitude of the solar daily magnetic variation is very nearly the same on storm days as on days preceding magnetic storms. It is accordingly concluded that the flux of solar radiation

absorbed in the E-region is about the same on storm days as on days prior to storms.

The immediate source of field during the sudden commencement, initial phase, and main phase of storms seems likely to be mainly atmospheric in location in higher latitudes, and this is also the case in the equatorial regions, except possibly in the field component of storms averaged around parallels of latitude.

Atmospheric processes which might facilitate concentrations of ionization along the auroral zone are discussed, and a simple dynamo theory of the auroral electrojet outlined. In connection with these, it is supposed that expansions of the auroral zone during hours of intense disturbance may be due to increased speed of meridional air-flow, accompanied by conservation of angular momentum. However, the average position of the auroral zone, as indicated by concentrated electric currents flowing along it, appears to vary little with season. It is not immediately clear that this observed condition is compatible with a heat-driven air-circulation of the upper atmosphere. This point merits careful consideration, as does the apparent nearly simultaneous appearance of electrojets in north and south polar regions. Although there are means whereby winds can provide an effective increase in transverse conductivity, it is not yet clear that these means are operative efficiently in the ionosphere. The sudden commencement and initial phase might arise from winds, but the mechanism responsible for the production of such winds is quite obscure.

References

[1] Balfour Stewart, Terrestrial magnetism, Encyclopedia Britannica, 9th ed., **16**, 181 (1882).

[2] A. Schuster, The diurnal variations of terrestrial magnetism, Phil. Trans. R. Soc., A, **208**, 163-204 (1908).

[3] S. Chapman, The solar and lunar diurnal variation of the earth's magnetism, Phil. Trans. R. Soc., A, **218**, 1-118 (1919).

[4] A. E. Kennelly, Elec. World and Eng., **15**, 473 (1902).

[5] O. Heaviside, Encyclopedia Britannica, 9th ed., **33**, 215 (1902).

[6] E. V. Appleton and M. A. F. Barnett, Proc. R. Soc., A, **109**, 621-641 (1925).

[7] G. Breit and M. A. Tuve, Phys. Rev., **28**, 554-575 (1926).

[8] D. R. Bates and H. S. W. Massey, The negative ion concentration in the lower ionosphere, J. Atmos. Terr. Phys., **2**, 1-13 (1951).

[9] M. Hirono, J. Geomag. Geoelectr., **4**, 7-21 (1952).

[10] W. G. Baker and D. F. Martyn, Nature, **170**, 1090-1092 (1952).

[11] S. F. Singer, E. Maple, and W. A. Bowen, Jr., J. Geophys. Res., **56**, 265-281 (1951).

[12] O. R. Wulf, On the relation between geomagnetism and the circulatory motions of the air in the atmosphere, Terr. Mag., **50**, 185-197 (1945), *idem*, 259-278 (1945).

[13] H. B. Maris and E. O. Hulburt, A theory of auroral and magnetic storms, Phys. Rev., **33**, 412-431 (1929); E. O. Hulburt, Phys. Rev., **31**, 1038-1039 (1928).

[14] A. G. McNish, On the ultraviolet light theory of magnetic storms, Phys. Rev., **52**, 155-160 (1937).

[15] S. Chapman and J. Bartels, Geomagnetism, Oxford, Clarendon Press, Vol. 2, 870-875 (1940).

[16] L. Harang, The aurorae, New York, John Wiley and Sons, Inc. (1951), and references there cited.

[17] J. Bartels, Geophysik, Teil 1, Naturforschung und Medizin in Deutschland, 1939-1946, 74-75, Dieterich'sche Verlagsbuchhandlung, Wiesbaden (1948). (Fiat review of German science.)

[18] S. Chapman and V. C. A. Ferraro, Terr. Mag., **36**, 77-97, 171-186 (1931); **37**, 147-156, 421-429 (1932); **38**, 79-96 (1933); V. C. A. Ferraro, J. Geophys. Res., **57**, 15-49 (1952).

[19] D. F. Martyn, Nature, **167**, 92-94 (1951).
[20] S. Chapman, Proc. R. Soc., A, **95**, 61-83 (1918).
[21] E. H. Vestine and S. Chapman, Terr. Mag., **43**, 351-382 (1938).
[22] H. Alfvén, Cosmical electrodynamics, Oxford, Clarendon Press (1950).
[23] A. I. Lebedinski, Dok. Akad. Nauk SSSR, **86**, 913-916 (1952).
[24] C. N. Gartlein, Trans. Amer. Geophys. Union, **31**, 18-20 (1950).
[25] A. B. Meinel, Astrophys. J., **113**, 50-59 (1951).
[26] H. Siedentopf, A. Behr, and H. Elsässer, Nature, **171**, 1066-1067 (1953).
[27] G. J. Phillips, J. Atmos. Terr. Phys., **2**, 141-154 (1952).
[28] C. G. Little and A. Maxwell, J. Atmos. Terr. Phys., **2**, 356 (1952); Nature, **159**, 746 (1952).
[29] M. Ryle and A. Hewish, Mon. Not. R. Astr. Soc., **110**, 381-394 (1950).
[30] George H. Millman, A study of ionospheric winds and turbulence utilizing long radio waves, Scientific Report No. 37, The Pennsylvania State College, State College, Penn., 1-123 (1952).
[31] C. D. Salzberg and R. Greenstone, J. Geophys. Res., **56**, 521-533 (1951).
[32] L. A. Manning, O. G. Villard, and A. M. Peterson, Proc. Inst. Radio Eng., **38**, 877-883 (1950).
[33] G. H. Munro, Proc. R. Soc., A, **202**, 208-223 (1950).
[34] W. W. Kellogg and G. F. Schilling, J. Meteor., **8**, 222 (1951).
[35] H. Jeffreys, Q. J. R. Met. Soc., **48**, 29 (1922).
[36] N. Stoyko, Paris, C.-R. Acad. sci., **233**, 80-82 (1951).
[37] E. H. Vestine, L. Laporte, I. Lange, and W. E. Scott, The geomagnetic field, its description and analysis, Carnegie Institution of Washington Publication 580, Washington (1947).
[38] B. Cynk, Terr. Mag., **44**, 51-57 (1939).
[39] L. V. Berkner and H. W. Wells, Terr. Mag., **43**, 15-36 (1938).
[40] S. E. Forbush, Phys. Rev., **54**, 975-988 (1938).
[41] D. F. Martyn, Proc. R. Soc., A, **189**, 241–260 (1947).
[42] E. C. Bullard, Proc. R. Soc., A, **199**, 413-443 (1949).
[43] D. F. Martyn, Proc. R. Soc., A, **218**, 1-18 (1953).
[44] T. G. Cowling, Mon. Not. R. Astr. Soc., **93**, 90-98 (1932).
[45] K. Maeda, J. Geomag. Geoelectr., **2**, 45-53 (1950), and later papers.
[46] K. C. Westfold, Phil. Mag., **44**, 712-724 (1953), and references there cited.
[47] R. L. F. Boyd, Editor, Proceedings of the conference on dynamics of ionized media March 19-21 (1951); University College, London, April 1951.
[48] O. Jesse, Astr. Nachr., **140**, 161 (1896); C. Störmer, Astroph. Norvegica, **1**, 87-114 (1935) E. H. Vestine, J. R. Astr. Soc. Canada, **26**, 244-272, 303-317 (1934).
[49] A. G. McNish, Trans. Edinburgh Meeting, 1936, Internat. Union Geod. Geophys. Ass. Terr. Mag. Electr., Bull. No. 10, Edinburgh Meeting, 282-289 (1937).
[50] A. B. Meinel and D. H. Schulte, Astroph. J., **117**, 454-455 (1953).
[51] W. F. G. Swann, Phys. Rev., **43**, 217-220 (1933); L. Riddiford and S. T. Butler, Phil Mag., **43**, 447-456 (1952).
[52] N. Fukushima, Polar magnetic storms and geomagnetic bays, J. Fac. Sci., Tokyo Univ. 8, 293-412 (1953)—this valuable monograph includes an alternative form of the dynamo theory of storms and an excellent bibliography; T. Nagata and N. Fukushima, Geophys. Notes, Tokyo, 5, 85-97 (1952); T. Nagata and H. Ono, J. Geomag. Geoelectr., **4** 108-113 (1952).
[53] J. M. Stagg, British Polar Year Expedition, Fort Rae, 1932-33, **1**, p. 267, Royal Society London (1937).
[54] Carl Störmer, Geofys. Pub., **11**, 1-19 (1935).
[55] E. H. Vestine, Terr. Mag., **48**, 233-236 (1943).
[56] A. G. McNish, Terr. Mag., **42**, 109 (1937).
[57] E. V. Appleton and W. R. Piggott, Nature, **165**, 130-131 (1950).

GEOMAGNETIC AND SOLAR DATA

INTERNATIONAL DATA ON MAGNETIC DISTURBANCES, THIRD QUARTER, 1953

Preliminary Report on Sudden Commencements

S.c.'s given by five or more stations are in italics. Times given are mean values, ith special weight on data from quick-run records.

Sudden commencements followed by a magnetic storm or a period of storminess (s.s.c.)

1953 July *23d 08h 08m:* twenty-five.
1953 August *12d 00h 45m:* five.—*23d 00h 24:* thirty-three.
1953 September *15d 02h 59m:* thirty-six.—*18d 16h 09:* twenty-two.

Sudden commencements of polar or pulsational disturbances (p.s.c.)

1953 July 02d 02h 01m: SM Eb Va Hr.—02d 21h 52: Tr SM Ta El.—05d 00h 37: u Ta.—05d 05h 53: Te Am.—*06d 00h 37:* seventeen.—*07d 23h 18:* twelve.—8d 20h 31: Wn Fu IK Qu.—10d 14h 40: Ka To.—*11d 22h 51:* nine.—*12d 20h 26:* even.—*13d 20h 50:* eight.—15d 00h 23: Tl SF.—*18d 23h 34:* six.—*19d 20h 00:* five. -21d 00h 18: CF Tl.—*21d 21h 52:* twelve.—22d 21h 21: Ma Qu.—23d 21h 46: Tr M Ta.—24d 11h 48: Te Hr.—25d 23h 54: Ma Fu Ta.—26d 00h 35: Es Ma.—7d 18h 40: Es Ta.—28d 21h 48: Tr SM.—*29d 20h 12:* five.—*29d 23h 21:* eight.—0d 21h 00: Es Ma Fu SM.—31d 19h 07: Le Wn Ma IK.

1953 August *01d 20h 50m:* five.—*02d 19h 20:* five.—*05d 18h 58:* nine.—*05d 20h 4:* six.—*07d 01h 39:* seven.—*07d 23h 27:* five.—09d 19h 50: Fu Qu.—10d 21h 33: u Qu.—10d 21h 59: Le Qu El Hr.—11d 00h 05: Fu SM Ta.—*15d 19h 55:* twenty-ne.—*18d 01h 19:* nine.—18d 02h 02: IK Va.—20d 19h 30: El Tn.—20d 20h 40: El n.—20d 23h 16: Tl El Tn.—22d 20h 40: Qu Bi El.—24d 19h 10: Do Ta El.—4d 22h 40: Eb Ta Hr.—26d 21h 35: Fu Tl.—26d 21h 48: Ci SF El.—27d 19h 30: a Hr.—28d 20h 37: Tr Ta El.—*29d 20h 17:* seven.—30d 14h 46: IK Ka Ta Bi.—1d 20h 03: Ta Tn Hr.—31d 22h 46: Ta El.

1953 September *02d 01h 00m:* six.—*02d 01h 17:* ten.—02d2 2h 23: Le Es Wn Ta.—3d 17h 33: Wn Ci Ta El.—03d 22h 15: Ta El Hr.—*04d 18h 33:* five.—*04d 23h 44:* x.—05d 00h 27: Ci El.—05d 18h 48: So Wn.—05d 19h 34: Tr Fu.—*06d 20h 25:* xteen.—*06d 22h 58:* seven.—07d 16h 59: Fu IK.—*10d 22h 13:* twelve.—11d 00h 2: Wn Fu IK Te.—*11d 00h 53:* six.—11d 19h 56: Tr So Wn Fu.—12d 20h 32: Tr o Wn Fu.—*13d 21h 10:* fifteen.—20d 02h 00: Wn Ta.—21d 17h 04: Fu IK Qu.—*2d 01h 30:* ten.—*22d 18h 24:* five.—*22d 20h 24:* five.—22d 23h 32: Wn Fu Ta.—3d 16h 10: Fu IK.—*23d 21h 21:* eight.—*24d 19h 55:* seven.—24d 20h 16: Ci IK.—*5d 19h 03:* eleven.—*26d 21h 15:* five.—27d 02h 20: Fu Ta.—27d 23h 49: Fu Tl Ta,

Geomagnetic planetary three-hour-range indices Kp, preliminary magnetic character-figures, C, a final selected days, July to September, 1953

July 1953									
E	1	2	3	4	5	6	7	8	Sum
1	3+	4−	5−	6−	5−	2+	3−	3+	30+
2	4+	5−	5−	3+	4o	4−	4o	4o	33−
3	3+	2+	3+	3+	4o	3o	3o	3−	25o
4	3o	3+	4−	4+	4−	3o	3o	2o	26o
5	2o	3o	4o	3−	2+	2−	2o	2o	20−
6	5−	1+	2+	2+	1o	1+	1o	3o	17o
7	3+	4o	4−	2−	3+	3+	3o	4o	26+
8	4−	3−	3−	3o	2−	2+	4−	3o	23−
9	2+	1+	2o	2−	2o	2o	4o	3+	19−
10	3−	2o	3−	1−	1−	1+	1−	1−	11+
11	1+	3o	1−	1+	1+	0+	1−	1o	10−
12	1−	2−	0+	0+	2−	2−	5−	4+	15+
13	2o	2+	4−	3+	2+	2+	2o	3−	21−
14	1o	1−	1−	1o	2o	4o	4o	2+	16−
15	3o	4−	4−	3−	3+	3−	3−	1o	23−
16	1+	2−	1o	1−	0+	0+	0o	1−	6o
17	0+	1o	2+	2o	1+	1−	0+	1−	9−
18	2+	2−	1−	1+	2o	1−	0+	1+	10+
19	3−	2o	1+	1−	1−	0+	2−	2o	11+
20	3−	3−	1+	2o	2+	2o	0+	1o	14+
21	2−	1+	2+	2o	1−	1−	1−	2o	11+
22	0+	0+	2−	2−	1−	2o	1+	3o	11o
23	3+	4+	3+	5+	6−	5+	5−	5+	37+
24	4+	2−	1+	3+	3−	3o	3−	2+	21+
25	0+	1o	1+	1o	2o	3o	4−	3−	15o
26	4+	3o	3o	3o	4−	2+	4o	4o	27+
27	4+	6o	6−	4+	5−	5o	5−	3o	38−
28	4−	5−	5o	4−	3+	3+	4−	3+	31−
29	4o	5−	4+	4+	3+	4o	4+	5−	34−
30	4+	3o	4+	4−	4o	3+	3+	4o	30o
31	4o	3+	4−	4o	4−	2+	2o	2−	25−

August 1953									
1	3o	3o	2o	2o	3o	3o	3+	4−	23o
2	2+	3+	3−	3o	1+	2o	3−	2o	19−
3	2+	2−	2+	1−	2o	2−	2o	2−	14−
4	3o	2+	2o	1o	2−	3−	2+	2−	17−
5	1+	1o	2o	2o	1−	1−	3−	2o	12−
6	1−	1−	1+	2o	2−	3−	2o	2o	13o
7	4−	2+	2−	3o	1+	1+	2o	2+	18−
8	2+	2+	2+	2−	1+	1+	1−	2−	14−
9	3+	4−	3−	2o	3+	2+	4+	3−	24−
10	2+	2+	5o	3+	2+	3−	2+	4+	25−
11	4+	4+	3+	3−	2+	3+	3o	3−	26o
12	4+	5+	5o	5+	4+	6−	3+	3+	37−
13	4o	3+	3o	1o	4−	4−	5o	5−	28−
14	3+	4−	2−	2+	2−	2+	2+	2−	19o
15	2o	1+	2o	1+	2−	1o	4−	3−	16−
16	3o	2−	2o	4−	2o	2o	2+	2+	19o
17	2−	1o	1−	0+	2+	1+	1−	1−	9−
18	3−	2o	1−	0+	2−	2−	1o	2−	12−
19	2−	2−	1−	1o	2−	1o	1−	1−	9o
20	1+	0+	1−	1−	1−	0+	0+	1o	5−
21	1−	1o	1o	1o	1−	1−	0+	0+	6−
22	0+	2−	1+	1+	1+	1−	1o	1o	9−
23	4−	3+	3+	5+	4+	5o	5o	6+	36−
24	5+	6o	4+	4−	5−	6−	5+	7−	42−
25	4o	4+	5o	5+	5−	3−	3o	3−	32−
26	4o	5−	3+	2o	3+	3+	4o	5−	29−
27	5o	5o	4+	5o	5−	5+	5−	4o	38o
28	5−	5−	4o	5−	4−	5o	4o	5−	35−
29	3+	5o	5o	5+	4−	4+	5+	4o	36o
30	5+	5o	5+	5−	5o	6−	4o	4o	39o
31	5−	4+	3−	4−	5o	4o	3+	4−	31−

September 1953									
E	1	2	3	4	5	6	7	8	Sum
1	2+	3−	4−	3o	4o	3o	3−	2o	23+
2	5−	4o	4o	3−	3−	3+	3+	3o	28−
3	2+	2−	3−	3−	3o	5+	5+	7+	30+
4	7+	7−	5−	5o	4−	3+	5+	5−	41−
5	6o	4+	3o	2+	2+	1+	3+	3o	26−
6	1o	1+	5o	3−	3o	1−	3−	3o	19+
7	1+	3o	3+	3+	3−	3+	2−	3+	22o
8	3o	2+	3o	4−	2−	2o	2−	1−	18o
9	3o	3+	2−	1o	1−	1−	1−	1+	12+
10	1+	1−	2o	2−	2+	2o	2−	4−	15+
11	6−	3−	3o	2+	3o	1o	2−	1+	21−
12	2o	1+	2o	3o	2+	2o	3o	3+	19o
13	3o	3o	3+	3o	1+	1o	1o	2+	18o
14	0+	1−	1+	1−	0+	1−	1−	0o	5−
15	0o	3−	3−	3+	4o	4−	5o	3o	24+
16	3−	3−	2+	3o	3−	4−	4−	3−	23+
17	4o	3+	3+	2o	3o	2o	3o	2−	22+
18	2+	3−	3−	1o	1−	2+	4+	6−	22−
19	6+	6+	6o	6+	6o	7−	5−	5o	47+
20	5+	5+	4+	3+	4+	4+	4+	5−	36o
21	4+	4−	5o	4o	4o	4+	3o	3+	32−
22	5+	5−	6−	4−	3−	1+	4−	5−	32−
23	4o	5+	5+	5o	5+	5o	5o	4o	39o
24	4o	4o	5+	5−	5o	3−	4−	3o	32+
25	3o	2o	3+	3−	4−	3o	3−	2−	22o
26	1+	1+	2+	2o	2o	2−	2+	3+	16+
27	5−	5−	4+	3+	3o	2o	2o	1o	25o
28	3−	3+	2o	1o	1+	1+	2o	1o	15−
29	1−	1+	1−	1o	2−	2−	1−	0+	8o
30	0o	1+	2−	2o	2−	1+	3o	3−	14−
31									

Preliminary *C*, 1953		
July	Aug.	Sep.
1.1	0.8	0.8
1.1	0.6	0.9
0.8	0.4	1.5
0.8	0.5	1.7
0.6	0.4	1.1
0.7	0.4	0.8
1.0	0.6	0.8
0.8	0.3	0.5
0.6	1.0	0.3
0.2	1.0	0.6
0.2	1.0	0.9
0.6	1.4	0.6
0.8	1.2	0.5
0.6	0.8	0.0
0.8	0.6	1.3
0.0	0.6	1.0
0.1	0.1	0.7
0.2	0.2	1.0
0.2	0.1	1.8
0.4	0.0	1.4
0.2	0.0	1.2
0.4	0.1	1.1
1.5	1.6	1.4
0.8	1.6	1.2
0.6	1.3	0.8
1.0	1.1	0.5
1.4	1.5	0.9
1.2	1.3	0.3
1.2	1.4	0.2
1.0	1.5	0.5
0.8	1.3	

Final Selected Da		
July	Aug.	Sep
Five quiet		
11	17	9
16	19	14
17	20	28
18	21	29
21	22	30
Five disturbed		
1	12	3
2	23	4
23	24	19
27	27	20
29	30	23
Ten quiet		
10	3	8
11	5	9
16	6	10
17	8	12
18	17	13
19	18	14
20	19	26
21	20	28
22	21	29
25	22	30

Sudden impulses found in the magnetograms (s.i.)

1953 July 01d 12h 12m: Le Es Tn.—*07d 14h 25:* six.—07d 21h 34: SF Te.—*1d 17h 41:* eleven.—14d 19h 52: Ta Hr.—23d 19h 30: Te Ta.

1953 August 06d 16h 38m: Qu El.—11d 17h 00: Fu Ci. —12d 14h 24: Fu Ta.—2d 15h 24: Fu IK Ta. —13d 14h 43: Te Ta.—13d 15h 05: Ta Hr.—27d 13h 05: Fu b.

1953 September 03d 20h 48m: Te Ta Hr. —11d 14h 28: SM Ci Hu.—15d 14h 44: F Ka Ta Tn.—16d 09h 00: Ta Tn.—18d 18h 32: Te Ta Tn.

Preliminary Report on Solar-flare Effects

Effects confirmed by ionospheric or solar observations are in italics.

1953 July 07d 12h 27m–12h 47m: Va. —12d 18h 48–19h 09: Te (bay?). —12d 22h 5–22h 54: Te (bay?).—14d 14h 10–14h 50: Tu. —24d 00h 21–01h 03: Te.—7d 13h 27–13h 33: Te.—31d 15h 36–15h 48: Te.

1953 August 01d 21h 27m–21h 33m: Te.—06d 19h 32–19h 47: Te.—10d 00h 18–0h 40: Tu (s.i.?).—11d 17h 00–17h 15: Tu (s.i.?).—11d 22h 21–22h 33: Te.—3d 19h 41–20h 04: Te.—13d 21h 41–21h 51: Te (bay?).—14d 22h 01–22h 18: Te bay?). —23d 00h 24–00h 35: Tu (s.s.c.?).—23d 17h 18–17h 28: Te (s.i.?). —24d 13h 9–13h 25: Te.—24d 20h 20–20h 23: Te. —24d 22h 39–23h 26: Te (bay?). —27d 21h 2–21h 23: Te.—29d 14h 12–14h 18: Te.—31d 21h 23–21h 35: Te.

1953 September 03d 18h 19m–18h 25m: Te. —11d 14h 30–14h 37: Ch. —11d 19h 8–19h 29: Te.—11d 20h 18–20h 31: Te. —15d 14h 42–14h 51: SJ (s.i.?).—15d 14h 2–14h 50: Te (s.i.?).—18d 15h 35–15h 49: SJ.—23d 14h 31–14h 41: Te.

Ionospheric or solar disturbances without clear geomagnetic effect

None.

Minor disturbances reported by one station only are listed in the De Bilt uarterly circular, but omitted here.

COMMITTEE ON CHARACTERIZATION OF MAGNETIC DISTURBANCES

BARTELS, *Chairman*
University
Göttingen, Germany

J. VELDKAMP
Kon. Nederlandsch Meteorologisch Instituut
De Bilt, Holland

PROVISIONAL SUNSPOT-NUMBERS FOR OCTOBER TO DECEMBER, 1953

(Dependent on observations at Zurich Observatory and its station at Locarno and Arosa)

Day	Oct.	Nov.	Dec.
1	0	12	0
2	0	11	0
3	7	10	0
4	7	9	0
5	0	0	0
6	13	0	0
7	13	0	0
8	14	0	0
9	11	0	0
10	10	0	0
11	9	0	0
12	9	0	0
13	8	0	0
14	29	0	0
15	22	0	0
16	13	0	0
17	9	0	0
18	0	0	0
19	0	0	0
20	0	0	0
21	7	0	0
22	0	0	0
23	0	0	0
24	7	0	8
25	7	0	9
26	12	0	9
27	7	0	9
28	7	0	10
29	0	0	9
30	0	0	0
31	8		0
Means.....	7.4	1.4	1.7
No. days.....	31	30	31

Mean for quarter: 3.5 (92 days)
Mean for year 1953: 13.3 (365 days)

M. WALDMEIER

SWISS FEDERAL OBSERVATORY
Zurich, Switzerland

CHELTENHAM THREE-HOUR-RANGE INDICES *K* FOR OCTOBER TO DECEMBER, 1953

[*K*9 = 500γ; scale-values of variometers γ/mm: *D* = 5.4; *H* = 2.5; *Z* = 4.3]

Gr. day	October 1953			November 1953			December 19		
	Values *K*		Sum	Values *K*		Sum	Values *K*		Su
1	3411	3132	18	1122	1122	12	1111	0110	
2	2202	2111	11	1131	1112	11	1221	1010	
3	1332	2222	17	1011	1122	9	2211	2113	1
4	2101	2211	10	3111	1112	11	3222	2122	1
5	1122	0121	10	3333	2110	16	3221	0120	1
6	1121	1022	10	1031	2111	10	2111	2222	1
7	2153	2113	18	1222	1121	12	3211	0112	1
8	2221	2224	17	1122	1113	12	1221	2223	1
9	2442	1222	19	2210	0000	5	3001	1131	1
10	3210	2322	15	0000	0000	0	1022	1223	1
11	0011	2321	10	0000	2122	7	2434	5434	2
12	1211	1011	8	3222	3233	20	4442	3324	2
13	1100	1111	6	4653	6443	35	2322	2233	1
14	1210	1110	7	4543	5443	32	2222	2121	1
15	0022	6544	23	1445	5442	29	0112	1132	1
16	6531	2355	30	5633	2354	31	3132	1222	1
17	5344	3444	31	4332	2344	25	1111	2213	1
18	4444	4546	35	4423	3232	20	3012	1112	1
19	6556	4343	36	5533	5344	32	0021	1122	
20	4544	3443	31	3533	3444	29	1120	1222	1
21	3355	3222	25	4233	2222	20	2111	1013	1
22	2452	3333	24	2121	1012	10	1322	1221	1
23	3432	2121	18	1235	2443	24	1000	1122	
24	0023	4221	14	4332	1222	19	2321	1011	1
25	3422	1222	18	2432	3243	23	1111	1123	1
26	1221	1012	10	3221	1010	10	1001	0123	
27	4244	1132	21	3241	2112	16	1121	1313	1
28	4311	1212	15	0111	0012	6	3211	2222	1
29	2322	1333	19	3212	0000	8	2011	2323	
30	2121	1121	11	1010	1111	6	0211	1112	
31	3341	1101	14				1222	0101	

J. B. CAMPBELL
Observer-in-Cha

CHELTENHAM MAGNETIC OBSERVATORY
Cheltenham, Maryland, U.S.A.

EXCEPTIONALLY QUIET MAGNETIC DAYS, NOVEMBER 9 AND 10, 1953, AT THE CHELTENHAM MAGNETIC OBSERVATORY

The reproductions of the two Cheltenham magnetograms shown in Figure 1 for November 9 and 10, 1953, were kindly supplied by the United States Coast

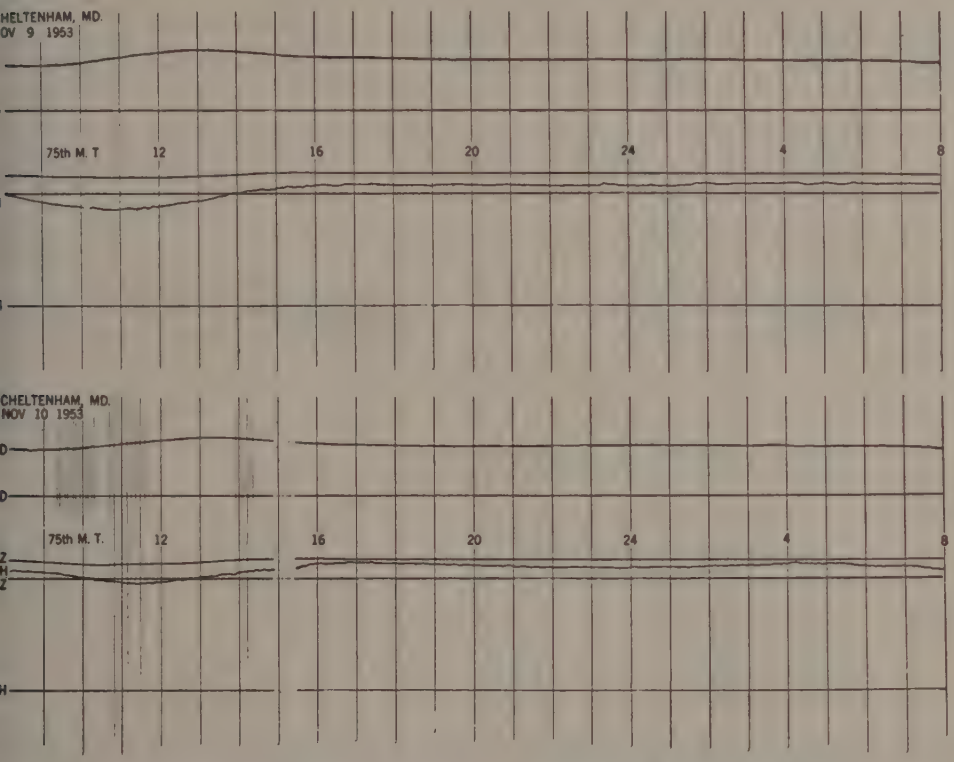

FIG. 1—PHOTOGRAPHIC REGISTRATIONS OF MAGNETIC ELEMENTS, CHELTENHAM OBSERVATORY, VERY QUIET DAYS OF NOVEMBER 9 AND 10, 1953

and Geodetic Survey. They are published (1) because they represent an approach to ideal quiet magnetic conditions, where all three elements describing the earth's magnetic condition (strength and direction) undergo smooth and regular variations, resulting in the assignment of three-hour-range indices K of 0 throughout the two days; and (2) for study of possible relations to other geophysical phenomena. Shown on the magnetograms is the traditional diurnal-variation with only slight disturbance superposed. Few days are so free from disturbance as these are; the last such occurrence at Cheltenham was the Greenwich day, November 8, 1949.

W. E. Scott

Department of Terrestrial Magnetism,
Carnegie Institution of Washington,
Washington 15, D. C., December 22, 1953
(Received December 23, 1953)

PRINCIPAL MAGNETIC STORMS

(Advance knowledge of the character of the records at some observatories as regards disturbances)

Observatory (Observer-in-Charge)	Greenwich date	Storm-time GMT of begin.	Storm-time GMT of ending[1]	Sudden commencement Type[2]	Amplitudes[2] D	H	Z	C-figure, degree of activity[4]	Maximal activity on K-scale 0 to 9 Gr. day	Gr. 3-hr. period	K-index	Range D	H
(1)	(2)	(3)	(4)	(5)	(6)	(7)	(8)	(9)	(10)	(11)	(12)	(13)	(14)
	1953	*h m*	*d h*		′	γ	γ					′	γ
College (C. J. Beers)	Oct. 15	08 50	21 16	s.c.*	−3	+21	−10	ms	15	5,6	7	330	1820
									17	3,4			
									18	3,5,6			
									19	3,4			
									20	3,4,5			
	Nov. 5	02 30	5 19	.....	....	....	....	ms	5	4,5	6	140	1220
	Nov. 12	08 30	16 22	.....	....	....	....	ms	13	4,5	7	320	2070
									14	4,5			
									15	4,5			
									16	4			
	Nov. 19	01 ..	21 15	.....	....	....	....	ms	19	5	7	200	1690
	Dec. 11	04 ..	12 21	.....	....	....	....	ms	11	5	7	220	1380
Sitka (T. L. Skillman)	Oct. 15	07 25	21 16	.....	....	....	....	s	19	4	8	127	1084
	Nov. 12	08 18	21 14	.....	....	....	....	ms	19	5	7	69	610
	Dec. 11	04 32	13 00	.....	....	....	....	ms	11	5	7	87	531
Cheltenham (J. B. Campbell)	Oct. 15	08 54	23 09	s.c.	0	5	0	ms	15	5	6	49	155
									16	1	6		
									19	1,4	6		
	Nov. 12	19 ..	23 14	.....	....	....	....	ms	13	2,5	6	41	126
									16	2	6		
	Dec. 11	04 37	13 06	s.c.	−2	3	−2	m	11	5	5	21	81
Tucson (M. L. Cleven)	Oct. 15	09 00	21 15	.....	....	....	....	ms	15	5,6	6	22	167
									19	1,3			
									20	2			
	Nov. 12	08 00	17 03	.....	....	....	....	ms	13	2,5	6	26	109
	Dec.	None											
San Juan (P. G. Ledig)	July	None											
	Aug.	None											
	Sep.	None											
	Oct. 15	08 47	16 06	s.c.	0	+8	−2	ms	15	5	6	8	163
	Nov.	None											
	Dec.	None											
Honolulu (R. F. White)	Oct. 15	08 45	21 15	.....	....	....	....	m	19	1,3,4	5	9	155
	Nov. 12	09 00	16 12	.....	....	....	....	m	13	5	5	6	99
	Dec.	None											
Instituto Geofísico de Huancayo (A. A. Giesecke, M. Casaverde)	Oct. 15	08 44	21 01	s.c.	0	+20	−2	ms	15	6	6	9	349
	Nov. 12	08 31	14 06	.....	....	....	....	m	12	5,6,7	5	7	178
	Nov. 15	04 23	17 22	.....	....	....	....	m	16	7	5	8	162
	Dec.	None											
Vassouras (Lelio I. Gama)	July 23	08 09	24 02	s.c.	+1	+7	+2	m	23	4	4	11	140
	Aug. 23	00 24	26 06	s.c.	+1	+17	+6	ms	24	1	6	8	129
	Sep. 15	03 00	16 21	s.c.	+1	+16	+6	ms	15	7	6	7	157
		(*Note*: The *K*-index and ranges for September 15 are estimated values due to partial power failure in the Greenwich three-hour period of maximum activity)											
	Sep. 18	16 10	20 05	s.c.	+1	+12	+2	ms	19	1	7	12	163

[1]Approximate time of ending of storm construed as the time of cessation of reasonably marked disturbance movements traces; more specifically, when the *K*-index measure diminished to 2 or less for a reasonable period.

[2]s.c. = sudden commencement; s.c.* = small initial impulse followed by main impulse (the amplitude in this case is that *main impulse only*, neglecting the initial brief pulse; ... = gradual commencement.

[3]Signs of amplitudes of *D* and *Z* taken algebraically; *D* reckoned positive if towards the east and *Z* reckoned positive cally downwards.

[4]Storm described by three degrees of activity: *m* for moderate (when *K*-index as great as 5); *ms* for moderately severe (*K* = 6 or 7); *s* for severe (when *K* = 8 or 9).

PRINCIPAL MAGNETIC STORMS—Continued

rvatory server- harge)	Green- wich date	Storm-time GMT of begin.	Storm-time GMT of ending[1]	Sudden commencement Type[2]	Amplitudes[3] D	H	Z	C-figure, degree of activity[4]	Maximal activity on K-scale 0 to 9 Gr. day	Gr. 3-hr. period	K-index	Ranges D	H	Z
(1)	(2)	(3)	(4)	(5)	(6)	(7)	(8)	(9)	(10)	(11)	(12)	(13)	(14)	(15)
	1953	*h m*	*d h*		′	γ	γ					′	γ	γ
	Oct. 6	23 59	8 00	s.c.	0	+10	−3	m	7	3	5	3	103	16
Gill)	Oct. 15	08 46	23 13	s.c.	0	+12	−4	ms	15	6	6	6	139	26
	Nov. 11	13 12	21 14	s.c.	0	+7	−2	m	13	5	5	7	88	27
	Nov. 23	06 ..	24 12	.....	.....	.....	.....	m	23	7	5	7	65	25
									24	1	5			
	Dec. 10	21 ..	13 00	.....	.....	.....	.....	m	11	5	5	7	104	17
anus	Oct. 14	*Note*: Solar-flare effects at 09h 50m and 14h 23m												
	Oct. 15	08 45	16 08	s.c.	0	+4	+3	ms	15	5,6,7	6	29	193	186
Wijk)	Oct. 16	15 ..	21 15	.....	.....	.....	.....	m	16	7,8	5	18	110	83
									17	5,6	5			
									19	3,4	5			
	Nov. 12	09 ..	14 23	.....	.....	.....	.....	m	13	5	5	21	117	80
	Nov. 15	04 ..	17 00	.....	.....	.....	.....	m	16	6,7	5	17	102	75
	Nov. 23	08 ..	24 07	.....	.....	.....	.....	m	23	7	5	14	59	62
	Dec. 10	21 ..	13 01	.....	.....	.....	.....	m	11	5	5	18	100	68
	July 23	08 08	24 00	s.c.	+1	+18	−2	m	23	4,5	...	4	153	7
roy)	Aug. 23	00 22	24 05	s.c.	+1	+19	−2	m	23	7,8	...	6	147	11
	Sep. 15	03 05	16 15	s.c.	+1	+20	−1	m	15	6,7	...	5	173	14
eroo	Oct. 15	08 44	21 16	s.c.	....	5	....	ms	15	5,6	6	21	150	155
Webb)									17	6				
									18	5				
	Nov. 12	10 30	21 18	.....	.....	.....	.....	m	13	4	5	14	97	129
									15	5,7				
									19	5				
	Nov. 23	05 50	24 12	.....	.....	.....	.....	m	23	4	5	15	75	108
	Dec.	None												
igi	Oct. 15	08 42	23 18	s.c.	....	+19	....	ms	15	6	6	....	.....	.....
d. Waal)									19	3,5				
	Nov. 12	09 ..	21 14	.....	.....	.....	.....	ms	19	5	6	.....	.....	.....
	Nov. 23	07 ..	24 12	.....	.....	.....	.....	m	23	4	5	.....	.....	.....
	1952													
uarie Isl.	Mar. 30	13 19	10 17	s.c.	+7	+118	−97	s	30	6	8	?	2039	1130
									3	6				
Gregor)	Apr. 21	05 ..	22 15	.....	.....	.....	.....	m	21	5	7	?	1231	715
	Apr. 27	22 14	8 22	s.c.	+3	−25	+19	ms	29	4	8	100+	1611	1098
									7	5				
	May 18	00 ..	20 18	.....	.....	.....	.....	m	18	4,6	6	?	821	611
									19	4,6				
		(*Note*: Commencement on May 18 obscured during record changing)												
	May 26	08 ..	31 ..	.....	.....	.....	.....	ms	27	4	7	?	1166	593
									28	5				
									30	3				
		(*Note*: Record incomplete after 06h, May 31)												
	June 8	05 ..	11 18	.....	.....	.....	.....	m	9	5	7	71	1230	658
	June 14	07 ..	17 20	.....	.....	.....	.....	m	14	4	7	?	828	498
	June 22	07 ..	24 21	.....	.....	.....	.....	ms	24	4,5,6	7	?	1075	505
		(*Note*: Record for June 23 incomplete from 10h, so ranges are approximate)												
	July 5	04 ..	5 16	.....	.....	.....	.....	s	5	6	8	120±	1453	1088
	July 20	11 06	22 13	s.c.	+20	−545	+408	ms	21	6	8	149	1406	570
	Aug. 17	04 ..	20 14	.....	.....	.....	.....	m	17	4	7	?	1034	513
									20	4				
		(*Note*: Records incomplete during adjustments on August 18 and 19, so ranges are approximate)												
	Aug. 31	22 ..	3 19	.....	.....	.....	.....	ms	1	4	7	87	1245	585
		(*Note*: Record incomplete after 04h, September 2, so ranges are approximate)												
	Sep. 7	17 ..	10 16	.....	.....	.....	.....	s	8	3,5,6	7	102±	1518	836
									9	4				

PRINCIPAL MAGNETIC STORMS—Concluded

Observatory (Observer-in-Charge)	Greenwich date	Storm-time GMT of begin.	Storm-time GMT of ending[1]	Sudden commencement Type[2]	Amplitudes[3] D	H	Z	C-figure, degree of activity[4]	Maximal activity on K-scale 0 to 9 Gr. day	Gr. 3-hr. period	K-index	Rang D	H
(1)	(2)	(3)	(4)	(5)	(6)	(7)	(8)	(9)	(10)	(11)	(12)	(13)	(14
	1952	*h m*	*d h*		′	γ	γ					′	γ
Macquarie Isl.	Sep. 28	03 30	30 19	.....	.....	.....	.....	s	29	5	8	?	175
—*Continued*	Oct. 3	12 06	6 19	s.c.	+9	−192	+163	s	5	3	8	?	128
(P. M.	Oct. 21	10 10	22 06	s.c.*	0	−33	+38	(Minor disturbance only)					
McGregor)	Oct. 25	10 17	27 14	.....	.....	.....	.....	m	26	5,6	7	?	158
		(*Note*: A p.s.c. with large bay occurred October 26, $02^h\ 04^m$)											
	Oct. 29	09 ..	2 18	.....	.....	.....	.....	ms	30	6	7	143+	144
									31	5,6			
									1	5			
	Nov. 26	06 ..	29 00	.....	.....	.....	.....	s	27	4,5	8	?	150
	Dec. 1	08 30	5 15	.....	.....	.....	.....	ms	2	5,6	7	137	115
									4	4			
	Dec. 13	04 ..	13 17	.....	.....	.....	.....	m	13	4	7	99	83
	Dec. 24	01 15	25 17	s.c.	−3	+11	−12	m	24	5	7	80	92
	Dec. 28	11 55	2 20	s.c.	−4	−120	+91	ms	29	6,7	7	?	163
									30	6			
									31	5,6			
	1953												
	Jan. 5	05 45	7 03	.....	.....	.....	.....	ms	5	3,6,7	7	126	106
	Jan. 19	01 30	20 15	.....	.....	.....	.....	m	19	2,4	6	60	86
									20	5			
	Jan. 25	08 ..	30 20	.....	.....	.....	.....	s	27	4	8	125+	132
									28	6			
		(*Note*: The *H* range for storm of January 25 is doubtful because of adjustments during January 24-27)											
	Feb. 22	09 29	28 22	.....	.....	.....	.....	s	23	3	7	90 +	128
									24	4,5,6			
									25	3,4,5			
									26	3,4			
									27	4			
	Mar. 1	19 16	3 15	s.c.	−4	−19	+14	ms	2	5	8	?	151
	Mar. 8	09 ..	10 20	.....	.....	.....	.....	m	9	4	7	83 ±	106
									10	4			
	Mar. 20	19 ..	28 22	.....	.....	.....	.....	s	23	6	8	122+	153
									24	4			

[*N.B.* According to advice supplied by P. B. Nye, Director, in listing the degree of activity of a storm at the Macquarie Island Magnetic Observatory, the scheme given in footnote 4 of the standard form was not strictly followed. In several instances, an intense short-term movement of the type associated with aurorae on otherwise undisturbed days, produced a *K*-index which would have given a higher activity degree than the general appearance of the record suggested. Again, during another storm, the activity seemed higher than that given by the maximum *K*-index. In fixing the degree of activity, the relative appearances of storms and the frequency of high *K*-indices were used as a guide.]

REVIEWS AND ABSTRACTS

TAKESI NAGATA: *Rock-magnetism*. Tokyo, Maruzen Co., Ltd., 225 pp. + subject and author indexes of 6 pp. (1953). 24 cm.

Within the past few years, there has been increasing interest in the challenges presented by the subject of rock-magnetism. The basic problem is to recognize, isolate from one another, and account for the magnetic moment vectors a given rock-sample may have acquired at various times, starting with the occasion of its formation and extending to the present day, under the influence of geologic conditions, time, and magnetic fields. This problem is made particularly complex by the natural variability of ferromagnetic oxides and their associated minerals.

In *Rock-magnetism*, Nagata has presented an up-to-date comprehensive summary of the contributions that have been made in the subject by workers throughout the world. No other survey has previously been published. The scope of his treatment is best indicated as follows: Chapter I, Magnetic properties of rock-forming ferromagnetic minerals, 49 pages, 50 references, 42 illustrations; Chapter II, Measuring apparata for magnetic properties of rocks, 33 pages, 15 references, 22 illustrations; Chapter III, General magnetic properties of rocks, 38 pages, 15 references, 21 illustrations; Chapter IV, Thermo-remanent magnetism of igneous rocks, 70 pages, 54 references, 54 illustrations; Chapter V, Natural remanent magnetism of sedimentary rocks, 20 pages, 9 references, 21 illustrations; Chapter VI, Geophysical problems relating to rock magnetism, 13 pages, 21 references, 4 illustrations. The liberal use of excellent illustrations, many of them copied from original and oftentimes unavailable works, has tremendously enhanced the usefulness of the volume. The careful coverage of the important literature of all languages (except Russian) stems from the author's long experience in the subject and his linguistic ability. Although the English style occasionally is cumbersome, there are no ambiguities. The proof-reading was excellent; the binding, paper, and printing are good.

In any developing science, there can be exciting controversies, and the subject of rock-magnetism is no exception. Nagata has treated these with restraint and has done a good service by assembling many pertinent contributions with conservative statements on difficulties accompanying their interpretation. It is obvious from *Rock-magnetism* that many more studies will be needed before any definitive solution to the basic problem of the subject is known to be at hand. Nagata's book will be a great help to anyone taking up a part of the problem.

JOHN W. GRAHAM

LETTER TO EDITOR

A NOTE ON SWEEP-FREQUENCY BACKSCATTER OBSERVATIONS

The technique of making sweep-frequency studies of oblique-incidence point-to-point observations on directive antennas by means of slowly sweeping ionosphere recorders[1] led directly to observations of sweep-frequency backscatter. First observations were made before July 1951 at the Sterling, Virginia, laboratory of the National Bureau of Standards. Greatly improved results were made possible by December 1953 as a result of reducing the receiver band-width and improving the video clamping. A rhombic antenna beamed to the west was used.

In the lower left-hand part of Figure 1 may be recognized a conventional $h'f$

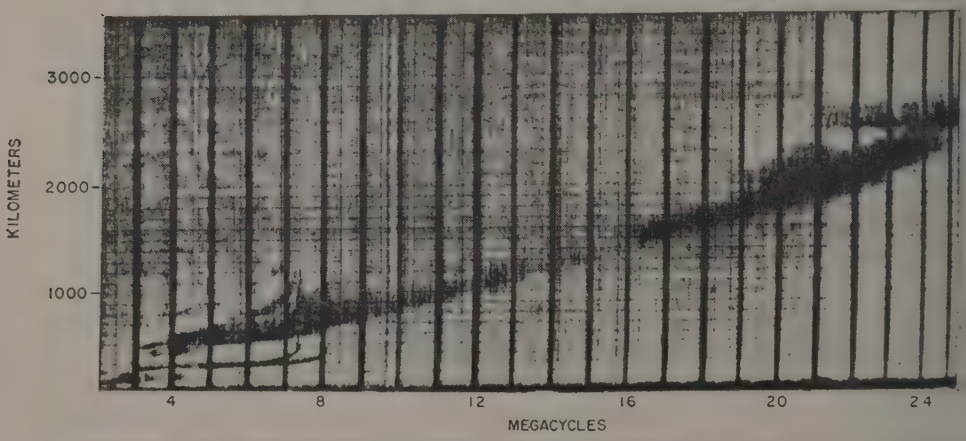

FIG. 1—MULTIFREQUENCY SWEEP FOR DECEMBER 15, 1952, AT 12^h57^m EST, SHOWING BACKSCATTER

sweep on a 4,000-km height (slant range) scale with an $F2$-layer critical frequency of 7.3 Mc. The backscatter echoes are the diffuse, dark traces which develop out of the second-order echoes, as theory would indicate, and extend across the frequency scale at continuously increasing range. The echo beginning at 21 Mc at a fixed slant range of 2,500 km appears to be scatter from the Rocky Mountains. Under various conditions, scatter propagated by the $F1$ and E layers can also be identified. Disturbed-day scatter records are often very turbulent.

Results of analyzing backscatter records and simultaneous vertical-incidence records at a station along the beam indicated that the question of whether the

[1]E. E. Ferguson and P. G. Sulzer, Sweep-frequency oblique-incidence ionosphere measurements over a 1,150 km path, Proc. Inst. Radio Eng., **40**, 1124 (1952). [Letter to Editor.]

source of $F2$-propagated backscatter is the distant E layer[2] or the distant ground[3,4] is still not completely resolved. It appears that on certain type of disturbed days the scatter may be from the former.

Richard Silberstein

Central Radio Propagation Laboratory,
National Bureau of Standards,
Washington 25, D. C., October 12, 1953

(Received October 13, 1953)

[2]T. L. Eckersley, Analysis of the effect of scattering in radio transmissions, J. Inst. Elec. Eng., **86**, 548-563 and discussion 563-567 (1940).

[3]W. L. Hartsfield, S. M. Ostrow, and R. Silberstein, Back scatter observations by the Central Radio Propagation Laboratory—August 1947 to March 1948, J. Res., Nation. Bur. Stand., Washington, **44**, 199-214 (Feb., 1950). [RP 2071.]

[4]A. M. Peterson, The mechanism of F-layer propagated back-scatter echoes, J. Geophys. Res., **56**, 221-237 (1951).

NOTES

(1) *Proposed magnetic survey of the oceans*—The *Princess Waimai*, a 48-ton 74-foot yawl, sailed from Hamble, near Southampton, England, the early part of November 1953, to begin a magnetic survey of the Pacific and other oceans, the first since the cruises (1909-29) of the non-magnetic ship *Carnegie*, which unfortunately was destroyed by fire at Apia, Samoa, November 29, 1929. Dr. B. M. Cwilong, associate professor of physics in the University of British Columbia, is in command of the expedition. Since a non-magnetic vessel is highly desirable, Dr. Cwilong has designed a small 34-foot vessel, *Non-magnetic III*, which is nearing completion in Vancouver. The *Princess Waimai* will serve as a base-ship when the two ships join forces in Hawaii for the survey work in the Pacific, which is scheduled to take three years. On the first leg of the cruise to the Bahamas, Dr. Cwilong hopes to make meteorological and atmospheric-electric observations.

(2) *Australian scientists to establish their first station in the Antarctic*—Ten Australian scientists and technicians sailed from Melbourne during their summer month of January 1954 to set up Australia's first scientific station on the mainland of Antarctica. Most of the men are veterans of service on the lonely Heard and Macquarie Islands between Australia and Antarctica. The expedition will set up a base southwest of Western Australia in a 2,472,000 square-mile segment of Antarctica. This area, claimed by Australia, is almost as large as Australia itself. The advance party will erect buildings and carry on limited land surveying during the first year. Later, detailed studies will be made of weather conditions, geology, biology, geophysics, and cosmic rays. Australians are convinced that air traffic between their country and South Africa and South America will pass over Antarctica. Australia is only 1,500 miles from its nearest point to the south polar continent.

(3) *Radio astronomy conference, Washington, D. C.*—A three-day conference on radio astronomy, sponsored by the National Science Foundation, the Carnegie Institution of Washington, and the California Institute of Technology, was held at the Carnegie Institution of Washington, January 4-6, 1954. Some 75 astronomers and radio engineers were invited and in attendance. Thirty-five formal papers on various topics were presented under the following general headings: (1) Survey of world progress in radio astronomy; (2) problems and theory in radio astronomy; and (3) antenna and equipment problems. Dr. John P. Hagen, of the U. S. Naval Research Laboratory, Washington 20, D. C., served as conference secretary.

(4) *Plans for new Cheltenham Magnetic Observatory*—Plans are on the drawing board for the new Cheltenham Observatory, which is to be located on the A. P. Hill Military Reservation, about 10 miles from Fredericksburg, Virginia. According to the U. S. Coast and Geodetic Survey, efforts are being made to make this proposed geomagnetic observatory the foremost in the world, so that it may serve as a basic observatory for all others of its kind. It will include laboratories for research and the development of instruments for study of the earth's magnetic field.

(5) *Geomagnetic activities of the United States Coast and Geodetic Survey*—An active program of intercomparison of world magnetic charts for epoch 1955.0 in the manuscript stage has been inaugurated among the Coast and Geodetic Survey, the Dominion Observatory of Canada, and the Royal Observatory of Great Britain, with a view to eliminating major differences in the isomagnetic and isoporic lines from the charts to be published by those agencies.

Mr. Masahisa Sugiura, graduate student at the Geophysical Institute, University of Alaska, spent several weeks in the offices of the Coast and Geodetic Survey studying old magnetic records from the Bureau's observatories.

Mr. C. T. Whalen, of the Inter-American Geodetic Survey, Canal Zone, made a study of the geomagnetic charting operations in the Coast and Geodetic Survey.

(6) *Spring meeting of URSI and IRE*—The USA National Committee of the International Scientific Radio Union (URSI) and the Institute of Radio Engineers Professional Group on Antennas and Propagation and Microwave Theory and Techniques (PGMTT) are jointly sponsoring a meeting consisting of technical sessions on May 3, 4, 5, and 6, 1954, at the National Bureau of Standards, Washington, D. C. A combined technical session of interest to all participants is scheduled for the morning of May 4, to be followed by one or more sessions in each of the following fields of radio science: (1) Radio measurement methods and standards; (2) tropospheric radio propagation; (3) ionosphere radio propagation; (4) terrestrial radio noise; (5) radio astronomy; (6) radio waves and circuits, including general theory and antennas; and (7) electronics. A Symposium on Millimeter Waves, planned jointly by the PGMTT and URSI Commission 6, will be a feature of the meeting. Additional details and advance registration will be available through the Secretary of the USA National Committee, W. E. Gordon, School of Electrical Engineering, Cornell University, Ithaca, New York.

(7) *Personalia*—Dr. *Serge A. Korff*, of New York University, was appointed reporter for cosmic rays on the U. S. National Committee that is developing a program for the International Geophysical Year (IGY), 1957-58. At a meeting of the National Committee in Washington, D. C., on January 14, 1954, Dr. Korff presented a report on the suggested U. S. program of cosmic-ray observations to be made during the IGY. His recommendations, together with those to be made in other scientific fields, will be transmitted to the International Council of Scientific Unions, the agency which plans the IGY.

Prof. *Hannes Alfvén*, of the Royal Institute of Technology, Stockholm, Sweden, and Visiting Research Professor, University of Maryland, presented a talk on "Sunspots," February 10, 1954, the initial lecture in a series of four sponsored by the University of Maryland, at College Park.

The February 1954 number of the "Proceedings of the Indian Academy of Sciences" commemorates the sixtieth birthday of Dr. *K. R. Ramanathan*, whose interests in science have been terrestrial magnetism, seismology, and meteorology (thermal structure and movements of the upper air). He held posts as director of the Colaba and Alibag observatories at Bombay and the Solar Physics Observatory at Kodaikanal. Following his retirement from government service in February 1948, he joined the physical research laboratory at Ahmedabad and is now actively engaged on investigations of the physics of the upper atmosphere.

NICHOLAS HUNTER HECK, 1882-1953

Captain Nicholas H. Heck, USC&GS (Ret.), internationally known scientist and engineer, died December 21, 1953, at Mount Vernon Hospital, Washington, D. C. For more than 20 years, Captain Heck was Chief of the Division of Terrestrial Magnetism and Seismology (now the Division of Geophysics), of the United States Coast and Geodetic Survey. At the time of his retirement on April 30, 1945, he was serving as Scientific Assistant to the Director of the Bureau.

Captain Heck was born in Heckton Mills, Pennsylvania, September 1, 1882. He was graduated from Lehigh University with an A.B. degree in 1903, and received a degree in civil engineering from the same University the following year and an Honorary Sc.D. degree in 1950. Fordham University also conferred an Honorary Sc.D. degree upon him in 1941.

Captain Heck entered the commissioned service of the Coast and Geodetic Survey on June 17, 1904, and served continuously with the Bureau for a period of more than 41 years. He made important contributions to the development of the wire drag for use in locating pinnacle rocks which constitute a hazard to navigation. His early field assignments with the Bureau included hydrographic surveys in Puerto Rico, Alaska, and along the east coast of the United States. He also served as commanding officer of several of the Bureau's largest ships.

During World War I, Captain Heck served in the United States Navy on various scientific research projects. It was during this period that he recognized the possibilities of applying to hydrographic surveying the propagation of sound waves in water, resulting in the development of radio acoustic ranging. He also served as a consultant for special scientific subjects during World War II.

Captain Heck was an international authority on seismology and author of a popular book on the subject entitled "Earthquakes," published by Princeton University Press in 1936. He was author of various Bureau publications concerning wire drag and sweep work of the Coast and Geodetic Survey, compensation of the magnetic compass, velocity of sound in sea-water, radio acoustic method of determining position in hydrography, and earthquake history of the United States. He also wrote numerous articles relating to magnetism and seismology, which were published in this country and abroad.

Captain Heck was a member of many scientific and engineering societies, both national and international. He was a former president of both the Seismological Society of America and the Philosophical Society of Washington, D. C. He was also president of the Seismological Association of the International Union of Geodesy and Geophysics, a member of the Washington Academy of Sciences, president (1938) of the District of Columbia Chapter of Sigma Xi, and held membership in the Federal Club, Cosmos Club, American Society of Civil Engineers, Society of American Military Engineers, and the National Geographic Society.

LIST OF RECENT PUBLICATIONS

BY W. E. SCOTT

Department of Terrestrial Magnetism,
Carnegie Institution of Washington,
Washington 15, D. C.

(Received January 4, 1954)

A—*Terrestrial Magnetism*

BARTELS, J., AND J. VELDKAMP. International data on magnetic disturbances, second quarter 1953. J. Geophys. Res., 58, No. 4, 543-545 (1953).

BEAGLEY, J. W. Ionospheric and geomagnetic effects of solar flares. N. Z. J. Sci. Tech., B, 35, No. 2, 141-151 (1953).

BODLE, R. R. Cheltenham three-hour-range indices *K* for July to September, 1953. J. Geophys. Res., 58, No. 4, 546 (1953).

BULLEN, J. M., AND C. H. CUMMACK. The lunar diurnal-variation of the earth's magnetic field for all elements at Amberley, New Zealand. J. Geophys. Res., 58, No. 4, 554-556 (1953). [Letter to Editor.]

CHERNOSKY, E. J. The phased-superposed-epoch method of analysis, and an application to geomagnetic activity. Trans. Amer. Geophys. Union, 34, No. 4, 519-528 (1953).

EGEDAL, J. The lunar-diurnal variation of the magnetic declination in Rude Skov 1908-1951. Pub. Danske Meteorol. Inst., No. 21, 17 pp. (1953). 25 cm.

GAIBAR-PUERTAS, C. Contribución al estudio del geomagnetismo pirenaico. Observatorio del Ebro, Misc. Pub. No. 9, 106 pp. + 10 tables + 60 pls. (1952). 24 cm.

GEOGRAPHICAL SURVEY INSTITUTE. The observation of the vertical deflection in Japan. Bull. Geog. Surv. Inst. Japan, 3, Pts. 2-4, 149-232 (March, 1953).

GEOGRAPHICAL SURVEY INSTITUTE. Magnetic survey of Japan, 1951. Bull. Geog. Surv. Inst. Japan, 3, Pts. 2-4, 119-148 (March, 1953).

GERARD, V. B. Note on a proposed three-component aeromagnetometer. N. Z. J. Sci. Tech., B, 35, No. 1, 1-3 (1953).

GERARD, V. B. Aeromagnetic observations over the Banks Peninsula area and the Mernoo Bank. N. Z. J. Sci. Tech., B, 35, No. 2, 152-160 (1953).

GOLDBERG, J., J. BATURIĆ, J. MOKROVIĆ, AND M. KASUMOVIĆ. Measurement of the magnetic declination in the Yugoslav area of the Adriatic Sea in the year 1949. Mem., Yugoslav Acad. Sci. Arts, Dept. Math. Phys. and Tech. Sci., Vol. I, No. 2, 26 pp. (1952). 28 cm. [English summary.]

GRIFFITHS, D. H. Remanent magnetism of varved clays from Sweden. Nature, 172, 539-540 (Sept. 19, 1953).

HEEZEN, B. C., M. EWING, AND E. T. MILLER. Trans-Atlantic profile of total magnetic intensity and topography, Dakar to Barbados. Repr., Deep-sea research, London, Pergamon Press, Ltd., 1, 25-33 (1953).

INTERNATIONAL UNION OF GEODESY AND GEOPHYSICS, ASSOCIATION OF TERRESTRIAL MAGNETISM AND ELECTRICITY. Circular letter from Prof. E. Thellier, chairman, to the members of the Committee on Observational Technique. Bull. d'Information, 2, No. 3, 491-497 (juillet 1953).

ISTANBUL-KANDILLI OBSERVATORY. Annuaire magnétique. Service Magnétique, Istanbul, Ibrahim Horoz Basimevl, 58 pp. (1953). 28 cm. [Contains hourly values of *D*, *H*, and *Z* for year 1949.]

JONES, H. S., AND P. J. MELOTTE. The harmonic analysis of the earth's magnetic field, for epoch 1942. Mon. Not. R. Astr. Soc., Geophys. Sup., 6, No. 7, 409-430 (1953).

KALINOWSKA, Z. Some remarks on the secular variations of the earth's magnetic field in Poland. Acta Geophys. Polonica, **1**, No. 3-4, 208-217 (1953). [Contains annual means and secular changes at Swider Observatory for years 1921-1950.]

LAURSEN, V. Circular letter No. 312-53/8 to magnetic observatories and geophysical institutions. J. Geophys. Res., **58**, No. 4, 557-558 (1953). [Letter to Editor.]

MAURITIUS. Annual report of the Observatory Department for the year 1951. Port Louis, J. E. Felix, Govt. Printer, No. 1, 13 pp. (1953). [Contains mean values of the magnetic elements for 1951.]

MURPHY, T. The magnetic survey of Ireland for the epoch 1950.5. Dublin Institute for Advanced Studies, Geophys. Mem. No. 4, 27 pp. (1953). 34 cm.

NAGATA, T. Rock-magnetism. Tokyo, Maruzen Co., Ltd., 225 pp. + subject and author indexes of 6 pp. (1953). 24 cm.

NAGATA, T. Self-reversal of thermo-remanent magnetization of igneous rocks. Nature, **172**, 850-852 (Nov. 7, 1953).

NAGATA, T., S. AKIMOTO, AND S. UYEDA. Origin of reverse thermo-remanent magnetism of igneous rocks. Nature, **172**, 630-631 (Oct. 3, 1953). [Letter to Editor.]

NEW ZEALAND. Report on magnetic survey on Pacific Islands, August-September 1952 (prepared by A. L. Burrows, Magnetic Survey, Christchurch). Department of Scientific and Industrial Research, 9 pp. + 3 tables, mim. (rec'd Sept. 14, 1953). 26 cm.

PACAULT, A., B. LEMANCEAU, ET J. JOUSSOT-DUBIEN. Nouvelle méthode de mesure des susceptibilités magnétiques. Paris, C.-R. Acad. sci., **237**, No. 19, 1156-1158 (1953). [Remarque sur la Note par M. P. Pascal, p. 1158.]

PRICE, A. T. Magnetic properties of the earth's interior. Nature, **172**, 786-787 (Oct. 31, 1953). [Discussion held on Sept. 4, 1953, by Section A (Mathematics and Physics) of the British Association at its Liverpool meeting.]

ROQUET, M. J. Sur les rémanences magnétiques des oxydes de fer et leur intérêt en géomagnétisme. Theses présentées a la Faculte des Sciences de l'Université de Paris pour obtenir le grade de Docteur ès Sciences Physiques, Sér. A, 162 pp., typed, + 52 figs. (Oct. 12, 1953). 27 cm.

SABBEN, D. VAN. Solar-flare effects and magnetic storms. J. Atmos. Terr. Phys., **3**, No. 5, 270-273 (1953).

SUGIURA, M. The solar diurnal variation in the amplitude of sudden commencements of magnetic storms at the geomagnetic equator. J. Geophys. Res., **58**, No. 4, 558-559 (1953). [Letter to Editor.]

TAKEUCHI, H., AND Y. SHIMAZU. On a self-exciting process in magneto-hydrodynamics. J. Geophys. Res., **58**, No. 4, 497-518 (1953).

VESTINE, E. H. Note on geomagnetic disturbance as an atmospheric phenomenon. J. Geophys. Res., **58**, No. 4, 539-541 (1953).

VESTINE, E. H. The immediate source of the field of magnetic storms. J. Geophys. Res., **58**, No. 4, 560-562 (1953). [Letter to Editor.]

WINGST OBSERVATORIUM. Magnetogramme 1952 (1. Januar bis 31. Dezember). D. Hydrogr. Inst. Hamburg, No. 2503, 98 pp. (1953). 25 cm.

YOKOYAMA, I. A new method for regulating electric currents and its application to measurements of geomagnetic field. Bull. Earthquake Res. Inst., **31**, Pt. 3, 211-217 (1953).

YOSIDA, K. Theory of antiferro magnetism. Ann. Rep. Sci. Wks., Fac. Sci., Osaka Univ., **1**, for 1952, 19-38 (1953).

B—*Terrestrial Electricity*

BENNETT, W. H., AND E. O. HULBURT. Magnetic self-focusing of auroral protons. Phys. Rev., **91** No. 6, 1562 (1953).

CHAPMAN, S., AND D. W. N. STIBBS. Solar eclipses and the aurora borealis. Sky and Telescope, **13** No. 2, 35-39 (1953).

GUNN, R., AND C. DEVIN, JR. Raindrop charge and electric field in active thunderstorms. J. Met. **10**, No. 4, 279-284 (1953).

JACKA, F. The southern auroral zone as defined by the position of homogeneous arcs. Aust. J. Phys., **6**, No. 2, 219-228 (1953).

KIMBALL, D. S. The aurora. Sky and Telescope, **13**, No. 2, 40-42 (1953).

MCDONALD, J. E. On the electrical conductivity of the lower stratosphere. Trans. Amer. Geophys. Union, **34**, No. 4, 529-533 (1953).

MILES, V. G. Radar echoes associated with lightning. J. Atmos. Terr. Phys., **3**, No. 5, 258-262 (1953).

MORRISON, R. B. The variation with distance in the range 0-100 km of atmospheric wave-forms. Phil. Mag., **44**, No. 356, 980-986 (1953).

NOLAN, P. J., AND P. S. MACCORMAIC. The nuclei produced by disruptive discharge at a water surface. School of Cosmic Physics, Dublin Institute for Advanced Studies, Geophys. Bull. No. 7, 19 pp. (July 1953). 28 cm.

SCHONLAND, B. F. J. The pilot streamer in lightning and the long spark. Proc. R. Soc., A, **220**, No. 1140, 25-38 (1953).

STÖRMER, C. Results of the observations and photographic measurements of aurora in southern Norway and from ships in the Atlantic during the Polar Year 1932-1933. Geofys. Pub., Oslo, **18**, No. 7, 117 + 3 pls. (1953). 30 cm.

VEGARD, L., AND E. TÖNSBERG. Results from auroral spectrograms obtained at Tromsö during the winter 1950/51. Geofys. Pub., Oslo, **18**, No. 8, 20 pp., 3 pls. (1952). 31 cm.

WEXLER, R. Radar echoes from a growing thunderstorm. J. Met., **10**, No. 4, 285-290 (1953).

C—*Cosmic Rays*

BRUNBERG, E. Å. Experimental determination of electron orbits in the field of a magnetic dipole. Tellus, **5**, No. 2, 135-156 (1953); and Part II (by E. Å. Brunberg and A. Dattner), No. 3, 269-292 (1953).

DAUDIN, A., ET J. DAUDIN. Effets atmosphériques sur les gerbes d'Auger. J. Atmos. Terr. Phys., **3**, No. 5, 245-257 (1953).

MACHADO, E. A. M. Los procesos estocásticos de la radiación cósmica. Meteoros, **3**, Nos. 2-3, 174-193 (1953).

SARABHAI, V., AND R. P. KANE. Effects at Godhavn and lower latitudes of changes in energy and composition of solar cosmic rays. Phys. Rev., **91**, No. 3, 688-689 (1953).

SARABHAI, V., AND R. P. KANE. Effects of the geomagnetic field on solar cosmic rays. Phys. Rev., **92**, No. 2, 415-419 (1953).

TRUMPY, B. Time variations of cosmic ray intensity associated with geomagnetic and solar activity. Physica, **19**, No. 7, 645-667 (1953).

TRUMPY, B., AND H. TREFALL. On the correlation between the cosmic ray intensity and the meteorological conditions. Physica, **19**, No. 7, 636-644 (1953).

YNGVE, V. H. The time variation of cosmic-ray heavy nuclei. Phys. Rev., **92**, No. 2, 428-435 (1953).

D—*Upper Air Research*

ALLCOCK, G. McK. The application of high-frequency radio-propagation predictions in the New Zealand area. N. Z. J. Sci. Tech., B, **35**, No. 2, 198-212 (1953).

APPLETON, E. V. A note on the "sluggishness" of the ionosphere. J. Atmos. Terr. Phys., **3**, No. 5, 282-284 (1953). [Research Note.]

ARGENCE, E., AND M. MAYOT. Méthode de détermination des hauteurs vraies des couches de l'ionosphere. II—Utilisation de la valeur exacte de l'indice de réfraction (cas du rayon ordinaire). J. Geophys. Res., **58**, No. 4, 493-496 (1953).

ARMSTRONG, E. B. A note on the use of the Fabry-Perot etalon for upper atmosphere temperature measurements. J. Atmos. Terr. Phys., **3**, No. 5, 274-281 (1953).

BANERJI, R. B. Recombination coefficient in the *F*-region: A possible new process of ionization of nitrogen molecules. Nature, **172**, 953-954 (Nov. 21, 1953).

BANERJEE, S. S., D. K. BANERJEE, AND V. D. RAJAN. Scattering of short wave radio signals and their bearing on the ionosphere. J. Sci. Industr. Res., New Delhi, **12**, No. 6, 278-282 (1953).

BECKER, W. Typische Streuprozesse radiofrequenter Strahlung an Elektronenwolken der sporadischen E_s-Schicht, dargestellt an Hand ausgewählter Echolotungsaufnahmen mit veränderlicher Frequenz. Archiv. Elektr. Uebertrag., **7**, Heft 8, 375-378 (1953).

Bramley, E. N. Direction-finding studies of large-scale ionospheric irregularities. Proc. R. Soc., A, **220**, No. 1140, 39-61 (1953).

Brown, R. H., and C. Hazard. A model of the radio-frequency radiation from the galaxy. Phil. Mag., **44**, No. 356, 939-963 (1953).

Chalmers, J. A. The charge on the ionosphere. J. Atmos. Terr. Phys., **3**, No. 6, 345-346 (1953). [Letter to Editor.]

Chamberlain, J. W., and N. J. Oliver. Stellar absorption lines in night-sky spectra. Astroph. J., **118**, No. 2, 197-199 (1953).

Chamberlain, J. W., and N. J. Oliver. Atomic and molecular transitions in auroral spectra. J. Geophys. Res., **58**, No. 4, 457-472 (1953).

Chappell, D. W. G., L. B. Hainsworth, and I. M. Moorat. Some statistical results on the phenomena associated with ionospheric storms. J. Atmos. Terr. Phys., **3**, No. 6, 301-320 (1953).

Chatterjee, B. Nature and origin of sporadic *E* regions as observed at different hours (over Calcutta). J. Atmos. Terr. Phys., **3**, No. 5, 229-238 (1953).

Chatterjee, B. Oblique propagation of radio waves over a curved earth. Indian J Phys., **27**, No. 5, and Proc. Indian Assoc. Cultivation Science, **36**, No. 5, 257-268 (1953).

Christiansen, W. N., and J. A. Warburton. The distribution of radio brightness over the solar disk at a wavelength of 21 centimeters. Aust. J. Phys., **6**, No. 2, 190-202, and No. 3, 262-271 (1953).

Chvojková, E. Über die Entstehung der F_1-Schicht. Bull. Astron. Inst. Czechosl., **4**, No. 5, 101-109 (1953).

Covington, A. E., and H. W. Dodson. Absorption of 10.7-centimetre solar radiation during flare of May 19, 1951. J. R. Astr. Soc. Can., **47**, No. 5, 207-211 (1953).

Crompton, R. W., L. G. H. Huxley, and D. J. Sutton. Experimental studies of the motions of slow electrons in air with application to the ionosphere. Proc. R. Soc., A, **218**, No. 1135, 507-519 (1953).

Cutolo, M. Measurements of the terrestrial magnetic field in the *E*-layer. Nature, **172**, 774-775 (Oct. 24, 1953).

Das, A. K., and B. N. Bhargava. Radio noise-bursts from solar *M*-regions. Nature, **172**, 855-856 (Nov. 7, 1953). [Letter to Editor.]

Das, A. K., and K. Sethumadhavan. Eruptive prominence of February 26, 1953, and associated radio noise-burst. Nature, **172**, 446-447 (Sept. 5, 1953).

Dodson, H. W., E. R. Hedeman, and L. Owren. Solar flares and associated 200 Mc/sec radiation. Astroph. J., **118**, No. 2, 169-196 (1953).

Dufay, J., P. Berthier, et B. Morignat. Nouvelle évaluation de l'altitude de la couche atmosphérique émettant la raie verte de l'oxygène dans la lumière du ciel nocturne. Paris C.-R. Acad. sci., **237**, No. 15, 828-830 (1953).

Ellis, G. R. *F*-region triple splitting. J. Atmos. Terr. Phys., **3**, No. 5, 263-269 (1953).

Elterman, L. A series of stratospheric temperature profiles obtained with the searchlight technique. J. Geophys. Res., **58**, No. 4, 519-530 (1953).

Gardner, F. F., and J. L. Pawsey. Study of the ionospheric *D*-region using partial reflections. J. Atmos. Terr. Phys., **3**, No. 6, 321-349 (1953).

Greenstein, J. L., and R. Minkowski. The Crab nebula as a radio source. Astroph. J., **118**, No. 1, 1-15 (1953).

Greenwich Observatory. Greenwich photo-heliographic results, 1941. London, H. M. Stationery Office, vii + 95 (1953). 30 cm.

Hanson, G. H., H. V. Serson, and W. Campbell. Maximum usable frequencies and lowest usable frequencies for the path Washington to Resolute Bay. J. Geophys. Res., **58**, No. 4, 487-499 (1953).

Hardwick, B. Two cases of large F_2 region disturbance associated with small magnetic disturbance. J. Atmos. Terr. Phys., **3**, No. 6, 347-349 (1953). [Letter to Editor.]

Hoyle, F. Cosmic origin of radiation at radio frequencies. Nature, **172**, 296-297 (Aug. 15, 1953). [Letter to Editor.]

Huxley, L. G. H. Alternative developments in the theory of radio wave interaction. Proc. R. Soc., A, **218**, No. 1135, 520-536 (1953).

Ionospheric Research Committee (Japan). Special report No. 1 on ionospheric storms. Science Council of Japan, 55 pp. approx. (March, 1953). 25 cm.

Jones, R. E. Physical characteristics of the lower *E*-region as deduced from the measurement of changes in phase path of long radio waves. Pennsylvania State College, Ionosphere Res. Lab., Sci. Rep. No. 48, 88 pp., mim. (Aug. 25, 1953). 28 cm.

Kaiser, T. R. Radio echo studies of meteor ionization. Adv. Phys., 2, No. 8, 495-544 (1953).

Kelso, J. M. On the coupled wave equations of magneto-ionic theory. J. Geophys. Res., 58, No. 4, 431-436 (1953).

Kraus, L. Further discussion of Kelso's paper on a method for determination of the distribution of electron density in the ionosphere. J. Geophys. Res., 58, No. 4, 551-553 (1953). [Letter to Editor.]

Lien, J. R., R. J. Marcou, J. C. Ulwick, D. R. McMorrow, L. B. Linford, and O. C. Haycock. Bifurcation of the *E* region. Phys. Rev., **92**, No. 2, 508-509 (Oct. 15, 1953). [Letter to Editor.]

Mariani, F. Densità elettronica nell'atta atmosfera *E* interpretazione delle curve $h'(f)$ dell'altezza virtuale della ionsfera. Ann. Geofis., Roma, **6**, No. 1, 21-45 (1953).

McCue, C. G. Concerning Green's reinterpretation of the magneto-ionic theory. J. Atmos. Terr. Phys., **3**, No. 5, 239-244 (1953).

McKinley, D. W. R. Effect of radar sensitivity on meteor echo durations. Can. J. Phys., **31**, 758-767 (July, 1953).

Meek, J. H. Correlation of magnetic, auroral, and ionospheric variations at Saskatoon [Part 1]. J. Geophys. Res., **58**, No. 4, 445-456 (1953).

Meinel, A. B. Origin of the continuum in the night-sky spectrum. Astroph. J., 118, No. 2. 200-204 (1953).

Miley, H. A., E. H. Cullington, and J. F. Bedinger. Day-sky brightness measured by rocket-borne photoelectric photometers. Trans. Amer. Geophys. Union, **34**, No. 5, 680-694 (1953).

Mitra, A. P. A tentative model of the equilibrium height distribution of nitric oxide in the high atmosphere and the resulting *D*-layer. Pennsylvania State College, Ionosphere Res. Lab., Sci. Rep. No. 46, 53 pp. + refs., mim. (May 15, 1953). 28 cm.

Munro, G. H. Reflexions from irregularities in the ionosphere. Proc. R. Soc., A, **219**, No. 1139, 447-463 (1953).

Nicolet, M. Aeronomical problem of nitrogen oxides. Pennsylvania State College, Ionosphere Res. Lab., Sci. Rep. No. 52, 36 pp., mim. (1953). 28 cm.

Parkinson, R. W. Instrumentation for the measurement of coupling phenomena at 150 kc/s and preliminary results. Pennsylvania State College, Ionosphere Res. Lab., Sci. Rep. No. 47, 57 pp., mim. (Aug. 10, 1953). 28 cm.

Petrie, W., and R. Small. The intensities of atomic and molecular features in the auroral spectrum. Can. J. Phys., **31**, 911-926 (Sept., 1953).

Ramanathan, K. R., and Bh. V. R. Murthy. Daily variation of amount of ozone in the atmosphere. Nature, **172**, 633-634 (Oct. 3, 1953).

Roy, R., and J. K. D. Verma. Irregularities in the ionosphere. J. Geophys. Res., 58, No. 4, 473-485 (1953).

Saha, A. K. On the law of the variation of *E*-region maximum with the zenith distance of the sun. Indian J. Phys., **27**, No. 9, and Proc. Indian Assoc. Cultivation Science, **36**, No. 9, 431-438 (1953).

Scheuer, P. A. G., and M. Ryle. An investigation of the H II regions by a ratio method. Mon. Not. R. Astr. Soc., **113**, No. 1, 3-17 (1953).

Schrag, R. L. Instrumentation for the observation of long delay echoes at 150 kc/s. Pennsylvania State College, Ionosphere Res. Lab., Sci. Rep. No. 50, 87 pp., mim. (1953). 28 cm.

Scott, J. C. W. The distribution of F_2 region ionization at high latitudes. J. Atmos. Terr. Phys., **3**, No. 6, 289-294 (1953).

Scott, J. C. W. Real and complex wave polarization in the ionosphere. J. Geophys. Res., 58, No. 4, 437-443 (1953).

SIEDENTOPF, H. Radioastronomie II: Beobachtungsergebnisse über kosmische Radioquellen. Archiv. Elek. Uebertrag., 7, Heft 11, 507-517 (1953).

SILBERSTEIN, R. High-frequency scatter sounding experiments at the National Bureau of Standards. Science, 118, 759-763 (Dec. 25, 1953).

SOMAYAJULU, Y. V., B. R. RAO AND E. B. RAO. Investigation of travelling disturbances in the ionosphere by continuous-wave radio. Nature, 172, 818-820 (Oct. 31, 1953). [Letter to Editor.]

STOREY, L. R. O. An investigation of whistling atmospherics. Phil. Trans. R. Soc. London, A, 246, No. 908, 113-141 (1953).

VAN DE HULST, H. C. The galaxy explored by radio waves. Observatory, 73, No. 875, 129-139 (1953).

WEISS, A. A. The structure of the *F* region of the ionosphere. Aust. J. Phys., 6, No. 3, 291-303 (1953).

WILD, J. P., J. D. MURRAY, AND W. C. ROWE. Evidence of harmonics in the spectrum of a solar radio outburst. Nature, 172, 533-534 (Sept. 19, 1953).

WULF, O. R. On the production of glow discharges in the ionosphere by winds. J. Geophys. Res. 58, No. 4, 531-538 (1953).

WYATT, S. P., JR. A radio model of the galaxy. Astroph. J., 118, No. 2, 304-313 (1953).

E—*Earth's Crust and Interior*

BÅTH, M. Comparison of microseisms in Greenland, Iceland, and Scandinavia. Tellus, 5, No. 2, 109-134 (1953).

BONDI, H., AND R. A. LYTTLETON. On the dynamical theory of the rotation of the earth. II—The effect of precession on the motion of the liquid core. Proc. Cambridge Phil. Soc., 49, Pt. 3, 498-515 (1953).

BULLEN, K. E. The rigidity of the earth's inner core. Ann. Geofis., Roma, 6, No. 1, 1-10 (1953).

GASKELL, T. F., AND J. C. SWALLOW. Seismic refraction experiments in the Indian Ocean and in the Mediterranean Sea. Nature, 172, 535-537 (Sept. 19, 1953). [Experiments carried out by H.M.S. *Challenger* during her world cruise of 1950-52.]

GUTENBERG, B. Wave velocities at depths between 50 and 600 kilometers. Bull. Seis. Soc. Amer. 43, No. 3, 223-232 (1953).

HALES, A. L. The thermal contraction theory of mountain building. Mon. Not. R. Astr. Soc. Geophys. Sup., 6, No. 7, 458-466, and No. 8, 486-493 (1953).

HODGSON, J. H. A seismic survey in the Canadian Shield. I: Refraction studies based on rockbursts at Kirkland Lake, Ont.; and II: Refraction studies based on timed blasts. Dominion Observatory, Ottawa, Vol. XVI, Nos. 5 and 6, 113-163 and 169-181 (1953). 29 cm.

JACOBS, J. A. The earth's inner core. Nature, 172, 297-298 (Aug. 15, 1953). [Letter to Editor.]

SIMON, F. E. The melting of iron at high pressures. Nature, 172, 746-747 (Oct. 24, 1953).

TATEL, H. E., L. H. ADAMS, AND M. A. TUVE. Studies of the earth's crust using waves from explosions. Proc. Amer. Phil. Soc., 97, No. 6, 658-669 (1953).

UREY, H. C. On the concentration of certain elements at the earth's surface. Proc. R. Soc., A, 219, No. 1138, 281-292 (1953).

VALLE, P. E. Una equazionale di stato per i solidi. Ann. Geofis., Roma, 6, No. 2, 183-197 (1953). [English translation available. Istituto Nazionale di Geofisica, Rome, Pub. No. 273.]

F—*Miscellaneous*

CHAPMAN, S. The International Geophysical Year 1957-58. Nature, 172, 327-329 (Aug. 22, 1953).

CONSEIL INTERNATIONAL DES UNIONS SCIENTIFIQUES. Année Géophysique Internationale, Bulletin d'information No. 1. Extract, Bulletin d'Information de l'Union Géodésique et Géophysique (I.U.G.G. News Letter), 2° année, No. 3, 601-673 (juillet 1953).

NEWELL, H. E., JR. High altitude rocket research. New York, Academic Press, Inc., xiv + 298 + 93 figs. + 37 tables (Dec. 1953).

TER HAAR, D. The age of the universe. Sci. Mon., 77, No. 4, 173-181 (1953).

WALDMEIER, M. Provisional sunspot-numbers for July to September 1953. J. Geophys. Res., 58, No. 4, 546 (1953).

WASHINGTON CONFERENCE ON RADIO ASTRONOMY—1954

A conference on radio astronomy was held in Washington, January 4, 5, and 6, 1954, jointly sponsored by the National Science Foundation, the California Institute of Technology, and the Carnegie Institution of Washington. The meetings were held in Elihu Root Hall of the Carnegie Institution at 1530 P Street, N.W., Washington 5, D.C. The meeting was organized by a committee under Dr. Jesse L. Greenstein of the California Institute of Technology as Chairman, with Dr. J. B. Wiesner, Massachusetts Institute of Technology, Dr. Bart J. Bok, Harvard Observatory, Dr. Merle A. Tuve, Carnegie Institution, Dr. John P. Hagen, Naval Research Laboratory, as members, and with Dr. Raymond J. Seeger representing the National Science Foundation.

The conference was called to bring together not only those actively working in radio astronomy, but also a group of other astronomers, physicists and electronics men, and a number of advanced graduate students and young research men who might undertake work in this area if they were more fully acquainted with its challenges and opportunities. An effort was made to present a comprehensive survey of the present status of research in this field, to examine in some detail the most critical problems now evident, and to indicate, as far as possible, some of the directions for profitable future activity.

The JOURNAL is indebted to the participants and to Dr. John P. Hagen, Secretary of the conference, for the following summaries and abstracts, which give a goodly fraction of the material presented during three intensive and very interesting days. A subsidy from the special fund for the conference, which was provided by the National Science Foundation, has made it possible to publish these notes on the conference. (EDITOR)

Monday, January 4, 9:45 A.M.—12:30 P.M.

L. A. DuBridge, Chairman

Greetings from the Carnegie Institution: Paul A. Scherer, Executive Officer

SURVEY OF WORLD PROGRESS IN RADIO ASTRONOMY

(1) B. Y. MILLS, *Australia, C.I.W.*: (*a*) **CSIRO results on shapes, sizes, and spectra of radio sources; and** (*b*) **The galactic noise background.** Some recent Australian experiments have been directed at a more detailed study of the stronger radio sources. Information sought has been the radio spectra of the sources and the shapes and sizes of the emitting areas. It is hoped that this information will aid in determining the unknown process causing the emission.

Measurements of source spectra have been made over a range of wavelengths from 16 meters to one meter. More than 20 sources have been observed over portions

of this range, but only three over the whole range. There are variations in the slopes of the spectral curves, but all exhibit an increase in intensity with increasing wavelength. Approximate shapes and sizes, ranging from the order of 1′ of arc to several degrees, have been determined for 14 sources.

The background radiation has been studied over limited regions of the sky, including the galactic centre, at frequencies of 150 Mc and 18 Mc, and over a wider range at 97 Mc. The aerial resolution is insufficient in these surveys for detailed quantitative analysis, being 6°, 17°, and 8°, respectively, but it is possible to draw some general conclusions. These are (*a*) near the galactic centre the radiation shows a very pronounced concentration towards the plane of the galaxy, (*b*) the distribution in longitude along the galactic plane is irregular near the centre of the galaxy, (*c*) there is evidence that in the direction of the centre of the galaxy the 18-Mc radiation is undergoing absorption by the ionized interstellar gas. Because of irregularities in the distribution and the difficulty of allowing for the effect of localised sources, higher resolution surveys at different frequencies are required to give a reliable quantitative picture of galactic structure.

(2) R. HANBURY-BROWN, *Manchester*: (*a*) **The survey with the 218′ paraboloid**; (*b*) **measures of the angular diameters of sources; and** (*c*) **Extra-galactic radiation.** The work which is described here has been carried out at the Jodrell Bank Experimental Station of the University of Manchester, England.

Survey with the 218′ diameter paraboloid—The antenna system used in this survey consists of a paraboloid of diameter 218 feet and focal length 126 feet. The surface of the paraboloid is formed by a mesh of parallel wires, spaced 8 inches apart, and it has a reflection coefficient of about 65 per cent at a wavelength of 1.9 meters. The accuracy of the profile of the surface is about ± 5 inches. The beam-width is 2° between half-power points at 1.9 meters, and the side lobes are of the order of one or two per cent. The paraboloid is fixed with its axis vertical; however, the central tower, which supports the primary feed, may be swung in the north-south plane, so that the beam may be directed to different declinations. The maximum beam tilt which has been used is about 15°, and under these conditions there appears to be no serious distortion of the beam shape.

The antenna has been used in conjunction with a 1.9-meter receiver to survey an area of sky contained within a strip ± 15° on either side of the zenith.

The isophotes show the distribution of the general galactic background radiation in the strip, together with several discrete sources. The two most intense sources, Cygnus A and Cassiopeia A, lie within the strip. The presence of a source, which appears to be extended, close to Cygnus A, can clearly be seen, and this source corresponds to the Cygnus X reported by Piddington. Another source of considerable interest is in the position of Tycho Brahe's Supernova. An examination of the distribution of the sources found in this survey shows a very marked concentration of the intense sources towards the galactic plane.

Measurements of the angular diameters of the sources—Measurements of the angular diameters of the discrete sources Cassiopeia A and Cygnus A have been carried out during the past two years and are still in progress. Before the order of magnitude of the diameters of these sources was known, it was assumed that they

night be comparable in apparent diameter with the stars. For this reason, a new type of interferometer was developed, which is capable of operation at extremely long base-lines. This instrument operates at 125 Mc/sec, and uses two aerial systems of about 500 square meters in aperture. The apparent diameter of a source is derived by measuring the correlation coefficient between low frequency components in the envelope of the signal received at the two ends of the interferometer. It can be shown that this correlation coefficient is proportional to the sum of the squares of the Fourier sine and cosine transforms of the intensity distribution across the source. The principal disadvantage of the instrument is that it is relatively insensitive to weak sources.

Measurements of Cassiopeia A show that it is roughly symmetrical radially, and that its apparent angular diameter is of the order of 5 minutes of arc.

Measurements of Cygnus A show that it is markedly asymmetrical in shape, with a ratio of major to minor axis of about 4 to 1. The position angle of the major axis of the source is uncertain, but is believed to be about 90°. The observations made along a direction close to the major axis show that the correlation coefficient drops to a very low value with a base-line of about 1,250 wavelengths and increases to a secondary maximum at about 2,000 wavelengths. The height of the secondary maximum indicates that Cygnus A must contain at least two radiating centers, and the simplest model which will fit the present observations consists of two centers of angular size 51″ × 30″, spaced with the centers 1′ 28″ apart. The measurements on Cygnus A are continuing, and it is proposed to extend the base-line of the interferometer further so that the model of Cygnus A may be improved.

It is of interest to note that the size of the object which is radiating at 125 Mc/sec is apparently far greater than the image of the two colliding galaxies observed with the 200-inch telescope.

Extra-galactic radiation—The 218-foot diameter paraboloid at Jodrell Bank has been used to search for the radiation from extra-galactic sources at a wavelength of 1.9 meters. The first extra-galactic nebula to be detected was the Great Spiral Nebula in Andromeda (M 31), and since then a further five discrete sources have been associated with nebulae. The most recent result is the detection of M 81.

A comparison of the radio flux from these nebulae with their light flux suggests that the ratio is constant. This result applies only to late-type spirals, and it is of great interest to discover whether the ratio also holds for other types of nebulae.

A search has also been made for the radiation from large numbers of nebulae. In 1952, the presence of extended bands of radiation were reported and were associated with the irregularities in the distribution of extra-galactic nebulae. Observations of these bands have been extended over the range of declinations between N 40° and N 70°. The band centered at 12 hours of right ascension appears to correspond with a band of bright nebulae which extends across the sky, and this conclusion is strengthened by the results of Kraus and Ko, who here reported a similar band at lower declinations.

An attempt to detect the radiation from clusters of nebulae has shown the presence of a radio source in the position of the Perseus cluster. This source may be associated with the cluster as a whole or with the peculiar nebula NGC 1275.

Calculations have been made to estimate the intensity to be expected from the

irregularities in the distribution of extra-galactic nebulae from the clusters and from the so-called "isotropic component." In each case, it may be shown that when all the obvious corrections have been taken into account the observed intensity of the radiation is greater than that to be expected if all nebulae radiate in the same way as normal late-type spirals, but the discrepancy is no more than two magnitudes.

(3) C. G. LITTLE, *Manchester*: (*a*) **The Jodrell Banks program on meteors aurorae and ionosphere; and** (*b*) **the effects of the ionosphere on extra-terrestrial radio sources.** The three main spheres of meteor research at Jodrell Bank—the routine determination of meteor radiants, velocities and heights—are continuing by methods already fully described. I hope that members of this conference who were present at the recent Boston AAAS meetings will forgive me if I now refer to the newer aspects of our radar work at Jodrell Bank, which I also described at that meeting.

Firstly, I would like to tell you about the work now being carried out by Dr Greenhow. He has been applying the meteor radar technique to investigate the ionosphere winds at heights of the order of 90 km. His original work was based on a direct measurement of the changes in the range of the meteor trail after formation. These measurements were limited by the range discrimination available from his three-microsecond pulses (about 50 yards). He has recently made use of the coherent pulse technique, whereby changes in range of only a yard can readily be detected. Each pulse is coherent in phase with all preceding pulses, and the echo signals are mixed at the receiver with some of the original C. W. signal supplied to the pulse transmitter. Owing to the changes in range of the meteor trail, the relative phase of the two signals varies, and so the output of the receiver varies as the two signals beat together. The radial velocity of the echoing point is determined from the rate at which these beats occur. The radial motion in the north-south and east-west directions are measured by running with the aerial alternatively pointing due north or due east, for five-minute periods; these north-south and east-west components are then averaged separately for hourly intervals and then combined to give the average direction and velocity of the meteor trails during that hour.

The two slides show some of his results. The first slide shows 24 successive hourly wind-vectors in the form of polar plots; the dotted circles indicate the scatter of the observations during each hour. The second slide summarises two days of continuous observations; in this case, the variation of the north-south and east-west vectors are plotted separately. Both slides show clearly the semi-diurnal clockwise rotation of the wind vector, superposed on a systematic drift towards the east of approximately 10 metres per second.

Although aurorae are not common in England, a certain amount of aurora echo work is being done by Mr. Bullough. He is using a horizontally-beamed twin Yagi array at 74 Mc/sec; the beam-width of his aerial is about $\pm$ 10° in azimuth whilst ground reflection lifts his beam to an elevation of approximately 10°. The aerial is rotated continuously at 10 complete rotations per hour. Any echoes are

recorded by photographing A-scope and intensity modulated displays on moving film.

These range-time plots are readily transformed into range-azimuth plots—the slide shows the location during three successive aerial rotations of the auroral echoing regions, during an aurora which occurred recently to the north of the British Isles. When corrections are applied for the aerial beam-width, it is found that the echoing points lie on a relatively thin strip accurately parallel to the lines of geomagnetic latitude.

The third piece of radar work which I would like to mention is that being carried out by Dr. Kaiser, Mr. Murray, and Mr. Hargreaves. They are using a moon radar equipment, and are already getting some very interesting results. The equipment operates on a frequency of 120 Mc sec, with a pulse length of 30 milli-seconds, a band-width of 28 cycles sec, and a p.r.f. of one pulse per two seconds. The aerial, as shown in the slide, consists of ten banks of eight full-wave dipoles, λ 4 above reflecting screens inclined at 45° to the earth's surface. The banks are separated by $\sqrt{2}'$ λ along the ground in the north-south direction. The beam-width is ±6° azimuth and ±2°.5 in elevation. The beam is fixed in azimuth, but can be moved in declination (by changing the relative phase between the banks of dipoles), from $\delta = 0°$ to $\delta = +30°$. In this way, the moon can be observed at transit for a period of about 3 4 hour, whenever it is at positve declination; that is, for about 14 transits per month.

This equipment has been operating for about three months in its present form. The echoes show a rapid fading from pulse to pulse as shown in the slide; this fading has been shown to possess a Rayleigh distribution. A very interesting result is that the echoes obtained about dawn show a long-period fade of duration about 1/2 hour. It is suggested that this is due to the Faraday effect—the rotation of the plane of polarisation of the radiation field as the radiation traverses the ionosphere in to the presence of a magnetic field. Experiments are now in progress to check this theory—if the explanation is correct, the technique should prove an accurate method for determining the *total* thickness of the ionosphere.

The second part of my talk relates to the effect of the ionosphere on the incoming extra-terrestrial radio-waves.

The ionosphere makes its presence known to radio astronomers by three main effects; by absorption, refraction, and scintillation effects.

The least investigated effect is probably that of absorption, both regular and that associated with radio fadeouts. The effect is small, except at long wavelengths, and little work has been done in this field. Kerr and Shain used moon echoes at 20 Mc/sec at low angles to obtain some information on absorption—more recently, Shain has made a fuller investigation, working at 18.3 Mc/sec and using galactic radiation at vertical incidence. Amongst the interesting results he has already published is that the *F*2-region contributes largely to the total absorption, and that the *E*-region plays a comparatively small part. During an S.I.D., of course, *D*-region effects become very marked and have been observed by several workers.

The second effect is that of ionospheric refraction. This has been investigated by Kerr and Shain using moon echoes, and by the Australian workers using sea-

interferometers on the sun or the more-intense, localised radio sources. This work relates to high angles of incidence—near the zenith the effects are much smaller, but the precision position-finding measurements of Smith at Cambridge enabled the tilting of the ionosphere in the zenith at dawn or dusk to be investigated.

The third ionospheric effect of importance is the scintillation of the radio stars. This has been investigated comparatively fully, and I would like to indicate very briefly how the study of radio scintillation phenomena has been used to obtain information about the ionosphere.

The next slide shows typical radio star scintillations. It has been found that these scintillations are due to the presence of irregularities in the *F*-region. The radio sources scintillate not only in intensity but also in position, and, to some degree, "in colour." Thus, the high-resolution Cambridge interferometers have shown that during strong scintillation activity the radio star's apparent position may vary through several minutes of arc; work at Cambridge and at Jodrell and more recently in Holland has shown that there is a fair degree of correlation between scintillations recorded at one site at frequency differences of up to a ratio of 1:1.5.

The scale of the amplitude distribution may be determined by using spaced receivers; the next slide shows simultaneous records taken by two such equipments. The scale and intensity of the irregularities in phase which occur at ground level have been investigated at Cambridge by Hewish, using interferometer techniques. He has found that the phase irregularities are approximately the same size as the amplitude variations, and have an intensity of up to at least one radian at 80 Mc/sec. A combination of these amplitude and phase measurements has shown that the ionospheric irregularities are about 4 km in size.

The study of the scintillation records using three triangularly-spaced receivers about one kilometer apart enables the motion of the ionospheric irregularities to be investigated. The next slide shows fluctuations recorded by three such equipments and reveals marked systematic time displacements between the three records. The next slide shows some of the results of this *F*-region wind measuring technique; it has been found that the motions are predominantly towards the west in the evening and reverse direction rather abruptly at about midnight.

One factor in the scintillation phenomena which soon becomes apparent to anyone working in the field is the extreme variability of the speed of the fluctuations, which may vary about one hundredfold. An early analysis, shown in the next slide, revealed that the scintillation rate was, on the average, four times more rapid during aurorae than in their absence; a more quantitative result was obtained by plotting the fluctuation rate against the geomagnetic *K*-index, as shown in the next slide. This revealed a more or less linear relationship between the two phenomena. It has also been shown that the fluctuation rate is proportional to the wind velocity, a result which means that the wind velocity can now be estimated with (say) a 20 per cent accuracy from measurements of the fluctuation rate at a single receiver.

The last slide shows a rather unusual decrease in the extra-terrestrial signal at 80 Mc/sec which occurred during an aurora. The decrease was attributed to the reflection away from the receivers of some of the extra-terrestrial signal by

intense auroral ionization—this explanation seems plausible, since strong auroral echoes were obtained during this period at a frequency of 72 Mc/sec.

(4) F. G. Smith, *Cambridge, C.I.W.*: (*a*) **Radio star scintillations; and** (*b*) **the Cambridge program on discrete sources and solar activity.** The diurnal variation of the ionospheric condition causing the scintillation of "radio stars" has been studied by Hewish at the Cavendish Laboratory, Cambridge, England. The study is now being extended to observing stations in Finland, the Gold Coast, and in the U.S.A. At Washington, this work is being done at the Department of Terrestrial Magnetism, Carnegie Institution of Washington. The diurnal variation has been shown to be markedly different from that at Cambridge, and the experiment is being continued through a whole year to observe the seasonal variations.

At the Cavendish Laboratory, experiments continue along the lines reported in *Monthly Notices* of the Royal Astronomical Society (**112**, 298, 1953). The occultations of the radio source in Taurus by the solar corona were observed in 1952 and 1953, and it has been shown that the radio waves are scattered in inhomogeneities of the corona at distances up to 15 $R_\odot$.

A new interferometer is in use at the Cavendish Laboratory with which it is hoped to observe a large number of discrete sources of cosmic radio waves. The interferometer consists of four aerial systems, each one being a parabolic cylinder about 12,000 square feet in area, at the corners of a rectangle about 1,800 feet by 180 feet. This instrument is at present being used to survey the radiation for the northern hemisphere at a wavelength of 3.7 metres. Accurate location will be determined for many of the discrete sources. One identification of an intense radio source has already been found, although the analysis of most of the recordings has not yet been made. This source is the galactic nebula IC 443. Brightness distribution measurements have been made which show that the source is about 1/2° across, corresponding well with the optical appearance of the nebula.

2-5 P.M.

John Hagen, Chairman

(5) F. T. Haddock, C. H. Mayer, and R. M. Sloanaker, *N.R.L.*: **Radiation at 10 cm from discrete sources and the Orion Nebula.**[1] From November 27 to December 10, 1953, observations were undertaken for the first time using the Naval Research Laboratory 50-foot paraboloidal reflector (Fig. 1) and a microwave radiometer at a wavelength of 9.4 cm or 3,200 Mc/sec. During this period, radio waves from beyond the solar system were detected for the first time at a wavelength of less than 21 cm. Radiation was measured from sources situated both within and external to the Milky Way stellar system. This work extends the short-wave limits of the radio spectra on the previously known six brightest cosmic radio sources by factors of 2.5 to 12. These are the well-known sources in the constellations of Cassiopeia, Taurus, Cygnus, Sagittarius, Centaurus, and Virgo.

[1]Astroph. J. (in press); also presented at AAAS Meeting, Boston, December 27, 1953.

Knowledge of radio spectra is of value in finding the proper radiation mechanism in these sources. In fact, the mechanism in all previously known cosmic radio sources is not yet understood.

Besides the measurement of these six brightest sources known at meter wavelengths, two new radio sources were discovered. They were also identified with bright gaseous nebulae in our Galaxy; the Omega or Swan Nebula in Sagittarius, and the Great Nebula in Orion (Figs. 2 and 3).

(HADDOCK, MAYER, SLOANAKER)

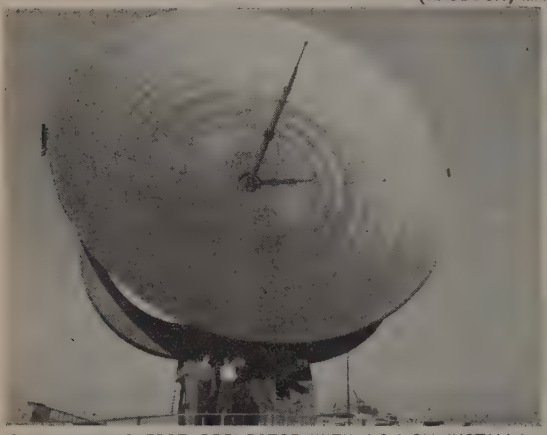

FIG. 1—NRL 50-FOOT REFLECTOR WITH λ9.4 CM-INSTALLATION (NRL PHOTO)

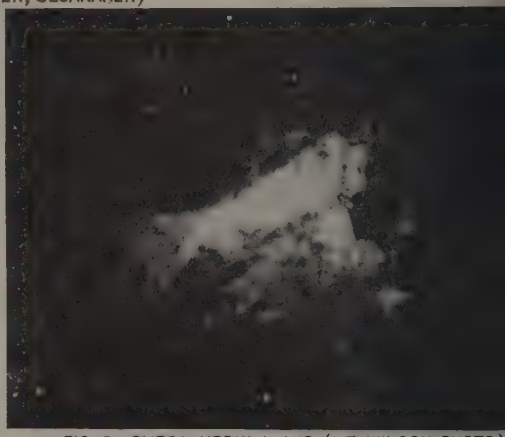

FIG. 2—OMEGA NEBULA, M17 (MT. WILSON PHOTO)

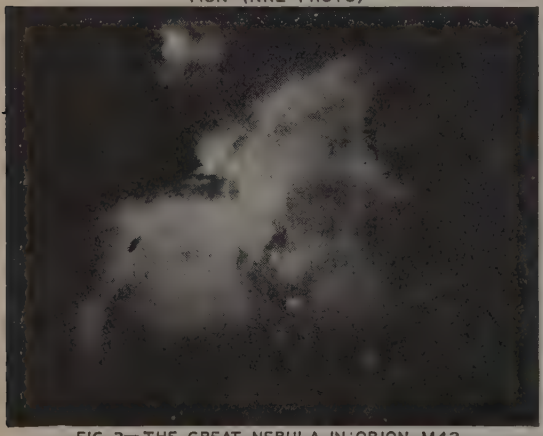

FIG. 3—THE GREAT NEBULA IN ORION, M42 (MT. WILSON PHOTO)

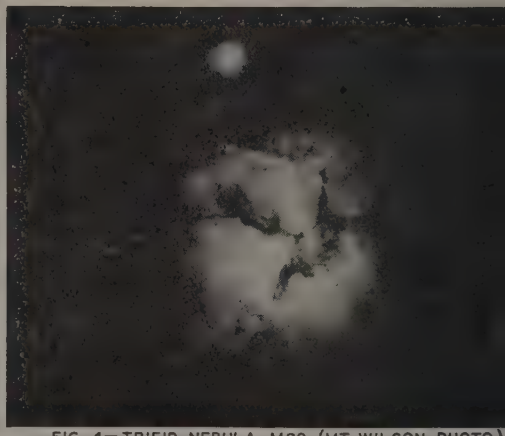

FIG. 4—TRIFID NEBULA, M20 (MT. WILSON PHOTO)

From the size and intensity of the radio source in Orion found at 9.4 cm wavelength,[1] from the failure to detect this source at longer wavelengths,[2] and from results of optical studies of the Orion Nebula,[3] it appears that the observed radio emission arises thermally from free electron collisions with positive ions. If further studies confirm this, it will be the first discrete radio source whose radiation

[2]J. E. Baldwin, Observatory, **73**, 155 (1953).

[3]J. L. Greenstein, Astroph. J., **104**, 114 (1946); also J. L. Greenstein and R. Minkowski, Astroph. J., **118**, 1 (1953).

nechanism is understood. The known spectra of other sources indicate decreasing ntensity with increasing frequency, whereas the Orion source spectrum appears o be the inverse. Thus, the Orion Nebula may represent a new class of discrete adio sources.

(HADDOCK, MAYER, SLOANAKER)

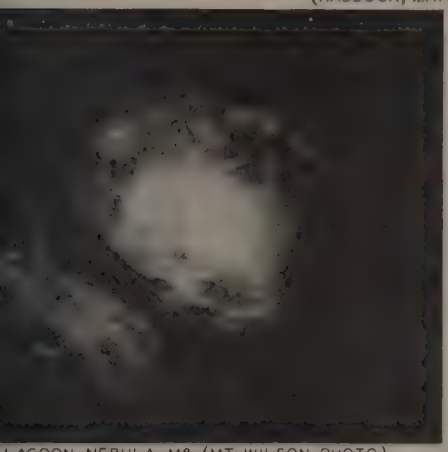

LAGOON NEBULA, M8 (MT. WILSON PHOTO)

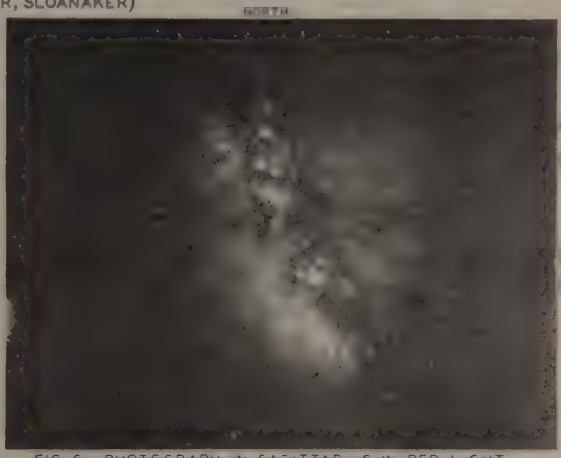

FIG. 6—PHOTOGRAPH IN SAGITTARIUS IN RED LIGHT
(DR. BART J. BOK PHOTO)

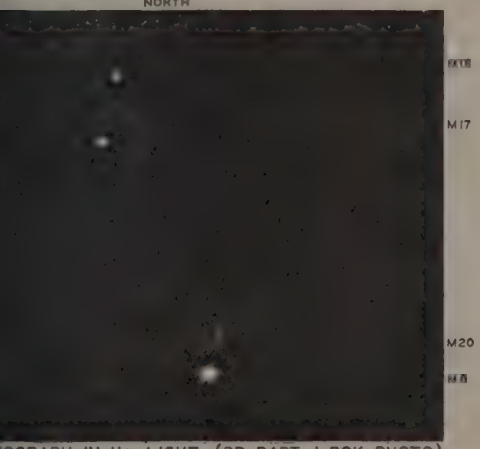

OGRAPH IN Hα LIGHT (DR. BART J. BOK PHOTO)

The Orion Nebula was suggested as a thermal radio source several years ago by J. L. Greenstein[4] because it was a very dense ionized hydrogen (H II) region strongly emitting the (Balmer) hydrogen-alpha line at 6563 A.

The other new source, the Omega Nebula, NGC 6618, is also a bright hydrogen emission region which has not been detected at longer wavelengths, although it is fifty per cent brighter than the Orion Nebula at 9.4 cm. Thus it also appears to be a thermal source. In addition, observations at 9.4 cm in the directions of the Trifid Nebula, NGC 6514, and the Lagoon Nebula, NGC 6523 (Figs. 4 and 5), gave definite evidence of radiation. Now these are also bright hydrogen emission

[4] J. L. Greenstein, Observatory, **67**, 25 (1947), and Astr. J., **54**, 121 (1949).

regions. B. Y. Mills[5] reported a source at 101 Mc/sec whose uncertainties i position include the Trifid Nebula.[6] Figures 6 and 7 are photographs of the sam region, one in red light and the other in hydrogen-alpha light. The four brigh hydrogen emission nebulae stand out clearly in the hydrogen-alpha photograph They are from north to south: NGC 6611 (not searched for at 9.4 cm); the Omeg Nebula, NGC 6618; the Trifid Nebula, NGC 6514; and the Lagoon Nebula NGC 6523.

One other source was detected at 9.4 cm which agreed in position with a sourc first detected at 25 cm wavelength.[7] It was later found at 300 cm (101 Mc/sec by Mills[5] and appears at all three wavelengths as a discrete source superimpose on an extended source of weaker intensity. The observed position for this sourc at 9.4 cm was $17^h\ 42^m.5 \pm 2$ minutes in right ascension and $-29° \pm 0°.1$ in declina tion. This position is in a region of several hydrogen-alpha emission nebulae.[8]

We are grateful to Mr. J. Edwin Sees, NRL, for preparing the antenna contro system. We are indebted to Drs. John P. Hagen, Naval Research Laboratory and F. Graham Smith, Cavendish Laboratory, for their interest in these obser vations.

(6) G. REBER, *Hawaii, Research Corporation*—**Interferometric work in Hawai** The random variations of intensity of signals from point sources caused by th ionosphere greatly affect studies of cosmic static. Most of the time, the interfero meter pattern for a discrete radio source rising over the horizon is so disturbed an modified by these ionospheric effects as to become unusable and, indeed, ofte unrecognizable. One cause of these fluctuations is the condition known as sprea *F*, which indicates the presence of diffuse and irregular echoes from the *F*-regio of the ionosphere. Analyses of spread *F* over Hawaii were completed for the perio 1944–1953. The diurnal and seasonal properties were discussed and a conclusio reached regarding latitude and longitude effects. Some properties of scintillation at decameter waves were described.

(7) J. D. KRAUS, *Ohio State University*—**Some results of the Ohio State Uni versity radio astronomy project.** No abstract was submitted.

(8) J. HAGEN, *N.R.L.*: **Some results of solar research with radio astronom techniques.** It is apparent that the sun is a vastly different object when viewed a meter wavelengths than when seen at decimeter or at centimeter wavelengths. Th difference between the quiet sun and the disturbed sun becomes progressivel greater as the wavelength increases. Much effort has been put into gaining a understanding of the mechanism for radiation in the sun, and I think it is no apparent that the mechanism back of the quiet sun is well understood. This wi be brought out later in the talk. Figure 1 illustrates in a schematic fashion th

[5]B. Y. Mills, Aust. J. Sci. Res., A, 5, 266 (1952).

[6]R. J. Coates suggested this optical identification.

[7]J. H. Piddington and H. C. Minnett, Austr. J. Sci. Res., A, 4, 459 (1951).

[8]We are indebted to Dr. Bart J. Bok for showing us a catalogue of hydrogen-alpha regio prior to publication. *Cf* S. Sharpless, Astroph. J., 118, 362 (1953).

ariation of the radiation with wavelength and with different levels of activity n the sun. The lower full curve is a curve of the variation of quiet sun temperature ith wavelength, varying from somewhat less than 10^4 °K at millimeter wave-ngths to about 10^6 degrees at meter wavelengths. The next curve is that of the sturbed sun, with the effective temperature varying from about 10^4 degrees at ort wavelengths to something like 10^7 or 10^8 degrees at the longer wavelengths. here is a part of this disturbed component which is highly correlated with sunspot tivity, and in the diagram this has been separated out. This is most apparent at wavelength of about 10 cm. The uppermost curve indicates the level to which ie radiation of the sun rises at the time of chromospheric flares. It is seen that the are-associated effect is apparent even at 8-mm wavelength with an increase in tensity of only a few per cent, whereas at the longest wavelength, that is, around meters or so, the equivalent temperature rises by a factor of 10^4 or 10^5. If we ok at the quiet sun component by itself, as shown in Figure 2, it is seen that the mperature rises smoothly from about 7,000 or 8,000 degrees at 8 mm to a million egrees in the meter wavelength band. This has been shown to be consistent with ermal radiation from the ionized gas of the sun's atmosphere, where the absorp-on in the atmosphere is due to free-free transitions between protons and electrons, ith the resultant absorption coefficient being proportional to the square of the ectron density and the square of the wavelength and inversely proportional to ie three-halves power of the temperature. When an analysis is made of the radio diation from the sun in this manner, it is possible to assign an electron density istribution and a temperature gradient of the atmosphere in such a way that the eoretically predicted temperatures will agree with those measured. This has been one and the resultant temperature and pressure gradients are shown in Figure 3. he important point is that the temperature seems to remain at a low level through-ut the chromosphere and then at a height of 10,000 km it rises steeply to a mperature of about a million degrees at the base of the corona.

It is important to find ways and means to check this result by experiment. o do so, leads to a search for ways and means to obtain high resolution in scanning ie sun. Since the temperature gradient in the atmosphere is a rising one in the gion where the principal absorption for the radio waves takes place, then one ould expect for that group of waves a radial brightness distribution with a bright mb. That this is so can be seen by the following argument. Figure 4 shows the ffective emission per unit thickness for the different layers in the sun's atmosphere or four different wavelengths, all based on the model referred to earlier. It is seen iat with the 50-cm wavelength, for example, there is considerable emission from ie corona, but that the principal emission takes place from that region of the un's atmosphere between 15,000 and 30,000 km above the photosphere. Similarly, or 10 cm, the principal emission originates in a region somewhat lower and there s less radiation from the corona, as would be expected. In the extreme, at 8.5 mm, ost of the emission comes from a region around 7,500 km above the photosphere, ith practically no contribution from the corona. Thus, each of these wavelengths llows us to probe regions in the sun's atmosphere, and one would expect them hen to reflect the temperature of each of these layers. At these wavelengths, the ndex of refraction remains very near unity in the regions of the sun in which we

are interested. Near the limb of the sun, a ray must travel tangentially throug the sun's atmosphere and so will be absorbed sooner than would a ray entering t atmosphere at the center of the sun. Now, since the temperature is rising in t sun's atmosphere, the principal emission for the limb ray will arise in a region high in the atmosphere than for the central ray and will consequently be at a high temperature. The type of limb brightening expected on this model is shown

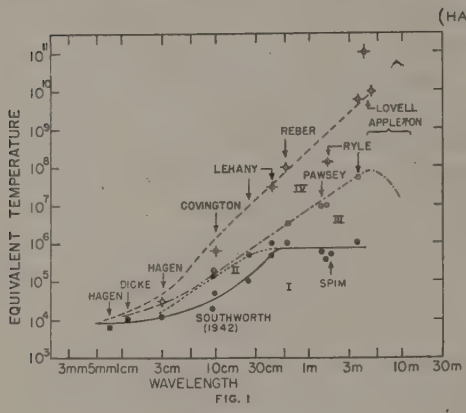

FIG. 1

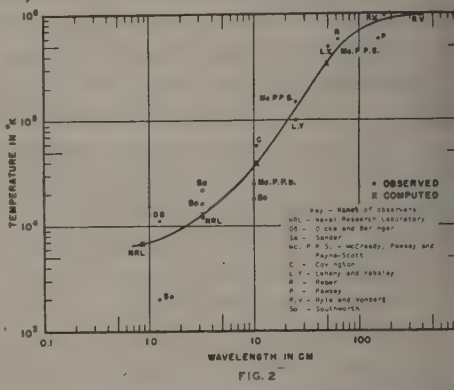

FIG. 2

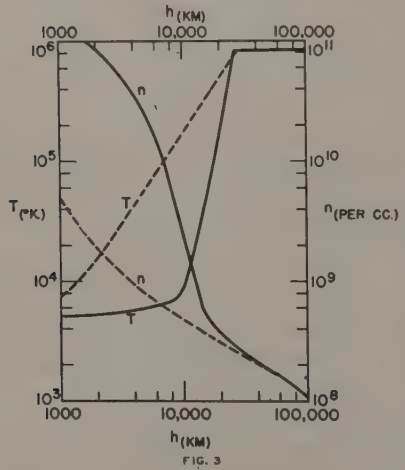

FIG. 3

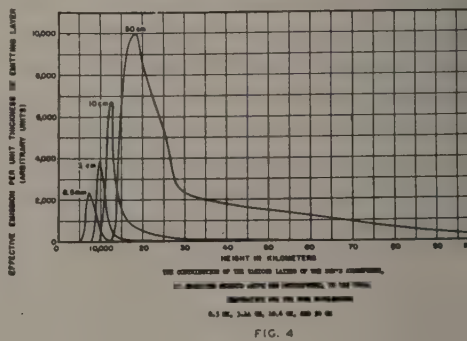

FIG. 4

Figure 5, where it is seen that in every case, in the wavelength range 8 mm to cm, the effective diameter of the sun is greater than the photospheric diamet becoming progressively greater as the wavelength becomes longer, and that limb brightening is not very great at 8 mm, as one would expect, and becor greater as we go towards 10 cm, where it appears to reach a maximum. At 50 c while the diameter of the sun is greater, the relative brightness of the limb is so great as at 10. The problem arises then how best to measure this radial brig ness distribution and thereby to get a confirmation of the theory of the quiet s There are two or three methods immediately available. One of them is to obt high resolution by building an antenna with a large aperture, such as the 50-f

antenna at the Naval Research Laboratory, which can resolve the sun when used at short centimeter and millimeter wavelengths. This has also been done by Covington in Canada, where a linear antenna operated at 10 cm and capable of resolving the sun has been built. A second method would be to use an interferometer. The best example is the multiple element interferometer of Christiansen in Australia. This is operated at 20-cm wavelength. Christiansen's and Covington's antennas, of course, have resolution in only one plane, but can discern limb brighten-

(HAGEN)

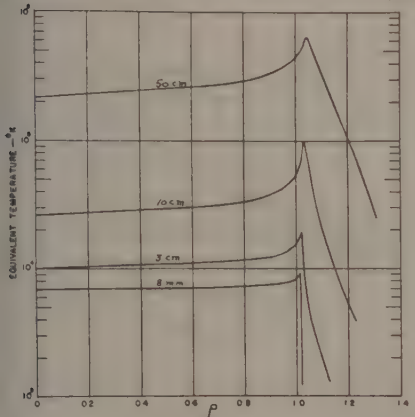

FIG. 5

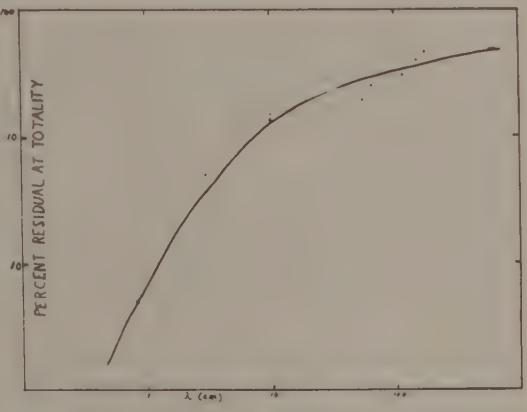

FIG. 6

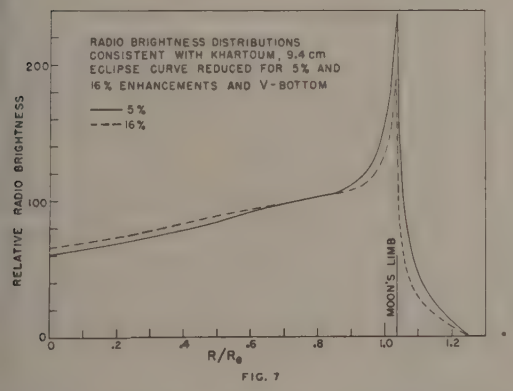

FIG. 7

ing. A third method that is particularly usable in the centimeter range and which yields the highest resolution is that of eclipse measurement. Referring to the sketch of the radial brightness distribution for various wavelengths, it is clear that during an eclipse as the moon covers the surface of the sun an observation of the resultant eclipse curve should reveal by its residual at totality the outer structure of the radial brightness distribution curve. In addition, careful analysis of the shape of the eclipse curve will yield the radial brightness distribution curve existing for that wavelength on the sun. This will be discussed in detail in a later paper, but it should be pointed out here that this is a powerful method in the centimeter wavelength range and becomes not so good at longer wavelengths where the effective diameter of the sun is much larger. The most recent eclipse of the sun in 1952,

nearly central at Khartoum, was measured by the Naval Research Laboratory group at a wavelength of 9.4 cm and also at 8.5 mm. The 9.4-cm equipment used a 6-foot dish which had a 4-degree beam, and therefore effectively saw the sun as a point source. The 8.5-mm equipment used a larger antenna, 16 feet by 2 feet in aperture, which therefore had a fan-beam 8 minutes by one degree in outline. This beam was so oriented on the sun that the long dimension of the beam went across the center of the sun and enclosed the track of the moon. This made the analysis of the eclipse somewhat simpler and helped considerably by avoiding active areas.

The results obtained since 1947 at total eclipses of the sun by all workers are shown in the following slides. First is shown the 1951 eclipse observed by Blum of France at a wavelength of 178 cm. Note the round bottom of the eclipse curve with a residual of 47 per cent. The 1947 eclipse was observed by Haikin and Chikhachev at a wavelength of 150 cm. Here the sun was much more active, but the residual at this wavelength was 40 per cent. Then, in order of wavelength, is shown the 1952 eclipse measured at Khartoum by Laffineur, at a wavelength of 117 cm and 55 cm. The residuals were, respectively, 30.5 and 19.5 per cent. As the wavelength becomes shorter, it is to be noted that the eclipse curves begin to take form and have a sharper bottom. The next slide shows the results of the 1950 eclipse observed by the Naval Research Laboratory party at Attu. The wavelengths here were 65, 10, and 3 cm. The residuals, in order, were 25, 15, and 5 per cent. The NRL data for 10 cm taken at the 1952 eclipse, Khartoum, are shown on the next slide with a residual of 13 to 14 per cent. The next slide shows the 1947 eclipse measured by the Naval Research Laboratory from a ship in the Atlantic at a wavelength of 3 cm. Here the residual is 3 per cent. It should be noted that this and the observation at 150 cm by the Russians, Haikin and Chikhachev, represent the first total eclipse measured by radio astronomy. Analysis of the 3-cm data for this eclipse at this early date clearly showed the effect of sunspots and also limb brightening. Finally, we have the NRL Khartoum eclipse curve at a wavelength of 8.5 mm and here the residual has fallen to 0.5 per cent. When one compares the residuals measured at various wavelengths, it becomes clear that the residual is a direct function of the wavelength, becoming smaller as the wavelength decreases. It should be noted that these data refer to the sun over a period of five years and during that time there were tremendous changes in the activity of the sun, yet the data hang together quite well (Fig. 6).

The NRL 10-cm eclipse curve taken at Khartoum in 1952 has been carefully analyzed for the effect of spots and then has been reduced for the resultant radial brightness distribution (Fig. 7). The method of doing this will be described in detail later by Mr. Haddock, but let us point out here that the resultant radial brightness distribution curve shows marked limb brightening and is quite consistent with that predicted by the theory referred to earlier. The 8-mm curve has been analyzed in somewhat the same fashion, but with the striking result that, in addition to limb brightening in about the amount predicted, there appears also to be a bright center to the sun. This is consistent with measurements made with the 50-foot dish at this wavelength, and a theory is in the process of being worked out to explain this situation. The theory is based on a model of the chromosphere in which

here are two gases, a hot and a cold, disposed in vertical columns suggested by picules.

It is felt that the theory of the quiet sun is in fairly good shape and the resultant picture of the middle portion of the sun's atmosphere is good, that is, for that region just above the middle chromosphere and extending through the lower corona. Further work in the very short wavelength region from 8 mm on down in wavelength will serve to clarify the picture somewhat deeper in the chromosphere, and work in the meter range of the quiet sun is required to fully clarify a picture of the outer corona.

(9) E. G. Bowen, *Australia, C.S.I.R.O.*: **Some recent results in the study of radio emission from the sun**—(*a*) **Solar research at CSIRO; and** (*b*) **a new phenomenon in solar radio noise.** Two results which have recently been obtained in the study of radio emission from the sun are as follows:

(1) Using two multiple-beam interferometers in the E-W and N-S planes, respectively, Christiansen has found that on a wavelength of 20 cm, no limb brightening occurs along the N-S axis of the sun, while at the same time there is pronounced limb brightening along the E-W direction. This leads to a radio "picture" of the sun which is not circularly symmetrical and is analogous to the visual concept of the corona.

(2) The radio spectrometer of Paul Wild for determining changes in the radio frequency spectrum of the sun with time has been extended in range to operate from 40 to 240 Mc/sec. When a flare occurs on the sun, it is already known that particles are emitted with velocities from 500 to 1,000 km/sec. A new result obtained with the spectrometer is that, coincident in time with the flare, fast particles are also emitted with a velocity of a fifth or a tenth the velocity of light. This result may have an important bearing on theories of origin of cosmic rays.

(10) A. E. Covington, *National Research Council of Canada*: **Solar noise at 10 cm.** Since 1947, routine observations of the 10.7-cm solar flux have been made in Ottawa at the National Research Council and have provided measures of the steady daily flux, as well as any superimposed bursts of radiation. The bursts usually show simple variations of intensity and are classified according to a system of few terms. A pronounced 27-day variation in the daily level indicates the presence of bright radio spots on the solar surface. These radio sunspots have been located by a directional antenna with a fan-shaped beam (half power points, 1/8° in E-W direction and 20° in N-S direction). Some relationships between the radio and optical features of the sunspot are outlined.

Regular observations of the 10.7-cm solar flux have been made in Ottawa at the National Research Council with a 4-foot reflector. This antenna has a resolving power of 7°, so that the total radiation from the whole disk is received. The antenna is motor driven so that the solar output may be recorded throughout the day.

Slide 1—Record of the solar flux for one day
Burst is eliminated; level remains steady
Calibration
Sunset

The bursts at 10 cm are essentially single events in comparison to bursts o meter wavelengths. They are relatively rare and few terms are sufficient to classif anything that may be observed.

Slide 2—In six years of observations involving 12,000 hours

Single s/n	—34 per cent	Pre — 5 per cent	1947— 1083	56
Simple	—32 per cent	Post—25 per cent	48— 1826	61
Complex	—20		49— 2185	103
Groups	—11 per cent		50— 1675	78
Periods of irregularities	— 3 per cent		51— 2225	106
			52— 2761	28
			11755	432
			53—	30
				462

Slide 3—Example of bursts
Slide 4—Recently discovered type; gradual rise and fall May 25, 1952

Several observatories throughout the world are now engaged in watching th radio sun. Ultimately we should be able to follow solar activity 24 hours a da rain or shine. Slide (No. 5) shows the daily level of the 10-cm solar flux as recorde in 1952 at five different stations (Fig. 2).

	Mc
Ottawa	— 2800
Sydney	— 3000
Tokyo	— 3000
Osaka	— 3260
Nagoya	— 3750

If the outer curves—daily levels from Ottawa and Nagoya—are compared, it wi be seen that there is good agreement and that the same sun is being observed. Th curves in between show the same general trend, but there is considerably mo scatter.

The showly varying component of the daily level in the decimetre range ha been associated with the appearance of sunspots and shows high correlation wit indices such as the total area of sunspots present on the disk. This is shown in slide.

The same data are also shown in a scatter diagram. The intercept of the straigh line gives the flux from the spotless sun (an equivalent temperature of 45,000° for an assumed 1/2° solar disk), while the slope of the line gives the flux from un sunspot area (equivalent temperature of 14×10^6°K for a spot area of one millionth of solar hemisphere).

The scatter diagram is based upon a simple model of the radio spot in whic an extensive volume of coronal material is related to the underlying optical spo The equivalent temperature of this radio emitting surface is of the order of 10^6°K

Directional studies by means of a large antenna have located radio sources o the solar disk. The slotted waveguide antenna is 150 feet long and is shown in slide.

CLASSIFICATION OF 10 CM. SOLAR NOISE BURSTS

EMISSION:

(1) Single Burst--(Simple - One Peak / Complex - Two or more peaks)

(2) Group of Bursts -- Series of single bursts

(3) Gradual Rise and Fall -- Small Amplitude, long duration

(4) Miscellaneous -- Periods of irregularities

(5) Secondery Features of Bursts -- (a) superimposed fluctuations
(b) precursor
(c) post-burst increase

FIG. 1

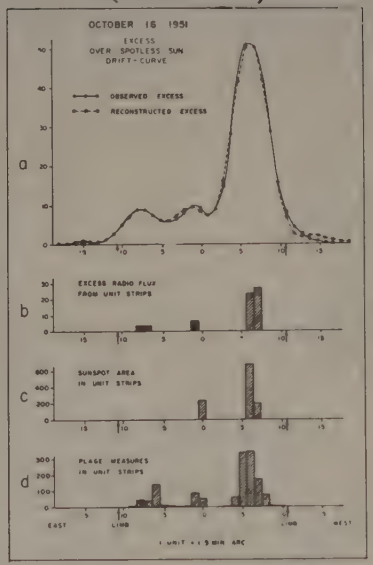

FIG. 3

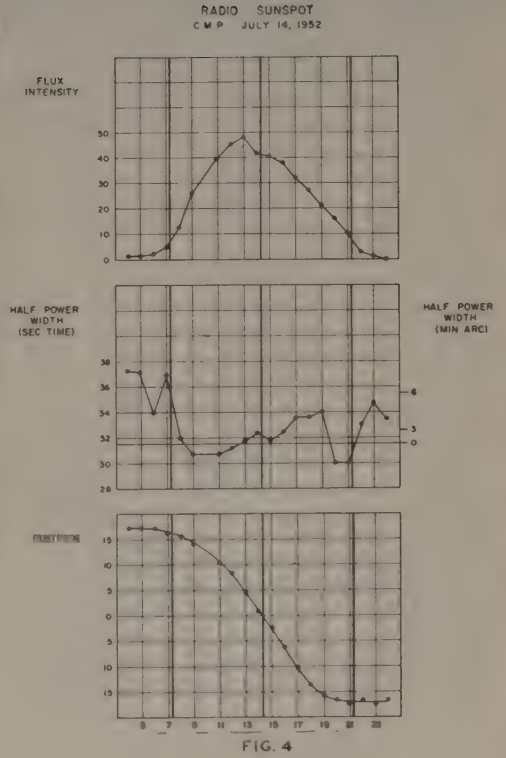

FIG. 4

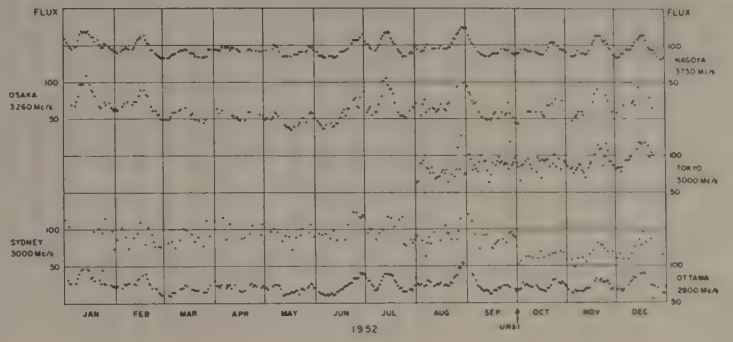

FIG. 2

This antenna produces a fan-shaped beam 1/8° in the E-W plane and 20° in the N-S plane. The horn is 18 inches wide, 150 feet long with the slotted waveguide lying in the bottom. This structure is mounted on a shaft and may be pointed to any elevation. An observation is taken when the sun drifts through the antenna pattern. Information is obtained in strips.

Solar activity is represented by the excess above the quiet-sun drift curve. On October 16, 1951, the excess curve showed three radio sources. When the antenna pattern is removed, one obtains the E-W position of three radio sources as shown in curve *b* of Figure 3. The sunspot areas from the Naval Observatory have been found in strips and are shown as curve *c*, while certain plage measures were made by Dr. Dodson and are shown in curve *d*. The best agreement appears between the radio sunspots and the plage measures.

When a well-developed radio spot is followed across the solar disk, the radius of the sphere on which it is located can be found. Three different spots give values of radius 1.1 times that of the photosphere. This places the radio spot at an elevation of 65,000 km.

Waldmeier has identified the 10-cm radio sunspots with bright features of the corona which he calls condensations. One such feature was observed during the eclipse of February 25, 1952, and is shown in a slide.

In conclusion, one might say that the radio sunspot is such a condensation with the bright plage and dark sunspot at the base.

Open House

Monday, January 4, 8 P.M.

Informal get together, with light refreshments, at the C.I.W. building, 1530 P Street

Tuesday, January 5, 9:45 A.M.—12:30 P.M.

B. J. Bok, Chairman

(11) C. R. BURROWS AND W. E. GORDON, *Cornell University*: **Some results of the Cornell radio astronomy project.** Cornell University started research in radio astronomy with the support of the Office of Naval Research on May 1, 1946. The first task was the design and construction of a 204-inch reflector which could be used for receiving extra-terrestrial radiations. This telescope, shown in Figure 1, is the result of the cooperative efforts of the Schools of Mechanical Engineering, Civil Engineering, and Electrical Engineering. The eight-ton instrument is mounted on a circular track, supported by concrete foundations. In addition to its vertical axis, it has three other axes, one of which may be aligned with the axis of rotation of the earth, and another at right-angles to this, which then becomes a declination axis. The fourth allows rotation around the axis of the parabola. The two axes in addition to those of the normal equatorial mount were provided in order to facilitate the measurement of the directive characteristics of the antenna.

It was originally intended to set the astronomical axes so that the antenna was directed horizontally and then by rotating it about the other two axes it would be possible to obtain the directional characteristics of the antenna in all meridian

lanes by placing a test transmitter a suitable distance away on the earth's surface. Ve later found that this method of calibration was unnecessary, since in periods f quiet sun the sun itself could be used as a test transmitter.

At Cornell, we were not even satisfied with this method of calibrating the radio elescope and, hence, supplemented it with an auxiliary calibration, which will be lescribed later.

This telescope was first provided with a 200-Mc feed, which has later been hanged to 1,420 Mc, with provisions to later use it on both frequencies. While he telescope was under construction, measurements were made by using a 268 adar antenna mount, which is shown in Figure 2. The Quonset hut which houses he electronic equipment and the concrete foundation for the large telescope, nder construction at the time, are also shown in Figure 2. The electronic equipnent associated with this antenna is a straight-forward superheterodyne receiver, vith precautions taken to maintain stability. Day-to-day variations are of the rder of magnitude of 0.1 per cent of the first circuit noise. Routine daily measurements of the radiation from the sun on 200 Mc were begun using this equipment n July 1948. At first the measurements were limited to a couple of hours around noon, but in October 1949 the measurements were extended over the entire period hat the sun is above the horizon. Later these were shortened to just cover the normal working day, since early in the morning and late in the afternoon the presence of the ground affects the observations.

In June 1948, the Air Force Cambridge Research Center asked the School of Electrical Engineering at Cornell to establish a solar radio observatory at Sacramento Peak, New Mexico, to be operated in cooperation with the optical observatory being established by Harvard University. Figure 3 shows the antennas and laboratory of this observatory. The two antenna mattresses on the left of the cross-arm are used to observe the radiation from the sun at 200 Mc on circular polarization. The dipole antennas of these arrays are at right-angles, so that by inserting an extra quarter wavelength of line in first one or the other feed line, right-hand or left-hand circular polarization can be received. The two Yagi antennas on the right arm are for measurement on 50 Mc, while the parabolic reflector in the center is for 3,200 Mc. Since this is an altitude-azimuth mount, an analog computer is used to keep these antennas directed toward the sun throughout the day. This is driven by a clock-motor on the polar axis, and the signals are taken off the altitude and azimuth axes which drive the servomechanism control for the antenna. The first circuits of the electronic equipment are mounted as near the antenna as possible, the signals being brought into the laboratory at intermediate frequencies, and the remaining electronic equipment is in the laboratory building.

The daily measurements of the intensity of the solar flux at 200 Mc as obtained at Ithaca, together with interferometer measurements giving the position of bursts, have been used for an intensive study of the active regions of the sun in cooperation with Dr. Helen Dodson,[1] of the McMath-Hulbert Observatory. Since another conference paper by Dr. Dodson not only includes the results of the relationship of optical measurements of solar activity to these measurements at

[1]H. W. Dodson, E. R. Hedeman, and L. Oren, Solar flares and associated 200-Mc/sec radiation, Astroph. J., 118, 169–196 (1953).

200 Mc, but also the measurements made by Mr. Covington of Ottawa at 2,80 Mc, this will not be described further. The classification of distinctive events whic has been made at Ithaca by Mr. Owren in connection with this cooperative effor is of interest.

(BURROWS, GORDON)

FIG. 1

200 MC 3200 MC 55 MC

FIG. 3

FIG. 2

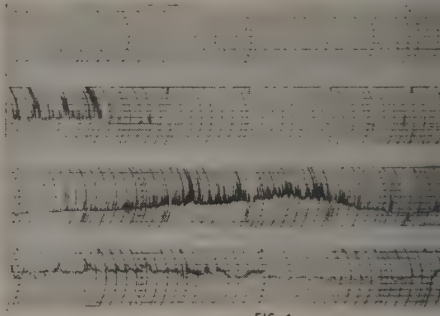

FIG. 4

FIG. 1—204-inch radio telescope equipped to receive 200-Mc radiation

FIG. 2—Radio astronomy observatory, Ithaca, New York, 1948, showing laboratory buildin telescope base, and SCR 268 antenna mount

FIG. 3—Solar radio observatory, Sunspot, New Mexico, showing laboratory building and antenn mount

FIG. 4—Characteristics of radiation from the sun at 200 Mc: Q = quiet sun, E = sudden com mencement of activity, N = noise storm, and W = high level with little activity

Figure 4 shows samples of the Esterline-Angus recording of the radiation fron the sun at 200 Mc as measured at Ithaca. The first record shows a quiet sun. Thi is substantially a straight line, except for the semi-hourly interruptions for th calibration of the equipment. The second record shows a sudden commencemen of activity. The third record shows a temporary increase of activity and media flux, which has been referred to as a "noise storm." The last record on this slid (Fig. 4) shows a series of small-amplitude long-period fluctuations superimpose on an increase in median flux. Figure 5 shows some of the types of distinctiv events. The upper left-hand example, labeled S, is of a single burst of rather larg

nplitude. The next record (C) shows a complex burst, and the third (K) a compact oup of bursts. The last record on the left (T) is a rise and fall of flux during a nall time (a matter of a few minutes) with an increase in burst activity, while ıe record marked R shows a rise and fall of flux in a short time-interval without

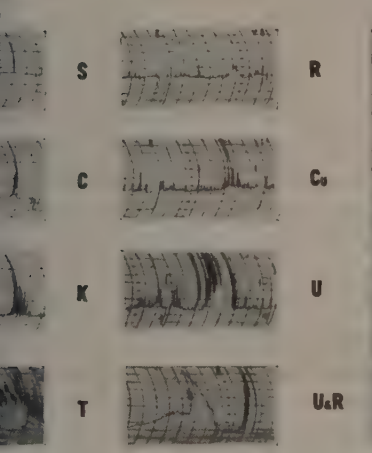

FIG. 5

(BURROWS, GORDON)

FIG. 6

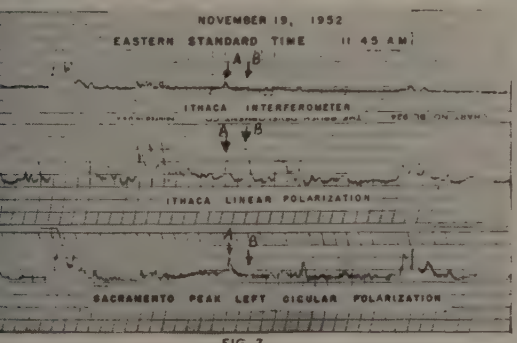

FIG. 7

G. 5—Distinctive events in the solar records at 200 Mc: S = simple burst, C = complex burst, = compact group of bursts, T = rise in flux with increase in activity, R = rise in flux with no increase in activity burst, and U = outburst

G. 6—Radio astronomy observatory, Ithaca, New York, 1953, showing laboratory building, nergency power truck, and antennas from left to right as follows: Equatorial mount for solar servations, NE interferometer station, radio telescope, W interferometer station, one of calibration antennas, and SCR 268 mount

G. 7—Comparison of burst activity as observed on an interferometer, a linear polarized, and a circularly polarized antenna

ı accompanying increase in activity. The remaining records on the right are rge amplitude bursts of duration longer than a few minutes, normally referred) as "out-bursts."

In addition to searching for distinctive events, as illustrated by these samples, ıe daily record of radiation received from the sun at 200 Mc is reduced by hourly tervals to give the median flux and the relative amount of activity. These data

are submitted for publication in the Quarterly Bulletin and to Dr. DeVoogt i Holland for his monthly reports for Commission Va, URSI.

Figure 6 shows a more recent picture of the radio astronomy laboratory a Ithaca. The antenna on the high mast is one of a pair of antennas that have bee used to obtain an absolute measurement of the radiation received from the su on 200 Mc. These antennas are so arranged that one can be used to transmi energy to the other, or both can be used to receive signals from the sun. In th former case, the product of the gains of the two antennas is obtained; and, in th latter case, the ratio of the gains is obtained. This allows a determination of th absolute gain of either antenna and, hence, the radiation from the sun can b obtained in watts per square meter per cycle per second. This type of measuremer requires radiation from the sun to be reasonably constant over an interval of tim

The 204-inch telescope appears in the Figure and another 200-Mc antenna o a much less elaborate equatorial mount. All of the recent measurements of th sun on 200 Mc have been made with this antenna. There are three antennas com prising two interferometers; the westernmost antenna can be seen in the Figur the one east of it is not in the Figure, but an antenna can be seen just back of th emergency power supply truck. The "268" antenna mount has been set on permanent concrete pier, visible on the right. When this antenna was still mounte on its trailer with only jacks to take the trailer off its wheels, Seeger and William son[2] made a study of the distribution of radiation in the galaxy in an effort t determine the plane of the galaxy. The internal consistency of the data taken wit this setup greatly exceeded the accuracy with which the direction in regard to i axes was known. Accordingly, this antenna was mounted in a more permaner fashion and the experiments have been repeated. These are now in the process being analyzed.

The use of the interferometer, both in locating active regions on the sun an discrete sources, has led to the conclusion that greatly improved accuracy ma be obtained by properly designing an interfometer to be as free as possible fro the major errors of this one. Proper design should make possible an accuracy of th order of one part of the 10^5 in angle. This requires that the antennas be mounte on a sufficiently firm foundation that their positions do not change by as much a a fraction of a millimeter over a period of time, and that the antennas may b inverted or interchanged without introducing this much uncertainty in positio It is also desirable that three sets of transmission lines be used by the antenna and the radiometer, so that the small differences in their electrical length can b calibrated out. It probably is unnecessary to say that there must be no pr amplifiers in the interferometer circuit, since they could introduce a variab phase. With this improved interferometer, it is planned to determine the positio of the brighter point sources repeatedly, night after night, in order to statistical determine the errors of measurement. It is hoped that similar measurements w be made of the same point sources at other observatories, so that the residu observatory error can be removed from all of the measurements.

One of our graduate students, Mr. Edward Reinhart, has made a rather e

[2]C. L. Seeger and R. E. Williamson, The pole of the galaxy as determined from measureme at 205 MC/sec, Astroph. J., 113, 21–49 (1951).

austive theoretical study of radiation from the quiet sun at various frequencies. ecently, he has calculated the occultation of the Taurus radio star by the solar orona. His theoretical investigation, assuming an eight-minute diameter at 80 Mc and a 15-minute diameter at 40 Mc, shows that there will be an occultation n van de Hulst's[3] electron density distribution for the solar corona on 40 Mc, ut no occultation on 80 Mc. When he assumes the distribution of electronic ensity suggested by Ryle, there results a complete eclipse on both frequencies. The apparent size of the Taurus image increases as the sun is approached, but the pread of the image is too small to account for the observed decrease in amplitude n the interferometer pattern as reported by Machin and Smith.[4] Mr. Reinhart as studied the effect of enhancements of the sun's radiation at the time of the Taurus transit and suggests that this may account for some of the departures rom the smooth curve by Machin and Smith. He is now studying the effect of ccultation of a non-uniform radio star by a non-symmetric corona.

Dr. Takeo Hatanaka,[5,6] who has been visiting us from the Tokyo Observatory or the past 17 months, has made a detailed study of the position and polarization f bursts at 200 Mc. Figure 7 shows the type of data with which he works. The pper curve shows the output of the interferometer (spacing of 51 wavelengths) t Ithaca. The record is too short to show a complete fringe. The second curve hows the received radiation on a linear polarized antenna, and the bottom curve hows the data obtained at Sacramento Peak with left-handed circular polariza- ion. The burst marked *A* in the center of the Figure apparently is not located at he minimum of the interferometer pattern and the left-handed circular polariza- ion component of it is seen in the bottom trace. About a second earlier, there is nother burst indicated as *B*, which shows up on the linear polarization record ut is absent both on the circular polarization record and the interferometer ecord. This burst apparently is located at a different part of the sun, and had a ifferent polarization. By a statistical study of the ratios of the amplitudes of hese records, Dr. Hatanaka has been able to separate bursts according to their olarization and position on the sun. He has made two simple assumptions with egard to the nature of the radiation. One is that the radiation of a burst consists f two circular polarizations of different intensity and a random phase. The other s that the radiation, in general, is represented by an elliptically polarized radiation. The latter is equal to assuming a constant phase difference in the former case. It s found that neither of these assumptions is adequate to explain the observed lata.

Part of the difficulty in interpreting these data is that they are taken with dif- erent equipments. Accordingly, a time-sharing system is planned in which the ignals on right-handed polarization, left-handed polarization, and the two linear

[3]H. C. van de Hulst, The electron density of the solar corona, Bull. Astron. Inst. Netherlands, No. 410 (Feb. 1950).

[4]K. E. Machin and F. G. Smith, Occultation of a radio star by the solar corona, Nature, 170, 319–320 (1952).

[5]T. Hatanaka, A solution for the path of radio waves through the solar atmosphere by elliptic ntegrals, Cornell University, Res. Rep. E.E. 181 (Jan. 1954).

[6]T. Hatanaka, Position and polarization of solar radio bursts on 200 Mc/sec, Cornell Uni- ersity, Res. Rep. E.E. 179 (Dec. 1953).

polarizations are obtained both with and without an interferometer arrangement on the basis of some 50 pieces of data a second, so as to produce substantially simultaneous records of all of the data using the same radiometer. It is hoped that with these data it will be possible to obtain a better understanding of the nature of these increases in solar radiation from the sun.

(12) HELEN W. DODSON, *McMath-Hulbert Observatory, University of Michigan* **Solar flares and associated radiation at 200 Mc/sec and 2,800 Mc/sec.** During 1951 and 1952, we at the McMath-Hulbert Observatory and the radio astronomers at Cornell University and the National Research Council of Canada, carried out two cooperative studies of solar radiation at radio frequencies at the time of solar flares. The first study was an investigation of 200-Mc/sec radiation as recorded at Cornell at the time of 194 flares. Our Cornell colleagues were Dr. Charles R. Burrows and Mr. Leif Owren. The second study was a similar survey of 2,800 Mc/sec radiation as recorded at Ottawa at the time of 386 flares and subflares. Our colleague in this work was Mr. A. E. Covington. The present report brings together for comparison some of the main features of these two studies.

Comparison of the results of the studies of flares at these two radio frequencies reveals certain similarities and certain differences. A higher percentage of flares was apparently associated with a distinctive event at 200 Mc/sec (78 per cent) than was the case at 2,800 Mc/sec (40 per cent). At 2,800 Mc/sec, the percentage of flares with associated radio-frequency events increased rapidly with importance of the Hα flare (19 per cent for subflares to 87 per cent for flares of importance two and three). This was not the case at 200 Mc/sec; the percentage was practically independent of flare importance.

The basic form of the flare-associated event at these two radio frequencies appears to be fundamentally similar. In both cases, the fully-developed flare event exhibits two parts, but either of these two parts may occur separately. At 200 Mc/sec, the first or "early" part of the double pattern is a sudden major burst of complex shape, which starts with the commencement of the flare and is usually over by the time Hα maximum has been attained. The second or "late" component is an enhancement of the 200-Mc/sec radiation, which starts more gradually. It begins after the start of the Hα flare, often after Hα maximum has been attained and reaches its maximum as the flare is fading. When fully developed, this second part appears to be identical with the feature known as "noise storm."

At 2,800 Mc/sec, the first or early part is a sudden single burst, which may be either simple or complex in structure. This burst commences with the start of the Hα flare and is usually over by the time Hα maximum has been attained. The second part of the typical flare event at this frequency is the gradual diminution of flux, termed by Covington a "post-burst increase." When only this second part of the flare-event occurs, the distinctive event at 2,800 Mc/sec is classified as a "gradual rise and fall." At this higher frequency, the "second part" seems to start simultaneously with the flare, and with the "first part," contrary to its late aspect at 200 Mc/sec.

At both frequencies, flares in all importance categories were associated with practically all types of flare-associated events. However, at both frequencies

here was a higher percentage of important flares in the Hα brightenings associated ith bursts followed by second or late parts than with comparable but purely urst-type features.

Sudden ionospheric disturbances accompanied 46 per cent of the flares (sub-ares excluded) in the 200-Mc/sec study and 42 per cent of those in the 2,800-Ic/sec investigation. Separation of the flares according to the presence or absence f an associated radio event did not introduce any marked change in the percentage ith SID's when 200-Mc/sec events were considered (46 per cent for flares with ssociated events and 42 per cent for the nulls). A similar division made a con-picuous difference when 2,800-Mc/sec events were considered. SID's accompanied 1 per cent of the flares with distinctive events at 2,800 Mc/sec, but only 18 er cent of the null cases. Furthermore, within each importance category, the ccurrence of a 2,800-Mc/sec event favored the occurrence of a sudden ionospheric isturbance. Although the mere occurrence of a 200-Mc/sec event with the flare id not appear to alter the probability of an ionospheric disturbance, it should be ointed out that flares associated with 200-Mc/sec events of high energy excesses nd conspicuous second parts had more than the average numbers of associated ID's.

(Comment) H. C. VAN DE HULST: **Fast recordings of solar radiation at 200 Ic/sec.** In connection with the preceding paper, attention may be called to the ossibility of making recordings of solar radiation with a very high time-resolution. n 1950, the Microwave Astronomy Project at Cornell University acquired equip-ent for making such records at 200 Mc/sec with a Brush recorder. Results from sample of these records have been reported by Charles L. Seeger at an URSI-IRE eeting, Washington, D.C., in 1950. Recently Seeger, now at Leiden Observatory, as reexamined these samples. The speed is 120 inches per minute, or one mile per ght hours. The finest details shown extend over one-fifth of a second, or one milli-eter, except for car-interference, which is very much sharper. The variety of etail makes these tracings even harder to interpret than the tracings taken at rdinary speed. However, the new examination has brought out two features that ay be important.

(1) The records show a distinct difference between activity associated with stormy days" and activity of another kind, of which the strongest bursts are seen be associated with flares. The flare-type events are characterized by a long me constant, of the order of three seconds. Some such events were found coincide with a reported flare, that was previously thought to have no associated dio emission.

(2) Those cases that could be studied in detail show that a major flare-type vent has leaders and followers. The leaders may be simple bulges, with an equally ng duration of three seconds, and sometimes as low as a 20 per cent increase over e quiet sun's intensity. They may precede the major event by half an hour or ore and a periodicity in time is suspected. Further study is needed and it is still mpossible to tell whether a flare prognosis may be based on these hints.

(13) W. O. ROBERTS, *High Altitude Observatory, Boulder, Colorado*: **Radio nission from active regions of the corona.** Phenomena of the sun's atmosphere

may be divided into the following two principal classes: (1) Those associated wit the steady level of emission of energy to space from the "undisturbed" sola surface, and (2) those associated with variably disturbed active regions of th sun. Radio emission effects of importance are associated with both classes o phenomena.

The solar chromosphere, perhaps made up principally of small jet-like spicule is a major phenomenon of the undisturbed sun and is undoubtedly a source of substantial part of the radio noise of the "quiet" sun. The fact that the chromo sphere is not a simple, uniform atmospheric layer and does not decrease in densit equally along all solar radii is of primary importance in theories of its radio emissio

We speculate that the electron (or white-light) corona arises from two source as follows: (1) The ion streams represented by spicules found at all latitudes, an (2) the grosser jets and streams found over active solar regions, which are characte ized by solar flares, plages, sunspots, and emission-line coronal maxima. We furth suggest that net magnetic fields possessing roughly radial orientation diverge fro active regions. These fields, we speculate, have field strengths at coronal heigh roughly comparable with the sun's general field, and are, together with the gener field, responsible for channeling spicule ions into the rays and streamers observe at solar eclipse, and which have been suggested by others[1] as the cause of recurre geomagnetic storms. Concordantly, we conceive of the active centers themselves a sources of relatively dense, hot coronal material infused into the solar atmosphe at times of solar-flare activity, which slowly spreads from the centers with spee of the order of one kilometer per second, giving rise both to optical and rad noise[2] phenomena.

Particularly important for an understanding of the corona are the followi radio emission studies: (1) Of the polarization of active-region emission at met wavelengths similar to those of Payne-Scott and Little,[3] for information on magne fields in the solar corona; (2) of active region radio-noise at times of low sol disturbance, because of the ease with which the active region phenomena can isolated and unambiguously identified; and (3) of bursts and other noise phenome occurring in the absence of active centers, and thus perhaps associated wi electron coronal streamers, as suggested by recent observations of Das a Bhargava.[4]

Research leading to the speculations stated above has been a joint effort several staff members of the High Altitude Observatory and was in part support by the Office of Naval Research.

(14) F. T. HADDOCK, *N.R.L.*: **Eclipse measurements at centimeter wavelen and their interpretation.*** Radio observations of the solar eclipses are made

[1]C. W. Allen, Mon. Not. R. Astr. Soc., **104**, 13 (1944).
[2]J. H. Piddington and R. D. Davies, Nature, **171**, 692 (1953).
[3]R. Payne-Scott and A. G. Little, Aust. J. Sci. Res., A, **4**, 508 (1951).
[4]A. K. Das and B. H. Bhargava, Nature, **172**, 855 (1953).

*This talk covers material presented before the URSI-IRE meeting in Washington, D.C April 27–30, 1953, by John P. Hagen, "Naval Research Laboratory Solar Eclipse Expedition February 1952"; by C. H. Mayer and D. R. J. White, "The radio telescope used at Khartou at a wavelength of 9.4 cm"; and by F. T. Haddock and R. M. Sloanaker, "Observational eviden for solar limb brightening at a wavelength of 9.4 cm."

determine (*a*) the radio "brightness" distribution over the solar disk, and (*b*) the size, position, and intensity of localized regions of enhanced emission. It is necessary to determine (*b*) in order to find (*a*), which is difficult because of the low angular resolving power generally available with radio telescopes. An eclipse of the sun is valuable because it is geometrically precise and thus capable of fixing the absolute scale of size. Although the analysis of eclipse data is complex, the effective angular resolving power for centimeter waves is of the same order as that obtainable optically on the sun.

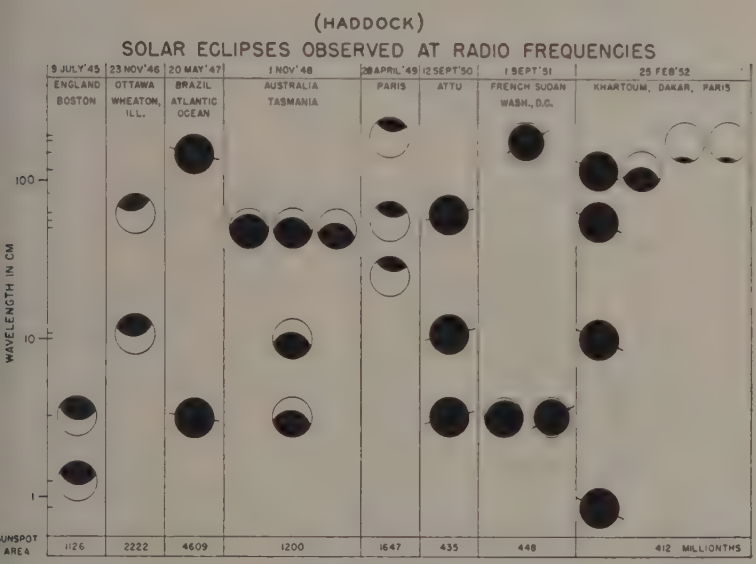

FIG. 1

Each year since 1945 a solar eclipse has been observed at more than one radio frequency by various research groups. More than two dozen separate measurements have been made on wavelengths ranging from 0.8 to 200 cm. (Fig. 1 displays pictorially the eclipse magnitude and the path of moon over the sun as seen from the various radio eclipse sites. The date, observing wavelengths, and sunspot area for each eclipse is also given.)

The measurement of the February 25, 1952, total solar eclipse at a wavelength of 9.4 cm was obtained at Khartoum, Sudan. This eclipse offered a good opportunity to test the hypothesis of a bright ring of emission about the solar limb predicted at this wavelength, since the ring would just be obscured by the moon at optical totality. As the variation of received solar flux near mid-totality is most sensitive to the presence of a bright ring near the sun's limb, it is believed that a total solar eclipse is required for its detection. Accurate and precise data are also needed because by the nature of the observation small uncertainties in the received flux lead to large uncertainties in the derived brightness distribution.

The 9.4-cm eclipse curve obtained at Khartoum was modified for the presence of enhanced emission from two active regions, one on the west limb and one on the east limb of the sun, under the assumption of circular symmetry in the radial

brightness distribution centered on the solar disk. (Fig. 2 shows the track of the moon over the sun and the active regions.) The range of modifications possible in this case was limited by the small amount of excess emission, about 8 per cent, which could be arbitrarily assigned to the active regions. (Fig. 3 shows the observed

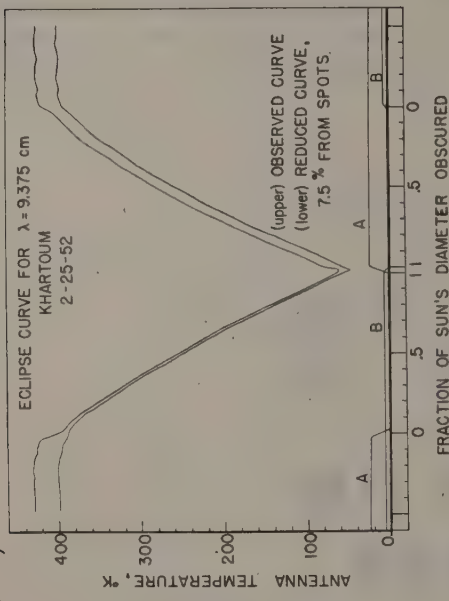

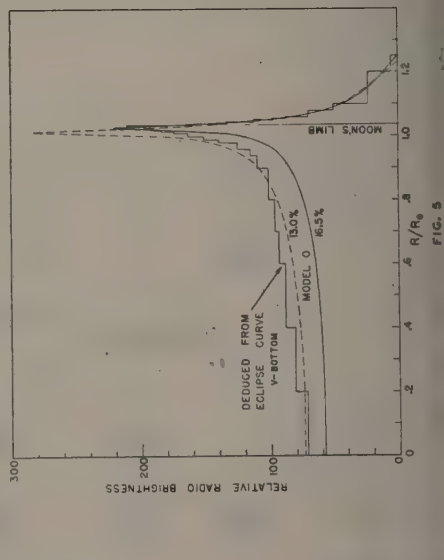

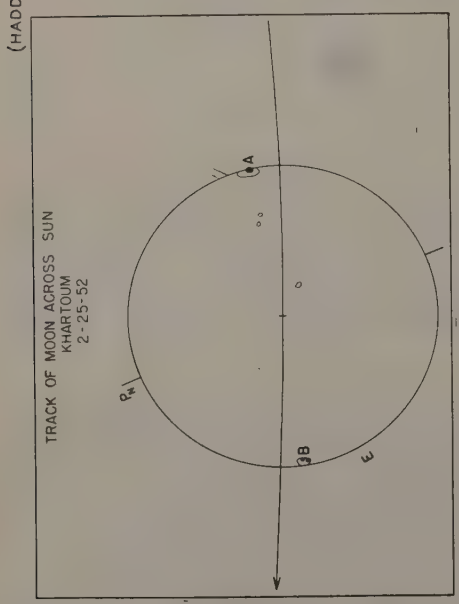

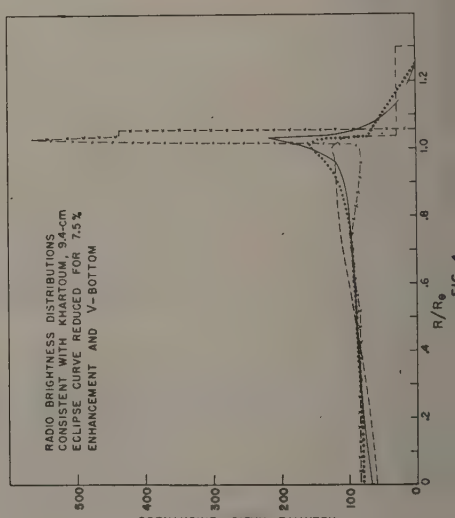

(HADDOCK)

eclipse curve with a modified symmetrical eclipse curve below it.) A set of possibl radial brightness distributions consistent with the modified eclipse curve wer derived. They all show evidence of increased radio brightness near the limb of th visible sun. (Fig. 4 shows the set of possible radial distributions.)

Good agreement is obtained between a derived radial distribution chosen from the possible solutions on the basis of physical considerations and a predicted distribution based upon a model of the sun's atmosphere given by Hagen.[2] A slight contraction in the radial scale of model improves the agreement. (Fig 5. shows the derived radial distribution deduced from the modified eclipse curve with a Vee-shaped bottom and the predicted distributions. The dashed curve is the predicted distribution, the scale of which is reduced so that the flux at mid-eclipse is 13 per cent of the uneclipsed value.) A radio measurement of a total eclipse offers perhaps the best method for determining the radial scale of electron density and temperature distributions in the solar chromosphere.

[Because of the number and variety of contributions on solar problems, additional discussion was postponed until Wednesday afternoon, January 6.]

PROBLEMS AND THEORY IN RADIO ASTRONOMY

(15) R. Minkowski, *Mount Wilson and Palomar Observatories, Carnegie Institution of Washington and California Institute of Technology*: **Progress report on astronomical observations of radio sources.** It is now well established that a variety of astronomical objects can be strong radio emitters. A detailed investigation of such objects is of obvious importance, but at the present stage only a few of them offer the possibility of obtaining significant results.

Little can be done at present from the astronomical side to help understand the radiation from normal extragalactic nebulae, including the Galaxy. The bulk of this radiation seems to originate from sources which are similar to the bulk of the stars in the way in which they are distributed within the Galaxy, but only improved radio observations can decide finally the question of whether stars are the source of the radio emission of normal galaxies.

Most of the peculiar extragalactic nebulae identified as radio sources seem to be systems in which the radio emission is due to a collision of two galaxies. Since in such a collision strong interaction occurs only between the gas, while the stars are essentially unaffected, it seems obvious that the collision of gas clouds produces the radio emission. The strongest source of this type, Cygnus A, is a nebula of the 18th magnitude, too faint to easily permit a detailed investigation. The radio-interferometric measures suggest that a large part of the radio emission occurs in the most outlying parts of the system, which are too faint to be observed optically. Another type of peculiarity seems to be represented by NGC 4486, but no explanation can be suggested why and how the astronomical peculiarity, a small straight jet extending from the nucleus, produces the strong radio emission which seems to originate, not in this jet, but in the nebula as a whole.

Most accessible for a detailed investigation are the galactic sources. Three different types of galactic emission nebulosities are now recognized as radio sources. That in these objects the radio emission originates in a mass of gas, is beyond all doubt. The problem is this: Which peculiar conditions lead to radio emission of much

[2] J. P. Hagen, Temperature gradients in the sun's atmosphere measured at radio frequencies, Astroph. J., 113, 547 (1951).

higher intensity than the weak thermal emission of the bulk of the gas in normal emission nebulae, such as the Orion nebula? The three types are represented by the following objects:

(1) The nebulosity discovered by Baade in the position of the Cassiopeia source represents a new type of object. It consists of broken bits of nebulosity scattered within an area of about 6′ diameter, which coincides in position and size with the radio source. The optical emission is strongest near the northern edge, but the whole area seems to contribute to the radio emission. Thus, optical and radio emission are not directly related. The nebulosity consists of two different kinds of condensations: sharp broken bits visible only in red light and diffuse small clouds. The diffuse clouds have very large radial velocities (−1,800 to ±4,500 km/sec); the internal motions in individual clouds are of the order of 500 km/sec. Many of these clouds have changed their shape to such a degree in two years that their proper motion cannot be determined. For a few more stable condensations, Baade has found outward motions of the order of 0.25 second of arc/year. All motions are irregular to such a degree that they hide entirely the effects of any systematic expansion. This condition is fundamentally different from the behavior of supernova shells, such as the Crab nebula. The sharp broken bits show small radial velocities (0 to 150 km/sec), small internal motions of the order of 100 km/sec, and no observable proper motion in two years. It is possible, but not certain, that these features define a mass which is expanding with a velocity of about 100 km/sec. The spectrum of the diffuse condensations shows strong forbidden lines with unusual relative intensities, but no permitted lines of H or He have been observed. The interpretation of these spectra is difficult, possibly owing to the instability of these condensations, in which probably the ionization is determined, not by the present state, but depends on the previous history. No exciting star seems to be present; the excitation may be due to transformation of mechanical energy in collisions. The electron temperature is probably of the order of 15,000° to 20,000°, the electron density of the order of 10^3 to 10^4 cm^{-3}. The sharp filaments show Hα and the [N II] lines, which are absent in the diffuse condensations, in addition to very faint lines of [O I]. This suggests higher density and lower electron temperature than in the diffuse condensations.

(2) The Crab nebula, the remnant of the supernova of 1054, is an expanding mass of gas. The inner part of the nebula consists of diffuse nebulosity which shows a continuous spectrum. This is surrounded by a system of filaments which have a spectrum consisting of forbidden and permitted lines. No observational evidence permits one at present to decide whether the radio emission originates in the inner or outer part of the nebula. The Crab nebula is long known to be an expanding system, with a velocity of expansion of 1,200 km/sec. Superposed are irregular motions. Recent observations show that these irregular motions are of the order of 300 km/sec. In some places, they suggest the existence of secondary centers of expansion, which may explain the scalloped appearance of the edge of the nebula.

(3) The nebula IC 443, recently identified as a source by Baldwin on the basis of Ryle's new survey, is a rare type of circular filamentary nebulosity, rather similar to the Cygnus loop (NGC 6960/6992). These nebulae seem to be slowly expanding. Very small outward proper motions of the edge of the nebula have

recently been observed in IC 443 by Baade. The spectroscopic evidence is not yet adequate to establish the existence of expansion. Random motions, however, have been observed. They seem to be of the order of 100 km/sec, definitely much larger than the random velocities of the order of 10 km/sec which seem to be present in typical diffuse nebulosities.

The presence of large random motions in all three objects suggests that there may be a connection between the presence of large random motions and the radio emission. To make a first preliminary test of such an assumption, it is necessary to compare the velocity spread with the radio emission per unit volume. If plausible values for the unknown distances of the Cassiopeia source and of IC 443 are assumed, one obtains the following data:

	Cassiopeia	Crab	IC 443
Diameter in minutes of arc.....	5	5	50
Distance in parsecs.....	(500)	1,000	(1,500)
Radio emissivity in ergs $cm^{-3}(c/s)^{-1}$..	1.1×10^{-30}	3.3×10^{-32}	0.7×10^{-35}
Order of velocity spread in km/sec...	2,000	300	100

The emission seems to increase faster than the square of the velocity spread, but the data are too preliminary to establish more than the probable existence of a relation between radio emission and velocity spread.

(16) J. L. Greenstein, *Mount Wilson and Palomar Observatories, Carnegie Institution of Washington and California Institute of Technology*: **Thermal emission from gases; and energy considerations in non-thermal sources.** The theory of thermal emission from ionized gases permits the computation of (1) the optical depth due to free-free absorption and (2) the emission at radio frequencies. Thermal emission should be detectable from galactic diffuse emission nebulae, galactic H II regions or groups of H II regions along spiral arms, planetary nebulae (when high resolution is available), and from the central plane of the Milky Way. Absorption by ionized gas of radiation from distant non-thermal sources would also appear along the Milky Way.

The optical thickness, allowing for stimulated emission, is 4×10^5 E.M./$f^2T^{3/2}$, where f is the frequency in Mc/sec and E.M. $= n_i n_e l$, is the emission measure; n_i, n_e are per cm^3 and l, the thickness, is in parsecs. From an optically thin emitter, we receive power $P = 5 \times 10^{-24}$ E.M. $g\theta^2T^{-1/2}$ watts/square meter per cycle per second. Here g is the Gaunt factor (near ten), and θ is the apparent angular diameter of the source in radians. For the Orion nebula, I adopt $n_i = n_e = 300/cm^3$, $l = 1$ psc, that is, $\theta = 2.5 \times 10^{-3}$. Then $\tau = 4$ at 100 Mc/sec, that is, the nebula is optically thick. The spectrum is flat at $P = 3.5 \times 10^{-25}$ for $f > 300$ Mc/sec and drops rapidly at $f < 100$ Mc/sec, where the optical thickness is large. These numbers predict somewhat less power than is observed by F. T. Haddock, of the Naval Research Laboratory. However, the E.M. given is a rough average value, and the results show the importance of better optical values of n_i, n_e and l. Antenna diameter of 50 feet or greater and frequencies of 1,000 Mc/sec are needed for work on emission regions of small E.M. A recent list of E.M.'s is given by H. Johnson (Astroph. J., **118**, 370, 1953), and may suggest other emission nebulae with observable values of radio-frequency power. Planetary nebulae have enormous

E.M. $\approx 10^5$ to 10^6, but are of such small angular size that they will be observable only at very high frequencies, or with very large antennae. It is possible that clusters of galaxies will contain sufficient neutral hydrogen to be detectable with 21-cm radiation.

The effect of free-free absorption superposed on non-thermal radio sources is to produce a maximum in the transmitted radio spectrum at a frequency 0.77 $(\text{E.M.})^{1/2}$ Mc/sec and to flatten the spectral energy curve.

The non-thermal sources apparently concentrate a large amount of noise power into the radio frequencies. Let us assume that gases in high-velocity collision are the energy source. In a forthcoming paper by Greenstein and Minkowski (Astroph. J., in press), estimates are made of the total kinetic energy available during collisions of large gas masses, and of the radio-frequency emission of the well-identified discrete sources. For example, the Cygnus A source emits 5×10^{-24} erg/cm^{3}sec; this is 5 per cent of the total kinetic energy of gas clouds of mass 10^9 $M_\odot$ colliding with a velocity of 1,000 km/sec. The duration of such a collision is only a million years. Small filaments such as occur in the Cassiopeia A source have a life of only 10 to 100 years; their kinetic energies would produce very high radio-noise emission rates if the energy were entirely dissipated during a collision.

(17) F. Hoyle, *Cambridge—California Institute of Technology*: **A mechanism for radio noise generation.** The optical identification of such strong radio sources as Cygnus A, Cassiopeia, the Crab, etc., constitutes an important step toward an understanding of the processes of origin of cosmic radio waves. For in all these cases, the physical conditions that are operative appear to be comparatively simple: the emitting sources seem to consist of highly diffuse gaseous masses occupying regions from about a parsec to 10,000 parsecs in their dimensions; with large internal motions—several hundred km/sec to several thousand km/sec; and perhaps with magnetic fields of intensities from 10^{-3} to 10^{-4} gauss. These appear to be the principal ingredients of the problem, other complicating factors, such as appear in the case of solar radio emission, being apparently absent.

An interesting possibility that merits consideration as a generating mechanism is that of synchrotron-type emission by relativistic electrons.[1] It is to be emphasised that electrons are necessary, not protons or positive ions which radiate at much too small a rate. At first sight, this might be thought a somewhat implausible requirement. Electrons not only seem to be absent from cosmic rays but considerations of the type first discussed by Fermi[2] would seem to provide a strong reason why relativistic electrons should not be present in interstellar space; namely, that the rate of energy loss from inelastic collisions with neutral interstellar hydrogen gas is about a thousand times greater than the rate of gain of energy through "magnetic collisions." It may however be possible to overcome this objection. The Fermi acceleration mechanism gives a gain-rate that is proportional to the square of the mean random dynamical velocity of the gas masses that carry the magnetic field. Fermi's original calculations were based on a mean velocity of 30 km/sec. In strong radio sources such as Cassiopeia and Cygnus A, a velocity of

[1] J. Schwinger, Phys. Rev., 75, 1912 (1949).
[2] E. Fermi, Phys. Rev., 75, 1169 (1949).

3,000 km/sec would be more appropriate, thereby increasing the gain-rate by a factor 10^4—more than sufficient to overcome the discrepancy. It would seem, therefore, that the above-mentioned criticism can be countered. Indeed, the special conditions required for an electron-acceleration mechanism to operate may very well prove an advantage, since it apparently explains why the normal interstellar gas is comparatively weak in radio emission and why high dynamical velocities seem always to accompany strong emission, a point that is emphasised by Minkowski.[3]

Turning now to the quantitative aspects of the matter, a relativistic electron of velocity ω radiates mainly at frequencies close to the value of ν given by

$$\nu = 4.19 \times 10^6 B\gamma^2 \text{ cps}$$

when B is the magnetic intensity in gauss, and $\gamma = (1 - \omega^2/c^2)^{-1/2}$, so that the electron energy is γ times its rest mass. For $\nu = 10^8$ cps, and $B = 10^{-3}$ gauss, the appropriate value of γ is about 150. The power radiated by a relativistic electron is

$$1.58 \times 10^{-15} B^2\gamma^2 \text{ ergs/sec}$$

The latter formula implies that a relativistic electron radiates an appreciable fraction of its energy in radio waves in a time of order

$$5 \times 10^8 B^{-2}\gamma^{-1} \text{ sec}$$

Using the above relation between γ and ν, this may be expressed by saying that an electron radiating a frequency close to ν loses an appreciable fraction of its energy in

$$10^{12} B^{-3/2}\gamma^{-1/2} \text{ sec}$$

Inserting $\nu = 10^8$ cps, $B = 10^{-3}$ gauss, gives a time of about 10^5 years, which, cosmically speaking, is a very short interval —implying that the present process is a powerful one. Furthermore, it can readily be estimated that if the total energy of all relativistic electrons now present within the Cygnus colliding galaxies (for example) is only a fraction 3×10^{-5} of the total energy of the collision itself (this assumes 10^{44} gm for the mass of colliding gas), then an adequate intensity in the radio band is emitted. Thus, the emission is not only rapid when considered from the point of view of an individual electron, but can be a highly efficient converter into radio energy of the dynamical energy of mass motion of cosmic material.

It remains to add that these ideas can be put to a test. It is possible, given the energy spectrum of the relativistic electrons, to use the above formulas to obtain the frequency spectrum of the emitted radio waves. Suppose that the number of relativistic electrons in the range γ to $\gamma + d\gamma$ is proportional to $d\gamma/\gamma^3$, this being similar to the normal cosmic-ray spectrum. Since each electron emits at a rate proportional to γ^2, it follows that the total emission by all electrons in the range γ to $\gamma + d\gamma$ is proportional to $d\gamma/\gamma$, which by the formula relating γ and ν is proportional to $d\nu/\nu$. Hence, the frequency spectrum of the radio wave should follow a $d\nu/\nu$ dependence. This may be compared with the observed dependence of about

[3]R. Minkowski, private communication.

$d\nu/\nu^{1\cdot2}$. The agreement is satisfactory in view of uncertainty in the energy spectrum of the electrons.

2-5 P.M.

J. B. Wiesner, Chairman

(18) F. G. SMITH, *Cambridge—C.I.W.*: **The nature of the problems of radio astronomy.** (No abstract was submitted.)

(19) H. K. SEN, *C.R.P.L., National Bureau of Standards*: **Noise generation by oscillating plasmas, and non-linear plasma theory.** A brief review was given of plasma oscillations and electron-wave tubes, indicating the need for extension of the small signal theory. The non-linear theory of space-charge waves in moving, interacting electron beams developed by the author was described.

A consideration of the complete (without the linear approximation) equations of the interaction of two moving electron beams of given densities (with sufficient numbers of ions to make the charges macroscopically neutral) showed that propagation of steady-state space-charge wave is a function of its amplitude and phase velocity. For small amplitudes, the oscillation is simple harmonic, and the characteristic dispersion equation of the first-order theory was obtained. For a given phase velocity of the wave, the period increases with the amplitude, and the oscillation becomes increasingly anharmonic. Beyond a particular value of the amplitude (which is a function of the phase velocity of the wave), the oscillation becomes discontinuous and exhibits the phenomenon of jump (well known in non-linear oscillation theory).

An application of the above theory to estimate the intensity of the second-harmonic component in the solar noise generated by solar corpuscle motion in a static corona showed that the higher harmonics would be progressively weaker in intensity. The oscillation amplitude at the point of discontinuity gave a radio intensity far in excess of that observed, indicating the possibility of an extremely low efficiency-factor of conversion of space-charge into electromagnetic-wave energy. On the assumption of a constant coversion-factor for the fundamental and the higher harmonics, absorption near the critical plasma frequency was invoked to bring the theory in line with the recent interesting discovery by Australian workers[1] of the second-harmonic component in solar radio noise. This component exhibits the characteristic frequency drift of the fundamental and is comparable to it in intensity.

The importance of the low efficiency-factor for conversion of space-charge into electromagnetic-wave energy was stressed as making it possible for the plasma to radiate even under weak coupling between longitudinal plasma and transverse (electromagnetic) waves brought about by any means such as non-linear effects, magnetic fields, or transverse velocities. An estimate based on the antenna theory of plasma radiation (first proposed by J. Feinstein[2]), for example, gave a solar radio flux of the order of magnitude of the observed flux.

[1]Personal communication by J. P. Wild to the author.
[2]Letter to the Editor, Phys. Rev., 85, 145 (1952).

The trend for further work in this field was indicated.

(20) This paper was withdrawn.

(21) J. D. KRAUS, *Ohio State University*: **The O.S.U. Antenna.** (No abstract was submitted.)

(22) B. Y. MILLS, *Australia—C.I.W.*: **The pencil beam antenna.** A new method of constructing a pencil beam aerial of high resolution but low effective area and low cost has been devised. It is particularly useful for observations of cosmic noise, including discrete sources, at wavelengths of a few metres. A small scale model, giving an 8° beam at 97 Mc, has been constructed and put into operation. A large model designed to give a beam-width of 0°8 at a frequency of 86 Mc is under construction.

(23) R. HANBURY-BROWN, *Manchester*: **The Manchester paraboloid.** A large paraboloid is under construction at the Jodrell Bank Experimental Station of the University of Manchester. The instrument is financed jointly by the Department of Scientific and Industrial Research and the Nuffield Foundation.

The paraboloid is of 250 feet diameter with a focal length of 62 feet 6 inches. The accuracy of the profile and the size of the mesh will determine the maximum usable frequency, and this cannot yet be stated with certainty. However, it is intended to use at least the central 100 feet of the paraboloid for observations up to about 1,500 Mc/sec.

The bowl of the instrument is supported on an alt-azimuth mount, and it can be rotated through 360° in azimuth and elevation. The instrument will be electrically driven and will be capable of a complete rotation in about a quarter of an hour. The accuracy with which the beam can be pointed is to be of the order of 1/5 degree. The instrument is to be controlled from a computer which will convert celestial coordinates into azimuth and elevation, and which will also allow the instrument to be controlled in terms of any other system of coordinates, such as galactic coordinates.

The weight of the bowl is about 300 tons and the weight of supporting structure is about 1,200 tons. The instrument will be mounted on a circular railway track of 300 feet diameter, which in turn is supported on a reinforced concrete circle on a ring of piles. The foundations of the instrument are now complete; the railway track is at present being laid; and it is expected that construction of the actual instrument will begin in the spring of 1954. The instrument should be at least in partial operation at some time during 1955.

(24) J. P. HAGEN, *N.R.L.*: **The 50-foot antenna—design, construction, and use.** A large precision parabolic reflector has been installed at the Naval Research Laboratory. The reflector is 50 feet in diameter and is made of solid aluminum, with a surface machined to such a tolerance that it may be used at wavelengths of 3 mm and longer. The object in building a large antenna was to obtain the highest resolution and gain possible so that the instrument could be used to study the

radiation of the sun and moon in detail, and to search for radiation from the galaxy and from particular regions of the galaxy, such as the hot hydrogen regions. The reflector itself, weighing 30,000 pounds, is made of 30 pieces of aluminum, separately cast and edge machined. The reflector was machined at the plant of the Collins Radio Company, and brought to the Laboratory and reassembled on the roof of one of the buildings. The surface tolerance is better than we had planned in the beginning. It has been measured by means of a templet; also as a check it has been surveyed as though it were a field by the Coast and Geodetic Survey, the two measurements checking against one another very well. In addition, the pattern obtained at the various wavelengths serves also as a check on the over-all tolerance of the surface. The pointing accuracy to date has been all that could be desired.

The reflector is supported in a steel yoke, which in turn rests upon a standard Navy gun mount. The normal motion of the gun-mount is in azimuth and altitude. In order to effect an equatorial mount, a computer was built which transforms equatorial to alt-azimuth coordinates. This is done with an error of less than five minutes of arc. The machine, of course, is inoperative within a degree or two of the zenith, and, in order to reach the zenith, the antenna must be trained through the gun-mount controls directly. The beam-width of the antenna at 8 mm is three minutes of arc; the calculated gain is 2×10^7, the calculated and measured beam-width at 3 and 10 centimeters being 10 minutes of arc and 26 minutes, respectively. As an example of the resolution obtained with the antenna, drift curves for the sun and moon are shown. In the first instance, drift curves taken at 3 cm are shown, indicating the motion of a radio spot across the sun for three different days. The second illustration shows a single drift curve of the sun taken at 8 mm. The non-uniformity of the surface of the sun can be seen and also the irregularities caused by a spot region. The third curve shows a drift curve of the moon at 8-mm wavelength, and it is clearly seen that there is a considerable temperature gradient across the surface of the moon. The longest wavelength at which this antenna has been used is 21 cm, where it is presently planned to use the antenna for a study of the hydrogen-line emission from selected regions of the galaxy. It is also planned to complete a survey of the sky at 10-cm wavelength, to do some work with the sun at 10 cm, and then to repeat the 10-cm search at 3 cm. In the meantime, the antenna will be used for a high resolution study of the sun and the moon at 8-mm wavelength.

Tuesday, January 5, 6:30 P.M. Dutch-treat dinner followed by a free discussion on antenna design (lead off by E. G. Bowen)

(25) E. G. BOWEN, *Australia—C.S.I.R.O.*: **A new radio telescope design; the big antenna versus the interferometer array.** A disadvantage of a giant radio telescope mounted on a conventional altitude-azimuth mount is that by far the greatest proportion of constructional material goes into the mount and the foundations, and not into the parabolic dish itself. In addition, as the dish is supported only at two points near its periphery, asymmetrical flexure of the surface becomes a problem.

An alternative design which overcomes both of these disadvantages is now

(HAGEN)

proposed. In this design, a 250-foot diameter paraboloid is mounted on a portion of a sphere, as shown in the sketch. The sphere is approximately 120 feet in diameter, and it is allowed to float in a pool of water or light oil in the fashion of a ball joint.

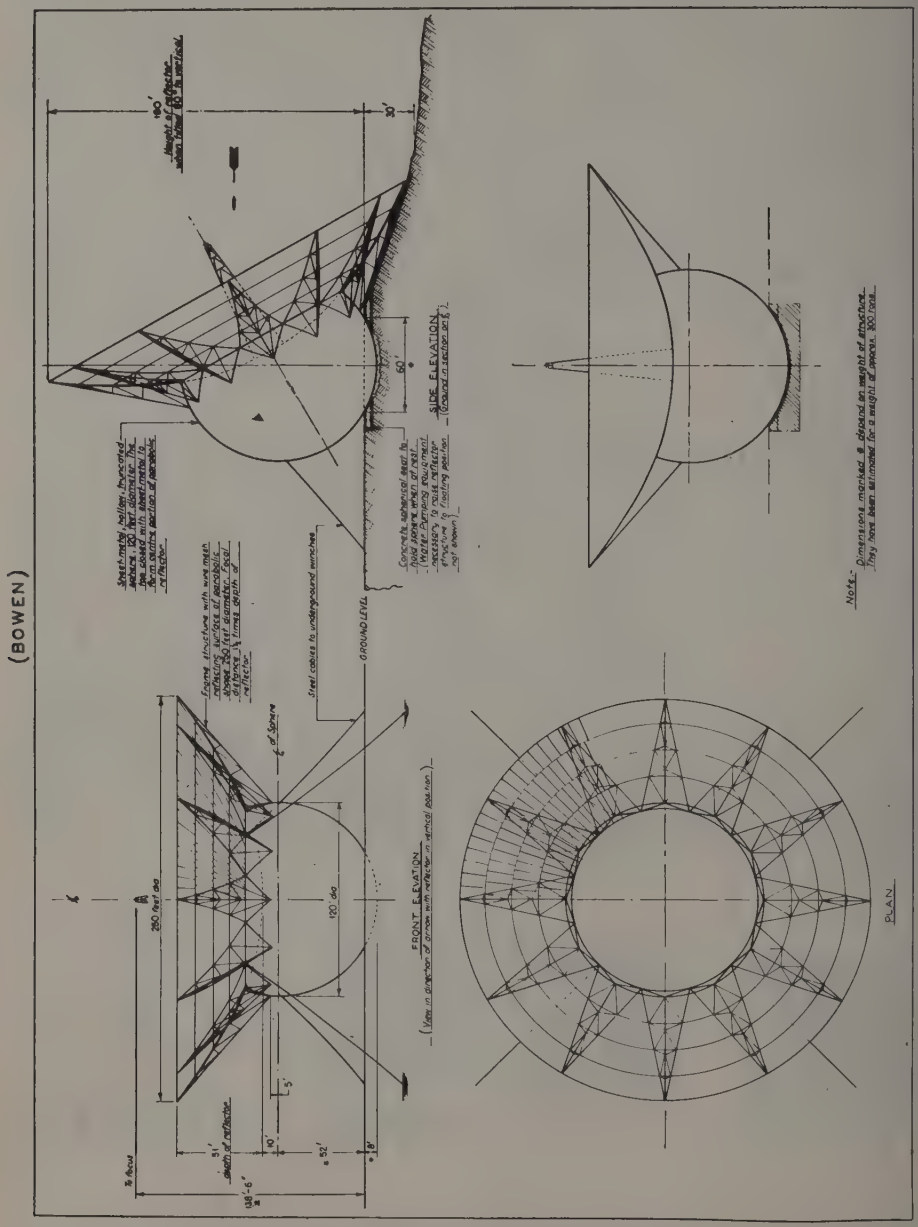

The sphere could be of 1/4″ or 3/8″ welded steel construction; it would be pressurised to provide stiffness and to maintain its shape. The design has a number of advantages over others, as follows:

(*a*) No elaborate foundations are required.
(*b*) Circular symmetry is maintained and there should be few problems maintaining the central portion of the paraboloid to sufficiently close tolerances to operate at a frequency of 1,420 Mc/sec.
(*c*) The structure can be "parked" pointing in any required direction by reducing the level of fluid in the pool.
(*d*) The total weight of the structure is estimated to be 300 or 400 tons as compared with 1,500 tons for conventional designs.

Along with these advantages go certain disadvantages, perhaps the most serious being that of providing an accurate drive. One method of carrying this out would be by means of four cables in the north, south, east, and west directions, respectively. Alternatively, the design is amenable to a relatively simple form of polar axis drive.

Wednesday, January 6, 9:45 A.M.—12:30 P.M.

Merle A. Tuve, Chairman

(26) H. I. Ewen, *Harvard University*: **21-cm equipment at Harvard.** (No abstract was submitted.)

(27) C. G. Little, *Manchester*: **21-cm receiver at Jodrell Bank.** The aerial to be used initially in the Jodrell Bank H-line programme is a 30-foot focal-plane-aperture paraboloid on an alt-azimuth mounting. The surface of the paraboloid, which is accurate to about $\pm 1/2$ inch, is made of 3 8-inch mesh expanded copper. The aerial is steered by means of two electric motors (one azimuth, one elevation).

The range of speed available from the motors is not sufficient to enable the paraboloid to be moved continuously; to track a source, the aerial has to be moved in a series of steps. Since the beam-width of the aerial is only 1°.5, it is necessary to move the aerial about once per minute. This would be rather laborious if done manually, so we have devised a semi-automatic scheme. A magslip is driven at a constant speed equal to the mean angular rate at which the aerial is to be moved in azimuth. The output of this magslip is compared with the azimuth-position magslip on the aerial; as soon as an error of 1/5° has accumulated, relays are tripped, the azimuth motor is started, and the paraboloid moves until it is 1/5° ahead of the correct position, when the motor is switched off. A similar system is used for the elevation control. Using this technique, it is sufficient to check the position of the aerial about every half-hour, and to apply manually any small corrections required to compensate for the non-linear rate of change of azimuth and elevation.

The receiver is similar in principle to the original apparatus used by Ewen, and involves the comparison 30 times per second of the received power on equal bandwidths (each 20 kc/sec wide) separated by 1 Mc/sec. These comparison bands are produced by switching the frequency of the first L.O. 30 times per second through 1 Mc/sec; the receiver is tuned by slowly varying the frequency of the two first

L.O. frequencies, keeping their frequency separation of 1 Mc/sec constant. No radio frequency amplifier is used; all local oscillator frequencies in the double superheterodyne receiver are crystal controlled.

One of the disadvantages of the original Ewen-type receiver is the fact that the receiver is only observing the H-line half of the time; the remaining half, the receiver is tuned to the comparison band. This disadvantage is overcome in our receiver by the use of two parallel 2nd I.F. strips separated by 1 Mc/sec (that is, by the frequency through which the 1st L.O. is switched). In this way (if the receiver is tuned to the correct frequency), the H-line radiation is alternatively amplified, first in one 2nd I.F. strip and then in the other; that is, it is being observed all the time in one or the other channel. This leads to an increase in sensitivity of $\sqrt{2}$ compared with the original Ewen-type equipment. It also has considerable advantages in the suppression of any R. F. interference.

(28) H. E. TATEL, *C.I.W.*: **21-cm equipment at the Carnegie Institution of Washington.** (No abstract was submitted.)

(29) N. T. LAVOO, *General Electric Company*: **Tube noise and circuit problems at high frequency.** (No abstract was submitted.)

(30) C. H. MAYER, *N.R.L.*: **Improved noise power measurements through the use of ferrites.**[1] One of the limitations on the accuracy of measuring small radio noise powers is the dependence of the receiver output response on the radio-frequency impedance connected to the receiver input. Errors in relative measurements result when the antenna is replaced by calibration sources with different impedances and line lengths, or when the receiver frequency changes with time. The impedance of the antenna adds an additional uncertainty to absolute measurements. Even with well-matched impedances and good receiver performance, uncertainties of five to ten per cent may result at microwave frequencies. This talk will describe two ways in which ferrite circuit elements have been used to reduce this source of error at a wavelength of 3.15 cm.

The sketch (Fig. 1) shows the apparatus used to observe the effect of a mismatched source impedance. The input of a comparison-type receiver, similar to that described by Dicke, was connected to a long waveguide transmission line. A dielectric plug, which was terminated in a lossy vane and adjusted for a known reflection coefficient, was drawn through the long waveguide at a uniform rate.

Figure 2 shows recordings of the output of a 3.15-cm receiver when plugs with voltage reflection coefficients of 4/10 and 2/10 were drawn through the waveguide. The short period of the variation corresponds to a line length of about ½ local oscillator wavelength. The long period of the variation results from the response of the superheterodyne receiver to both the signal and the image frequencies, and corresponds to a line length which is ½ wavelength longer for the image than for the signal; in this case about six feet. The amplitude of the variations shown here

[1]Text of papers presented to the URSI-IRE meeting, October 5–8, 1953, at Ottawa, Canada, and to the Radio Astronomy Conference, January 4–6, 1954, at the Carnegie Institution of Washington.

could have been reduced by proper mixer phasing, and the reflection coefficients used were several times larger than would be used in practice.

When ferrite materials with good dielectric properties at microwave frequencies

(MAYER)

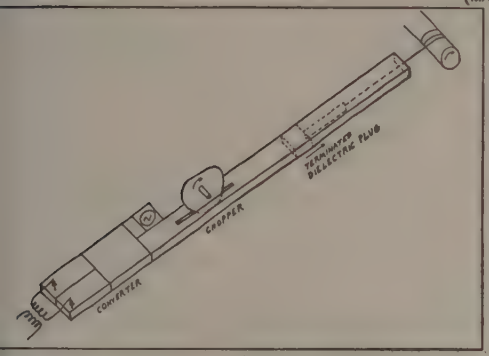

FIG. 1

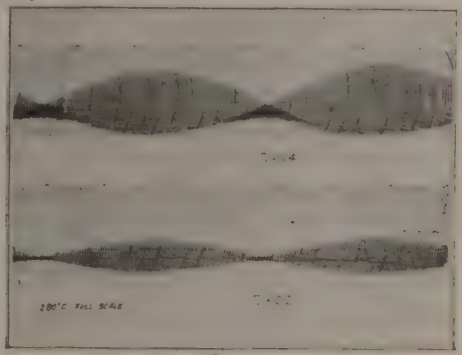

FIG. 2

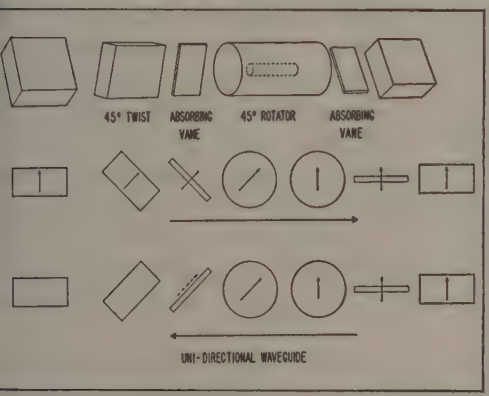

FIG. 3

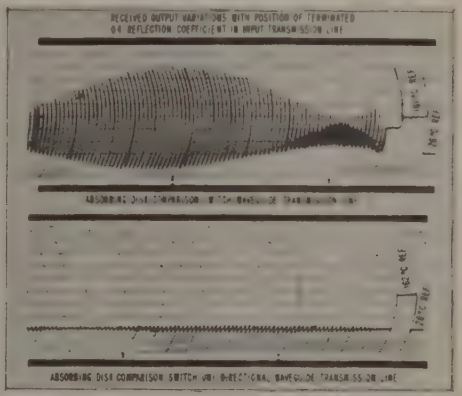

FIG. 4

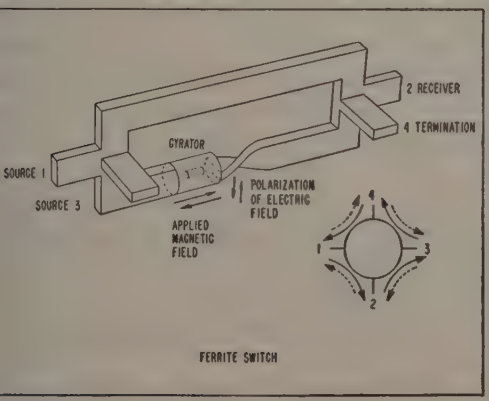

FIG. 5

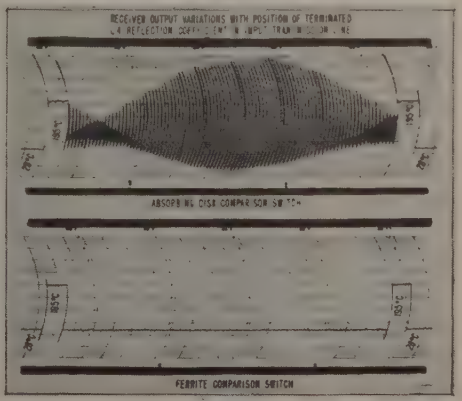

FIG. 6

became available, it was possible to construct a non-reciprocal waveguide transmission line which could be used to isolate the receiver from the source with little loss in sensitivity. A commercially-available one-way waveguide with attenuations

of ½ decibel and 20 decibels for the two directions of propagation was used for the test described here. The diagram (Fig. 3) illustrates the operation of the one-way waveguide. A longitudinal magnetic field is applied to the ferrite with a permanent magnet, so as to rotate the plane of polarization of an incident wave by 45°. Reversal of the direction of propagation is equivalent to reversal of the applied magnetic field; consequently, a wave fed into one end is rotated into the plane of the output waveguide and is transmitted, while a wave fed into the other end is rotated into a plane normal to the output waveguide and is absorbed in a lossy vane.

The upper chart in Figure 4 shows the output of the receiver when the plug with a reflection coefficient of 4/10 was drawn through the waveguide. The lower chart shows a repeat of this procedure with the one-way waveguide inserted between the chopper and the mixer of the receiver. The receiver output variation was reduced to 10 per cent of its former value. The decrease in signal response caused by the transmission loss of the isolator is demonstrated by the output from the noise source. For increased isolation, a better ferrite isolator can be built, or several isolators can be cascaded.

In the second application, the rotating lossy-disk chopper was replaced by a ferrite switch. The diagram (Fig. 5) shows a device which was described as a circulator by Hogan (Bell System Tech. J., **31**, 1-31,1952). A 90° ferrite rotator connects two cross-polarized waveguides in one branch of a hybrid circuit. The length of the other branch was adjusted for transmission from 1 to 2 for one direction of applied magnetic field. The 90° rotator introduces an effective phase-change of 180° for the reverse direction of propagation, so that transmission occurs from 2 to 3 instead of from 2 to 1 for the same applied field. The operation is summarized in the circuit symbol suggested by Hogan. Transmission follows the solid arrows for one direction of applied magnetic field and the dashed arrows for the reverse field.

To make a radio-frequency switch with built-in isolation, an alternating magnetic field was applied to the ferrite by exciting a solenoid wound around the waveguide with a square-wave current. In order to compare the ferrite switch with the lossy-disk chopper, the antenna line was connected to 1, the receiver to 2, and matched terminations to 3 and 4. The solenoid was excited at 30 cps. The experimental model, which was assembled from laboratory components, had a transmission loss of 4/10 decibel and a switching ratio of 26 decibels.

The upper chart in Figure 6 shows the receiver output variation with the lossy-disk chopper. The lower chart shows the receiver output variation with the ferrite switch. In both cases, the plug with a reflection coefficient of 4/10 was drawn through the waveguide. The magnitude of the output variation with the ferrite switch was about two per cent of that with the chopper.

The ferrite switch has several other characteristics which may be desirable in radio astronomy applications.

The switching is all electrical, and switching rates throughout the audio-frequency range can be realized.

A second receiver can be connected to terminal 4 of the switch which was not used in the previous example.

Switching can be accomplished between two arbitrary sources; for example,

irect comparisons between antenna and sky, or between the radiation in two ifferent polarizations.

At the present time, we have attempted these ferrite applications only in the egion of 3-cm wavelength. Whether similar results can be realized at other wave-engths depends on the properties of the ferrites. It seems probable that these echniques can be successfully applied at shorter wavelengths and at longer wave-engths, at least to 10-cm wavelength.

HYDROGEN AND OTHER LINE RADIATIONS

(31) H. C. VAN DE HULST, *Leiden Observatory, Holland*: **Structure of the Galaxy rom 21-cm line observations.** (No abstract was submitted.)

(32) B. Y. MILLS, *Australia—C.I.W.*: **Observations of the Magellanic Clouds.** Radio-frequency emission from the Magellanic Clouds has been observed in Australia, both at a wavelength of 21 cm from neutral hydrogen and at a wave-ength of 3 meters. The line radiation was received from large areas of both Clouds, eaching beyond the optical limits. The observations, which were made with a esolution of 1° in angle and 8 km/sec in radial velocity, gave the line profiles for bout 250 independent points.

Optical observations have shown that the Large Cloud contains substantially nore obscuring dust than the Small Cloud. The radio observations allow the total nass of neutral hydrogen in the Clouds to be calculated, and it is found to be of he same order in both. Thus, the ratio of gas to dust is very different in the two ystems. In the Large Cloud, the distribution of gas has been found to be similar o that of the stars, but in the Small Cloud an envelope of gas extends well beyond he core of stars.

The distribution of radial velocities over the whole of the two Clouds has been btained. Analysis of the mean radial velocities, derived from the line profiles, ndicates regular motions of (*a*) rotation as a binary system and (*b*) translation.

The 3-meter radiation from the Clouds has been detected with an 8° pencil-beam erial. The Small Cloud is not resolved with this beam-width, but the Large Cloud ives an indication of a finite angular size. The ratio of the radio flux to the light ux emitted by each of the Clouds is approximately the same and roughly equal to hat of the Andromeda and other "normal" galaxies.

(33) R. H. DICKE, E. M. PURCELL, AND J. WITTKE, *Princeton and Harvard Universities*: **Excitation of the 21-cm line.** (No abstract was submitted.)

(34) C. H. TOWNES, *Columbia University*: **Microwave spectra of astrophysical nterest.** (No abstract was submitted.)

Discussion by B. F. BURKE, *Department of Terrestrial Magnetism, Carnegie Institution of Washington*, following Towne's paper at Radio Astronomy Conference, January 4–6, 1954: It is suggested that interstellar lines due to the hydrogen nolecule-ion, H_2^+, might be observable. Transitions are possible between several

levels whose energy difference should lie in the radio-frequency and microwave region, since there is a ρ-type doubling of rotational levels and a hyperfine splitting analogous to the observed splitting in the ground state of the hydrogen atom.

(35) B. J. Bok, *Harvard University*: **Astronomical problems connected with the 21-cm line.** The discovery of the 21-cm line of neutral hydrogen by Purcell and Ewen,[1] promptly confirmed by Dutch[2] and Australian[3] teams, opened up a new era in galactic research. Oort, van de Hulst, and Muller[4] have been the first to take full advantage of the new technique for the study of the hydrogen cloud in the more remote parts of our galactic system, and from their researches ha come new and basic information regarding the spiral structure of our galaxy t distances which we had never thought it possible to reach by optical means. Sinc van de Hulst has already spoken at this symposium about the progress made t date by himself and associates in Holland, it would be redundant to discuss agai the related problems of spiral structure, galactic rotation, and the difficult problem of the distribution and motion of the neutral hydrogen clouds in the inner parts o our galaxy. No general survey of the topic, however, would be complete withou stressing the fundamental importance of the lines of research now being pursue by the Dutch research workers. Another very promising line of research has bee developed by Kerr and Hindman,[5] but since their work has already been discusse at this symposium by Mills, it will not be necessary here to do more than mentio it and emphasize the importance of further studies of the distribution and motion in the aura of neutral hydrogen in which the two Magellanic Clouds appear to b imbedded. In out presentation of problems connected with the 21-cm line, w shall, therefore, stress in particular those that are either now under investigatio with Harvard's Agassiz Station radio telescope, or which we intend to investigat in the near future. I should state that in my report on our work at Agassiz Statio I am speaking for myself and associates, principally Dr. Harold I. Ewen, co-directo of the project, David S. Heeschen and A. Edward Lilley, graduate students, an John A. Campbell, project engineer.

The Agassiz Station radio telescope is a 24-foot equatorially-mounted parabol which is driven in hour angle by means of a servo-hydraulic system. For the 21-c line, the antenna half-power point separation is approximately 1°.7. The telescop is located at the Agassiz Station of Harvard Observatory. Support for the proje has been provided by a friend of Agassiz Station and through a grant from th National Science Foundation.

Ewen has described in detail how the receiver continuously compares an records the difference of the average D.C. noise power in two sections of th galactic microwave spectrum. These are the signal and comparison bands. Th comparison band is centered 3 Mc/sec above the signal band and has a fixed ban width of 2 Mc/sec. The receiver is essentially a double conversion superheterodyn

[1]Nature, **168**, 356 (1951).
[2]Nature, **168**, 357 (1951).
[3]Nature, **168**, 358 (1951).
[4]Observatory, **73**, 129 (1953); and Ciel et Terre, **69**, 117 (1953).
[5]Astr. J., **58**, 218 (1953).

odified to act as a comparison radiometer. Tuning of the local oscillator effectively ides both signal and comparison bands along the galactic spectrum, and the signal and is allowed to encounter the hydrogen emission line. The line profile which esults from such a "scan" presents the structure of the line superimposed on the alactic background spectrum and is not a measure of the background itself.

Several features of the equipment are of fundamental importance to the stronomer. The knowledge of velocities rests upon the knowledge of the frequency hroughout the scan. The Harvard equipment has automatic frequency-marking ircuits developed by Ewen. They indicate intervals of 100 kc/sec and 10 kc/sec on the bottom and top of each scan, respectively. At the hydrogen-line frequency of 1,420 Mc/sec, an interval of 10 kc/sec corresponds to a Doppler shift of 2.13 km/sec.

The fundamental frequency standard for the equipment is a 5-Mc/sec crystal, which the operator continuously maintains in approximate "zero beat" with WWV. With this arrangement, the equipment indicates the frequencies on each record with a precision that amounts to an uncertainty in velocity of about one-fifth of a kilometer per second.

The detail revealed in the line profile depends upon the band-width of the signal band. Four band-widths are available with the present equipment. They are 200 kc, 50 kc, 15 kc, and 5 kc per second, respectively, corresponding to widths of 43 km, 11 km, 3 km, and 1 km per second. For most problems, it is desirable to employ the smaller band-widths. The observations reported here were all taken with a signal band-width of 15 kc/sec.

The calibration of the receiver in temperature depends upon a knowledge of the noise figure of the receiver. For measurement of the noise figure, we use the method developed by W. W. Mumford at the Bell Telephone Laboratories. This technique employs a fluorescent tube as a noise source. The noise figure is measured at least once on each day of operation; the estimated error of our calibrations is $\pm 10°$K on the conventional scale of brightness temperature. The probable error of a point derived as a mean from four separate scans is $\pm 4°$K, and the minimum detectable signal with our present equipment is $\pm 5°$K.

Construction of the electronic, hydraulic, and mechanical components of the Harvard telescope began in the fall of 1952. The assembly at Agassiz Station was completed during the summer of 1953. Final electronic tuning and mechanical and hydraulic adjustments were completed during the fall, and this permitted our galactic research program to start the end of November, 1953.

During the last week of November and first three weeks of December, the equipment was operated 20 hours a day by Heeschen and Lilley. They obtained slightly more than 200 good-quality scans. Reduction has been completed for fifty per cent of these observations, and some interesting first-results can be presented at this time.

The Agassiz Station radio telescope is shown in Figure 1. We show in Figures 2 and 3 some sample unreduced profiles. The profile in Cepheus at $l = 87°$, $b = 0°$ has two peaks 270 kc/sec apart in frequency, to which corresponds a difference in radial velocity of 57 km/sec. The brighteness temperatures for peak intensity of both maxima are approximately 50°K. In Cygnus, at $l = 52°$, $b = 0°$, three peaks

are shown, separated in radial velocity by 38 and 32 km/sec. The brightness temperatures of the maxima are approximately 70°, 50°, and 30°K. From these and other profiles for the same direction, we find that the brightness temperature between the minima cannot amount to more than 5°K.

In the initial program for the Agassiz Station radio telescope, we are concentrating on regional surveys, with the emphasis at first on the sections of the galactic center and anti-center. The initial program for the section of the center (Heeschen) has 39 centers between $l = 317°$ and 336°, $b = -10°$ to $+50°$; whereas the program for the section of the anti-center (Lilley) has 90 centers between $l = 141°$ and 153°, $b = -50°$ to $+50°$. We intend to obtain a minimum of four acceptable scans per center; the initial program is at present about one-third completed.

For the section of the galactic center, the results of 57 scans are shown. In Figure 4, the reduced profiles are displayed by galactic position. The line at $l = 327°$, $b = 0°$ is of special interest. Presumably, this is the direction toward the galactic center, or near it, and galactic rotation effects should be small. However, the profile has two maxima 50 kc/sec apart, corresponding to a difference in radial velocity of 11 km/sec. A plot of peak brightness temperature *versus* galactic latitude reveals some interesting features (Fig. 5). The following listing of estimated peak brightness temperatures indicates the general nature of our preliminary results:

Galactic latitude	Peak brightness temperature
°	°
−10	43
0	79
+10	45
+20	49
+30	41
+40	28
+50	15

The most notable feature is the secondary maximum at 20° north galactic latitude.

Figure 6 shows, for the anti-center section, the reduced profiles arranged according to galactic position. For $l = 147°$, the plot of peak brightness temperature *versus* galactic latitude (Fig. 7) reveals a marked asymmetry, which is produced by a strong shoulder in the curve on the south side of the plane. The peak brightness temperature remains relatively high, 30° to 40°, south of the plane, but a different characteristic is revealed north of the plane. Figure 7 shows that the line breadths of the profiles at northern galactic latitudes are large compared to those for similar positions on the south side. The total width of the line at $b = -12°$ is 80 kc/sec (16 km/sec), whereas 12° north of the plane the total width is 134 kc/sec (27 km/sec).

For both the center and anti-center profiles, it is interesting to note that the secondary maxima in the curves of peak brightness temperature *versus* galactic latitude are associated with positions where marked dark nebulae occur. For the

FIG. 1

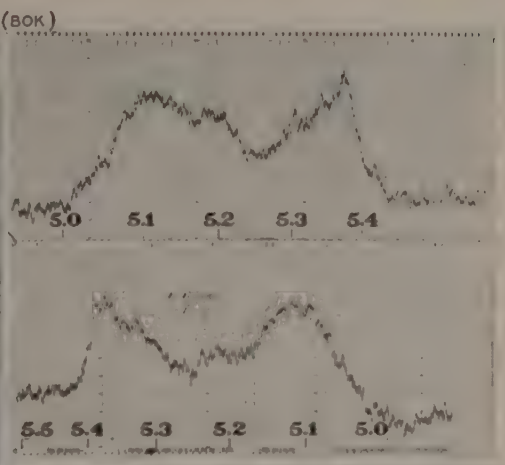

FIG. 2

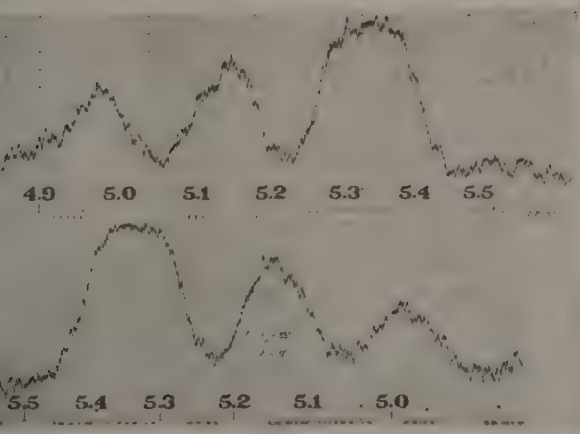

FIG. 3

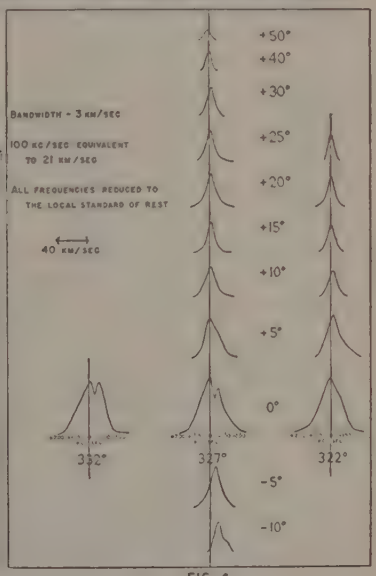

FIG. 4

FIG. 1—The Agassiz Station radio telescope

FIG. 2—Observed profiles at galactic longitude 87°, latitude 0°: The two profiles were obtained one with the scanning frequency increasing, the other decreasing. The bold figures along the bottom of each scan represent the beat-frequencies with the local oscillator. For galactic longitude $l = 87°$, the value of $l - l_0 = 120°$, which corresponds to an assumed value of the longitude of the galactic center $l_0 = 327°$.

FIG. 3—Observed profiles at galactic longitude 52°, latitude 0°: See the legend for Figure 2

FIG. 4—Reduced profiles for the section of the galactic center (Heeschen)

center and anti-center, these are respectively the Ophiuchus and Taurus dark nebulae complexes.

The two initial Harvard surveys are purposely concerned primarily with the two directions in the sky for which galactic rotation effects play the least rôle.

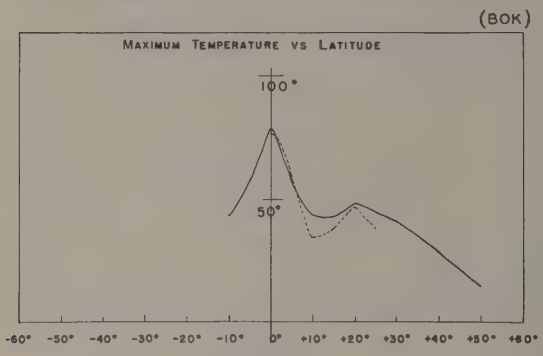

FIG. 5

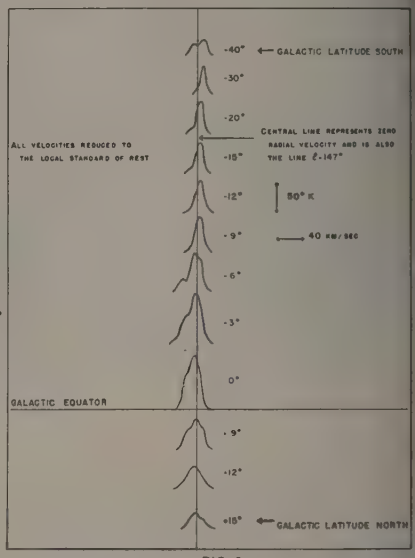

FIG. 6

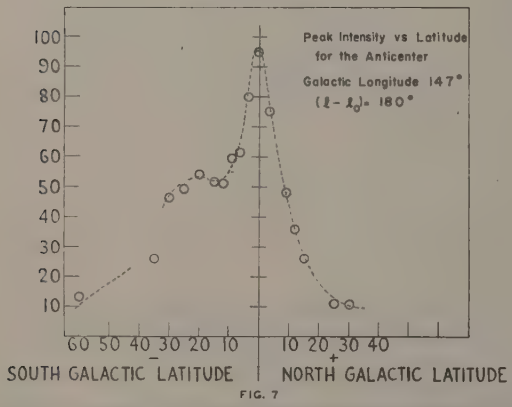

FIG. 7

FIG. 5—Variation of peak brightness temperature with galactic latitude for the section of the galactic center (Heeschen): The full-drawn curve is for $l = 327°$, the dotted curve for $l = 322°$

FIG. 6—Reduced profiles for the section of the anti-center, $l = 147°$ (Lilley)

FIG. 7—Variation of peak brightness temperature with galactic latitude for the section of the anti-center (Lilley)

To supplement these surveys, we have already begun work on two additional regional surveys, one for the very complex section between $l = 45°$ and $62°$; the other for the section between $l = 100°$ and $110°$. In the first section, a careful study, point-by-point in the sky and extending from $b = -30°$ to $+30°$ at least, promises valuable results with regard to the separation of effects produced by nearby local features of galactic structure and by features related to remote spiral structure. For the section between $l = 100°$ and $110°$, we seem to have an excellent opportunity to distinguish clearly between effects produced by the spiral arm in which the sun is located and the thin outermost spiral arm of Morgan[6] (compare with Münch's[7] results for multiple interstellar lines in this section).

[6]Astroph. J., 118, 318 (1953).

[7]Pub. Astr. Soc. Pacific, 65, 179 (1953).

Regional surveys, like those we have sketched above, promise results of importance if we correlate the details of the radio features with the known optical features. The results of Heeschen and Lilley (Figs. 5 and 7) may possibly suggest that dark nebulae and complexes of dark nebulae may have important effects on the emission of 21-cm radiation, but it would be premature to analyze the preliminary data in detail. It seems likely, however, that from regional surveys we shall be able to draw valuable conclusions regarding temperature conditions inside dark nebulae and regarding the constancy of the ratio between gas and dust in interstellar space. Among the optical features that especially deserve attention are dark nebulae, complexes as well as single nebulae, and—for high angular resolution surveys—globules. We shall certainly find it worth while to study also with highest attainable precision sections of the Milky Way in which multiple interstellar absorption lines have been detected, and the possible effects of extended H (II) regions is similarly worthy of detailed investigation. Our results to date indicate that maximum brightness temperature of a given line is only one of several important parameters; half-width of the line total intensity will have to be considered.

In future surveys, considerable importance should be attached to detailed astrophysical analysis of observed line profiles. The importance of such studies has become evident from research by Wild[8] and Heeschen,[9] but to date we cannot say that we have really begun the detailed analysis of observed line profiles with due attention to problems of optical depth, variable brightness temperature along the line of sight, and dispersion in random radial velocities. We shall have to consider separately models with cloud structure and models with more nearly uniform distribution of the gas in the spiral arms. The importance of such studies cannot be overstressed, but it should be realized that observational data of the highest caliber will be required for results of significance. High resolution in angle, which is critically important, and in frequency (radial velocity) are necessary. These conditions make it necessary that the research be done with the largest available parabolic antennas and with recording equipment providing high resolution in frequency; a good first goal seems to be a parabolic antenna with an aperture of at least 50 to 80 feet and recording equipment with a signal band-width of 5 kc/sec (1 km/sec). It may be that lower resolution in frequency will suffice, but this has not yet been proved to be the case.

We should emphasize at this point the importance of studies of the brightness temperature for the general background radiation upon which the observed 21-cm profiles are superimposed. A comparison radiometer specifically excludes measurement of the brightness temperature of the continuous background radiation, and this important observational quantity must be obtained separately and by a different observational technique. The simple assumption of a background temperature of 10°K, which is often made in our analyses, will not suffice for future research.

The current 21-cm research has only served to whet the astronomer's appetite for other line absorption or emission features. The paper by Townes, presented at

[8] Astroph. J., 115, 206 (1952).
[9] Astr. J., 58, 40 (1953).

this symposium, has provided us with a listing of other possible absorption or emission features which must be looked for, however small the prospects for their detection may seem at present. For the case of deuterium (327 Mc/sec), a negative result will already be of value in providing an upper limit to the abundance of deuterium relative to hydrogen. Finally, Townes's calculations give strong support to Shklovsky's[10] suggestion that we should search for evidence of OH in the vicinity of 1,665 Mc/sec.

In our brief survey of problems, we should refer to the need for studies of the radiation, very weak but presumably detectable, that reaches us from outside our own galaxy. It would be most helpful if we could detect and study the radiation from the great spiral in Andromeda, M31. The considerable range in radial velocity (more than 600 km/sec, equivalent to a little more than 3 Mc/sec in frequency!) observed optically for objects in M31, makes this a very difficult object for study by 21-cm techniques, but the attempt must be made. This is primarily a project for a large parabolic antenna. Correlation between radio data, observed radial velocities, and structural features observed optically should produce information of relevance to studies of the dynamical properties of M31. The spiral M33 may in some ways prove to be more accessible to radio studies, since the range of radial velocity observed optically over this galaxy is relatively small, which should at least facilitate detection. Furthermore, the smaller average radial velocity for M33 relative to our sun (-167 km/sec) makes this a somewhat easier object than M31, with an average radial velocity of -250 km/sec.

In conclusion, we wish to mention the importance that attaches to studies in high galactic latitudes. Our observations at Agassiz Station have already confirmed the results of Christiansen and Hindman,[11] which show considerable 21-cm emission from fields at high galactic latitudes. Since these observations refer to relatively small radial velocities, the clouds that produce these features belong almost surely to our own galaxy; they may be related (as mentioned by Minkowski in the discussion at the Washington symposium) to the faint nebulous patches observed in high galactic latitudes on some of the Mount Palomar Schmidt photographs. The considerable breadth and even duplicity shown by some of the profiles at high galactic latitudes observed at Agassiz Station suggest that further study of these galactic neutral hydrogen clouds at great distances from the galactic plane may be quite profitable. Still another potential field of research in high galactic latitudes lies in the search for possible extra-galactic background radiation from neutral hydrogen at frequencies corresponding to high velocities of recession, but it seems futile at this point to do more than mention research in this area.

DISCUSSION OF SPECIAL TOPICS

"We will hold this period for those who wish to comment on and discuss topics insufficiently touched on by formal papers. Will those who wish to initiate such discussions inform Greenstein, so that topics of interest to the conferees can be covered."

[10]Astron. Zhurnal, **26**, 10 (1948), and **29**, 144 (1952).
[11]Aust. J. Sci. Res., A, **5**, 437 (1952).

L. Field, *California Institute of Technology*: **Noise generation in plasmas.**

J. W. Dungey, *Pennsylvania State University*: **The neutral point theory of olar flares.***[1] The mechanism for the acceleration of charged particles to high nergies is explained. This occurs in a "discharge," which is a thin sheet of very rge electrical current density. It is shown that discharges will occur in the eighborhood of neutral points but not elsewhere. Only very rough numerical alues can be given, but these agree with the observed duration of a flare and ggest a voltage of $\sim 10^{10}$ volts for an intense flare. The number of particles ccelerated is sufficient to account for the increase in cosmic-ray intensity some-mes observed shortly after a flare.

R. H. Dicke, *Princeton University*: **Non-linear effects in noise.**

A. E. Covington, *National Research Council, Canada*: **Evidence for increased bsorption of solar noise at the time of a flare.**

H. C. van de Hulst, *Leiden Observatory, Holland*: **Spicules as the optical hromosphere.**

W. O. Roberts, *High Altitude Observatory, Boulder, Colorado*: **Holes in the hromosphere.**

B. F. Burke, *Department of Terrestrial Magnetism, Carnegie Institution of Vashington*: **A possible mechanism for 200-Mc/sec noise generation.**

OPEN HOUSE AT NAVAL RESEARCH LABORATORY

Captain Beltz and Dr. John Hagen invite members of the conference to visit the Naval Research Laboratory late Wednesday afternoon. Please leave names at the egistration desk."

The following invited participants attended the Radio Astronomy Conference:

H. Alfvén, Royal Institute of Technology, Stockholm, and University of Maryland
L. H. Aller, University of Michigan
Philip Barnhart, University of Indiana
A. Blaauw, Yerkes Observatory
Bart J. Bok, Harvard College Observatory
H. G. Booker, Cornell University
E. G. Bowen, Commonwealth Scientific and Industrial Research Organization, Australia
R. Britten, Department of Terrestrial Magnetism, Carnegie Institution of Washington
R. H. Brown, Jodrell Bank Experimental Station, England
B. F. Burke, Department of Terrestrial Magnetism, Carnegie Institution of Washington
C. R. Burrows, Cornell University

*The preparation of this paper was sponsored by the Geophysics Research Division of the Air Force Cambridge Research Center, under Contract AF19(122)–44.

[1]See Phil. Mag., **44**, 725 (1953).

Solomon Charp, Franklin Institute
C. E. Cleeton, U.S. Naval Research Laboratory
R. J. Coates, U.S. Naval Research Laboratory
Arthur Code, University of Wisconsin
H. H. Corbett, U.S. Naval Research Laboratory
A. E. Covington, National Research Council, Canada
R. H. Dicke, Palmer Physical Laboratory
Helen W. Dodson, McMath-Hulbert Observatory
Lee A. DuBridge, California Institute of Technology
J. W. Dungey, Pennsylvania State University
H. I. Ewen, Harvard College Observatory
W. R. Ferris, U.S. Naval Research Laboratory
G. Field, Princeton University
Lester Field, California Institute of Technology
J. Firor, Department of Terrestrial Magnetism, Carnegie Institution o Washington
S. E. Forbush, Department of Terrestrial Magnetism, Carnegie Institutio of Washington
Kenneth L. Franklin, University of California
J. E. Gibson, U.S. Naval Research Laboratory
V. L. Goerke, National Bureau of Standards, Colorado
W. E. Gordon, Cornell University
J. L. Greenstein, California Institute of Technology
F. T. Haddock, U.S. Naval Research Laboratory
J. P. Hagen, U.S. Naval Research Laboratory
J. Hall, U.S. Naval Observatory
David S. Heeschen, Harvard College Observatory
L. Helfer, Department of Terrestrial Magnetism, Carnegie Institution o Washington
N. Hepburn, U.S. Naval Research Laboratory
F. Hoyle, Cambridge, England, and California Institute of Technology
E. O. Hulburt, U.S. Naval Research Laboratory
Robert Jones, Pennsylvania State University
J. D. Kraus, Ohio State University
N. T. Lavoo, General Electric Company
A. Edward Lilley, Harvard College Observatory
C. G. Little, Harvard College Observatory
Sol Matt, Ohio State University
Tom Matthews, Harvard College Observatory
E. Maxwell, Massachusetts Institute of Technology
C. H. Mayer, U.S. Naval Research Laboratory
J. H. McMillen, National Science Foundation
A. G. McNish, National Bureau of Standards
G. C. McVittie, University of Illinois

B. Y. Mills, Commonwealth Scientific and Industrial Research Organization, Australia, and Department of Terrestrial Magnetism, Carnegie Institution of Washington
Rudolph Minkowski, Mount Wilson and Palomar Observatories
A. P. Mitra, India, and Pennsylvania State University
L. Owren, Norway, and Department of Terrestrial Magnetism, Carnegie Institution of Washington
G. Reber, Wailuku, Maui, Territory of Hawaii
W. O. Roberts, High Altitude Observatory, Boulder, Colorado
Paul Scherer, Carnegie Institution of Washington
Ed. Schiffmacher, Cornell University
Richard Sears, Indiana University
R. J. Seeger, National Science Foundation
H. K. Sen, National Bureau of Standards
Alan Shapley, National Bureau of Standards
S. L. Sharpless, U.S. Naval Observatory
Fred Singer, University of Maryland
R. M. Sloanaker, U.S. Naval Research Laboratory
F. G. Smith, Cambridge, England, and Department of Terrestrial Magnetism, Carnegie Institution of Washington
L. Spitzer, Princeton University
Frank Tangherlini, Consolidated Vultee Aircraft Corporation
H. Tatel, Department of Terrestrial Magnetism, Carnegie Institution of Washington
C. H. Townes, Columbia University
M. A. Tuve, Department of Terrestrial Magnetism, Carnegie Institution of Washington
L. C. Van Atta, Hughes Aircraft Company
H. C. van de Hulst, Leiden Observatory, Holland
E. H. Vestine, Department of Terrestrial Magnetism, Carnegie Institution of Washington
Constance Warwick, Harvard University
James Warwick, Harvard University
H. W. Wells, Department of Terrestrial Magnetism, Carnegie Institution of Washington
A. E. Whitford, University of Wisconsin
J. B. Wiesner, Massachusetts Institute of Technology
R. E. Williamson, Los Alamos Scientific Laboratory
M. Wrubel, Indiana University

NOTICE

When available, single unbound volumes can be supplied at $3.50 each and single numbers $1 each, postpaid.

Charges for reprints and covers

Reprints can be supplied, but prices have increased considerably and costs depend on the mber of articles per issue for which reprints are requested. It is no longer possible to publish a edule of reprint charges, but if reprints are requested approximate estimates will be given when ley proofs are sent to authors. Reprints without covers are least expensive; standard covers ith title and author) can be supplied at an additional charge. Special printing on covers can also supplied at further additional charge.

Fifty reprints, without covers, will be given to institutions paying the publication charge of 00 per page.

Alterations

Major alterations made by authors in proof will be charged at cost. Authors are requested, refore, to make final revisions on their typewritten manuscripts.

Orders for back issues and reprints should be sent to Editorial Office, 5241 Broad Branch Road, W., Washington 15, D.C., U.S.A.

Subscriptions are handled by The Editorial Office, 5241 Broad Branch Road, N.W., Washington , D.C., U.S.A.

CONTENTS—Concluded